

# Mesoscopic physics of nanomechanical systems

Adrian Bachtold<sup>\*</sup>


ICFO—Institut de Ciències Fòniques, The Barcelona Institute of Science and Technology,  
08860 Castelldefels, Barcelona, Spain

Joel Moser<sup>†</sup>

School of Optoelectronic Science and Engineering  
Soochow University, Suzhou 215006, People's Republic of China

M. I. Dykman<sup>‡</sup>

Michigan State University, East Lansing, Michigan 48823, USA

 (published 8 December 2022)

Nanomechanics has brought mesoscopic physics into the world of vibrations. Because nanomechanical systems are small, fluctuations are significant, the vibrations already become nonlinear for comparatively small amplitudes, and new mechanisms of dissipation come into play. At the same time, the exquisite control of these systems makes them a platform for studying many problems of classical and quantum physics far from thermal equilibrium in a well-characterized setting. This review describes, at a conceptual level, basic theoretical ideas and explicative experiments pertaining to mesoscopic physics of nanomechanical systems. Major applications of nanomechanics in science and technology are also outlined. A broad range of phenomena related to the conservative as well as dissipative nonlinearity and fluctuations are discussed within a unifying framework. They include the linear response of single and coupled vibrational modes as well as nonlinear effects of periodic driving. Such driving breaks the continuous time-translation symmetry and the detailed balance, with conspicuous consequences for fluctuations, particularly in the presence of the driving-induced bistability and multistability. Mathematical techniques are described in the appendixes to provide an introduction to the theory. The goal of the review is to show the richness of the physics at work. The continuous experimental and theoretical advances make nanomechanical systems a vibrant area of research with many new phenomena to discover.

DOI: [10.1103/RevModPhys.94.045005](https://doi.org/10.1103/RevModPhys.94.045005)

## CONTENTS

I. Introduction	2	C. Quantum description of the mode dynamics	15
II. Nanoresonators at a Glance	3	1. The power spectrum and the susceptibility of a weakly damped mode	15
A. Phenomenological description of the dynamics of a linear nanoresonator	3	V. Relaxation Mechanisms of Nanomechanical Resonators	15
B. Most common types of nanomechanical resonators	4	A. Scattering by phonons	16
C. Driving resonators	7	1. Clamping losses	16
D. Frequency control	8	2. Anelastic relaxation and dissipation dilution for flexural modes	17
E. Detection of displacement	8	3. Landau-Rumer relaxation	18
1. Quantum regime	9	4. Thermoelastic and Akhiezer relaxation	19
F. Measurement of the spectral response	9	B. Losses due to surface effects and two-level systems	21
III. Sensing and Clocks	10	C. Electronic relaxation	22
A. Force sensing	10	VI. Conservative and Dissipative Nonlinearity	23
B. Mass sensing	11	A. Mechanisms of conservative nonlinearity	24
C. Photothermal-based sensing	12	B. Mechanisms of nonlinear friction	26
D. Clocks and clock-based systems	12	C. Effect of the nonlinearity on the spectra	27
IV. Fluctuation-Dissipation Theorem and the Reaction Force from the Thermal Bath	12	1. Spectral effects of the Duffing nonlinearity	27
A. Coupling of the oscillator to a thermal bath	13	2. Dispersive coupling of a nanomechanical mode to a qubit	28
B. Brownian motion of the complex vibration amplitude	14	3. Broadening of the power spectrum due to nonlinear friction	30
		VII. Nonlinear Resonant Phenomena: A Laboratory for Studying Physics Far from Thermal Equilibrium	30
		A. Bistability of resonantly excited vibrations	30
		B. Parametric excitation	32
		C. Fluctuations of driven modes	32

<sup>\*</sup>adrian.bachtold@icfo.es

<sup>†</sup>j.moser@suda.edu.cn

<sup>‡</sup>dykman@pa.msu.edu

1. Fluctuation squeezing	33
D. Rare large fluctuations far from thermal equilibrium	34
1. Dynamics of nonequilibrium systems in rare large fluctuations	35
2. Scaling behavior of the rates of switching between stable vibrational states	36
3. A kinetic phase transition	37
VIII. Resonant Mode Coupling	38
A. Linear resonant coupling	38
B. Nonlinear resonant coupling	40
C. Parametrically induced resonant coupling	42
IX. Frequency Fluctuations	44
A. Allan variance	45
B. Eigenfrequency fluctuations	46
X. Outlook and Challenges	48
List of Symbols and Abbreviations	50
Acknowledgments	50
Appendix A: Method of Averaging: Weak Nonlinearity and Weak Damping	50
1. Nonlinear vibrations with no damping	50
2. Effect of the coupling to a bath	51
3. Ohmic dissipation	52
Appendix B: Oscillator Decay Rate in the Born Approximation and the Quantum Kinetic Equation	52
1. Master equation	53
Appendix C: Driving-Induced Cooling and Heating for Coupled Modes	54
Appendix D: Forced Vibrations	55
1. Resonant driving	55
a. Universality of fluctuations near a bifurcation point	56
2. Parametrically excited vibrations	57
a. Fluctuation squeezing in the linear regime	58
b. Squeezing of fluctuations about the state of resonantly or parametrically excited vibrations	58
Appendix E: Spectra of Nonlinear Underdamped Vibrational Modes: Quantum and Classical	59
1. “Paradox” of the quantum harmonic oscillator	59
2. The susceptibility in the explicit form	60
3. Dispersively coupled vibrational modes	61
4. Classical limit	61
1. “Paradox” of the quantum harmonic oscillator	59
2. The susceptibility in the explicit form	60
3. Dispersively coupled vibrational modes	61
4. Classical limit	61
Appendix F: The Action-Angle Variables	62
Appendix G: Thermoelastic and Akhiezer Relaxation	63
1. Kinetic equation	64
a. Thermoelastic relaxation	65
b. Akhiezer relaxation	66
1. Kinetic equation	64
a. Thermoelastic relaxation	65
b. Akhiezer relaxation	66
Appendix H: Allan Variance in the Limiting Cases	67
References	67

## I. INTRODUCTION

Studying vibrational motion has been one of the major areas of physics at least since the time of Galileo. The advent of nanomechanical vibrational systems (NVs) has opened a new direction in these studies. NVs are resonators for

mechanical vibrations. As an example, one can consider a string of a musical instrument downscaled to a diameter  $\lesssim 100$  nm and a submicron length. The vibration frequencies range from kilohertz to gigahertz and can be tuned not only through the dimensions and the shape of a device but also *in situ* by electrostatic and optical means. In addition, the lifetime of vibrations has now been increased to hundreds of seconds and more thanks to progress in nanofabrication.

By their nature NVs are mesoscopic. Because they are small, they display many features of microscopic systems. At the same time, they are sufficiently large to enable studying an individual vibrational system rather than resorting to ensemble measurements, as in conventional molecular or solid-state vibrational spectroscopy.

NVs were developed in the 1990s (Travis, 1994; Cleland and Roukes, 1996, 1998) and quickly attracted interest. Their vibrational eigenmodes display a rich dynamics that involves a broad range of many-body effects stemming from the coupling to electrons, propagating phonons, photons, and two-level fluctuators. They are also of significant interest for various applications that range from ultrasensitive mass, charge, and force detection to clocks. For example, the adsorption of mass onto a NV can be detected with a resolution approaching 1 yg, while a force can be resolved with a sensitivity approaching  $1 \text{ zN/Hz}^{1/2}$ . Over the years different aspects of the studies of NVs along with their applications have been reviewed in a number of works (Cleland, 2003; Ekinci and Roukes, 2005; Lifshitz and Cross, 2008; Poot and Zant, 2012; Aspelmeier, Kippenberg, and Marquardt, 2014b; Schmid, Villanueva, and Roukes, 2016; Steeneken *et al.*, 2021).

In this review, we focus on the mesoscopic physics of NVs, including dissipation, fluctuations, and nonlinear and far from thermal equilibrium phenomena in these systems. While these basic physical phenomena have been intensely investigated during the last few years, they have not yet been reviewed from a general perspective. Our aim is to provide a coherent and unifying description of the underlying concepts along with the experimental and theoretical results and to put them into a broad physics context. Details of the mathematical techniques are provided in the appendixes.

We describe the dissipation and thermal fluctuations of nanomechanical vibrations as resulting from the coupling to a thermal reservoir of a general form. Such a description applies to both flexural and localized compression- and shear-type modes. It allows us to analyze various specific dissipation mechanisms. They include the Landau-Rumer, Akhiezer, and thermoelastic relaxation due to scattering by propagating phonons and the phonon-induced clamping losses, as well as relaxation associated with the electrons in the nanoresonators and the leads and with the two-level systems.

A consequence of the small size of NVs expected from the general arguments of statistical physics is the occurrence of comparatively strong quantum and classical fluctuations. These fluctuations play a significant role in the vibration dynamics. Another important aspect of the dynamics is the vibration nonlinearity. Because of the small system size, vibrations with even comparatively small amplitudes become nonlinear. Not

only does the restoring force display nonlinearity, but also the rate of dissipative losses becomes amplitude dependent, a phenomenon associated with nonlinear friction.

The exquisite control of the NVSs and their versatility make them invaluable as a tool for studying the interplay of nonlinearity and fluctuations. This interplay leads to a broad range of phenomena that manifest themselves in different settings, in both the classical and quantum domains. Revealing and understanding them is an ongoing effort. We describe several of these phenomena studied with the NVSs, including the nondissipative broadening of the vibration spectra, nonlinear intermode energy exchange, and self-modulation and cross modulation of the vibration frequencies.

We also describe how the nonlinearity makes NVS vibrations a testing ground for exploring nonequilibrium phenomena. Several general types of such phenomena emerge where the vibrations are driven by a resonant field. Because the decay rates of the vibrations are usually small, even a weak field can lead to a significantly nonequilibrium behavior, such as the occurrence of bistability and multistability or chaos. Of particular interest, which goes beyond NVSs as such, are fluctuation effects away from thermal equilibrium. They range from noise-induced switching between coexisting metastable vibrational states to fluctuation squeezing. Since, on the one hand, driven nonlinear vibrations lack detailed balance while, on the other hand, the vibrations of NVSs are well characterized, these vibrations provide a unique opportunity for addressing many generic problems of quantum and classical statistical physics far from thermal equilibrium.

## II. NANORESONATORS AT A GLANCE

### A. Phenomenological description of the dynamics of a linear nanoresonator

We describe the dynamics of a NVS mode in terms of the coordinate  $q$  and momentum  $p$  of an oscillator. The mechanical displacement in the mode  $\mathbf{u}(\mathbf{r}, t)$  as a function of the coordinate  $\mathbf{r}$  has a spatial profile  $\boldsymbol{\varphi}(\mathbf{r})$ , whereas  $q(t)$  describes how the displacement varies in time,

$$\mathbf{u}(\mathbf{r}, t) = q(t)\boldsymbol{\varphi}(\mathbf{r}), \quad \int \boldsymbol{\varphi}^2(\mathbf{r})d\mathbf{r} = V, \quad (1)$$

where  $V$  is the volume of the resonator. The momentum of the oscillator is  $p = M\dot{q}$ , where  $M$  is the oscillator mass, and  $M = \int \rho(\mathbf{r})\boldsymbol{\varphi}^2(\mathbf{r})d\mathbf{r}$  [ $\rho(\mathbf{r})$  is the mass density]. Functions  $\boldsymbol{\varphi}(\mathbf{r})$  for different modes are orthogonal. We note that in the analysis of the experimental data a different normalization is sometimes used, i.e.,  $\max |\boldsymbol{\varphi}(\mathbf{r})| = 1$ . With this normalization, the maximal value of  $q(t)$  is the displacement amplitude.

The simplest theoretical model employed in the study of nanomechanical modes is a classical harmonic oscillator that performs Brownian motion (Risken, 1996), with a friction force proportional to the velocity and with fluctuations due to thermal noise. The noise is assumed to be Gaussian and  $\delta$  correlated in time. If the oscillator coordinate is  $q$  and the mass is  $M$ , the motion is described by the Langevin equation

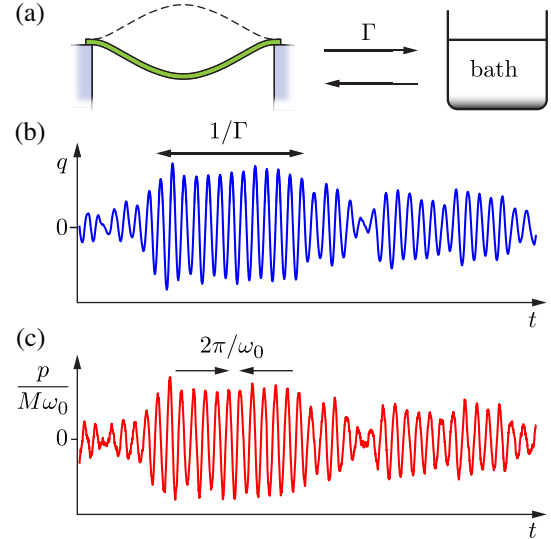


FIG. 1. (a) Mechanical oscillator coupled to a thermal bath. The coupling is quantified by the rate  $\Gamma$  for an oscillator quantum to be transferred into the bath. The parameter  $\Gamma$  enters both the friction force and the noise intensity in Eq. (2). (b),(c) Time evolution of the displacement and the momentum of the oscillator performing Brownian motion. The characteristic correlation time of the amplitude fluctuations is given by  $1/\Gamma$ . One can measure  $\Gamma$  using the spectral density of the displacement fluctuations:  $\Gamma$  is the half width at half maximum of the spectral peak; see Eq. (5).

$$M\ddot{q} + 2M\Gamma\dot{q} + M\omega_0^2q = f_T(t),$$

$$\langle f_T(t)f_T(t') \rangle = 4M\Gamma k_B T \delta(t - t'). \quad (2)$$

In Eq. (2)  $\omega_0$  is the mode eigenfrequency and  $\Gamma$  is the friction coefficient, which determines the decay rate of the vibrations in the absence of noise.

Without noise, the model of a damped oscillator has been long used in physics; for example, it was used by Lorentz in 1878 to describe the polarizability of matter. Later it was realized that with friction there comes noise. Both result from the coupling of the oscillator to a thermal reservoir (thermal bath); see Fig. 1. A microscopic analysis was started by Einstein and Hopf (1910). A detailed classical study was performed by Bogolyubov (1945), whereas the studies of the quantum dynamics were started in the late 1950s–early 1960s; see Toda (1958), Krivoglaz (1961), Senitzky (1961), Schwinger (1961), Ford, Kac, and Mazur (1965), Ullersma (1966), and Louisell (1990). More references can be found in the paper by Ford, Lewis, and O’Connell (1988). Many of these papers used a model in which the thermal bath was described by a set of harmonic oscillators and the coupling to the considered oscillator was linear in  $q$ . Over the years, such a model of the bath, often called a “bosonic bath,” has been one of the most frequently used in the study of quantum relaxation; cf. Feynman and Vernon (1963), Caldeira and Leggett (1981), and Grabert, Schramm, and Ingold (1988).

NVSs are one of the best examples of systems where dissipation described by the linear in  $q$  coupling to a bosonic bath can play an important role. In this case, the bath is often formed by phonons in the resonator and in its support. Different mechanisms of the phonon-induced dissipation,

such as clamping losses and thermoelastic, Landau-Rumer, and Akhiezer dissipation, are discussed in Sec. V.A. Nonlinear in  $q$  coupling to a bosonic bath can also play a major role in the NVS dynamics.

The most common way of characterizing the dynamics of NVSs is based on measuring either the spectral density of fluctuations of the displacement,

$$S(\omega) = \int_{-\infty}^{\infty} dt \langle q(t)q(0) \rangle \exp(i\omega t), \quad (3)$$

or the susceptibility  $\chi(\omega)$ , which characterizes the response to an external force at frequency  $\omega$ . It is defined by the relation between the force-induced displacement  $\delta q(t)$  and the force  $F \exp(-i\omega t)$  added to the right-hand side of Eq. (2) as

$$\langle \delta q(t) \rangle = \chi(\omega) F \exp(-i\omega t). \quad (4)$$

The absolute value and the argument of  $\langle \delta q(t) \rangle$  define the amplitude and the phase of the response.

The susceptibility and the spectral density of fluctuations are related by the fluctuation-dissipation theorem (see Sec. IV), with  $\text{Im} \chi(\omega) = (\omega/k_B T) S(\omega)$  in the classical limit. In addition, the real and imaginary parts of the susceptibility  $\text{Re} \chi(\omega)$  and  $\text{Im} \chi(\omega)$  are related by the Kramers-Kronig relation (Landau and Lifshitz, 1980);  $\text{Re} \chi(\omega)$  and  $\text{Im} \chi(\omega)$  determine, respectively, the in-phase and out-of-phase components of the force-induced displacement, whereas  $|\chi(\omega)|$  determines the displacement amplitude.

Of particular interest for NVSs is the situation where the oscillator decay rate  $\Gamma$  is small compared to the eigenfrequency  $\omega_0$ . In this case both  $S(\omega)$  and  $\text{Im} \chi(\omega)$  have sharp resonant peaks at frequency  $\omega_0$ . From Eq. (2) we find that near  $\omega_0$  both functions have a Lorentzian peak,

$$S(\omega) = \frac{k_B T}{M \omega_0^2} \frac{\Gamma}{\Gamma^2 + (\omega - \omega_0)^2},$$

$$\chi(\omega) = \frac{i}{2M\omega_0} [\Gamma - i(\omega - \omega_0)]^{-1}, \quad |\omega - \omega_0| \ll \omega_0. \quad (5)$$

Measuring the position and the half-width of the peak of  $S(\omega)$  and/or  $\text{Im} \chi(\omega)$  is commonly used to determine  $\omega_0$  and  $\Gamma$ . It thus enables finding the quality factor  $Q$ , which characterizes the energy relaxation and is conventionally defined as the ratio of the stored vibrational energy to the energy dissipated per cycle multiplied by  $2\pi$ ,

$$Q = 2\pi \frac{\text{stored energy}}{\text{dissipated energy per cycle}} \rightarrow \frac{\omega_0}{2\Gamma}. \quad (6)$$

Equation (6) is independent of the vibration amplitude for a linear mode.

A central role in the dynamics of NVS modes is played by the fluctuations of the mode eigenfrequencies. Such fluctuations can arise from the fluctuations of the resonator mass due to attachment or detachment of molecules, fluctuations of the spring constant due to charge and voltage fluctuations in the system, or the interplay of the thermal fluctuations of the amplitude and the vibration nonlinearities. These frequency

fluctuations increase the half-width of the spectral peak of  $S(\omega)$  and  $\text{Im} \chi(\omega)$  and, in general, can change the shape of the spectrum. Therefore, it is convenient to introduce an effective quality factor

$$Q_\omega = \omega_0 / 2\Delta\omega. \quad (7)$$

The parameter  $\Delta\omega$  takes into account frequency fluctuations and replaces the decay rate  $\Gamma$  in the standard expression (6). We employ two different symbols  $Q$  and  $Q_\omega$  to emphasize this difference. The factor  $Q_\omega$  does not describe energy relaxation but refers to the results of spectroscopic measurements. To draw a parallel to the description of the spin or qubit relaxation, we note that  $2\Gamma$  corresponds to  $1/T_1$ , whereas  $\Delta\omega$  is an analog of  $1/T_2$  in those systems. The physics behind frequency fluctuations in nanomechanics is fairly different and is discussed at length in the review. However, in this section we do not separate the spectral broadening mechanisms and set  $Q = Q_\omega$ . In Tables I–III we provide the reported values of the quality factor in several types of nanomechanical systems.

## B. Most common types of nanomechanical resonators

The first practical nanomechanical system was based on a silicon nanobeam (Cleland and Roukes, 1996, 1998). Since then a variety of nanomechanical resonators have been explored. Tables I and II summarize the characteristics of resonators based on low-dimensional materials, such as carbon nanotubes, semiconductor nanowires, graphene, semiconductor layered membranes, and levitating particles. Table III summarizes those of resonators nanofabricated from bulk material using the top-down approach. In many of these examples the vibrational modes correspond to bending (flexural) modes of the resonator, a microscopic analog of the vibrations of a string or a membrane. Carbon nanotubes are the narrowest resonators: their diameters typically range from 1 to 3 nm. Graphene and semiconductor monolayers are the thinnest membranes, as they are atomically thin. Other types of vibrational modes have been investigated, such as torsional modes in mechanically based torque resonators (Hauer *et al.*, 2013), the bulk Lamé modes in micromechanical resonators (Chandorkar *et al.*, 2008) and layered nanomaterial resonators (Zalalutdinov *et al.*, 2021), and the localized modes in optomechanical crystals; see Eichenfield *et al.* (2009), MacCabe *et al.* (2020), and references therein.

Advances in fabrication have led to a steady improvement of the quality factor of the NVSs. Optimizing the surface of resonators turned out to be central. The microscopic nature of the dissipation due to surface defects is not clear, but it might be related to additional relaxation channels that open due to the surface contamination and the degradation of crystallinity near the surface. In particular, the quality factor of mechanical resonators based on nanotube and graphene becomes extremely large at cryogenic temperatures (Hüttel *et al.*, 2009), reaching the range of  $10^6 - 10^7$  (Moser *et al.*, 2014; Güttinger *et al.*, 2017; Urgell *et al.*, 2020). The demonstration of such large quality factors came as a surprise. For many years, researchers observed that quality factors would decrease with the volume of the resonator, and for this reason



TABLE I. Figures of merit of mechanical resonators based on nanoscale systems.

$M$ (kg)	$k$ (N/m)	$\omega_0/2\pi$ (Hz)	Carbon nanotube		Reference
			$Q$ or $Q_\omega$	Description	
$3.3 \times 10^{-21}$ $4.8 \times 10^{-22}$ $5.3 \times 10^{-21}$	$4 \times 10^{-4}$ $1 \times 10^{-3}$ $2.7 \times 10^{-2}$	$2.4 \times 10^6$	$1.7 \times 10^2$ at 300 K	Single-clamped multiwall	Poncharal <i>et al.</i> (1999)
		$8.5 \times 10^8$	40 at 4 K	Double-clamped single-wall bundle	Reulet <i>et al.</i> (2000)
		$5.5 \times 10^7$	80 at 300 K	Double-clamped single-wall nanotube	Sazonova <i>et al.</i> (2004)
		$2.3 \times 10^8$	$2 \times 10^2$ at 6 K	Double-clamped single-wall nanotube	Chiu <i>et al.</i> (2008)
		$3.6 \times 10^8$	$1.2 \times 10^5$ at 20 mK	Double-clamped single-wall nanotube	Hüttel <i>et al.</i> (2009)
		$1.1 \times 10^{10}$	$4.2 \times 10^2$ at 4 K	Double-clamped single-wall nanotube	Chaste <i>et al.</i> (2011)
$5 \times 10^{-19}$ $4.4 \times 10^{-21}$ $7.9 \times 10^{-19}$ $2.7 \times 10^{-21}$	$5.1 \times 10^{-6}$ $5.2 \times 10^{-4}$ $4.5 \times 10^{-8}$ $8.9 \times 10^{-4}$	$3.9 \times 10^{10}$	$3.3 \times 10^4$ at 0.1 K	Double-clamped single-wall nanotube, device produced once	Laird <i>et al.</i> (2012)
		$5.1 \times 10^5$	250 at 300 K	Double-clamped single-wall bundle	Stapfner <i>et al.</i> (2013)
		$5.5 \times 10^7$	$4.8 \times 10^6$ at 30 mK	Double-clamped single-wall nanotube	Moser <i>et al.</i> (2014)
		$3.8 \times 10^4$	$2.2 \times 10^3$ at 300 K	Single-clamped single-wall nanotube	Tavernarakis <i>et al.</i> (2018)
		$9.1 \times 10^7$	$6.8 \times 10^6$ at 70 mK	Double-clamped single-wall nanotube	Urgell <i>et al.</i> (2020)
$M$ (kg)	$k$ (N/m)	$\omega_0/2\pi$ (Hz)	Semiconductor nanowire		Reference
			$Q$ or $Q_\omega$	Description	
$2.3 \times 10^{-17}$	6.0	$8.0 \times 10^7$	$1.3 \times 10^4$ at 300 K	Double-clamped Si wire	Feng <i>et al.</i> (2007)
$1.6 \times 10^{-17}$	$4.6 \times 10^{-2}$	$8.5 \times 10^6$	$1.0 \times 10^3$ at 300 K	Single-clamped GaN wire	Henry <i>et al.</i> (2007)
$9.8 \times 10^{-15}$	$7.2 \times 10^{-4}$	$4.3 \times 10^4$	$1.6 \times 10^5$ at 300 K	Single-clamped SiC wire	Perisanu <i>et al.</i> (2007)
$1.6 \times 10^{-17}$	$2.8 \times 10^{-5}$	$2.1 \times 10^5$	$1 \times 10^4$ at 300 K	Single-clamped Si wire	Nichol <i>et al.</i> (2008)
$5.5 \times 10^{-16}$	0.1	$2.2 \times 10^6$	$2 \times 10^3$ at 300 K	Single-clamped Si wire	Gil-Santos <i>et al.</i> (2010)
$1.5 \times 10^{-17}$	1	$4.1 \times 10^7$	$5 \times 10^2$ at 300 K	Double-clamped Si wire	Sansa <i>et al.</i> (2012)
$3.5 \times 10^{-16}$	$1.5 \times 10^{-4}$	$1.1 \times 10^5$	$2.9 \times 10^3$ at 300 K	Single-clamped SiC wire	Gloppe <i>et al.</i> (2014)
$3.5 \times 10^{-15}$	$8.6 \times 10^{-2}$	$7.9 \times 10^5$	$5.8 \times 10^3$ at 4.2 K	Single-clamped GaAs/AlGaAs wire	Montinaro <i>et al.</i> (2014)
$1 \times 10^{-16}$	14	$5.9 \times 10^7$	$2.8 \times 10^3$ at 16 K	Double-clamped InAs wire	Mathew <i>et al.</i> (2015)
$5.9 \times 10^{-17}$	$6.8 \times 10^{-5}$	$1.7 \times 10^5$	$5.9 \times 10^4$ at 4 K	Single-clamped Si wire	Sahafi <i>et al.</i> (2020)

TABLE II. Figures of merit of mechanical resonators based on nanoscale systems.

$M$ (kg)	$k$ (N/m)	$\omega_0/2\pi$ (Hz)	Graphene		Reference
			$Q$ or $Q_\omega$	Description	
$1.4 \times 10^{-18}$	0.3	$7.0 \times 10^7$	78 at 300 K	Double-clamped monolayer	Bunch <i>et al.</i> (2007)
$7.8 \times 10^{-17}$	10	$5.7 \times 10^7$	$3 \times 10^3$ at 300 K	Multilayer graphene oxide drum	Robinson <i>et al.</i> (2008)
$2.2 \times 10^{-18}$	1.4	$1.3 \times 10^8$	$1.4 \times 10^4$ at 5 K	Double-clamped monolayer	Chen <i>et al.</i> (2009)
		$7.5 \times 10^7$	$9 \times 10^3$ at 10 K	Double-clamped monolayer	van der Zande <i>et al.</i> (2010)
$1.9 \times 10^{-17}$	3	$6.4 \times 10^7$	$2.5 \times 10^2$ at 300 K	Double-clamped monolayer	Singh <i>et al.</i> (2010)
$3.9 \times 10^{-19}$	0.35	$1.5 \times 10^8$	$1.0 \times 10^5$ at 90 mK	Double-clamped monolayer	Eichler, Moser <i>et al.</i> (2011)
$2.2 \times 10^{-17}$	2.8	$5.7 \times 10^7$	$1.4 \times 10^3$ at 4.2 K	Double-clamped monolayer	Song <i>et al.</i> (2012)
$2.7 \times 10^{-16}$	14	$3.6 \times 10^7$	$2.2 \times 10^5$ at 14 mK	Multilayer drum	Singh <i>et al.</i> (2014)
$7.9 \times 10^{-16}$	$6.5 \times 10^{-2}$	$1.4 \times 10^6$	$8.2 \times 10^2$ at 300 K	Monolayer drum	Cole <i>et al.</i> (2015)
$9.6 \times 10^{-18}$		$4.6 \times 10^7$	$1.0 \times 10^6$ at 15 mK	Multilayer drum	Güttinger <i>et al.</i> (2017)
$M$ (kg)	$k$ (N/m)	$\omega_0/2\pi$ (Hz)	Semiconductor layer		Reference
			$Q$ or $Q_\omega$	Description	
		$2.6 \times 10^7$	$1.1 \times 10^2$ at 300 K	Monolayer MoS <sub>2</sub> drum	Castellanos-Gomez <i>et al.</i> (2013)
		$2.0 \times 10^7$	$7.1 \times 10^2$ at 300 K	Multilayer MoS <sub>2</sub> drum	Lee, Wang <i>et al.</i> (2013)
		$2.2 \times 10^7$	41 at 300 K	Monolayer MoS <sub>2</sub> drum	van Leeuwen <i>et al.</i> (2014)
		$4.1 \times 10^7$	$6.9 \times 10^2$ at 300 K	Double-clamped MoS <sub>2</sub> bilayer	Samanta, Yasasvi Gangavarapu, and Naik (2015)
$2.3 \times 10^{-17}$	2.9	$5.7 \times 10^7$	$4.7 \times 10^4$ at 3.5 K	Monolayer WSe <sub>2</sub> drum	Morell <i>et al.</i> (2016)

(Table continued)

TABLE II. (*Continued*)

$M$ (kg)	$k$ (N/m)	$\omega_0/2\pi$ (Hz)	$Q$ or $Q_\omega$	Semiconductor layer	Reference
				Description	
$4.3 \times 10^{-17}$	2.2	$1.8 \times 10^7$	48 at 300 K	Multilayer MoS <sub>2</sub> drum	Davidovikj <i>et al.</i> (2017)
		$8.4 \times 10^6$	$2.1 \times 10^2$ at 300 K	Multilayer black phosphorus drum	Islam, van den Akker, and Feng (2018)
		$3.6 \times 10^7$	$3.7 \times 10^4$ at 3 K	Monolayer MoSe <sub>2</sub> drum	Morell <i>et al.</i> (2019)
$M$ (kg)	$k$ (N/m)	$\omega_0/2\pi$ (Hz)	$Q$ or $Q_\omega$	Other layered crystals	Reference
				Description	
$1.8 \times 10^{-15}$	41	$2.4 \times 10^7$	$2.1 \times 10^2$ at 10 K	Double-clamped NbSe <sub>2</sub> multilayer	Sengupta <i>et al.</i> (2010)
$3.7 \times 10^{-17}$	4.0	$5.2 \times 10^7$	$2.4 \times 10^5$ at 15 mK	NbSe <sub>2</sub> -graphene-NbSe <sub>2</sub> drum	Will <i>et al.</i> (2017)
$1.3 \times 10^{-15}$	12	$1.5 \times 10^7$	690 at 300 K	Graphene-MoSe <sub>2</sub> drum	Kim, Yu, and Zande (2018)
		$1.5 \times 10^7$	$9.3 \times 10^4$ at 20 mK	Bi <sub>2</sub> Sr <sub>2</sub> CaCu <sub>2</sub> O <sub>8+<math>\delta</math></sub> drum	Sahu <i>et al.</i> (2022)
$M$ (kg)	$k$ (N/m)	$\omega_0/2\pi$ (Hz)	$Q$ or $Q_\omega$	Levitating particles	Reference
				Description	
$3.1 \times 10^{-14}$	$1.1 \times 10^{-4}$	$9.7 \times 10^3$	$2.1 \times 10^4$ at 300 K	SiO <sub>2</sub> particle in optical trap	Li, Kheifets, and Raizen (2011)
$3.1 \times 10^{-18}$	$1.7 \times 10^{-7}$	$3.7 \times 10^4$	$1 \times 10^7$ at 300 K	SiO <sub>2</sub> particle in optical trap	Gieseler <i>et al.</i> (2012)
$8.3 \times 10^{-17}$	$1.1 \times 10^{-6}$	$1.8 \times 10^4$	$1.8 \times 10^4$ at 300 K	SiO <sub>2</sub> particle in optical trap	Millen <i>et al.</i> (2015)
$\sim 1 \times 10^{-18}$	$\sim 2 \times 10^{-10}$	$2.1 \times 10^3$	$1.1 \times 10^3$ at 300 K	Charged particle in Paul trap	Conangla <i>et al.</i> (2018)
$\sim 1 \times 10^{-13}$	$\sim 7 \times 10^{-7}$	$4.1 \times 10^2$	$9.2 \times 10^1$ at 542 K	Diamagnetic particle in magnetic trap	O'Brien <i>et al.</i> (2019)
$\sim 6 \times 10^{-10}$	$\sim 7 \times 10^{-5}$	$5.6 \times 10^1$	$2.1 \times 10^6$ at 4.2 K	Ferromagnetic particle in Meissner trap	Vinante <i>et al.</i> (2020)

it was unthinkable that nanotubes and graphene resonators could exhibit such large quality factors. The large  $Q$  factors reflect the high crystallinity of these nanoscale systems and show that surface contamination is reduced to a minimal amount.

Levitating particles feature large quality factors of up to  $10^8$  even at room temperature (Ricci *et al.*, 2017). In many

experiments, the particles are trapped by a laser beam; the resonant frequency is given by the optical gradient force. Damping, which arises from collisions with the gas molecules in the sample chamber, becomes low at high vacuum. Recently particles have been levitated using new schemes, including ferromagnetic particles in Meissner traps made from superconducting materials (Gieseler *et al.*, 2020;

TABLE III. Figures of merit of mechanical resonators fabricated from bulk material with the top-down approach.

$M$ (kg)	$k$ (N/m)	$\omega_0/2\pi$ (Hz)	$Q$ or $Q_\omega$	Top-down nanofabricated resonators	Reference
				Description	
$5.6 \times 10^{-14}$	$6.5 \times 10^{-6}$	$1.7 \times 10^3$	$6.7 \times 10^3$ at 4.8 K	Single-clamped Si beam	Stowe <i>et al.</i> (1997)
$3.4 \times 10^{-17}$	$1.3 \times 10^3$	$1.0 \times 10^9$	$5 \times 10^2$ at 4.2 K	Double-clamped SiC beam	Huang <i>et al.</i> (2003)
$1.9 \times 10^{-15}$	1.5	$4.5 \times 10^6$	$2.1 \times 10^5$ at 300 K	Double-clamped Si <sub>3</sub> N <sub>4</sub> beam	Verbridge <i>et al.</i> (2006)
$1.4 \times 10^{-10}$	$1 \times 10^2$	$1.4 \times 10^5$	$1.1 \times 10^5$ at 2.5 K	Double-clamped GaAs/AlGaAs resonator	Mahboob and Yamaguchi (2008b)
$3.3 \times 10^{-16}$	$6.3 \times 10^4$	$2.2 \times 10^9$	$2.7 \times 10^3$ at 300 K	Optomechanical Si crystal	Eichenfield <i>et al.</i> (2009)
$7.7 \times 10^{-15}$	$1.2 \times 10^8$	$2 \times 10^{10}$	$\sim 1 \times 10^3$ at 300 K	GaAs/AlAs microcavity	Fainstein <i>et al.</i> (2013)
$1.6 \times 10^{-12}$	$6.7 \times 10^{-2}$	$3.2 \times 10^4$	$1.5 \times 10^6$ at 3 K	Single-clamped diamond beam	Tao <i>et al.</i> (2014)
$4 \times 10^{-12}$	$3 \times 10^{-1}$	$4.1 \times 10^4$	$4.5 \times 10^7$ at 300 K	Si <sub>3</sub> N <sub>4</sub> trampoline	Reinhardt <i>et al.</i> (2016)
		$1.4 \times 10^5$	$1 \times 10^8$ at 300 K	Si <sub>3</sub> N <sub>4</sub> tethered membrane	Norte, Moura, and Gröblacher (2016)
		$1.4 \times 10^7$	$4.3 \times 10^4$ at 25 mK	Torque Si resonator	Kim <i>et al.</i> (2016)
$1.6 \times 10^{-11}$	$3.7 \times 10^2$	$7.7 \times 10^5$	$2.1 \times 10^8$ at 300 K	Si <sub>3</sub> N <sub>4</sub> membrane with engineered mode	Tsaturyan <i>et al.</i> (2017)
$4.1 \times 10^{-15}$	$1.1 \times 10^{-4}$	$2.5 \times 10^4$	$1.6 \times 10^5$ at 0.14 K	Single-clamped diamond ladder	Heritier <i>et al.</i> (2018)
$\sim 5 \times 10^{-15}$	$\sim 1$	$\sim 2.5 \times 10^6$	$\sim 1 \times 10^8$ at 300 K	Si <sub>3</sub> N <sub>4</sub> nanobeam with engineered mode	Ghadimi <i>et al.</i> (2018)
		$1.0 \times 10^7$	$2.6 \times 10^6$ at 300 K	Lamé-mode Si resonator	Rodriguez <i>et al.</i> (2019)
$1.3 \times 10^{-16}$	$1.5 \times 10^5$	$5.3 \times 10^9$	$4.9 \times 10^{10}$ at 7 mK	Optomechanical Si crystal	MacCabe <i>et al.</i> (2020)
$\sim 1 \times 10^{-20}$	$\sim 3$	$3 \times 10^9$	$1.2 \times 10^3$ at 20 mK	Double-clamped Si beam	Zhang, Hu <i>et al.</i> (2020)

Vinante *et al.*, 2020), diamagnetic particles in magnetic traps (Hsu *et al.*, 2016; O'Brien *et al.*, 2019), and charged particles in Paul traps (Alda *et al.*, 2016; Delord *et al.*, 2020).

High-stress silicon nitride is the material used by many groups to produce top-down resonators endowed with high quality factors (Kozinsky *et al.*, 2006; Verbridge *et al.*, 2006; Unterreithmeier, Weig, and Kotthaus, 2009; Unterreithmeier, Faust, and Kotthaus, 2010; Wilson-Rae *et al.*, 2011; Maillet *et al.*, 2017; Zhou *et al.*, 2019; Bothner *et al.*, 2020). Dissipation in the bulk of this high-stress material is notably low. The quality factor can be further enhanced by structuring high-stress silicon nitride films into trampoline geometries (Norte, Moura, and Gröblacher, 2016; Reinhardt *et al.*, 2016) and nonuniform phononic crystal patterns (Tsaturyan *et al.*, 2017; Ghadimi *et al.*, 2018). Engineering the shape of mechanical eigenmodes enables a reduction of losses near their supports. Quality factors as high as  $8 \times 10^8$  can be achieved at room temperature (Ghadimi *et al.*, 2018) and  $1.5 \times 10^9$  at 30 mK (Seis *et al.*, 2022).

An important role in studying nonlinear phenomena and the effects of mode coupling has been played by single and coupled nanoresonators based on narrow nanowires grown by electrodeposition (Kozinsky *et al.*, 2007), thin nanofabricated structures (Defoort *et al.*, 2015), and suspended GaAs and AlN heterostructures that exploit the piezoelectric effect to actuate and control the vibrations (Masmanidis *et al.*, 2007; Mahboob and Yamaguchi, 2008b; Karabalin, Cross, and Roukes, 2009; Karabalin *et al.*, 2009, 2011; Yamaguchi, 2017).

### C. Driving resonators

The most straightforward way to excite nanomechanical resonators is by driving them with a directly applied force at an angular frequency  $\omega_F$  close to the eigenfrequency  $\omega_0$ . Owing to the nonlinearity of the system, such a direct drive can also efficiently excite vibrations when  $\omega_F \simeq \omega_0 N$  or  $\omega_F \simeq \omega_0/N$  with an integer  $N > 1$ , but their amplitude is usually smaller for the same drive amplitude (Nayfeh and Mook, 2004). Another method that is often employed consists in modulating the spring constant (Rugar and Grütter, 1991; Turner *et al.*, 1998). Such parametric driving is equivalent to the modulation of the resonant frequency. It is most efficient when the drive frequency is close to  $2\omega_0$ . The vibration amplitude is nonlinear in the amplitude of the parametric drive. The amplitude remains small until the driving amplitude reaches a threshold value, after which the resonator vibrates at half the drive frequency. Still, even before the threshold is reached, a resonator can amplify a probe drive at a frequency close to half the drive frequency, and also at exactly half the drive frequency (Rugar and Grütter, 1991; Eichler, Chaste *et al.*, 2011). A resonant probe field can be amplified by a nanoresonator also if the drive frequency is  $\omega_F \approx \omega_0$  (Dykman and Krivoglaz, 1979; Ochs *et al.*, 2021b).

The actuation of a nanoscale resonator was achieved for the first time with the magnetomotive drive [Fig. 2(a)] (Cleland and Roukes, 1996, 1998). In this method, flexural vibrations of a conducting nanobeam are excited by the Lorentz force, which emerges when an alternating current is applied through the nanowire placed in a perpendicular magnetic field. The

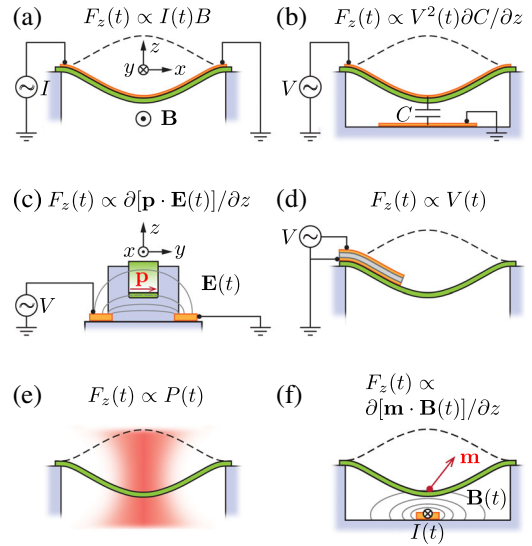


FIG. 2. Excitation of flexural vibrations. (a) Magnetomotive force, which is generated by a static magnetic field and an alternating current along the mechanical beam (shown in green). (b) Capacitive force, which is created by applying an oscillating voltage between the bottom gate electrode and the mechanical beam (green) that is conducting. (c) Dielectric force, which is acting on a mechanical beam (green) made from a dielectric material using a time-modulated electric field gradient. Depicted is a cross section of the device (see the coordinate frame). (d) Piezoelectric force, where the mechanical beam (green) is actuated with a piezoelectric film (gray) sandwiched between two metal electrodes. (e) Optical force, which is obtained by modulating the intensity of the laser beam (red) focused on the mechanical beam (green). (f) Magnetic force, where either the magnetic moment of the mechanical beam (green) or the magnetic field gradient is modulated (or both).

vibrations are detected by measuring the electromotive force generated along the length of the nanobeam using a network analyzer.

A widely used drive is the capacitive force; see Fig. 2(b) (Rugar and Grütter, 1991). It is implemented by applying a static voltage  $V_g^{\text{dc}}$  and an oscillating voltage with a comparatively low amplitude  $\delta V_g^{\text{ac}}$  between the resonator and a nearby gate electrode. The force is

$$F^{\text{ac}} = C'_g V_g^{\text{dc}} \delta V_g^{\text{ac}}, \quad (8)$$

where  $C'_g \equiv \partial C_g / \partial q$  is the derivative of the gate-resonator capacitance with respect to the mode displacement  $q$ . As a rough estimate,  $C'_g$  is given by the ratio of the capacitance to the characteristic distance between the resonator and the gate. For simplicity, we omit the work function difference between the resonator and the gate electrode in Eq. (8), which leads to an offset in  $V_g^{\text{dc}}$ . This driving force is effective when the resonator is an electrical conductor or is covered with a metal plate. A resonator made of a dielectric material can be driven by applying an electric field gradient between two electrodes structured near the resonator [Fig. 2(c)] (Unterreithmeier,

Weig, and Kotthaus, 2009). A dielectric material in vacuum moves toward the region with the highest electric field. This dielectric force has the same origin as the capacitive force since they are both related to the displacement-induced electrostatic energy gain of a capacitor. When the resonator is made of a piezoelectric material, a piezoelectric force is created by applying an electric field between two electrodes that are usually patterned on the resonator itself [Fig. 2(d)] (Masmanidis *et al.*, 2007; Mahboob and Yamaguchi, 2008b).

Optical drive is also frequently used [Fig. 2(e)]. Photothermal forces are straightforward to apply to nanoscale resonators. One simply needs to modulate the intensity of the laser focused on the resonator. Absorption-induced heating displaces the resonator through thermal expansion (Bunch *et al.*, 2007). Care has to be taken if one wants to keep the resonator temperature low. This requires weak absorption. When the absorption is sufficiently suppressed, the force from the heating is overcome by the force traditionally associated with radiation pressure that comes from the reflection of photons by the resonator. This force is often small, but it has the advantage of not causing heating. It is used in quantum optomechanics experiments where losses are detrimental to the manipulation of quantum states (Aspelmeyer, Kippenberg, and Marquardt, 2014b). Various available optical excitation protocols now enable the driving of different types of NVS vibrations, including the vibrations localized at defects in phononic optomechanical crystals; see MacCabe *et al.* (2020) and references therein.

Magnetic forces are usually used in magnetic resonance force microscopy experiments to detect electron and nuclear spins (Poggio and Degen, 2010). In some of these experiments, the spins located on the mechanical resonators are periodically flipped using magnetic resonance techniques. The associated time-modulated magnetic moment together with the magnetic field gradient of a nearby magnet results in an oscillating force [Fig. 2(f)]. Alternatively, the magnet is placed on the mechanical resonator and the spins on the surface of a chip.

#### D. Frequency control

The eigenfrequency  $\omega_0$  of a flexural mode of a NVS can be tuned by direct forces in two different ways. The frequency depends on the static gradient of the force. In the case of the capacitive force, the shift of the spring constant is given by

$$\Delta k = -\frac{\partial F}{\partial q} = -\frac{1}{2} C_g'' (V_g^{\text{dc}})^2. \quad (9)$$

Usually  $C_g'' \equiv \partial^2 C_g / \partial q^2 > 0$  and a dc gate voltage directly leads to an electrostatic softening of a resonator (Kozinsky *et al.*, 2006; Solanki *et al.*, 2010; Eichler, Moser *et al.*, 2011; Wu and Zhong, 2011; Stiller *et al.*, 2013).

In addition, the eigenfrequency can be tuned by the dc force via the change of the equilibrium position and the associated elongation of the resonator. Through nonlinear elasticity, such a change modifies the mechanical tension in the resonator. This effect leads to an increase in the frequency. The mechanism is broadly used with the capacitive force for frequency control in soft resonators such as carbon nanotubes

(Purcell *et al.*, 2002; Sazonova *et al.*, 2004; Rehnitz *et al.*, 2021). Overall, the effect of the gate voltage on the mode eigenfrequency depends on the geometry and the mode polarization (Kozinsky *et al.*, 2006). Piezoelectric actuators can also be used to tune  $\omega_0$  by enhancing the separation between the supports of a doubly clamped resonator. Using this technique, the eigenfrequency of a carbon nanotube could be increased by more than 20 times (Ning *et al.*, 2014).

Time-dependent frequency control is important in various applications, such as parametric drive. In the case of frequency control with the capacitive force, the eigenfrequency can be modulated in time using a combination of dc and ac gate voltages (Rugar and Grütter, 1991). An alternative and highly efficient approach is based on time-dependent piezoelectric actuation (Yamaguchi, 2017).

#### E. Detection of displacement

The detection of motion becomes increasingly difficult when resonators get smaller. A variety of methods have been developed to address the problem. The most broadly used methods are based on magnetomotive, capacitive, and optical or microwave measurements. Other methods include piezoelectric (Masmanidis *et al.*, 2007; Mahboob and Yamaguchi, 2008b), piezoresistive (He *et al.*, 2008; Lee, Truax *et al.*, 2013), scanning probe microscopy (Garcia-Sanchez *et al.*, 2007), scanning and transmission electron microscopy (Buks and Roukes, 2001; Niguès, Siria, and Verlot, 2015; Tsioutsios *et al.*, 2017), and field-emission (Purcell *et al.*, 2002) measurements.

The capacitive method relies on the motion-induced modulation of the capacitance  $\delta C_g$  between a conducting resonator and a nearby gate. Modulation of the capacitance in the presence of a gate voltage  $V_g^{\text{dc}}$  leads to the charge modulation  $\delta Q = \delta C_g V_g^{\text{dc}}$ . Where the vibrating resonator acts as a field-effect transistor, its conductance oscillates as  $\delta G = (\partial G / \partial Q) \delta Q$ . This causes a change of the current through the resonator  $\delta I = \delta G \delta V_{\text{sd}}$  in response to a voltage  $\delta V_{\text{sd}}$  applied across it. When  $\delta V_{\text{sd}}$  is oscillating at frequency  $\omega_{\text{sd}}$  close to  $\omega_0$ , the current can be conveniently measured at a low frequency  $\approx |\omega_{\text{sd}} - \omega_0|$ . This method was first applied to a GaAs resonator supporting a single-electron transistor made of aluminum (Knobel and Cleland, 2003) and to nanotube resonators (Sazonova *et al.*, 2004; Gouttenoire *et al.*, 2010). Yet another way to measure the oscillating capacitance is based on embedding a conducting nano-resonator in a superconducting cavity and measuring its radio-frequency reflection and transmission (Teufel *et al.*, 2008; Rocheleau *et al.*, 2010; Singh *et al.*, 2014; Song *et al.*, 2014; Weber *et al.*, 2014; Blien *et al.*, 2020; Zhou *et al.*, 2021). A similar method can be used with a dielectric resonator by integrating it with a nearby electric cavity (Faust, Krenn *et al.*, 2012).

In the optical frequency range, high-precision vibration detection is often based on interferometry. Vibrations of a nanoresonator embedded in an optical cavity can be detected from the modulation of the resonant frequency of the cavity measured by its transmission or reflection (Aspelmeyer, Kippenberg, and Marquardt, 2014b). Another method is based



on focusing a laser beam on the resonator and detecting the modulation of the reflected or scattered light (Carr and Craighead, 1997; Gloppe *et al.*, 2014; Yeo *et al.*, 2014). Here we describe optical detection of the vibrations of graphene-based resonators, a method used by many groups to detect vibrations of monolayer and few-layer systems (Barton *et al.*, 2012; Reserbat-Plantey *et al.*, 2012; Castellanos-Gomez *et al.*, 2013; Lee, Wang *et al.*, 2013). The laser beam illuminates a graphene membrane suspended over a metal gate. When the graphene monolayer is covered by an adsorbed contamination layer, an optical cavity is created between the monolayer and the gate, and the vibrations modulate this cavity. In contrast, in the case of a clean monolayer, a standing wave is formed by the interfering incident and reflected laser beams with the reflection from the metal gate. A clean graphene monolayer does not affect the standing wave much, since its reflection coefficient is small. In contrast, the absorption coefficient of graphene is about 0.02 for visible light, which is a notably large value considering that the material is only one atom thick. The displacement of the graphene layer changes the absorbed intensity. Therefore, the motion of the graphene resonator can be measured by recording the reflected light intensity.

Optical detection of micromechanical systems has attracted significant interest in the context of improving the sensitivity of LIGO detectors of gravitational waves, as these detectors are also based on vibrational systems. One of the important challenges is reducing the photon counting noise and the photon radiation pressure noise. It can be addressed using squeezed states of light, and the experimental results on measuring a micromechanical membrane with squeezed light were recently reported (Kleybolte *et al.*, 2020).

### 1. Quantum regime

Significant progress has been made in detecting small displacements that occur where a nanoscale or microscale vibrational system is in the quantum regime, in which case the vibration amplitude is  $\propto \hbar^{1/2}$ . Detecting vibrations and characterizing their energy distribution in this regime is one of the central problems of quantum optomechanics. An important approach is based on illuminating an optical or microwave cavity that contains a nanoresonator and measuring the spectrum of the emitted radiation. This spectrum contains lines shifted from the incident light frequency by the frequency of the vibrational mode. The ratio of the intensities of the lower- and higher-frequency lines, i.e., of the Stokes and anti-Stokes components, is determined by the effective temperature of the mode (Kippenberg and Vahala, 2008; Aspelmeyer, Kippenberg, and Marquardt, 2014b; Pfeifer *et al.*, 2016; Riedinger *et al.*, 2016; Clark *et al.*, 2017; Reed *et al.*, 2017; Delić *et al.*, 2020; Tebbenjohanns *et al.*, 2020). Detailed information about the vibrational quantum state of mechanical modes can be obtained by connecting these modes to a qubit (O’Connell *et al.*, 2010; Chu *et al.*, 2018; Satzinger *et al.*, 2018; Arrangoiz-Arriola *et al.*, 2019).

Mechanical resonators in the quantum regime open new directions of research, including quantum squeezing of the

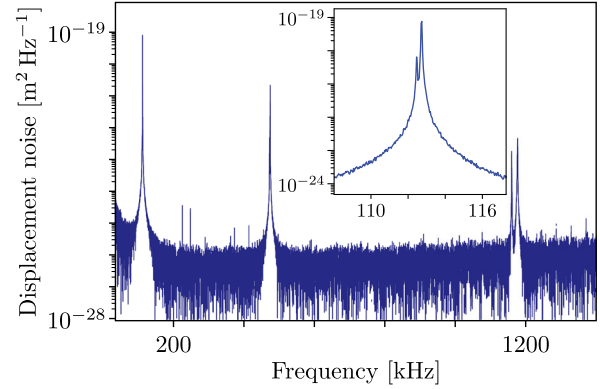


FIG. 3. Power spectrum  $S(\omega)$  of a single-clamped resonator based on a SiC nanowire measured optically at 300 K. The spectrum formed by the three lowest-frequency eigenmode “families” are shown. Each mode family is composed of two peaks (see inset), which correspond to the two eigenmodes that vibrate in perpendicular directions. The peaks allow one to determine the mode eigenfrequencies and the  $Q_\omega$  factors. The noise floor of the spectrum quantifies the displacement sensitivity of the detection. Adapted from Gloppe *et al.*, 2014.

mechanical motion (Lecocq *et al.*, 2015; Pirkkalainen, Damskägg *et al.*, 2015; Wollman *et al.*, 2015), measurement-based quantum control of mechanical motion (Wilson *et al.*, 2015; Rossi *et al.*, 2018), quantum backaction evading measurements (Suh *et al.*, 2014; Ockeloen-Korppi *et al.*, 2016; Möller *et al.*, 2017), entanglement between mechanical resonators (Ockeloen-Korppi *et al.*, 2018; Riedinger *et al.*, 2018; de Lépinay *et al.*, 2021; Kotler *et al.*, 2021; Wollack *et al.*, 2022), and fundamental measurements with levitating particles cooled to the ground state (Delić *et al.*, 2020; Magrini *et al.*, 2021; Tebbenjohanns *et al.*, 2021).

### F. Measurement of the spectral response

Measurement of the spectral response is the most common method for studying mechanical resonators. This response provides the important characteristics of a resonator. They include the resonant frequencies of the eigenmodes, their spectral bandwidth  $\Delta\omega$ , and the quality factor  $Q_\omega$  introduced in Eq. (7). There are two major approaches to measuring the spectral response. One of them is based on applying an oscillating force to the resonator, sweeping the frequency of the force, and measuring the displacement of the resonator with a lock-in amplifier. This gives the mechanical susceptibility  $\chi(\omega)$ , as discussed in Sec. II.A.

The other approach is to measure the power spectrum  $S(\omega)$ , i.e., to measure the spectrum of the displacement that results from thermal and quantum fluctuations with no regular external force applied. The power spectrum is measured by simply feeding the output signal of the resonator detector into a spectrum analyzer. In practice, the power spectrum is often more difficult to measure than the spectrum of response to a periodic drive, especially when no care is taken to reduce the noise in the measurement circuit. Figure 3 shows the measured power spectrum of a cantilever based on a SiC nanowire featuring different eigenmodes.

### III. SENSING AND CLOCKS

Nanomechanical resonators have attracted considerable interest due to their remarkable sensing capabilities. Because of their small mass, such resonators are exquisite sensors of external forces and mass deposition. We describe here the basics of sensing. Nanomechanical resonators are also used as clocks in commercial products.

#### A. Force sensing

Force sensing consists in converting a weak force into a displacement that is then measured by electrical or optical means. The linear response of the displacement  $q(t)$  to an external force  $F \cos \omega t$  is given by the mechanical susceptibility  $\chi(\omega)$ . If the noise is disregarded, the force-induced displacement increment is  $\delta q(t) = \text{Re}[\chi(\omega) F \exp(-i\omega t)]$ . The detection of an oscillating force is optimized by matching its frequency to the mechanical eigenfrequency, where  $|\chi(\omega)|$  is maximal.

The measured displacement is a superposition of the displacement induced by the force and thermal vibrations, i.e., a superposition of the signal and noise, respectively [Fig. 4(a)]. The fundamental limit of force sensing is set by the condition that the signal exceeds the thermal noise. Quantitatively, this limit can be characterized by noting that,

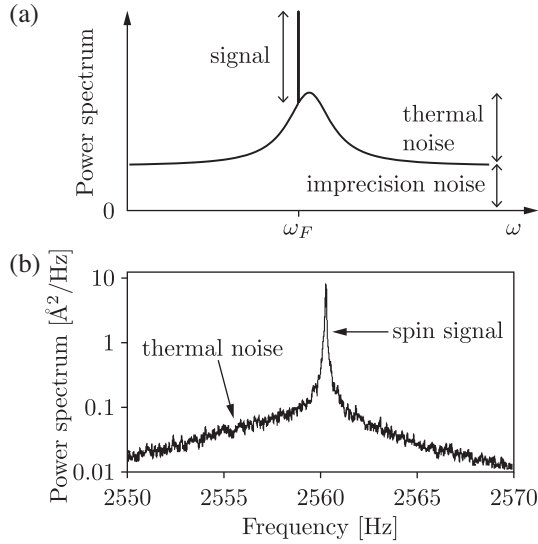


FIG. 4. (a) Sensing of a coherent external force using spectral measurements. The power spectrum has contributions from driving-induced displacement, thermal vibrations, and the imprecision in the vibration detection. The signal to be detected is the narrow peak at the frequency of the external force. The integration time  $\tau$  required to resolve this peak can be obtained by setting the resolution bandwidth  $\Delta f_{\text{RBW}}$  of the spectrum analyzer such that the signal-to-noise ratio is 1 ( $\tau = 1/\Delta f_{\text{RBW}}$ ). The peak height of the coherent external force in the spectrum gets larger as  $\Delta f_{\text{RBW}}$  is reduced. The effect of frequency noise is disregarded. (b) Power spectrum of the vibrations of a microcantilever in the force sensing of nuclear spin experiments. The signal induced by the periodically driven spins is the narrow peak. The imprecision in the vibration detection is negligible in this experiment. Adapted from Poggio *et al.*, 2007.

by its meaning, the power spectrum of the mode  $S(\omega)$  is the mean-square thermal displacement at frequency  $\omega$  per unit frequency. At the same time, it follows from the definition of the susceptibility  $\chi(\omega)$  [Eq. (4)] that the squared displacement induced by a regular force  $F \cos \omega t$  and averaged over the force period is  $\overline{(\delta q)^2} = |\chi(\omega)|^2 F^2 / 2$ . The ratio of these displacements, which is determined by the function  $S_F(\omega) = 2S(\omega)/|\chi(\omega)|^2$ , shows how strong the force should be for it to be detected with a signal-to-noise ratio equal to 1.

The ratio  $S_F(\omega)$  takes a particularly simple form in the important case where the power spectrum of the vibrations has a Lorentzian peak at the vibration eigenfrequency  $\omega_0$  with half-width  $\Delta\omega \ll \omega_0$ ; see Sec. IX.B. For such a spectrum, to the leading order in  $\Delta\omega/\omega_0$  the resonant susceptibility is [cf. Eq. (5)]

$$\chi(\omega) = \frac{i}{2M\omega_0} [\Delta\omega - i(\omega - \omega_0)]^{-1}, \quad \Delta\omega, |\omega - \omega_0| \ll \omega_0. \quad (10)$$

In the same range  $|\omega - \omega_0| \ll \omega_0$ ,

$$S_F(\omega) \approx 8k_B T M \Delta\omega \equiv \frac{4k_B T M \omega_0}{Q_\omega}. \quad (11)$$

The function  $S_F(\omega)$  is independent of frequency over the entire range of the peak in the spectrum of the resonator, that is, beyond the region  $|\omega - \omega_0| \lesssim \Delta\omega$ . Such broadband force sensing is somewhat nonintuitive given that the force response of the displacement is strongly frequency dependent. We emphasize that force sensing can be comparatively broadband even for high- $Q$  resonators. Forces with frequencies far from other resonances can be detected provided that thermal noise and imprecision noise in the displacement detection are low enough.

Equation (11) suggests a strategy for detecting small forces. The best force sensitivity has been achieved with carbon nanotubes, which are the operating resonators with the smallest mass [ $\sqrt{S_F} = (4.3 \pm 2.9) \times 10^{-21} \text{ N}/\sqrt{\text{Hz}}$ ] (de Bonis *et al.*, 2018). Resonators based on silicon carbide nanowires can reach  $\sqrt{S_F} = 4.0 \times 10^{-20} \text{ N}/\sqrt{\text{Hz}}$  (Fogliano *et al.*, 2021). Resonators microfabricated from bulk material are often better to use as sensors; their sensitivity has reached  $\sqrt{S_F} = (1.9 \pm 0.6) \times 10^{-19} \text{ N}/\sqrt{\text{Hz}}$  (Heritier *et al.*, 2018). Fluctuations of the nanoresonator frequency worsen the force sensitivity in Eq. (11), as they widen the mechanical linewidth and decrease the associated quality factor  $Q_\omega$  (Moser *et al.*, 2013).

The transduction of the mechanical vibrations into a measurable electrical or optical output signal is challenging with small resonators. The transduction can deteriorate the force sensitivity by adding noise. This so-called imprecision noise is quantified by the noise floor in the spectral measurement of a resonator [Fig. 4(a)].

Figure 4(b) shows a force sensing experiment of nuclear spins (Poggio *et al.*, 2007). The nuclear spins of  $^{19}\text{F}$  atoms in a  $\text{CaF}_2$  crystal are detected by attaching the crystal to a microcantilever. The nuclear spins are flipped back and forth at the mechanical resonant frequency. The associated time-modulated magnetic moment together with an applied

magnetic field gradient creates a force that drives the microcantilever. The measured power spectrum of the vibrations in Fig. 4(b) shows a narrow peak associated with the spins on top of the broad resonance of the thermal vibrations of the microcantilever. The goal of such experiments is to achieve magnetic resonance imaging with atomic resolution (Degen *et al.*, 2009; Nichol *et al.*, 2013).

Force sensing has been used with great success in recent advances in various fields. These include the Casimir force (Chan *et al.*, 2001, 2008; Klimchitskaya, Mohideen, and Mostepanenko, 2009; Gong *et al.*, 2021; Liu *et al.*, 2021), nanomagnetism (Forstner *et al.*, 2012; Losby *et al.*, 2015; Rossi *et al.*, 2019), scanning probe microscopy imaging of vectorial forces (Li, Tang, and Roukes, 2007; de Lépinay *et al.*, 2017; Rossi *et al.*, 2017), light-matter interaction (Gloppe *et al.*, 2014), persistent currents in normal metal rings (Bleszynski-Jayich *et al.*, 2009), and detection of a phonon flux in superfluid  $^4\text{He}$  (Guénault *et al.*, 2020).

## B. Mass sensing

Mass sensing relies on monitoring how the eigenfrequency of a nanomechanical resonator changes when an additional mass is adsorbed onto its surface. Most experiments are done with flexural modes (Ekinici, Yang, and Roukes, 2004; Yang, Lian *et al.*, 2006). If one assumes that this mass  $m_{\text{add}}$  is uniformly distributed over the resonator, that the resonator itself is uniform, and that  $m_{\text{add}}$  is small compared to the resonator mass  $M_{\text{NVS}}$ , then the relative change of the resonator eigenfrequency is

$$\delta\omega_0/\omega_0 = -m_{\text{add}}/2M_{\text{NVS}}. \quad (12)$$

As an example, Fig. 5(a) shows a series of downward shifts in  $\omega_0$  consistent with single adsorption events of naphthalene molecules onto a nanotube resonator.

There are different methods of monitoring the eigenfrequency. The simplest one relies on driving the resonator slightly off resonance while recording the vibration amplitude with a lock-in amplifier. A change in the eigenfrequency results in a change in the displacement amplitude  $A$  [Fig. 5(b)]. The resonator settles to a new amplitude and phase over the decay time. The frequency shift can be quantified from the measured change of  $A$  using the slope of the mechanical susceptibility at the drive frequency. Implied in the analysis is that the adsorbed mass does not change over the duration of the measurement, which itself exceeds the decay time; however, the analysis can also be extended to the case where adsorbates attach and detach with a rate comparable to the relaxation rate (Dykman *et al.*, 2010).

Phase-locked loop measurements are also often used to track the resonant frequency in mass sensing experiments. The method was first developed for high- $Q$  cantilevers in atomic force microscopy (Albrecht *et al.*, 1991). It was used for faster detection of the frequency shift than in the just-discussed method. However, a phase-locked loop is efficient when the imprecision noise in the detection of the displacement is small compared to the driven vibration amplitude. This is often hard to achieve for small resonators, such as nanotube resonators measured capacitively.

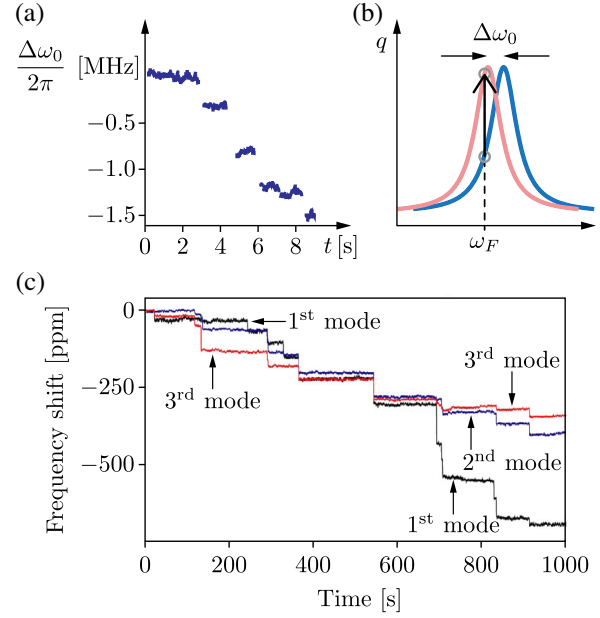


FIG. 5. (a) Sensing of the adsorption of naphthalene molecules onto a nanotube resonator by monitoring the resonant frequency as a function of time at 4.3 K. Each shift in the resonant frequency is associated with adsorption of one molecule. The suspended nanotube is  $\sim 150$  nm long, and its fundamental mode vibrates at 1.8 GHz. Adapted from Chaste *et al.*, 2012. (b) Mass sensing associated with one adsorption event. The resonator is driven at the frequency  $\omega_F$ . The change in the resonant frequency due to the adsorption event results in the increase of the driven vibration amplitude. (c) Real-time record of the eigenfrequencies of the first three flexural modes of the microcantilever exposed to a flux of gold nanoparticles. Similar measurements were carried out with protein macromolecules (Hanay *et al.*, 2012) and *E. coli* bacteria (Malvar *et al.*, 2016). Adapted from Malvar *et al.*, 2016.

Mass spectrometry of molecules and nanoparticles requires one to overcome the assumption of the uniform distribution of the adsorbed mass over the resonator. This can be achieved by tracking the resonant frequency of several flexural eigenmodes (Hanay *et al.*, 2012, 2015). The method utilizes the fact that the resonant frequency shift induced by an adsorbed molecule depends on both its mass and its position on the resonator. The frequency shift of an  $n$ th eigenmode due to a particle attached to a point  $\mathbf{R}$  on the surface of a nanoresonator is

$$\delta\omega_n(\mathbf{R})/\omega_n = -m_{\text{add}}\varphi_n^2(\mathbf{R})/2M_{\text{NVS}}. \quad (13)$$

Here  $\varphi_n(\mathbf{R})$  is the dimensionless displacement of the resonator at the point  $\mathbf{R}$  due to the  $n$ th eigenmode; see Eq. (1).

The frequency shift is largest when the molecule is located at the antinode of the eigenmode, where its vibration amplitude is maximal, while it is equal to zero when the molecule sits at a node. The more modes can be measured, the better the resolution of the mass of the absorbed molecule and of its location.

Figure 5(c) shows how the measured eigenfrequencies of a microcantilever get reduced due to adsorption of 100 nm



diameter gold nanoparticles (Malvar *et al.*, 2016). Quasi-instantaneous jumps are simultaneously observed in the frequencies of the first three flexural modes when a single nanoparticle is adsorbed. The frequency shift is different for the three modes since it depends on the nanoparticle location. The data analysis gives an average nanoparticle mass of  $11.6 \pm 3.8$  fg.

The notable sensing capabilities of mechanical resonators have enabled advances in many areas. These include characterizations of analytes using mass spectrometry (Hanay *et al.*, 2015; Malvar *et al.*, 2016; Sage *et al.*, 2018), the detection of large-mass biological particles that cannot be probed with commercial mass spectrometers based on mass-to-charge-ratio measurements (Dominguez-Medina *et al.*, 2018), weighing of biomolecules and single cells in fluid using microchannels integrated in resonators (Burg *et al.*, 2007), gas chromatography (Li *et al.*, 2010; Venkatasubramanian *et al.*, 2016), probing the density and viscosity of liquids (Gil-Santos *et al.*, 2015), the diffusion of adsorbed atoms on the surface of a resonator (Yang *et al.*, 2011), the formation and transitions between solid- and liquid-phase monolayers of adsorbed atoms (Wang *et al.*, 2010; Tavernarakis *et al.*, 2014), properties of helium superfluid thin films (Guénault *et al.*, 2019; Noury *et al.*, 2019; Sachkou *et al.*, 2019), and *in situ* nanofabrication (Gruber *et al.*, 2019).

The mass resolution of a resonator is limited by frequency fluctuations. As we see in Sec. IX, there is a fundamental limit on how small frequency fluctuations and the mass resolution can be. This fundamental limit in the linear regime is related to the thermal displacement noise. It was found that, for some resonators, to improve mass sensing in a linear regime one may want to decrease the  $Q$  factor (Roy *et al.*, 2018). It was proposed to further increase mass sensitivity by driving a nanoresonator into a nonlinear regime and using the squeezing of thermomechanical fluctuations (Buks and Yurke, 2006). Mass sensing measurements in the nonlinear regime were recently performed by Yuksel *et al.* (2019).

On the practical side, of particular importance are comparatively slow frequency fluctuations, with the correlation time comparable to or exceeding the decay time. Identifying the origin of such fluctuations is usually difficult. For instance, they can arise from the diffusion of atoms over the resonator surface (Atalaya, Isacsson, and Dykman, 2011a, 2011b; Yang *et al.*, 2011), the electrostatic interaction between the resonator and trapped charges in the substrate (Siria *et al.*, 2012), and temperature drifts that modify the resonator stress. Slow frequency fluctuations are usually quantified using the Allan deviation. Their mechanisms and the Allan deviation are discussed in Sec. IX. These frequency fluctuations can be reduced, enabling one to reach a mass resolution of  $(1.7 \pm 0.5) \times 10^{-27}$  kg with a 2 s integration time. This has been achieved with a nanotube thanks to its extremely small mass (Chaste *et al.*, 2012). This mass resolution is comparable to the mass of one proton.

### C. Photothermal-based sensing

Nanoresonators can be used for several kinds of sensing based on light absorption. The experiments are done using

resonators with tensile stress. The underlying idea is that photon absorption causes heating; the associated thermal expansion reduces the stress, changing the mechanical frequency of the resonator. Because the frequency can be detected with high accuracy, these experiments are exquisitely sensitive, with the sensitivity limited by frequency fluctuations, as in the case of mass sensing. Such photothermal sensing enables optical absorption spectroscopy of single particles and molecules located on the resonator (Larsen *et al.*, 2013), high-precision single-molecule imaging (Chien *et al.*, 2018), high-speed detection of electromagnetic radiation with graphene nanomechanical bolometers (Blaikie, Miller, and Aleman, 2019), and thermal transport measurements of phonons in MoSe<sub>2</sub> monolayer drums through the detection of the thermal gradient over these suspended devices (Morell *et al.*, 2019).

### D. Clocks and clock-based systems

Mechanical resonators are used with great success as ultrastable timing references. Although these resonators are produced mostly at the microscale, we mention them since they have an important technological impact on our society. The current generation of these devices utilizes silicon technology with a wafer-encapsulation process to keep the self-sustaining oscillators in vacuum (Kim *et al.*, 2007). They can now be found in nearly all mobile phones, for example. One of the leading manufacturers, SiTime, reports clocks for mobile and other battery powered devices with  $\pm 3$  ppm frequency stability over the industrial temperature range between  $-40$  and  $+85^\circ\text{C}$ , while the power consumption is kept low (below  $5\ \mu\text{W}$ ) (Zaliasl *et al.*, 2015). Telecommunication applications require still better clocks, and a frequency stability of  $< \pm 0.1$  ppm and an Allan deviation of about  $8 \times 10^{-11}$  at 1 s integration time in the temperature range between  $-45$  and  $+105^\circ\text{C}$  have been achieved (Roshan *et al.*, 2016).

Nanoscale electromechanical resonators have also been used as self-sustained oscillators. The challenge is to integrate the device into an electrical circuit so that it produces a continuous high-frequency signal when powered by a dc input in the feedback loop. The vibrations are transduced into an electrical signal that is amplified with an adjustable gain and phase before being fed back to the resonator. The difficulty is to obtain a sizable electrical signal with minimum imprecision noise added by the transduction of the vibrations. A frequency stability of  $\pm 2$  ppm was demonstrated in a single-crystal SiC electromechanical resonator, albeit over a short test time, less than 1000 s (Feng *et al.*, 2008). Interesting approaches to suppressing the noise that are based on using a resonator in the nonlinear regime near bifurcation points of the response to an external drive were proposed by Greywall *et al.* (1994), Yurke *et al.* (1995), and Kenig *et al.* (2012, 2013), and the possibility of going beyond the limit imposed by the thermomechanical noise was demonstrated (Villanueva *et al.*, 2013).

## IV. FLUCTUATION-DISSIPATION THEOREM AND THE REACTION FORCE FROM THE THERMAL BATH

A simple general model that leads to the Brownian dynamics (2) is based on the assumption that the



nanoresonator is an oscillator coupled to a thermal bath and that the coupling is linear in the oscillator coordinate. In this section we describe the connection between the phenomenological theory (2) and a microscopic theory. We specify the conditions of applicability of the phenomenological description, where the friction force is determined by the instantaneous value of the velocity and where the noise can be described as  $\delta$  correlated in time (the Markovian approximation). We then show that for resonators with a high  $Q$  factor, a significantly less restrictive formulation can be developed if one is interested in the dynamics of the vibration amplitude and the slow part of its phase. Such a dynamics is Markovian on times that largely exceed the vibration period even where the model (2) is inapplicable. The analysis provides an expression for the decay rate  $\Gamma$  in terms of the parameters of the thermal reservoir, and also shows that the frequency of the mode is changed as a result of the coupling and can become temperature dependent. The formulation immediately extends to the case where the mode dynamics is quantum.

### A. Coupling of the oscillator to a thermal bath

The description of dissipation of the oscillator is based on the picture in which the oscillator is coupled to a system with many degrees of freedom. In particular, a nanomechanical mode is coupled to phonons in the nanoresonator and in the substrate that supports the nanoresonator, to the electronic degrees of freedom, to an extended set of two-level fluctuators, etc. The many-degree-of-freedom system coupled to the oscillator can usually be thought of as a thermal bath. The leading term in the expansion of the coupling energy in the oscillator coordinate  $q$  is linear in  $q$  and can be written as

$$H_i = qh_b, \quad (14)$$

where  $h_b$  depends on the dynamical variables of the bath only. It gives the force  $F_b \equiv -h_b$  that the bath exerts on the oscillator. Because of the large number of dynamical variables, the excitation spectrum of the bath is (quasi)continuous. The form of the function  $h_b$  depends on the type of bath. For example, if the bath is formed by phonons in the resonator or the substrate,  $h_b$  is typically a series in the phonon coordinates. The nonlinear terms in this series are behind such familiar mechanisms of dissipation of a nanomechanical mode as the thermoelastic, Landau-Rumer, and Akhiezer relaxation; see Sec. V.A.

To formally describe the dynamics of the mode and the bath, we assume that for  $t \rightarrow -\infty$  they are uncoupled and the bath is in thermal equilibrium. Because the bath is “large,” it is only weakly perturbed by the coupling once the latter is turned on. The response of the bath can be then described using the linear response theory (Landau and Lifshitz, 1980),

$$h_b(t) \approx h_b^{(0)}(t) + \delta h_b(t). \quad (15)$$

In Eq. (15)  $h_b^{(0)}(t)$  is the function  $h_b$  in the absence of the coupling. The force  $-h_b^{(0)}(t)$  describes the effect of the thermal fluctuations of the unperturbed bath on the oscillator.

It is a random force, and it can be chosen to have zero mean,  $\langle h_b^{(0)}(t) \rangle = 0$ .

The term  $\delta h_b(t)$  is the perturbation caused by the coupling. When averaged over the fluctuations of the bath, it can be written as

$$\langle \delta h_b(t) \rangle = - \int_0^\infty dt' \mathcal{X}_b(t') q(t-t'). \quad (16)$$

The function  $\mathcal{X}_b(t)$  is the generalized susceptibility of the bath with respect to the oscillator coordinate  $q$ . Equation (16) is simply an expression of the causality principle: the response of the bath at time  $t$  depends on the values of  $q$  at earlier times.

Because the bath is in thermal equilibrium, its susceptibility and fluctuations are related by the fluctuation-dissipation theorem. This relation has the form

$$S_b(\omega) = 2\hbar[\bar{n}(\omega) + 1]\text{Im}\chi_b(\omega), \quad (17)$$

where  $\chi_b(\omega)$  is the Fourier transform of the susceptibility  $\mathcal{X}_b(t)$  [see Eq. (A7)],  $S_b(\omega)$  is the power spectrum of the bath fluctuations,

$$S_b(\omega) = \int_{-\infty}^\infty dt e^{i\omega t} s_b(t), \quad s_b(t) = \langle h_b^{(0)}(t) h_b^{(0)}(0) \rangle, \quad (18)$$

and  $\bar{n}(\omega) = [\exp(\hbar\omega/k_B T) - 1]^{-1}$  is the thermal occupation number of vibrations at frequency  $\omega$ . The real and imaginary parts of  $\chi_b(\omega)$  are related by the Kramers-Kronig relation. Therefore, Eq. (17) fully defines the bath susceptibility in terms of the power spectrum  $S_b(\omega)$ .

To the leading order in the coupling, one is tempted to replace  $\delta h_b(t)$  in Eq. (15) with  $\langle \delta h_b(t) \rangle$ . The force from the bath on the mode then takes the form

$$F_b(t) = F_b^{(r)}(t) - h_b^{(0)}(t), \quad F_b^{(r)}(t) \equiv -\langle \delta h_b(t) \rangle. \quad (19)$$

The term  $F_b^{(r)}(t)$  is the reaction force from the bath. It results, as seen in Eq. (16), from the perturbation of the bath by the oscillator and depends on the oscillator coordinate. The reaction force is often called the backaction (Clerk and Bennett, 2005; Kippenberg and Vahala, 2008; Clerk *et al.*, 2010). It is reminiscent of the backaction in the theory of quantum measurements, which describes the effect of the measuring apparatus on the measured quantum system and comes from the interaction between the apparatus and the system; cf. the Heisenberg microscope (Heisenberg, 1927). We note that the force  $F_b^{(r)}(t)$  emerges not only in the quantum but also in the classical description of the dynamics.

Equation (16) indicates that the force  $F_b^{(r)}(t)$  is retarded: it depends on  $q(t')$  with  $t' \leq t$ . One should keep in mind that  $F_b^{(r)}(t)$  is an approximation of the reaction force. It relies on the perturbation theory, and one should make sure that the perturbation theory holds for long times on the order of the lifetime of the considered vibrational mode.

In the classical theory, the previous approximation for the reaction force applies in the important case where the power spectrum  $S_b(\omega)$  of the thermal noise is almost constant for

frequencies ranging from much smaller to much larger than  $\omega_0$ . When the power spectrum is flat, the noise correlation function  $-h_b^{(0)}(t)$  is approximately a  $\delta$  function [ $h_b^{(0)}(t) \propto \delta(t)$ ]. This means that the noise part of the force from the bath  $F_b$  is white noise. One can show that the backaction part of  $F_b(t)$  has a term  $\propto -dq(t)/dt$ ; see Appendix A.3. This maps the dynamics of the mode onto the phenomenological equation of Brownian motion (2). In the quantum theory, the case was studied by Caldeira and Leggett (1981) for the bath being a set of harmonic oscillators and  $h_b$  being linear in the coordinates of these oscillators. This is called Ohmic dissipation.

### B. Brownian motion of the complex vibration amplitude

For a NVS mode, the analysis of the effect of coupling to a thermal bath can be extended to a significantly broader situation using the fact that the mode decay rate  $\Gamma$  is small compared to the eigenfrequency  $\omega_0$  or, equivalently, the  $Q$  factor is large. The approach that we describe allows one to also study nonlinear effects. In addition, it allows one to avoid the assumptions of the Ohmic dissipation model. The underlying physics is that a mode with a large  $Q$  factor is a “filter.” It is sensitive primarily to perturbations in a narrow frequency range around the eigenfrequency  $\omega_0$ . In particular, it is sensitive to the bath fluctuations in this frequency range. Of primary interest, therefore, is the amplitude and phase of the mode.

A natural approach to the analysis of the dynamics is offered by the Krylov-Bogoliubov method of averaging (Kryloff and Bogoliubov, 1947; Bogoliubov and Mitropolsky, 1961). Here the first step is to switch from the fast-oscillating coordinate  $q(t)$  and momentum  $p(t)$  of the mode to two new variables, the complex amplitude  $u \equiv u(t)$  and its conjugate,

$$\begin{aligned} q(t) &= u(t) \exp(i\omega_0 t) + u^*(t) \exp(-i\omega_0 t), \\ p(t) &= iM\omega_0 [u(t) \exp(i\omega_0 t) - u^*(t) \exp(-i\omega_0 t)]. \end{aligned} \quad (20)$$

The real and imaginary parts of  $u(t)$  have a simple physical meaning. They are simply the quadratures of the vibrations: if we write the mode displacement as  $q(t) = A(t) \cos[\omega_0 t + \phi(t)]$ , then  $\text{Re} u(t) = (1/2)A(t) \cos \phi(t)$  and  $\text{Im} u(t) = (1/2)A(t) \sin \phi(t)$ .

In the absence of coupling to a thermal bath, the mode oscillates at the frequency  $\omega_0$  with constant amplitude and phase, and then  $u(t) = \text{const}$ . Because of the coupling,  $u(t)$  will vary in time, but for weak coupling the change over the vibration period  $2\pi/\omega_0$  will be small. This can be used to show that, in “slow” time compared to  $2\pi/\omega_0$ , one can disregard retardation of the reaction force. This means that the value of  $F_b^{(r)}(t)$  at time  $t$  is determined by the value of  $u(t)$  at the same time  $t$ ; see Eq. (A8). Taking into account the explicit expressions for the reaction force (A8) and the thermal noise  $h_b^{(0)}(t)$ , we then obtain (see Appendix A.2)

$$\dot{u} = -(\Gamma - iP)u + \xi(t). \quad (21)$$

In Eq. (21) the term  $\xi(t) = (i/2M\omega_0)h_b^{(0)}(t) \exp(-i\omega_0 t)$  describes the noise that comes from the fluctuations in the thermal bath. The meaning of the parameters  $\Gamma$  and  $P$  is seen from the solution of Eq. (21) for the regular part of the complex amplitude  $\langle u(t) \rangle = \langle u(0) \rangle \exp[-(\Gamma - iP)t]$ . When combined with Eq. (20), this shows that  $\Gamma$  is the decay rate of the vibrations, whereas  $P$  is the change of their frequency due to the coupling to the bath,  $\omega_0 \rightarrow \omega_0 + P$ , i.e.,  $P$  is an analog of the polaronic effect for a vibrational system. Both  $\Gamma$  and  $P$  are expressed in terms of the bath susceptibility  $\chi_b(\omega)$  at the mode eigenfrequency (Appendix A.2),

$$\Gamma = \frac{\text{Im} \chi_b(\omega_0)}{2M\omega_0}, \quad P = -\frac{\text{Re} \chi_b(\omega_0)}{2M\omega_0}. \quad (22)$$

With an account taken of Eq. (17), the decay rate  $\Gamma$  is also simply expressed in terms of the power spectrum  $S_b(\omega_0)$  of the random force exerted by the bath. In the classical limit  $k_B T \gg \hbar\omega_0$  we have

$$\Gamma = (4Mk_B T)^{-1} S_b(\omega_0). \quad (23)$$

We later use Eq. (23) in the analysis of the decay of nanomechanical modes due to their coupling to phonons, two-level fluctuators, and electrons.

As seen in Eq. (22), both the decay rate  $\Gamma$  and the frequency shift  $P$  depend on the temperature. The temperature dependence of  $P$  is a simple microscopic mechanism of the temperature dependence of the measured eigenfrequency of NVSSs, and this dependence can be determined from the experimentally measured power spectrum or the response curves. For a carbon nanotube, such measurements were reported by Tepsic *et al.* (2021). In what follows, we incorporate  $P$  into the definition of  $\omega_0$ ; i.e., we replace  $\omega_0 \rightarrow \omega_0 + P$ .

The noise  $\xi(t)$  in Eq. (21) is Gaussian and zero mean. It is  $\delta$  correlated in the slow time compared to the vibration period  $2\pi/\omega_0$  and the time over which bath correlations decay,

$$\langle \xi^*(t) \xi(t') \rangle \approx (\Gamma k_B T / M\omega_0^2) \delta(t - t'), \quad (24)$$

whereas the correlator  $\langle \xi(t) \xi(t') \rangle$  and its complex conjugate can be disregarded (Appendix A.2). It is seen from the simple relations (21)–(24) between the decay rate of the mode and the noise from the thermal bath that the stationary distribution of the mode is the Boltzmann distribution and  $\langle |u|^2 \rangle = k_B T / 2M\omega_0^2$ .

The time evolution of the complex oscillator amplitude described by Eq. (21) is Markovian. There is no delay: the response of the bath is instantaneous in slow time. The corrections disregarded in Eqs. (21) and (24) are small if the bath susceptibility  $\chi_b(\omega)$  weakly varies with  $\omega$  in a comparatively narrow band centered at  $\omega_0$ . The width of this band is determined by the time dependence of  $u(t)$  and is  $\sim \Gamma, |P|$ . It is small compared to  $\omega_0$  and to the reciprocal correlation time of fluctuations in the bath at frequency  $\sim \omega_0$ . This is in contrast to the model of the Brownian motion described by Eq. (2), which requires a near constancy of  $\chi_b(\omega)$  in the frequency band broader than  $\omega_0$ .

We reiterate that the Markovian equation of motion (21) is an approximation. Its applicability has to be checked and the expressions for the decay rate and the polaronic frequency shift have to be derived using a microscopic model of the bath and the coupling.

### C. Quantum description of the mode dynamics

The previous analysis can be extended to the quantum regime. In quantum terms, the functions  $u(t)$  and  $u^*(t)$  become operators, with  $u^*$  understood as  $u^\dagger$ . They are simply the operators  $(1/2)[q(t) \mp ip(t)/M\omega_0] \exp[\mp i\omega_0 t]$  of a harmonic oscillator in the Heisenberg representation and are simply related to the ladder operators  $a^\dagger$  and  $a$ , with

$$\begin{aligned} u(t) &= (\hbar/2M\omega_0)^{1/2} a^\dagger(t) e^{-i\omega_0 t}, \\ [u(t), u^\dagger(t)] &= -\hbar/2M\omega_0. \end{aligned} \quad (25)$$

The equation of motion for  $u(t)$  [Eq. (21)] is linear. It applies not only in the classical case but also in the case where  $u(t)$  is an operator, becoming a *quantum Langevin equation*. The noise  $\xi(t)$  in this formulation is an operator too, and the operators  $\xi(t)$  and  $\xi^\dagger(t)$  do not commute ( $\xi^\dagger$  replaces  $\xi^*$ ). In particular, with the account taken of Eq. (17) we have instead of Eq. (24)

$$\begin{aligned} \langle \xi^\dagger(t) \xi(t') \rangle &\approx e^{\hbar\omega_0/k_B T} \langle \xi(t) \xi^\dagger(t') \rangle \\ &\approx [\hbar(\bar{n} + 1)\Gamma/M\omega_0] \delta(t - t'), \end{aligned} \quad (26)$$

where  $\bar{n} \equiv \bar{n}(\omega_0)$  is the thermal occupation number of the mode.

The noncommutativity of  $\xi(t)$  and  $\xi^\dagger(t)$  is important. Indeed, the mean values  $\langle u(t) \rangle$  and  $\langle u^\dagger(t) \rangle$  decay in time. However, the commutation relation between  $u(t)$  and  $u^\dagger(t)$  should be independent of time. Using Eq. (26) for the noise correlators, one immediately finds using Eq. (21) and the conjugate equation for  $u^\dagger$  that  $\langle [u(t), u^\dagger(t)] \rangle$  remains constant.

On the formal side, the approximations made in deriving the equations of motion (21)–(26) and the equivalent master equation (see Appendix B) correspond to the familiar ladder approximation in the diagrammatic technique (Abrikosov, Gorkov, and Dzyaloshinski, 1975). We note that a non-Markovian quantum Langevin equation has been also discussed in the literature; it has been consistently derived microscopically for the case of the coupling to a bath of harmonic oscillators, with the coupling effectively bilinear in the dynamical variables of the mode and the bath oscillators; see Ford, Lewis, and O'Connell (1988) and references therein.

The decay rate  $\Gamma$  in the quantum theory is simply related to the rate of transitions between the oscillator energy levels due to the coupling to the bath. As shown in Appendix B,  $\Gamma$  is half the rate  $W_{1 \rightarrow 0}$  of transitions from the first excited to the ground state of the mode due to the coupling to the bath for  $T = 0$ .

### 1. The power spectrum and the susceptibility of a weakly damped mode

The picture of the dynamics of the oscillator as vibrations at frequency  $\omega_0$  with slowly varying amplitude and phase

provides a physical insight into why the oscillator power spectrum  $S(\omega) = \int_{-\infty}^{\infty} dt \langle q(t)q(0) \rangle \exp(i\omega t)$  has a peak at frequency  $\omega$  close to  $\omega_0$ . Expressing the coordinate  $q(t)$  in terms of the complex amplitude  $u(t)$  and its complex conjugate in the classical limit or the operators  $u(t)$  and  $u^\dagger(t)$ , to extend to the quantum description we find using Eq. (20) that, for  $|\omega - \omega_0| \ll \omega_0$ ,

$$S(\omega) \approx 2\text{Re} \int_0^\infty dt \langle u^\dagger(t)u(0) \rangle e^{i\omega t}. \quad (27)$$

From Eqs. (21) and (26), for the considered linear oscillator

$$S(\omega) = \frac{\hbar}{M\omega_0} (\bar{n} + 1) \frac{\Gamma}{\Gamma^2 + (\omega - \omega_0)^2}. \quad (28)$$

Equation (28) extends the result (5) to the quantum domain. The frequency  $\omega_0$  here incorporates the polaronic shift  $P$ , and therefore the position of the maximum of  $S(\omega)$  is temperature dependent. We note that the peak of the power spectrum of the radiation emitted by a quantum oscillator is described by Eq. (28), where the factor  $\bar{n} + 1$  is replaced by the thermal occupation number  $\bar{n}$ .

The general expression for the oscillator susceptibility  $\chi(\omega)$  in response to a weak drive at frequency  $\omega$  near resonance  $|\omega - \omega_0| \ll \omega_0$  reads

$$\chi(\omega) = \frac{i}{\hbar(\bar{n} + 1)} \int_0^\infty dt \langle u^\dagger(t)u(0) \rangle e^{i\omega t}. \quad (29)$$

For a linear oscillator the susceptibility is given by Eq. (5).

We emphasize that the general expressions (27) and (29) for the power spectrum and the susceptibility are not limited to the case of a linear oscillator. They describe the power spectrum of a vibrational mode even where the vibrations are nonlinear as long as the spectrum has a narrow peak with a width much smaller than  $\omega_0$  and the reciprocal correlation time of the reservoir.

The quantum description becomes relevant for the experiments where the mechanical mode is close to the quantum ground state. This regime was first achieved in nanomechanics by O'Connell *et al.* (2010). In this experiment a mechanical breathing mode vibrating at 6 GHz was cryogenically cooled using a dilution fridge at 25 mK, and a nonclassical state of motion was created. Recently cryogenic cooling down to the quantum regime was accomplished for a nanomembrane flexural mode with  $\omega_0 = 2\pi \times 15.1$  MHz by lowering its temperature to 500  $\mu$ K (Cattiaux *et al.*, 2021). Mechanical modes endowed with long lifetimes have been cooled down into the quantum regime by coupling them to photon cavities and using parametric drive (Chan *et al.*, 2011; Teufel *et al.*, 2011; Verhagen *et al.*, 2012). This cooling was discussed in the review by Aspelmeyer, Kippenberg, and Marquardt (2014b).

## V. RELAXATION MECHANISMS OF NANOMECHANICAL RESONATORS

The general expression for the decay rate allows us to consider various microscopic mechanisms of energy



dissipation of low-frequency modes in NVs. The major types of the relevant thermal reservoirs are (i) phonons in the substrate, (ii) thermal phonons in the nanoresonator, (iii) electrons in the nanoresonator and in the leads, and (iv) two-level systems. We use the term “phonon” somewhat loosely, as the systems we are discussing do not necessarily have translational symmetry, or even spatial uniformity. However, the relevant eigenmodes, although not plane waves, are spatially extended and have a quasicontinuous frequency spectrum resembling phonons. In thin nanobeams and membranes the spectrum consists of bands of modes extended along the nanobeams or membranes and having different transverse spatial structures. Generally, in disordered systems there are also localized vibrational excitations, which we do not discuss here.

### A. Scattering by phonons

The problem of linear damping of low-frequency eigenmodes in nanoresonators due to phonon scattering overlaps with the problem of sound absorption in dielectrics, which has been intensely studied since the 1930s (Landau and Rumer, 1937; Akhiezer, 1938); see Woodruff and Ehrenreich (1961), Maris (1966), Gurevich (1988), Garanin and Lutovinov (1992), Collins *et al.* (2013), Lindinfeld and Lifshitz (2013), Feng, Qiu, and Ruan (2015), and references therein. It is also closely related to the problem of decay in low-frequency resonant modes and gap modes in crystals with defects (Krivoglaz, 1961; Brout and Visscher, 1962; Kagan and Ioselevskii, 1962; Krivoglaz, 1964).

#### 1. Clamping losses

The simplest decay mechanism of nanomechanical vibrations is radiation of vibrational excitations (phonons) into the supporting structure. This mechanism is an important contributor to the so-called clamping losses. Vibrations of the NVS create time-dependent strain and stress in the area where the resonator is clamped. They serve as phonon-radiating antennas. The supporting structure is much larger than the resonator, and its phonons are a thermal bath for the resonator. This picture of decay via phonon emission is common for nanomechanical and micromechanical systems. In micromechanical systems the corresponding losses are often called anchor losses.

The simplest model of the coupling to the bath of phonons in the support is where the coupling is linear both in the coordinate  $q$  of the NVS mode and in the phonon coordinates  $q_\kappa$ . The model is described by the Hamiltonian  $H_i = qh_b$  [Eq. (14)], with

$$h_b = \sum_\kappa V_\kappa (b_\kappa + b_\kappa^\dagger). \quad (30)$$

Here  $b_\kappa$  and  $b_\kappa^\dagger$  are the annihilation and creation operators of the  $\kappa$ th phonon,  $\omega_\kappa$  is the phonon frequency, and the index  $\kappa$  includes the wave vector and the branch of the phonon. The

full Hamiltonian of the coupled NVS mode and the phononic bath is

$$H = H_0 + H_i + H_b, \quad H_0 = \hbar\omega_0 a^\dagger a, \\ H_b = \sum_\kappa \hbar\omega_\kappa b_\kappa^\dagger b_\kappa \quad (31)$$

[remember that the mode coordinate is  $q = (\hbar/2M\omega_0)^{1/2}(a + a^\dagger)$ ].

The analysis in Sec. IV.B shows that, for the model (30), the decay rate  $\Gamma$  and the shift of the eigenfrequency  $P$  of the NVS mode have the form (Bogolyubov, 1945)

$$\Gamma = \frac{\pi}{4M\omega_0^2} g_{cl}(\omega_0), \quad P = \frac{1}{2M\omega_0} \oint d\omega \frac{g_{cl}(\omega)}{\omega^2 - \omega_0^2}, \quad (32)$$

where  $g_{cl}(\omega) = (2\omega/\hbar) \sum_\kappa |V_\kappa|^2 \delta(\omega - \omega_\kappa)$  is the phonon density of states weighted with the interaction. The decay rate (32) is independent of temperature; it cannot be eliminated by cooling down the nanoresonator. However, it is small for low-frequency NVS modes because the density of phonons at frequency  $\omega_0$  in a 3D support is  $\propto (\omega_0/\omega_D)^2 \ll 1$  ( $\omega_D$  is the Debye frequency). Using Eq. (32), the decay rate can be reduced by either decreasing the density of states of phonons in the support or the coupling to these phonons.

The phonon-radiation decay of nanoresonators or microresonators has been attracting significant attention both on the theory side [see Angelescu, Cross, and Roukes (1998), Cross and Lifshitz (2001), Park and Park (2004), Photiadis, Douglas and Judge (2004), Bindel and Govindjee (2005), and Wilson-Rae (2008)] and on the experimental side [see Yasumura *et al.* (2000), Judge *et al.* (2007), Anetsberger *et al.* (2008), Eichenfield *et al.* (2009), Pandey *et al.* (2009), Unterreithmeier, Faust, and Kotthaus (2010), Schmid *et al.* (2011), Cole *et al.* (2011), Wilson-Rae *et al.* (2011), Rieger *et al.* (2014), Villanueva and Schmid (2014), Chakram *et al.* (2014), Meenehan *et al.* (2014), Ghaffari and Kenny (2015), Pfeifer *et al.* (2016), Norte, Moura, and Gröblacher (2016), Tsaturyan *et al.* (2017), and Ghadimi *et al.* (2018), and references therein]. Approximate expressions for the decay in cantilevers and membranes were summarized by Schmid, Villanueva, and Roukes (2016).

Separating radiation decay from other decay mechanisms is not necessarily simple in an experiment; cf. Unterreithmeier, Faust, and Kotthaus (2010), Yu, Purdy, and Regal (2012), and Ghaffari and Kenny (2015). On the theory side, to find the coupling parameters  $V_\kappa$  one has to find the force that the resonator mode exerts on the phonons. For atomic displacements in the contact area, a separation of the contributions from vibrational modes of the resonator and of the support is nontrivial. Formally, the resonator and the support are a single system with a single set of eigenmodes. The resonator “mode” considered is a superposition of the exact eigenmodes, which have frequencies lying within a band centered at  $\omega_0$  with a width  $\sim \Gamma$  and have comparatively large amplitudes inside the resonator. This picture is reminiscent of the theory of tunneling decay in quantum mechanics, with the NVS mode being an analog of the state localized in a potential well and decaying into extended states outside the well. The extended



states are the analogs of the phonons of the support. Both formulations have a counterpart in the analysis of resonant vibrations in solids that are mostly localized on defects (Brout and Visscher, 1962; Kagan and Iosevskii, 1962); see Barker and Sievers (1975).

One of the approaches to the problem of clamping losses is based on calculating the transmission  $\mathcal{T}$  of elastic waves through the contact (the clamping area). Cross and Lifshitz (2001) performed detailed calculations of the transmission for the support and the resonator having the same thickness. They used a scalar model of elastic waves and the stress-free boundary conditions at the edges. The displacement field in the contact area was expanded into a superposition of incident and reflected waves on the resonator side and a propagating wave in the support while keeping the field continuous on both sides of the contact. Once  $\mathcal{T}$  has been calculated, it is easy to find the decay rate. For example, for an eigenmode of a cantilever, which is a standing wave formed as a superposition of two waves propagating in opposite directions,  $\Gamma \sim v_g \mathcal{T} / L$ , where  $v_g$  is the group velocity of the wave and  $L$  is the length of the cantilever.

Extensive calculations of the decay rate were done for several types of modes in nanoresonators by conditionally separating the displacement at the edge into that from the NVS mode and the phonons in the support (Wilson-Rae, 2008). This separation allowed Wilson-Rae to find the stress from the resonator mode in the contact area and then the force this mode exerts on the support modes, which gave the parameters  $V_\kappa$ . The model was compared to measurements on high-stress  $\text{Si}_3\text{N}_4$  membranes with circular and square geometries (Wilson-Rae *et al.*, 2011) and AlGaAs suspended-plate resonators (Cole *et al.*, 2011).

Significant progress in reducing clamping losses in micro-mechanical resonators has been made by creating gaps in the phonon density of states in the contact area. If phonons with frequencies close to  $\omega_0$  are decoupled from the resonator mode, the decay (32) is eliminated (in practice, suppressed). Different means of creating spectral gaps have been developed for micromechanical resonators; cf. Mohammadi *et al.* (2009), Pandey *et al.* (2009), Ghaffari *et al.* (2013), Bahr, Marathe, and Weinstein (2014), Yu *et al.* (2014), Gokhale and Gorman (2017), and MacCabe *et al.* (2020). One of the most common methods is based on the use of phononic crystals. This allows one to create a mode localized mostly within an interior of a membrane or a nanobeam near a “defect” of the phononic crystal, with the frequency in the gap of the crystal excitation spectrum; see Figs. 6(a) and 6(b). This significantly reduces the coupling to the support phonons. These localized modes are counterparts of the modes localized at defects in solids (Lifshitz, 1942a, 1942b, 1942c), which have frequencies that lie outside the phonon bands. Most of the studies of localized modes in crystals with defects have been done using ensemble measurements (Barker and Sievers, 1975), in contrast to NVSSs, where the modes are accessed individually.

The importance of clamping (anchor) losses has led to a development of various numerical algorithms, some of which have been incorporated into the standard software (COMSOL). An example is the method of a perfectly matched layer, which was first applied to the problem of anchor losses by Bindel and

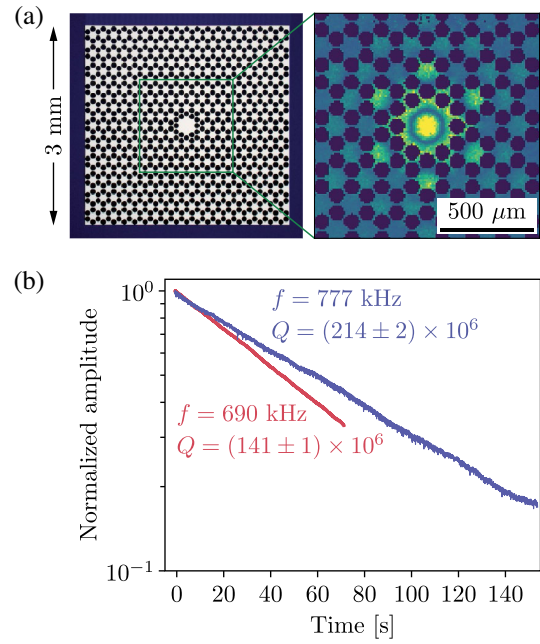


FIG. 6. (a) Engineered shape and support structure of the mechanical eigenmode. The measured shape of the localized flexural mode is indicated by the intensity of the yellow (light) color in the right panel. The silicon nitride membrane under tension is patterned with holes (shown in black) to (i) decrease clamping losses thanks to the quasi-band gap created by the phononic crystal in the membrane, and (ii) reduce dissipation with “soft clamping” by avoiding areas with large curvature. The membrane, which is about 100 nm thick, is supported by a silicon frame (left panel). (b) Energy decay measurements of two different modes at room temperature. Adapted from Tsaturyan *et al.*, 2017.

Govindjee (2005). In this numerical method, to avoid reflection of the irradiated phonons back into the resonator a layer is introduced adjacent to the boundary that truncates the unbounded support. The elasticity equations are artificially modified such that inside the layer the solution decays exponentially, which is technically accomplished using a complex-valued coordinate change in combination with a finite element implementation. At the same time, the solution in the region that includes the resonator is not changed (perfect matching).

## 2. Anelastic relaxation and dissipation dilution for flexural modes

At a phenomenological level, decay of vibrational modes in microresonators and nanoresonators is often described by anelastic relaxation. The term was introduced by Zener (1948). Anelastic relaxation comes from thermal relaxation, the motion of interstitial atoms, interstate transitions in two-level systems, grain boundary relaxation, and other processes (Zener, 1937, 1958; Nowick and Berry, 1972). In many cases the losses are described by assuming that the Young modulus has an imaginary part. One can think of this imaginary part as a result of the delay of the elastic response (hence the term “anelasticity”). Generally, the losses depend on the mode frequency and often display a characteristic peak as a function

of frequency (Zener, 1948). In this approach, a complex Young modulus is a property of a material; cf. Saulson (1990). However, the frequency dispersion of the complex Young modulus is often disregarded for the low-frequency modes studied in nanomechanical resonators, with the exception of thermoelastic relaxation (discussed later). The decay rate and the quality factor  $Q$ , which is defined by Eq. (6), are then expressed in terms of the imaginary part of the Young modulus.

To extend applications of nanomechanical and micromechanical systems, it is important to increase the quality factor. It was shown in the context of interferometric detectors of gravitational waves (González and Saulson, 1994) that, for flexural modes of a suspended loaded wire, the quality factor may become higher than the intrinsic  $Q$  of the material. This effect has become known as dissipation dilution. The physics of dissipation dilution is based on the fact that the elastic energy of a flexural mode in a stretched wire or, more generally, any stressed nanoresonator or microresonator comes not only from the internal stress associated with the strain but also from the externally applied tension, whereas the losses are often due to the intrinsic properties of the material.

Detailed understanding of dissipation dilution requires a careful analysis of the interplay between the tension and the losses. It was first shown numerically by Unterreithmeier, Faust, and Kotthaus (2010) that, in a multimode resonator, the effect can be accounted for by taking into account the actual shape of the flexural modes while assuming the complex Young modulus to be frequency independent. The results were successfully compared with their experimental data on up to nine modes in SiN nanostrings. In this approximation, the losses can be analyzed (Unterreithmeier, Faust, and Kotthaus, 2010; Schmid *et al.*, 2011; Yu, Purdy, and Regal, 2012) by writing the energy loss per vibrational cycle in the same form as the stress-related elastic energy and replacing the real Young modulus with its imaginary part  $E_2$ . For example, in a plate with a thickness  $h$  and a transverse displacement  $\zeta(x, y)$  in the  $z$  direction, the density of losses per unit area is

$$W_{\text{anelast}} = \frac{\pi h^3}{12\omega_0(1-\nu_p^2)} E_2 \{ (\partial_x^2 \zeta + \partial_y^2 \zeta)^2 + 2(1-\nu_p) [(\partial_x \partial_y \zeta)^2 - \partial_x^2 \zeta \partial_y^2 \zeta] \}, \quad (33)$$

where  $\nu_p$  is the Poisson ratio. Yu, Purdy, and Regal (2012) extended this expression to spatially nonuniform systems [ $E_2 \rightarrow E_2(x, y)$ ]. An explicit calculation for a nanobeam was done by Schmid *et al.* (2011).

As seen in Eq. (33), a major contribution to losses comes from the areas of the largest curvature. For clamped membranes and nanobeams under tension, these areas are close to the clamps. Therefore, one may expect to reduce the losses by engineering flexural modes so that they are localized to the central part of nanobeams or nanomembranes, i.e., away from the clamps. Such “soft clamping” has been successfully implemented using phononic crystals in multimode nanomembranes [Figs. 6(a) and 6(b)] (Tsaturyan *et al.*, 2017), as well as in multimode nanobeams (Ghadimi *et al.*, 2018). An alternative strategy consists in clamping a vibrating structure at the antinode of a perimeter mode (Bereyhi *et al.*, 2022).

Record-high  $Q$  factors were obtained along with high  $Q \times f$  factors, which in long nanobeams were as large as  $1.1 \times 10^{15} \text{ Hz}$  for  $f = 1.33 \text{ MHz}$  (Ghadimi *et al.*, 2018) at room temperature. Thus, isolating the modes inside suspended structures can be advantageous not only for reducing phonon emission into the substrate but also for reducing intrinsic material losses.

### 3. Landau-Rumer relaxation

At the microscopic level, a major intrinsic contribution to decay of low-frequency micromechanical and nanomechanical modes comes from their nonlinear coupling to other vibrational modes. The usually studied NVS modes have small frequencies compared to the Debye frequency  $\omega_D$ . Therefore, the density of states of higher-frequency modes is usually much larger than the density of states at  $\omega_0$ , and it is the coupling to such modes that leads to decay of the low-frequency modes. This decay is somewhat reminiscent of sound absorption in dielectrics, which has been intensely studied since the 1930s (Landau and Rumer, 1937; Akhiezer, 1938); see Maris (1966), Gurevich (1988), Garanin and Lutovinov (1992), Collins *et al.* (2013), Lindenfeld and Lifshitz (2013), Feng, Qiu, and Ruan (2015), and references therein. The relevant lowest-order nonlinearity is cubic. It leads to processes in which three vibrational modes are involved.

For cubic nonlinearity, the coupling (14) is described using the Hamiltonian  $H_i = qh_b$  with

$$h_b \equiv h_b^{(3)} = \sum_{\kappa\kappa'}' V_{\kappa\kappa'} b_{\kappa}^{\dagger} b_{\kappa'} + \sum_{\kappa\kappa'} (V'_{\kappa\kappa'} b_{\kappa}^{\dagger} b_{\kappa'}^{\dagger} + \text{H.c.}) \quad (34)$$

(the prime over the sum indicates that  $\kappa \neq \kappa'$ ). In Eq. (34)  $b_{\kappa}$  and  $b_{\kappa}^{\dagger}$  are the annihilation and creation operators, with  $\kappa$  now enumerating the modes localized mostly inside the resonator. Coupling to such modes is often stronger than it is to the modes in the support, and they serve as a thermal bath for the considered low-frequency mode. To simplify the language and to distinguish them from the considered mode, we call these high-frequency modes phonons.

Generally, because of the possible ripples and other inhomogeneities of the nanoresonator, the modes of the quasicontinuous frequency spectrum are not standard plane waves. This is why we use  $\kappa$  rather than the wave vector to enumerate them. The nanomechanical modes we are interested in are also not plane waves, whether these are flexural modes or modes localized near defects of a phononic crystal. Therefore, in distinction from the sound absorption problem, in the scattering described by the coupling  $qh_b$  the momentum is not conserved. This makes the problem similar to that of dissipation of modes localized on defects in disordered solids. Such a problem for the coupling Hamiltonian (34) was considered by Krivoglaz (1961, 1964).

The coupling parameters  $V_{\kappa\kappa'}$  have to be calculated with the account taken of the actual structure of the involved modes; cf. Atalaya *et al.* (2016), Iyer and Candler (2016), and MacCabe *et al.* (2020). The nonlinear coupling of the considered NVS modes to the modes in the support and the corresponding nonlinear clamping losses may also be

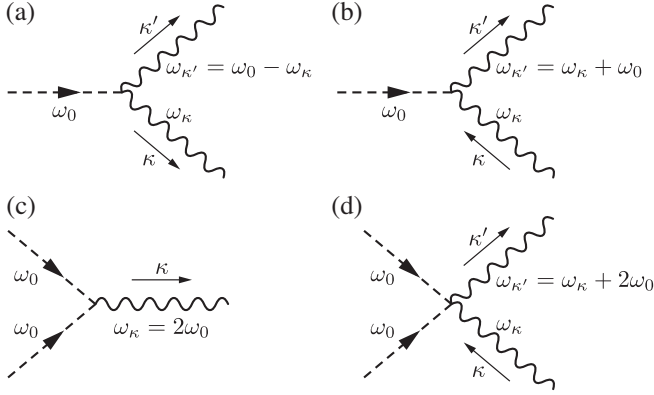


FIG. 7. Scattering of a considered NVS mode due to its nonlinear coupling to phonons.  $\omega_0$  is the NVS mode frequency, and  $\omega_{\kappa}$  and  $\omega_{\kappa'}$  are the frequencies of the phonons with quantum numbers  $\kappa$  and  $\kappa'$ . (a) Decay into two phonons. (b) Landau-Rumer mechanism: anti-Stokes scattering of a phonon  $\kappa$  into a phonon  $\kappa'$  by the NVS mode. (c) Scattering of two quanta of the NVS mode into a phonon, a process leading to nonlinear friction. (d) Analog of the Landau-Rumer scattering that leads to nonlinear friction.

important because of the same density of states argument. This coupling is described by the Hamiltonian (34), with  $\kappa$  referring to the modes primarily localized in the support. To our knowledge, this coupling has not yet been studied for nanoresonators either theoretically or in experiment.

The term  $\propto V'_{\kappa\kappa'}$  in Eq. (34) describes a decay process where one quantum of the NVS mode disappears and two quanta of the thermal bath (two phonons) emerge with the total energy  $\hbar\omega_0$ ; see Fig. 7(a). The rate of such scattering is small for low-frequency NVS modes because of the low density of states of the relevant phonons. For  $\hbar\omega_0 \ll k_B T$ , the process where a phonon is inelastically scattered off the considered NVS mode into another phonon is of a much higher probability; for example, a phonon  $\kappa$  is scattered into a phonon  $\kappa'$  and the energy difference  $\hbar\omega_{\kappa'} - \hbar\omega_{\kappa}$  is equal to  $\hbar\omega_0$ . This Raman-type scattering is sketched in Fig. 7(b). The coupling leading to this process is given by  $V_{\kappa\kappa'}$  in Eq. (34). The scattering probability is comparatively large when the thermal occupation numbers of the modes  $\kappa, \kappa'$  are large and their density of states is large too. This means that  $k_B T \gg \hbar\omega_0$ , a condition met in most experiments, with a few exceptions; see O'Connell *et al.* (2010), Chu *et al.* (2017, 2018), Satzinger *et al.* (2018), Arrangoiz-Arriola *et al.* (2019), MacCabe *et al.* (2020), Cattiaux *et al.* (2021), and Wollack *et al.* (2022), and references therein.

The phonons  $\kappa$  and  $\kappa'$  involved in the scattering shown in Fig. 7(b) are themselves experiencing decay. The rate of the decay of the considered low-frequency mode  $\Gamma$  strongly depends on the interrelation between the phonon relaxation time  $\tau_{\kappa}$  and the vibration period of the considered mode  $2\pi/\omega_0$ . If  $\omega_0\tau_{\kappa} \gg 1$ , we can disregard the decay of high-frequency phonons. Using Eqs. (23) and (34) we find that

$$\Gamma = \Gamma^{\text{LR}} = \frac{\pi}{2M\hbar\omega_0} \sum_{\kappa, \kappa'} |V_{\kappa\kappa'}|^2 [\bar{n}(\omega_{\kappa}) - \bar{n}(\omega_{\kappa'})] \delta(\omega_{\kappa} + \omega_0 - \omega_{\kappa'}). \quad (35)$$

Equation (35) has the same form as the expression for the decay rate of a mode localized on a defect (Krivoglaz, 1961, 1964) and is similar to the expression given by Landau and Rumer (1937) for the sound absorption coefficient in solids. An analysis of this expression in the case of a breathing mode in a nanobeam phononic crystal (MacCabe *et al.*, 2020) showed that the corresponding decay rate is much smaller than the observed value (which itself was extremely small, with the  $Q$  factor reaching  $5 \times 10^{10}$ ). Note that the density of states arguments and the symmetry arguments may lead to a four-quantum decay process having a higher rate than the three-quantum one (Landau and Khalatnikov, 1949a, 1949b; De Martino, Egger, and Gogolin, 2009).

#### 4. Thermoelastic and Akhiezer relaxation

Of primary interest for nanomechanical and micromechanical resonators is the situation where the decay rate of high-frequency phonons exceeds the frequencies of the considered modes. Phonon decay significantly complicates the calculation of the power spectrum of  $h_b^{(3)}$ , which gives the decay rate  $\Gamma$ ; see Eq. (23). In such a calculation the interaction between the phonons should be explicitly taken into account. This interaction comes from the nonlinearity of the crystalline lattice, which is described by nonlinear terms in the phonon Hamiltonian, i.e., the bath Hamiltonian. To the lowest order in the bath nonlinearity, one has to replace the bath Hamiltonian  $H_b$  given by Eq. (31) with  $H_b + H_b^{(3)}$ ,

$$H_b^{(3)} = \frac{1}{2} \sum_{\kappa_1 \kappa_2 \kappa_3} V_{\kappa_1 \kappa_2 \kappa_3} b_{\kappa_1}^{\dagger} b_{\kappa_2}^{\dagger} b_{\kappa_3} + \text{H.c.} \quad (36)$$

The Hamiltonian (36) describes processes where one phonon decays into two other phonons or, vice versa, two phonons annihilate and one phonon emerges such that the overall phonon energy is conserved,  $\omega_{\kappa_1} + \omega_{\kappa_2} = \omega_{\kappa_3}$ . Other cubic in  $b_{\kappa}, b_{\kappa}^{\dagger}$  terms have been dropped in Eq. (36), as they do not describe phonon decay, to the leading order.

In Appendix G we outline a way to calculate the decay rate of the low-frequency NVS mode using the general formulation of Sec. IV, with account taken of the nonlinear mode couplings (34) and (36). The calculation is somewhat involved. Here we give a qualitative phenomenological picture of two important limiting cases. We note, however, that both cases follow from the same general analysis.

The *thermoelastic relaxation* (TER) case is where the eigenfrequency  $\omega_0$  is so small that, because of the coupling (36), the high-frequency vibrations have time to come to thermal equilibrium locally in different parts of the vibrating nanoresonator. One can then introduce a local position-dependent temperature  $T(\mathbf{r})$  inside the nanoresonator. For flexural modes, this implies that the mean free path of thermal phonons  $l_T$ , which is determined by the coupling (36), is small compared to all dimensions, including the transverse dimension of the resonator.

The TER mechanism was proposed by Zener (1938). A detailed analysis of the TER for flexural modes was given by Lifshitz and Roukes (2000). The underlying physics can be understood (Landau and Lifshitz, 1986) if one thinks of



thermal expansion and of generating heat by bending a beam or a membrane. For a small temperature change  $\delta T$ , thermal expansion is proportional to  $\delta T$ ; that is, the relative change of the volume is  $\delta V/V = 3\alpha_T \delta T$ , where  $\alpha_T$  is the linear thermal expansion coefficient, which is determined by the coupling parameters (34); see the discussion after Eq. (39). On the other hand, it follows from the thermodynamics that there is an inverse process. Changing the volume leads to heating or cooling. The heat produced by a small volume increment  $\delta V$  is  $T \partial_T F_{V-T}$ , where  $F_{V-T}$  is the free energy density associated with thermal expansion:  $F_{V-T} = -E\alpha_T \delta T \delta V / (1 - 2\nu_p) V$ .

In flexural vibrations one part of the nanoresonator is periodically squeezed ( $\delta V < 0$ ), whereas the other part is stretched in the counterphase. Therefore, a temperature gradient emerges across the resonator. It dissipates via thermal conductivity, which leads to vibration decay.

If the thickness of the nanoresonator in the bending direction is  $l_\perp$ , the characteristic time of thermal diffusion across it is

$$\tau_Z = C\rho l_\perp^2 / \pi^2 \kappa_T, \quad (37)$$

where  $C$  is the specific heat per unit mass and  $\kappa_T$  is the thermal conductivity (Zener, 1938). If this time is small compared to the vibration period, the nanoresonator is essentially isothermal and TER is not efficient. In the opposite limit  $\omega_0 \tau_Z \gg 1$  TER is not efficient either, since the heat does not have time to propagate across the resonator over the vibration period and is locally averaged out over the compression-extension cycle. An intuitive approximation for the decay rate is provided by the Zener expression (Zener, 1938)

$$\Gamma^{\text{TER}} = \frac{E\alpha_T^2 T \omega_0}{2C\rho} \frac{\omega_0 \tau_Z}{1 + (\omega_0 \tau_Z)^2}. \quad (38)$$

In agreement with the previous qualitative arguments, the decay rate becomes small in the cases both where  $\omega_0 \tau_Z$  is large and where it is small.

A quantitative analysis of the dynamics of a flexural mode in a nanobeam can be done by writing the equation of motion for the displacement in the bending direction that, along with the elastic force, takes into account the force from the thermal expansion. This equation and the thermal diffusion equation form a system of two coupled linear equations. The complex eigenvalues of these equations describe the decay rate and the frequency shift of the flexural mode due to the thermoelastic effect (Lifshitz and Roukes, 2000).

On the experimental side, TER has been seen in both micromechanical and nanomechanical resonators at room temperature; see Roszhart (1990), Yasumura *et al.* (2000), Verbridge *et al.* (2006), Chandorkar *et al.* (2009), and Ghaffari and Kenny (2015). As the temperature is decreased, the decay rate (38) also decreases, and other decay mechanisms come into play. In addition, the mean free path of thermal phonons in nanoresonators can become larger than the resonator thickness such that the system is no longer in the TER regime.

**Akhiezer damping.**—The expression for the decay rate changes if  $\omega_0$  largely exceeds the rate of heat diffusion across the resonator ( $\omega_0 \gg \tau_Z^{-1}$ ), even though it can still be small or

comparable to the relaxation rate of thermal phonons. The phonons then do not have time to equilibrate locally to different temperatures in different parts of the resonator. The decay mechanism in this case was discussed by Akhiezer (1938) in the context of ultrasound absorption in solids. The corresponding mechanism of ultrasound absorption is called Akhiezer damping. It has been attracting significant attention and has been studied for various models of the phonon-phonon coupling; cf. Woodruff and Ehrenreich (1961), Maris (1966), Gurevich and Shklovskii (1968), Maris (1968), and Garanin and Lutovinov (1992), and references therein.

The concept of Akhiezer damping directly extends to the decay of low-frequency vibrational modes in nanomechanical and micromechanical systems. In this context it was analyzed in various papers (Kiselev and Iafrate, 2008; Kunal and Aluru, 2014; Atalaya *et al.*, 2016; Iyer and Candler, 2016; Hamoumi *et al.*, 2018). A detailed experimental study of the temperature dependence of Akhiezer damping in Si micromechanical resonator was described by Rodriguez *et al.* (2019); see also Ghaffari *et al.* (2013) for a review of the earlier work.

To give an idea of the mechanism, we consider the coupling of a low-frequency mode to high-frequency phonons in the deformation potential approximation (Gurevich, 1988). This approximation corresponds to the choice of the coupling parameters  $V_{\kappa\kappa'}$  in Eq. (34) based on the picture (Akhiezer, 1938) in which a low-frequency mode, with a spatially smooth displacement field  $\mathbf{u}(\mathbf{r})$ , weakly locally distorts the crystal. The distortion leads to coordinate-dependent changes  $\delta\omega_\kappa$  of the frequencies  $\omega_\kappa$  of high-frequency modes [remember that  $\boldsymbol{\varphi}(\mathbf{r})$  is the dimensionless local displacement due to the considered low-frequency mode],

$$\delta\omega_\kappa = -\omega_\kappa \gamma_\kappa^{(G)} \nabla \mathbf{u}, \quad \mathbf{u}(\mathbf{r}) = q\boldsymbol{\varphi}(\mathbf{r}). \quad (39)$$

The parameter  $\gamma_\kappa^{(G)}$  determines the coupling constants  $V_{\kappa_1\kappa_2}$  in Eq. (34). The average of  $\gamma_\kappa^{(G)}$  over the phonons with the weight given by the phonon heat capacities gives the Grüneisen parameter  $\gamma^{(G)}$ . This parameter is immediately related to the thermal expansion coefficient  $\alpha_T$ , i.e.,  $\gamma^{(G)} = E\alpha_T / C\rho(1 - 2\nu_p)$ . The approximation (39) is often generalized by replacing  $\nabla \mathbf{u}$  with the strain tensor associated with  $q\boldsymbol{\varphi}(\mathbf{r})$ , in which case  $\gamma_\kappa^{(G)}$  also becomes a tensor.

Finding the Akhiezer damping rate in nanomechanics requires, as a first step, solving the full quantum kinetic equation for the two-phonon correlation function of thermal phonons; see Appendix G. This equation goes beyond the conventional kinetic equation for the occupation numbers of phonons (Atalaya *et al.*, 2016). However, to see the Akhiezer effect qualitatively, one can start with Eq. (35), which describes phonon scattering off the low-frequency mode. Since high-frequency phonons have finite lifetimes, their energies are uncertain, and in Eq. (35) the  $\delta$  function of the energy conservation law  $\delta(\omega_\kappa - \omega_{\kappa'} + \omega_0)$  can be replaced by a Lorentzian with a half-width given by a phonon decay rate  $1/\tau_{\text{ph}}$ . This rate is the characteristic value of the decay rate  $\tau_\kappa^{-1}$  of the thermal phonons, which is quadratic in the parameters of the phonon-phonon coupling  $V_{\kappa_1\kappa_2\kappa_3}$ . From Eqs. (35) and (39), we then have



$$\Gamma^{\text{Akh}} = a^{\text{Akh}} C (\gamma^{(\text{G})})^2 \frac{\omega_0 \tau_{\text{ph}}}{1 + (\omega_0 \tau_{\text{ph}})^2}. \quad (40)$$

The lifting of the energy conservation constraint described by Eq. (40) leads to an increase of the decay rates of low-frequency NVS modes compared to the Landau-Rumer theory (35). It also leads to a specific temperature dependence of the decay rate. If the mean free path of the thermal phonons is small compared to the size of the resonator, this dependence is similar to the temperature dependence of ultrasound absorption. The parameter  $a^{\text{Akh}}$  in the latter case was found by Woodruff and Ehrenreich (1961) for a simple model of the coupling to acoustic phonons and for the ultrasound frequency  $\omega_0 \ll \tau_{\text{ph}}^{-1}$ , in which case  $a^{\text{Akh}} = \omega_0 T / 3 \rho v_s^2$ , where  $v_s$  is the average speed of sound. In this regime  $\Gamma^{\text{Akh}}$  weakly depends on temperature provided that  $T$  exceeds the Debye temperature. This is because the phonon scattering rate is proportional to the phonon occupation number, i.e.,  $\tau_{\text{ph}}^{-1} \propto T$  (Gurevich, 1988), whereas  $C$  is independent of  $T$ . For temperatures that are low compared to the Debye temperature, on the other hand,  $\Gamma^{\text{Akh}} \propto T^{-1}$  in clean systems, where  $\tau_{\text{ph}} \propto T^{-5}$ .

The decay rate (40) displays a pronounced dependence on the mode eigenfrequency  $\omega_0$ . It is small both for  $\omega_0 \tau_{\text{ph}} \ll 1$  and in the opposite limit  $\omega_0 \tau_{\text{ph}} \gg 1$ , where the decay is described by the Landau-Rumer-type theory.

The low-temperature behavior of  $\Gamma^{\text{Akh}}$  changes in thin nanoresonators. When the wavelength of thermal phonons becomes comparable to one of the dimensions of a resonator, the phonon spectrum is quantized and the density of states of the phonons is changed. This leads to a change of both the specific heat and the phonon decay rate. Moreover, nanoresonators can be (and often are) inhomogeneous on the scale of the phonon mean free path because of bending, twisting, ripples, etc., which requires a modification of the theory (Atalaya *et al.*, 2016). On the experimental side, in contrast to micromechanical resonators (Rodríguez *et al.*, 2019), the study of Akhiezer damping and the accompanying frequency shift in nanoresonators is at an early stage (Tepsic *et al.*, 2021).

To relate this to the previous discussion, we note that the decay of thermal phonons that underlies the Akhiezer relaxation is one of the microscopic mechanisms of the anelastic relaxation described by a complex Young modulus; see Sec. V.A.2.

## B. Losses due to surface effects and two-level systems

Nanomechanical resonators are characterized by a large surface-to-volume ratio. Therefore, surface scattering and the defects associated with surfaces may be an important source of mode relaxation; cf. Yasumura *et al.* (2000), Ekinici and Roukes (2005), Unterreithmeier, Faust, and Kotthaus (2010), Yu, Purdy, and Regal (2012), Faust *et al.* (2014), Villanueva and Schmid (2014), Hamoumi *et al.* (2018), and references therein. In particular, Villanueva and Schmid (2014) performed detailed measurements of surface losses in SiN membranes at room temperature as a function of the thickness and also compared different data in the literature; they concluded that the  $Q$  factor linearly increases with

increasing thickness. This is expected for surface losses if one thinks of the  $Q$  factor as the ratio of the energy stored, which is proportional to the volume, to the energy losses, which linearly increase with the surface area.

Generally, one can think of the surface losses as resulting from “static” and “dynamical” effects. A simple static effect comes from the static disorder, which leads to scattering of the thermal phonons. The effect is particularly strong where the phonon mean free path becomes comparable to the thickness. The disorder-induced scattering relaxes the momentum conservation law in phonon-phonon scattering, and thus decreases the lifetime of thermal phonons. This leads to a decrease of the relaxation rate of the low-frequency NVS modes in the Akhiezer regime for  $\omega_0 \tau_{\text{ph}} < 1$ , as seen from Eq. (40) (De, Kunal, and Aluru, 2016). However, as previously mentioned, one can also think of thermal phonons somewhat differently by associating them with the exact vibrational excitations of the disordered system in the harmonic approximation. The coupling of such thermal excitations to the low-frequency NVS modes is different than in a system with no disorder; cf. Atalaya *et al.* (2016). This can increase the Landau-Rumer and Akhiezer relaxation rates compared to those calculated in the absence of disorder.

The dynamical effects of surface disorder come from the defects with internal degrees of freedom, which can absorb energy from the low-frequency NVS modes. The best-known type of such defects are two-level systems (TLSs), which were introduced by Anderson, Halperin, and Varma (1972) and Phillips (1972) to explain the anomalous heat capacity and thermal conductivity of glasses at low temperatures. TLSs exist not only on surfaces but also in the bulk. Their density of states may be higher than the density of states of thermal phonons for low temperatures. For higher temperatures, where the density of states of thermal phonons is higher, the TLSs can “mediate” energy transfer from the low-frequency NVS modes to thermal phonons.

TLSs with level spacing that significantly exceeds  $\hbar\omega_0$  are believed to be important for the relaxation of low-frequency modes in nanoresonators. The relaxation is due not to resonant interlevel transitions of the TLSs, but instead to nonresonant processes. It has been discussed for a broad range of nanoresonators, such as gold (Venkatesan *et al.*, 2010), polycrystalline aluminum (Hoehne *et al.*, 2010), silica (Riviere *et al.*, 2011), aluminum covered silicon (Lulla *et al.*, 2013), SiN (Faust *et al.*, 2014) and GaAs (Hamoumi *et al.*, 2018) nanobeams as well as graphene-based heterostructure membranes (Will *et al.*, 2017), half-ring crystalline Si resonators (Hauer *et al.*, 2018), and phononic crystals (MacCabe *et al.*, 2020); see also Imboden and Mohanty (2014) for a review of early work.

The dominant mechanism of nonresonant coupling to a TLS is the modulation of the level spacing by the strain from the vibrational mode. This coupling is often called dispersive. It is easy to visualize if one thinks of the TLS states as intrawell states of a particle in a double-well potential, which are hybridized by interwell tunneling. The strain modulates the wells differently, which leads to a change of their relative depths, and thus to a change of the level spacing. The Hamiltonian of the coupling reads

$$H_{\text{TLS}} = C_{\text{TLS}} q (\hat{n}_2 - \hat{n}_1), \quad (41)$$

where  $\hat{n}_i$  is the operator of the occupation of the  $i$ th state of the TLS ( $i = 1, 2$ ),  $q$  is the NVS mode coordinate, and  $C_{\text{TLS}}$  is the coupling constant.

Relaxation of the mode results from the finite lifetime of the TLS states. By periodically modulating the TLS level spacing, the mode modulates the state populations with a delay determined by the interrelation between  $\omega_0$  and the interstate switching rate  $\tau_{\text{TLS}}^{-1}$ . This delay leads to the absorption of the mode energy, i.e., to the mode relaxation. If  $\omega_0 \ll \tau_{\text{TLS}}^{-1}$ , the TLS adiabatically follows the mode-induced strain, with essentially no absorption. In the opposite limit ( $\omega_0 \gg \tau_{\text{TLS}}^{-1}$ ) the TLS averages out the mode-induced strain, again with little absorption. Overall, the absorption coefficient  $\Gamma^{\text{TLS}}$  as a function of the mode eigenfrequency  $\omega_0$  is described by the so-called Debye peak, which was found by [Debye \(1929\)](#) in an analysis of the dielectric response due to a reorientation of polar molecules in crystals,

$$\Gamma^{\text{TLS}} \propto C_{\text{TLS}}^2 (k_B T)^{-1} \frac{\omega_0 \tau_{\text{TLS}}}{1 + \omega_0^2 \tau_{\text{TLS}}^2}. \quad (42)$$

Equation (42) can be immediately derived from the general formulation (17).

The TLS relaxation rate  $\tau_{\text{TLS}}^{-1}$  is determined by the coupling to phonons (or electrons). Generally, this rate depends on the geometry of the nanoresonator and the associated change of the phonon spectrum ([Behunin, Intravaia, and Rakich, 2016](#)). At low temperatures, it is dominated by interstate tunneling and single-phonon processes, with  $\tau_{\text{TLS}}^{-1} \propto \coth(E/2k_B T)$ , where  $E$  is the level spacing. At higher temperatures phonon scattering off TLSs comes into play. When the results are extended to still higher temperatures, TLSs are often thought of as particles in a double-well potential, with  $\tau_{\text{TLS}}^{-1}$  determined by the rate of activated interwell switching,  $\tau_{\text{TLS}}^{-1} \propto \exp(-\Delta U/k_B T)$ , where  $\Delta U$  is the barrier height; see [Enns and Hunklinger \(2005\)](#).

The overall temperature dependence of the decay rate of the low-frequency NVS modes is obtained by summing the contributions  $\Gamma^{\text{TLS}}$  for different TLSs. At low temperatures ( $T \lesssim 1\text{--}3$  K), it is often described by a power law ([Venkatesan et al., 2010; Lulla et al., 2013](#)), as expected for some models of the TLSs ([Seoáñez, Guinea, and Castro Neto, 2008](#)). For higher temperatures, because of the exponential falloff of  $\tau_{\text{TLS}}$  with the increasing temperature,  $\Gamma^{\text{TLS}}$  may display a peak as a function of temperature where  $\omega_0 \tau_{\text{TLS}} = 1$  ([Faust et al., 2014](#)). The overall behavior of the decay rate with temperature depends on whether there are various types of TLSs or, as in the case of certain surface defects, the distribution of the TLS parameters is narrow; cf. [Faust et al. \(2014\)](#) and [Hamoumi et al. \(2018\)](#).

Generally, resonant absorption by low-energy TLSs with the level spacing  $\hbar\omega_0$  can also contribute to the mode decay ([Remus, Blencowe, and Tanaka, 2009](#)). It would be characterized by absorption saturation and the associated decrease of the decay rate with the increasing mode amplitude, which is similar to ultrasound absorption ([Golding et al., 1973](#)) and the absorption of microwave radiation in superconducting cavities

([Gao et al., 2007](#)). However, this behavior is most clearly manifested for  $\hbar\omega_0 \gtrsim k_B T$ , a demanding condition in nanomechanics.

### C. Electronic relaxation

The thermal bath can be the electrons flowing through the resonator. It can also be the conducting electrons in a device capacitively coupled to the resonator. Both layouts are similar. Electron transport is used in many resonators to transduce mechanical vibrations into a measurable signal and to drive the motion via the capacitive force, i.e., by modulating the potential  $V_g$  between the gate electrode and the nanoresonator, as discussed in Sec. II. Conversely, the coupling to the electron system leads to the relaxation of mechanical vibrations via electrical dissipation.

The simplest relaxation mechanism is Ohmic losses in the electronic circuit. To illustrate this mechanism, we consider a mechanical resonator based on a suspended wire coupled to the gate electrode that, along with the elements of the electronic circuit, serves as the thermal reservoir; see Fig. 8(a). The coupling to the electronic degrees of freedom comes from the potential  $V_g$  in Fig. 8(b) that fluctuates due to the noise in the electron system. The coupling is described by the Hamiltonian

$$H_i = q h_b, \quad h_b = -C'_g \bar{V}_g \delta V_g. \quad (43)$$

We assume in Eq. (43) that the fluctuations of the potential  $\delta V_g$  are small compared to its mean value  $\bar{V}_g \equiv V_g^{\text{dc}}$ ; cf. Eq. (8). From the general expression (22), the contribution  $\Gamma_e$  of the coupling (43) to the decay rate  $\Gamma$  of the resonator in the classical case  $k_B T \gg \hbar\omega_0$  is

$$\Gamma_e = (4Mk_B T)^{-1} (C'_g V_g^{\text{dc}})^2 \int_{-\infty}^{\infty} dt e^{i\omega_0 t} \langle \delta V_g(t) \delta V_g(0) \rangle. \quad (44)$$

The power spectrum of the voltage fluctuations has a simple form for the Ohmic resistance in the device shown in Fig. 8(a), where we disregard the Coulomb interaction between the electrons as well as phase-coherent effects. For simplicity, we assume that the impedance of the circuit at the frequency  $\omega_0$  is given by large resistances  $R_{c1}$  and  $R_{c2}$  at the interface between the wire and the electrical leads. The corresponding resistors are connected in parallel to the ground [see Fig. 8(b)] such that the total resistance is  $R_{\text{eff}} = R_{c1} R_{c2} / (R_{c1} + R_{c2})$ . The

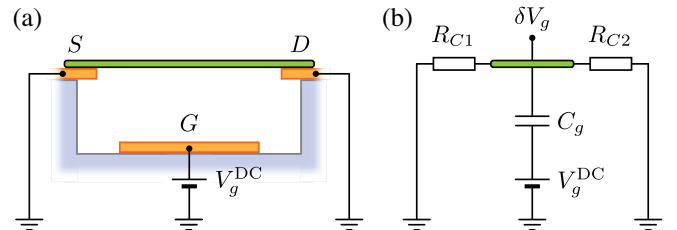


FIG. 8. (a) Schematic and (b) equivalent circuit of a suspended wire capacitively coupled to the gate electrode  $G$  and electrically contacted to the electrodes  $S$  and  $D$ . The resistances at the interface between the wire and the electrodes are  $R_{c1}$  and  $R_{c2}$ .

correlator of  $\delta V_g$  is then determined simply by the Johnson-Nyquist noise, resulting in

$$\Gamma_e = (C'_g V_g^{\text{dc}})^2 R_{\text{eff}} / 2M. \quad (45)$$

We note that Eq. (45) can be obtained directly from Eq. (43) by noting that the force on the resonator is  $C'_g \bar{V}_g \delta V_g$ . The motion of the resonator modulates the charge on it, leading to a current  $\approx C'_g V_g^{\text{dc}} \dot{q}$ . As a result, the potential  $\delta V_g$  is modulated. If the vibration frequency  $\omega_0$  is small compared to the relaxation rate of the circuit  $(R_{\text{eff}} C_g)^{-1}$ , then  $\delta V_g$  follows  $\dot{q}(t)$  adiabatically such that the corresponding part of  $\delta V_g$  has the form  $[\delta V_g]_q = -R_{\text{eff}} C'_g V_g^{\text{dc}} \dot{q}$ . By substituting this expression into the force on the resonator, we obtain the friction force  $-2M\Gamma_e \dot{q}$ . An alternative derivation based on calculating the energy loss due to the resistance of the nanoresonator was given by Song *et al.* (2012).

The electronic relaxation has been measured in resonators based on two-dimensional systems, such as graphene, WSe<sub>2</sub> monolayers, and van der Waals stacks (Song *et al.*, 2012; Morell *et al.*, 2016; Will *et al.*, 2017). The measured mechanical dissipation rate increases quadratically with  $V_g^{\text{dc}}$ , in agreement with Eq. (45). The electrical resistance obtained from the mechanical dissipation is in reasonably good agreement with the resistance of the device. A quantitative comparison is often challenging, especially when the spatial flow of the vibration-induced current is not precisely known due to the geometry of the device.

The electron-electron interaction can strongly modify the relaxation rate of a nanoresonator. The effect has been studied in several theoretical papers for low-resistive nanoresonators capacitively coupled to stationary normal and superconducting single-electron transistors (SETs) and in the layout where the nanoresonator itself is a SET that is capacitively coupled to an immobile gate electrode (Armour, Blencowe, and Zhang, 2004; Mozyrsky, Martin, and Hastings, 2004; Blencowe, Imbers, and Armour, 2005; Clerk and Bennett, 2005; Bennett and Clerk, 2006; Pistolesi and Labarthe, 2007; Micchi, Avriller, and Pistolesi, 2015). The underlying physics is related to the dependence of the potential of the SET island, and thus the tunneling rate, on the position of the nanoresonator. Experiments were carried out on SETs (Woodside and McEuen, 2002; Knobel and Cleland, 2003; Stomp *et al.*, 2005; Zhu, Brink, and McEuen, 2005; Lassagne *et al.*, 2009; Steele *et al.*, 2009; Bennett *et al.*, 2010; Ganzhorn and Wernsdorfer, 2012; Meerwaldt *et al.*, 2012; Benyamini *et al.*, 2014; Ares *et al.*, 2016; Deng *et al.*, 2016; Okazaki *et al.*, 2016; Willick, Tang, and Baugh, 2017; Blien *et al.*, 2020; Urgell *et al.*, 2020; Wen *et al.*, 2020; Vigneau *et al.*, 2021), superconducting SETs (LaHaye *et al.*, 2004, 2009; Naik *et al.*, 2006; Pirkkalainen, Cho *et al.*, 2015), and double-quantum dots (Benyamini *et al.*, 2014; Khivrich, Clerk, and Ilani, 2019).

The theory takes advantage of the fact that the response of a SET to the position is usually fast on the timescale of the vibration period; i.e.,  $\omega_0$  is small compared to the tunneling rate. The analysis can be formulated in terms of the linear response of the SET to the vibrations; cf. Sec. IV. Measurements have shown that the coupling can dramatically

increase the mechanical dissipation (Naik *et al.*, 2006; Lassagne *et al.*, 2009; Steele *et al.*, 2009). When the voltage applied between the source and the drain electrodes of the SET is larger than  $k_B T / e$ , the electronic bath is no longer in equilibrium and it can cool the thermal vibrations (Clerk and Bennett, 2005). In addition, such an out-of-equilibrium electronic bath in a SET can suppress the total dissipation rate of the mechanical resonator to zero, leading to self-oscillation (Usmani, Blanter, and Nazarov, 2007; Wen *et al.*, 2020). Cooling and self-oscillations can also be produced by an electrothermal reaction force associated with the electrical power dissipated in SETs (Urgell *et al.*, 2020).

The so-called electron shuttles (Gorelik *et al.*, 1998; Erbe *et al.*, 2001; Fedorets *et al.*, 2004; Koenig and Weig, 2012) can be operated in the self-oscillation regime too. These are devices where the metal island of the SET placed on a nanocantilever or microcantilever is oscillating between the source and drain leads (in each oscillation period, the island mechanically transfers a quantized number of electrons from one lead to the other).

The interplay of the NVS dynamics with other many-electron effects and the effects of the topology and coherence of the electron system has also been investigated. They include the Kondo (Götz *et al.*, 2018) and the quantum Hall effects (Singh *et al.*, 2012; Chen, Deshpande *et al.*, 2016), the electronic Fabry-Perot interference in a nanoresonator (Moser *et al.*, 2014), and the effect of Aharonov-Bohm oscillations in a topologically nontrivial nanowire (Kim *et al.*, 2019). Other manifestations of the coupling of the NVS modes and the electron subsystems were studied in ballistic *p-n* junctions (Jung *et al.*, 2019), field-effect transistors (Sazonova *et al.*, 2004), and quantum-point-contact devices (Poggio *et al.*, 2008).

## VI. CONSERVATIVE AND DISSIPATIVE NONLINEARITY

Vibration nonlinearity is one of the most important and interesting features of the NVS modes. As previously mentioned, since nanomechanical resonators are small, vibration nonlinearity already comes into play for small vibration amplitudes. Sometimes even thermal fluctuations can be sufficiently large to take the vibrations to a nonlinear regime. This regime is also reached with a modest resonant driving if the quality factor is high. In fact, for high- $Q$  modes care must be taken to stay in the linear regime.

Nonlinear effects are usually separated into conservative and dissipative categories. Conservative nonlinearity corresponds to the restoring force being a nonlinear function of the mode coordinate  $q$  or, equivalently, to the potential energy of the mode  $U(q)$  differing from  $M\omega_0^2 q^2/2$ . If  $U(q)$  has inversion symmetry,  $U(q) = U(-q)$ , as for bending modes in a straight nanotube or a flat membrane the leading non-parabolic term in  $U(q)$  is quartic in  $q$ . The potential energy of the mode then has the form

$$U(q) = \frac{1}{2} M \omega_0^2 q^2 + \frac{1}{4} M \gamma q^4. \quad (46)$$

This nonlinearity is often called the Duffing nonlinearity or, in terms of nonlinear optics, the Kerr nonlinearity. It has been seen in the majority of NVSs; cf. Aldridge and Cleland



(2005), Kozinsky *et al.* (2006), Feng *et al.* (2007), Castellanos-Gomez *et al.* (2013), and Yang *et al.* (2019).

In nonlinear dynamics the nonlinearity is conventionally considered to be strong where the nonparabolic part of the potential becomes of the same order of magnitude as the parabolic part (Arnold, 1989). In nanomechanics, in most studies the conservative nonlinearity of NVs is weak in this sense,

$$|\gamma|\langle q^4 \rangle \ll \omega_0^2 \langle q^2 \rangle. \quad (47)$$

However, even where the condition (47) holds, the effect of the nonlinearity on the dynamics can be strong provided that the decay rate of the mode is small, i.e.,  $Q \gg 1$ . This is clear from the following argument. The nonlinear part of the restoring force  $-M\gamma q^3$  shows that the effective “spring constant” gets effectively either stronger or softer with the increasing vibration amplitude, depending on whether  $\gamma > 0$  or  $\gamma < 0$ , respectively. Therefore, the resonant frequency becomes dependent on the vibration amplitude  $A$ . For weak nonlinearity, the shift in  $\omega_0$  is quadratic in  $A$  (see Appendix A.1),

$$\delta\omega_0 = \frac{3}{8} \frac{\gamma}{\omega_0} A^2. \quad (48)$$

The Duffing nonlinearity becomes important once this frequency shift becomes comparable to the frequency uncertainty associated with the decay rate  $\Gamma$ . In quantum terms, the energy levels of the mode become nonequidistant, and the nonlinearity becomes important once this nonequidistance becomes comparable to the level width  $\propto \hbar\Gamma$ ; see Appendix E.

Dissipative nonlinearity corresponds, in the phenomenological description, to the friction force being a nonlinear function of the velocity and coordinate. This function changes sign upon time reversal analogously to the linear friction force  $-2M\Gamma\dot{q}$ . In its simplest form, the nonlinear friction force is  $\propto q^2\dot{q}$  (van der Pol, 1926) or  $\propto \dot{q}^3$  (Rayleigh, 1945). As with the conservative nonlinearity, for weakly damped modes the nonlinear dissipative force is important where it is comparable to the linear friction force  $-2M\Gamma\dot{q}$ , which is much weaker than the restoring harmonic force  $-M\omega_0^2 q$ . In this section we discuss the mechanisms of nonlinearity and some of the key manifestations of nonlinearities in mechanical resonators. Nonlinear resonant phenomena are discussed in Sec. VII.

### A. Mechanisms of conservative nonlinearity

There are several mechanisms of nonlinearity for the restoring force in nanomechanics. The simplest of them is the nonlinear dependence of the stress (tension) on the displacement field of the mode. A familiar example is provided by a doubly clamped prestressed thin beam (Landau and Lifshitz, 1986). The change  $\Delta L$  of the length  $L$  of the beam due to the transverse displacement  $X(z, t)$  in a flexural vibrational mode is  $\Delta L \approx \int_0^L dz (\partial X / \partial z)^2 / 2$  for small  $|dX/dz|$  ( $z$  is the coordinate along the beam). The elongation leads to the tension  $ES\Delta L/L$ , where  $S$  is the area of the beam cross section. This tension adds to the tension  $T$  inside the beam such that the overall restoring force due to the tension is

$$F_T(z) \approx \left[ T + (ES/2L) \int dz (\partial X / \partial z)^2 \right] \partial^2 X / \partial z^2. \quad (49)$$

One can now substitute  $X(z, t) = q(t)\tilde{\varphi}(z)$ , where  $\tilde{\varphi}(z)$  is the spatial profile of the mode (which is sinusoidal for strong tension). The cubic in the  $X(z, t)$  term then leads to the force  $-\gamma M q^3$  in the equation of motion for  $q(t)$  [Eq. (2)], with  $\gamma = -(E/2L\rho) [\int dz (d\tilde{\varphi}/dz)^2]^2 [\int dz \tilde{\varphi}(z)^2]^{-1}$  (Lifshitz and Cross, 2008).

Nonlinear terms in the restoring force can also come from other sources. In particular, they can come from the nonlinear dependence of the resonator-to-gate capacitance  $C_g$  on the displacement of the resonator. As discussed in Sec. II.D, for a given mode the second derivative of  $C_g$  over the displacement associated with the mode leads to the change of the mode frequency. The higher-order derivatives of  $C_g$  lead to a force that is quadratic or cubic in the displacement, i.e., has the form  $-M\beta q^2 - M\gamma q^3$ ; cf. Kozinsky *et al.* (2006), Chan, Dykman, and Stambaugh (2008a), Eichler, Moser *et al.* (2011), Meerwaldt, Steele, and Zant (2012), and Eichler *et al.* (2013). The parameters  $\beta$  and  $\gamma$ , which are proportional to the third and fourth derivatives of  $C_g$ , respectively, are quadratic in the gate voltage; cf. Eq. (9). They scale approximately as the cube and the fourth power of the ratio of the displacement amplitude to the distance between the resonator and the relevant electrodes.

The nonlinearity can also result from electron-vibrational coupling (Lassagne *et al.*, 2009; Steele *et al.*, 2009; Meerwaldt *et al.*, 2012; Yang *et al.*, 2016; Moskovtsev and Dykman, 2017). Measurements on nanomechanical and micromechanical systems showed that the dependence of the vibration frequency on the amplitude, the so-called backbone curve, can be more complicated than Eq. (48) (Kacem and Hentz, 2009; Polunin *et al.*, 2016; Samanta, Arora, and Naik, 2018; Huang *et al.*, 2019; Ochs *et al.*, 2021a). This indicates that, in some cases, the restoring force can be proportional to higher powers of the displacement. The backbone curve can become nonmonotonic. At the extrema the vibration frequency is independent of the amplitude, leading to the so-called zero-dispersion phenomena (Soskin, Mannella, and McClintock, 2003).

The backbone curve of weakly damped modes, i.e., the relation between the frequency of the mode and the vibration amplitude, can be measured directly in the ringdown measurement. It is based on exciting vibrations to a comparatively large amplitude and measuring their frequency and amplitude as functions of time as the amplitude decays; see Figs. 9(a)–9(c) (Londoño, Neild, and Cooper, 2015; Polunin *et al.*, 2016; Güttinger *et al.*, 2017). This method applies where the nonlinearity is comparatively strong, so the overall frequency change is much larger than the decay rate.

Nanomechanical resonators usually have several well-resolved low-frequency eigenmodes at a time. They can be flexural or torsional modes or standing acoustic waves (Westra *et al.*, 2010; Barnard *et al.*, 2012; Castellanos-Gomez *et al.*, 2012; Eichler *et al.*, 2012; Mahboob *et al.*, 2013; Matheny *et al.*, 2013; Yamaguchi and Mahboob, 2013; Hanay *et al.*, 2015; Mathew *et al.*, 2016). They are nonlinearly coupled. The nonlinearity of the elasticity and of the capacitance are the



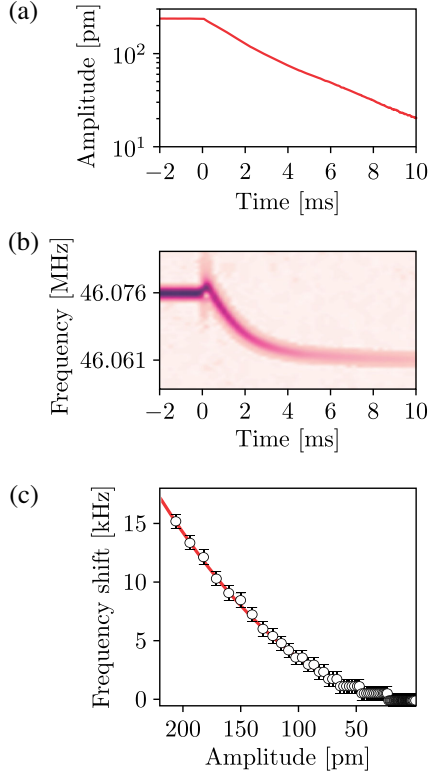


FIG. 9. Duffing backbone curve measured in a multilayer graphene drum. (a) Ringdown measurement. At time  $t = 0$ , the mechanical driving force is switched off and the vibrational amplitude starts to decay. (b) Time dependence of the short-time Fourier transform of the vibrations during the ringdown measurement. (c) Frequency shift as a function of vibrational amplitude. The solid red line is the quadratic dependence expected from Eq. (48). Adapted from Güttinger *et al.*, 2017.

leading sources of this coupling. For flexural modes this is seen in Eq. (49) if one takes into account the fact that  $X(z)$  is a sum of the displacements of different modes. In the case of nanobeams one should also take into account that nonlinear tension comes from modes that involve displacements in different directions. This is done by adding  $(\partial Y/\partial z)^2$  to  $(\partial X/\partial z)^2$  in Eq. (49) (Landau and Lifshitz, 1986). Similarly, the capacitance of the circuit that incorporates a resonator depends on different contributions to the displacement that come from different modes, leading to the mode coupling. A broad range of experiments have also been done on the modes in coupled nanoresonators (Buks and Roukes, 2002; Mahboob and Yamaguchi, 2008a; Karabalin, Cross, and Roukes, 2009; Okamoto *et al.*, 2009; Karabalin *et al.*, 2011; Mahboob, Mounaix *et al.*, 2014; Deng *et al.*, 2016; Dong, Dykman, and Chan, 2018).

The nonlinear part of the energy of the multimode nanoresonator is

$$U_{\text{nl}}(q_1, q_2, \dots) = \frac{1}{3}M \sum \beta_{n_1 n_2 n_3} q_{n_1} q_{n_2} q_{n_3} + \frac{1}{4}M \sum \gamma_{n_1 n_2 n_3 n_4} q_{n_1} q_{n_2} q_{n_3} q_{n_4} + \dots, \quad (50)$$

where the subscripts  $n_{1,2,3,4}$  enumerate the modes and summation over these subscripts is implied. The mass  $M$  here is

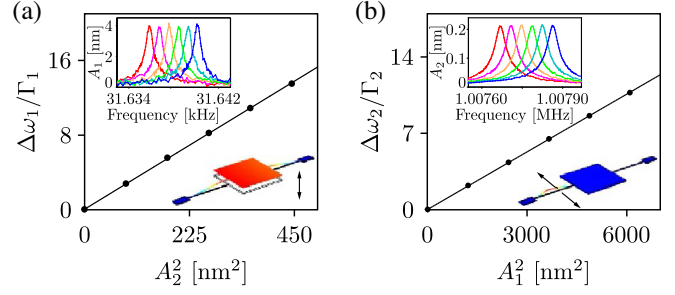


FIG. 10. Quadratic dependence of the shift of the mode frequency on the amplitude of another mode. The quadratic dependence indicates the dispersive mode coupling expected in Eq. (51). The resonator made of polycrystalline silicon consists of a plate supported on its opposite sides by two beams. Mode 1 involves the translational motion of the plate with both beams bending in the same direction, whereas only one of the beams vibrates in mode 2. Insets: spectra of the linear response of modes 1 and 2 upon increasing  $A_2^2$  and  $A_1^2$  (from left to right), respectively. Note the strong difference in the mode eigenfrequencies and decay rates. Adapted from Sun *et al.*, 2016.

chosen as an effective mass of one of the modes; cf. the discussion following Eq. (1).

For comparatively weak nonlinearity, the major effects of the nonlinear mode coupling can be conditionally separated into resonant and dispersive. Nonlinear resonant effects occur where a linear combination of the frequencies of several modes or their overtones is equal or close to the frequency of another mode or its overtone (Antonio, Zanette, and Lopez, 2012; Eichler *et al.*, 2012; Samanta, Yasasvi Gangavarapu, and Naik, 2015; De Alba *et al.*, 2016; Güttinger *et al.*, 2017; Czaplewski *et al.*, 2018; Houri *et al.*, 2019). The manifestations of the resonant couplings are discussed in Sec. VIII.

The dispersive coupling is important, on the other hand, where the mode frequencies are different and resonant conditions do not hold. The primary consequence of such coupling is the dependence of the vibration frequency of one mode on the amplitudes of other modes or, in quantum terms, the dependence of the spacing between the energy levels of one mode on the occupation numbers of the other modes (Ivanov, Kvashnina, and Krivoglaz, 1965; Dykman and Krivoglaz, 1971, 1973; Santamore, Doherty, and Cross, 2004; Westra *et al.*, 2010; Matheny *et al.*, 2013; Gloppe *et al.*, 2014; Miao *et al.*, 2014; Sun *et al.*, 2016; Gokhale and Gorman, 2017; Maillet *et al.*, 2017; Ari *et al.*, 2018; Gisler *et al.*, 2021). As in Eq. (48), if the amplitudes of the modes are  $A_m$ , the change  $\delta\omega_n$  of the frequency of the mode  $n$  due to the dispersive coupling described by the quartic in  $q_{n_i}$  terms in Eq. (50) is

$$\delta\omega_n = \frac{3}{4\omega_n} \sum'_m \gamma_{nnmm} A_m^2, \quad (51)$$

where the prime indicates that  $m \neq n$  in the sum over  $m$ .

Figure 10 shows measurements on two coupled NVS modes featuring the characteristic quadratic dependence of the shift of the eigenfrequency of one mode on the amplitude of the other mode. Dispersive coupling can also be measured

between modes of different natures, such as the flexural mode of a graphene drum and its optical phonon modes (Zhang, Makles *et al.*, 2020).

We note that the parameters  $\gamma_{nnmm}$  here have corrections  $\propto \beta_{nmk}^2$  due to the cubic in  $q_{ni}$  terms in Eq. (50), and also due to nonlinear coupling to phonons (Dykman and Krivoglaz, 1971, 1973). These are the renormalized parameters  $\gamma_{nnmm}$  that are accessible to the experiment, which are akin to the electron  $g$  factor renormalized due to the coupling to the electromagnetic field.

## B. Mechanisms of nonlinear friction

A basic microscopic mechanism of nonlinear friction in mesoscopic vibrational systems is a decay process in which two quanta of the considered mode scatter into excitations of a thermal reservoir (Dykman and Krivoglaz, 1975). The corresponding process is sketched in Figs. 7(c) and 7(d) [see also Fig. 32(b)]. An important contribution to nonlinear friction of low-frequency nanomechanical modes can come from the processes described using the quartic nonlinearity. In such processes, a thermal phonon with frequency  $\omega_\kappa \gg 2\omega_0$  is scattered off the considered nanomechanical mode with frequency  $\omega_0$  into another high-frequency phonon; see Fig. 7(d). Since the density of states of thermal phonons is often much higher than of the phonons with frequencies  $\approx \omega_0$ , these processes may be the leading cause of nonlinear friction. The frequency difference  $2\omega_0$  between the involved thermal phonons can be smaller than their decay rate. This complicates the analysis and makes it similar, to some extent, to the analysis of the thermoelastic or Akhiezer relaxation for linear friction (Atalaya *et al.*, 2016). Another contribution to nonlinear friction was discussed for nonlinear leakage of the flexural modes into bulk acoustic modes (Croy *et al.*, 2012), the nonlinear friction analog of standard clamping losses.

A general formulation of the theory of nonlinear friction is similar to that of the linear friction in Sec. IV (Dykman and Krivoglaz, 1975). The relevant Hamiltonian of the coupling of the mode to a thermal bath is quadratic in the mode coordinate to allow for processes where two vibrational quanta of the mode are created or annihilated,

$$H_i^{(nl)} = q^2 h_b^{(nl)}. \quad (52)$$

Here  $h_b^{(nl)}$  depends on the dynamical variables of the bath. As in the analysis of linear friction, one can express the coefficient of nonlinear friction  $\Gamma^{(nl)}$  in terms of the susceptibility of the bath with respect to the mode  $\chi_b^{(nl)}(\omega)$ ,

$$\Gamma^{(nl)} = \hbar^{-1} q_0^4 \text{Im} \chi_b^{(nl)}(2\omega_0), \quad q_0 = (\hbar/2M\omega_0)^{1/2}. \quad (53)$$

The susceptibility  $\chi_b^{(nl)}(\omega)$  is related by the fluctuation-dissipation relation (17) to the power spectrum  $S_b^{(nl)}(\omega)$  of the coupling  $h_b^{(nl)}$  calculated while disregarding the effect of the mode on the bath,

$$S_b^{(nl)}(\omega) = \int_{-\infty}^{\infty} dt e^{i\omega t} \langle h_b^{(nl)}(t) h_b^{(nl)}(0) \rangle.$$

If the fluctuation spectrum  $S_b^{(nl)}(\omega)$  is flat over a broad frequency range that significantly exceeds  $2\omega_0$ , the classical dynamics of the mode is the Brownian motion described by Eq. (2) with an additional term of the van der Pol friction force

$$f_{\text{vdP}} = -4M\Gamma^{(nl)}(q/q_0)^2 \dot{q}. \quad (54)$$

In the classical temperature range  $k_B T \gg \hbar\omega_0$  from Eq. (53),  $\Gamma^{(nl)} \propto q_0^4/\hbar \propto \hbar$ , and therefore  $\hbar$  drops out of the nonlinear friction coefficient  $\Gamma^{(nl)}/q_0^2$ . Important for a phenomenological description of nonlinear friction is that the thermal noise that comes along with the friction force  $f_{\text{vdP}}$  in Eq. (2) depends on the mode coordinate.

In the case of weakly damped modes, which is of interest for nanomechanics, the dynamics can be understood without requiring  $S_b^{(nl)}(\omega)$  to be flat over the range from  $\omega = 0$  to  $\omega \gg 2\omega_0$ . It suffices that  $S_b^{(nl)}(\omega)$  is smooth in the range centered at  $2\omega_0$  with a width that largely exceeds  $\Gamma, \Gamma^{(nl)}$ . The classical motion can be described using the slowly varying complex amplitude  $u(t)$  [Eq. (20)]; again, here we assume that the polaronic frequency shift has been incorporated into  $\omega_0$ . Instead of Eq. (21), the equation for  $u(t)$  now reads (Dykman and Krivoglaz, 1984)

$$\dot{u} = -\Gamma u - \left( \frac{2\Gamma^{(nl)}}{q_0^2} - i \frac{3\gamma}{2\omega_0} \right) u |u|^2 + \xi(t) + u^* \xi^{(nl)}(t), \quad (55)$$

where  $\xi^{(nl)}(t)$  is white Gaussian noise,  $\langle \xi^{(nl)}(t) [\xi^{(nl)}(t')]^* \rangle = (4\Gamma^{(nl)} k_B T / \hbar \omega_0) \delta(t - t')$  [we use the Stratonovich convention (Risken, 1996) for the multiplicative noise  $u^*(t) \xi^{(nl)}(t)$ ]. The nonlinear friction term in Eq. (55) has the same form for both the van der Pol and Rayleigh phenomenological nonlinear friction forces. We emphasize that if the nonlinear friction comes from the coupling to a thermal reservoir, the associated noise term necessarily depends on the dynamical variables of the mode, as seen in the last term in Eq. (55).

Along with the nonlinear friction, we have included the Duffing nonlinearity in Eq. (55); cf. Appendix A.1. The coupling to the bath of the form of Eq. (52) leads to a renormalization of the Duffing parameter  $\gamma$  (Dykman and Krivoglaz, 1975), which we assume to have been done.

Nonlinear friction in nanomechanical resonators was first measured in driven spectra by exciting the system to a comparatively large vibration amplitude (Eichler, Moser *et al.*, 2011; Zaitsev *et al.*, 2012). This friction notably results in a mechanical linewidth that changes as the vibration amplitude is increased. It can also be observed in ringdown measurements (Polunin *et al.*, 2016), where the decay rate varies as the vibration amplitude gets lower. The systems featuring nonlinear friction include carbon nanotubes as well as single-layer and multilayer graphene resonators (Eichler, Moser *et al.*, 2011; Miao *et al.*, 2014; Singh *et al.*, 2016; Güttinger *et al.*, 2017; Dolleman *et al.*, 2018; Keşkekler *et al.*, 2021), PdAu nanobeams (Zaitsev *et al.*, 2012), silicon MEMS (Nabholz *et al.*, 2018), and Si<sub>3</sub>N<sub>4</sub> membranes with engineered modes (Catalini *et al.*, 2021). A strong nonlinear friction was observed in a micromechanical resonator submerged into liquid helium at ultralow temperatures; it was related to the

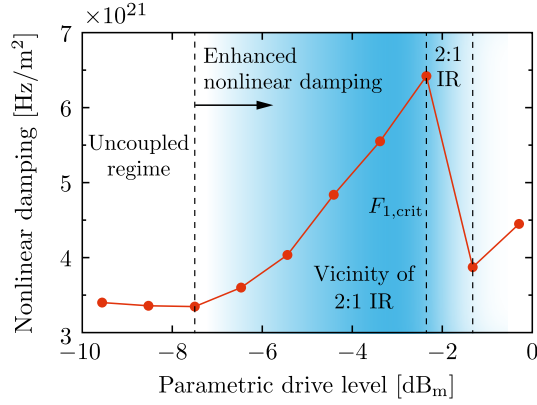


FIG. 11. Effective nonlinear damping coefficient of a parametrically driven mode when its vibration frequency is close to half the eigenfrequency of a second mode, i.e., near the 2:1 internal resonance (IR). Adapted from Keşkekler *et al.*, 2021.

amplitude-dependent attachment of vortices and provided a probe of quantized vorticity (Barquist *et al.*, 2020). Nonlinear friction plays an important role in the dynamics of coupled resonators when they are driven into the regime of self-sustained vibrations (Mahboob *et al.*, 2015, 2016). It also strongly affects parametric resonance (Lin, Nakamura, and Dykman, 2015), and related features can be used to develop new types of phase-locked loops (Miller *et al.*, 2019). Another application demonstrated by Chen, Zanette *et al.* (2016) is self-sustained micromechanical vibrations in a system with linear feedback.

As seen in Eq. (53), nonlinear friction is comparatively large if the power spectrum of the thermal bath, and thus the susceptibility  $\text{Im}\chi_b^{(nl)}(\omega) \propto S_b^{(nl)}(\omega)$ , is large for  $\omega \approx 2\omega_0$ . This happens if the considered mode is coupled to a mode with frequency close to  $2\omega_0$  and a relaxation rate much higher than  $\Gamma, \Gamma^{(nl)}$ . The nonlinear friction in this case corresponds to a process where two quanta of the considered mode scatter into a quantum of the second mode.

Figure 11 shows an experiment demonstrating the effect (Keşkekler *et al.*, 2021). The effective nonlinear friction of the parametrically driven lowest mode of a graphene nanodrum is seen to strongly increase with the drive amplitude, and thus with the vibration amplitude, where the drive frequency  $\omega_p \approx 2\omega_0$  was close to the eigenfrequency of the next lowest drum modes. In this system the inequality between the relaxation rates was not sufficiently strong, and to describe the observations it was necessary to go beyond the approximation of linear response of the higher-frequency mode underlying Eq. (53). This explains the behavior of the effective nonlinear damping in Fig. 11.

Nonlinear friction can be engineered by parametrically driving coupled mechanical modes at proper combination frequencies. The friction coefficient can be made not only positive but also negative, depending on the drive frequency (Dong, Dykman, and Chan, 2018). In microwave electromagnetic cavities, a positive nonlinear friction was engineered in order to create long-lived coherent quantum states, including cat states that can encode qubit states (Leghtas *et al.*, 2015; Touzard *et al.*, 2018).

### C. Effect of the nonlinearity on the spectra

As previously indicated, for underdamped vibrational systems the effects of the vibration nonlinearity become pronounced where the nonlinear part of the restoring or dissipative force is comparable to the linear friction force, while all these forces are much smaller than the linear restoring force  $-M\omega_0^2 q$ . The vibrations remain close to sinusoidal. However, the change of the dynamics can be dramatic. It is determined by the nontrivial interplay of the nonlinearity and linear damping.

#### 1. Spectral effects of the Duffing nonlinearity

For vibration amplitudes that are not too large, the primary effect of the conservative nonlinearity is the dependence of the vibration frequency on the mode amplitude [Eq. (48)] or mode amplitudes for coupled modes [Eq. (51)]. Owing to this dependence, the amplitude fluctuations of the mode (or, in quantum terms, fluctuations of the state populations) are converted into eigenfrequency fluctuations. This leads to spectral broadening and the overall change of the shape of the spectra, making the spectra profoundly non-Lorentzian. The theory of the spectra was first considered in several limiting cases in the quantum regime by Ivanov *et al.* (1966). Later a full classical and quantum theory was developed by Dykman and Krivoglaz (1971, 1973). Experimentally, the Duffing nonlinearity-induced evolution of the spectra with the varying fluctuation intensity was explored in different types of systems, such as silicon nitride nanobeams (Maillet *et al.*, 2017), levitated silica nanoparticles (Gieseler, Novotny, and Quidant, 2013; Amarouchene *et al.*, 2019), and a micro-mechanical trampoline resonator (Huang *et al.*, 2019). Maillet *et al.* (2017) studied not only the evolution of the power spectrum of nanoelectromechanical systems (NEMS) with varying noise intensity but also the in-phase and quadrature components of forced vibrations, which give the imaginary and real parts of the susceptibility of a mode with Duffing nonlinearity.

The classical physics of the effect can be readily understood (Dykman and Krivoglaz, 1971) by noting that the vibration amplitude fluctuates. In the harmonic approximation, the energy of the mode is  $M\omega_0^2 A^2/2$ , where  $A$  is the vibration amplitude. The mean-square amplitude in thermal equilibrium is  $\langle A^2 \rangle = 2k_B T/M\omega_0^2$ . The amplitude fluctuations lead to the spread of the vibration frequency. From Eq. (48), we determine that this spread, i.e., the characteristic magnitude of the frequency fluctuations, is  $\delta\bar{\omega}_0 = 3|\gamma|\langle A^2 \rangle/8\omega_0$ . A critically important parameter is the relation between  $\delta\bar{\omega}_0$  and the decay rate  $\Gamma$ , i.e., the parameter

$$\alpha_0 = \overline{\delta\omega_0}/2\Gamma = 3\gamma k_B T/8M\omega_0^3 \Gamma. \quad (56)$$

Equation (56) can be called the motional narrowing parameter to draw a similarity (although somewhat indirect) to the motional narrowing effect in nuclear magnetic resonance (Anderson, 1954; Kubo, 1954).

Indeed, the parameter  $\Gamma^{-1}$  is the correlation time of the amplitude fluctuations in the absence of nonlinear friction [cf. Eqs. (21) and (55)], and thus the correlation time of the



frequency fluctuations due to the Duffing nonlinearity. For  $|\alpha_0| \ll 1$  the correlation time is small compared to the time  $(\delta\omega_0)^{-1}$ . The frequency fluctuations are then averaged out and  $\delta\omega_0$  gives a characteristic shift of the mode frequency, while the width of the spectrum is determined primarily by the decay rate  $\Gamma$ . This is similar to the fast averaging of fluctuations that underlies nuclear magnetic resonance in liquids.

On the other hand, for  $|\alpha_0| \gg 1$  the spectrum of the oscillator can be thought of as a superposition of “partial spectra” centered at the frequencies  $\omega_0 + \delta\omega_0$  that depend on the instantaneous value of the amplitude  $A$ . The multitude of the frequencies is an analog of the inhomogeneous broadening in solid-state spectroscopy. The contribution of a partial spectrum at frequency  $\omega_0 + \delta\omega_0$  to the entire spectrum is determined by the probability density of having a given  $\delta\omega_0$ , which is determined by the Boltzmann distribution over  $\delta\omega_0 \propto A^2$ . The overall width of the spectrum is  $\sim \delta\omega_0 \gg \Gamma$ ; i.e., the spectral width is determined by the nonlinearity, not the decay, and the spectrum is strongly non-Lorentzian and asymmetric. The quantum picture is discussed in Appendix E.

The intermediate range  $|\alpha_0| \sim 1$  is the most interesting theoretically, as it shows how the partial spectra of the limit  $|\alpha_0| \gg 1$  shrink and deform with the decreasing nonlinearity or fluctuation intensity. Somewhat surprisingly, the spectrum is nevertheless described using a simple explicit expression in both the classical and quantum domains (Dykman and Krivoglaz, 1971, 1973); see Appendix E. Figure 35 shows the evolution of the spectrum with the varying  $\alpha_0$ .

Dispersive nonlinear coupling between the modes affects the spectrum in a similar way (Dykman and Krivoglaz, 1971, 1973). As seen in Eq. (51), the typical spread of the frequency of mode  $n = 0$  due to fluctuations of the amplitude of mode  $m > 0$  is  $\overline{\delta\omega_0} = 3|\gamma_{00mm}| \langle A_m^2 \rangle / 4\omega_m$ . The correlation time of the relevant fluctuations is the reciprocal decay rate  $\Gamma_m^{-1}$  of the mode  $m$ . Therefore, for  $\overline{\delta\omega_0} \gtrsim \Gamma_m$  the spectrum is broadened and becomes non-Lorentzian; see Appendix E. The corresponding spectral broadening has been suggested as a major broadening mechanism for flexural modes in carbon nanotubes (Barnard *et al.*, 2012), graphene sheets (Miao *et al.*, 2014), doubly clamped beams (Venstra, Leeuwen, and Zant, 2012; Matheny *et al.*, 2013), and microcantilevers (Vinante, 2014).

Figure 12 presents experimental results, which show how the power spectrum and the real and imaginary parts of the susceptibility are changed with the varying noise intensity. Figure 12(a) refers to the case where the dispersive coupling to other modes is small. The spectrum is determined by the internal mode nonlinearity and its shape evolves from a Lorentzian to a strongly asymmetric peak with the increasing  $\alpha_0$ . Figure 12(b), on the other hand, illustrates the effect of nonlinear dispersive mode coupling. The internal Duffing nonlinearity could be disregarded. The shape of the spectrum depends on the scaled coupling parameter  $\alpha_1 = 3\gamma_{0011}k_B T / 4M\omega_0\omega_1^2\Gamma_1$ .

Interesting behavior occurs where the number of modes dispersively coupled to the considered mode is large, even though the coupling to each mode taken separately is small. In this case the power spectrum  $S(\omega)$  may become Gaussian in its central part (Zhang and Dykman, 2015), as first found numerically by Barnard *et al.* (2012); see Appendix E.4.

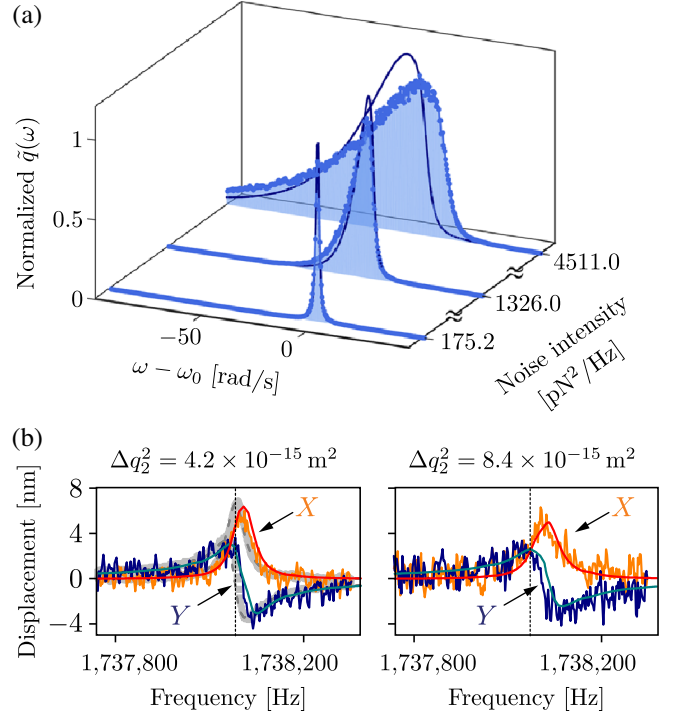


FIG. 12. (a) Evolution of the spectrum of a micromechanical trampoline resonator with the Duffing nonlinearity (46) upon increasing the effective temperature determined by the applied broadband noise. When the noise intensity is small, the spectrum is Lorentzian. At large noise intensity, the spectrum becomes highly asymmetric due to the interplay between the noise and the Duffing nonlinearity. At still larger noise intensities it was necessary to take into account higher-order nonlinearity. The solid lines correspond to the spectra expected without any free parameters. Adapted from Huang *et al.*, 2019. (b) In-phase and quadrature components of a weakly driven nanomechanical mode dispersively coupled to a fluctuating mode  $m = 2$  for different values of the mean-square displacement  $\Delta q_2^2$ . The displacement fluctuations of the  $m = 2$  mode are driven by electric noise. When these fluctuations are small, the response of the measured mode (gray data points) is symmetric with respect to the resonant frequency (vertical dashed line). For large fluctuations, the response becomes asymmetric. Adapted from Maillet *et al.*, 2017. The solid lines in (a) and (b) are calculations with no free parameters.

Dispersive coupling could be used for quantum nondemolition measurements of phonons (Santamore *et al.*, 2004). In such a measurement, the number of phonons of one mode would be continuously measured by recording the resonant frequency of the second mode. A realization of such an experiment in nanomechanics is challenging since it requires strong dispersive coupling compared to the decay rates of the modes.

## 2. Dispersive coupling of a nanomechanical mode to a qubit

A promising direction of nanomechanics is the study of the effects of coupling of nanomechanical vibrations to controllable two-level systems, qubits. The involved physics is closely related to the physics of the electronic states of defects coupled to phonons in solids (Stoneham, 2001), with N-V

centers being one of the defects of utmost current interest. Coupling nanomechanical modes to qubits opens a path toward studying the electron-phonon effects with unprecedented control. It also provides new means to manipulate and measure the quantum states of mechanical resonators operating in the gigahertz range (O'Connell *et al.*, 2010; Gustafsson *et al.*, 2014; Chu *et al.*, 2018; Satzinger *et al.*, 2018; Bienfait *et al.*, 2019). Compared to superconducting resonators, gigahertz mechanical resonators can have longer lifetimes (MacCabe *et al.*, 2020) and are usually much more compact (Safavi-Naeini *et al.*, 2019). These systems hold promise for scalable qubit architectures where quantum information is stored in bosonic systems (Ofek *et al.*, 2016; Hann *et al.*, 2019; Lescanne *et al.*, 2020).

In the systems studied thus far, the qubit-mode coupling energy was smaller than the mode level spacing  $\hbar\omega_0$ . In this case, if the level spacing of the qubit  $\hbar\omega_{\text{qbt}}$  is significantly different than  $\hbar\omega_0$ , of primary interest is the study of the dispersive coupling. This coupling has attracted significant attention in solid-state physics (Sild and Kristjan, 1988). If the qubit is described as a spin-1/2 system with the Hamiltonian  $H_{\text{qbt}} = \hbar\omega_{\text{qbt}}\sigma_z/2$ , where  $\sigma_z$  is the Pauli matrix, the dispersive coupling to the nanomechanical mode has the form

$$H_i^{\text{qbt}} = \frac{1}{2}\hbar\gamma_{\text{qbt}}\sigma_z q^2, \quad (57)$$

where  $\gamma_{\text{qbt}}$  determines the coupling energy.

The ensuing physics is similar to the physics of dispersively coupled vibrational modes. Thinking of the mode vibrations classically, one can see that the coupling-induced change of the qubit transition frequency is determined by the vibration amplitude  $A$ ,

$$\delta\omega_{\text{qbt}} = \frac{1}{2}\gamma_{\text{qbt}}A^2.$$

In the classical limit  $k_B T \gg \hbar\omega_0$ , the shape of the qubit spectrum is determined by the ratio of the characteristic value of the frequency shift  $\bar{\delta\omega}_{\text{qbt}} = \gamma_{\text{qbt}}k_B T/M\omega_0^2$  to the reciprocal correlation time of the frequency fluctuations  $\Gamma$ , going from the “motional narrowing” regime where this ratio is small to the “inhomogeneous broadening” regime where it is large.

In the quantum regime,  $\delta\omega_{\text{qbt}}$  takes on discrete values that correspond to different occupation numbers  $n_0$  of the vibrational mode,

$$\delta\omega_{\text{qbt}}(n_0) = (\hbar\gamma_{\text{qbt}}/M\omega_0)(n_0 + 1/2). \quad (58)$$

If  $\hbar\gamma_{\text{qbt}}/M\omega_0 \gg \Gamma(2\bar{n} + 1)$ , the lines at  $\omega_{\text{qbt}} + \delta\omega_{\text{qbt}}(n_0)$  with different  $n_0$  weakly overlap. This leads to a fine structure of the qubit spectrum and enables one to identify the population of the mode Fock states  $|n_0\rangle$ . The shape of the lines of the fine structure is close to Lorentzian, with a half-width  $\Gamma_{\text{qbt}} + 2\Gamma[\bar{n}(2n_0 + 1) + n_0]$  that linearly increases with  $n_0$ , which is similar to the case of dispersively coupled modes; cf. Eqs. (E4)–(E7). Here  $\Gamma_{\text{qbt}}$  is the half-width of the qubit spectral line in the absence of coupling to the mode. This regime is an analog of the inhomogeneous broadening.

If  $\hbar\gamma_{\text{qbt}}/M\omega_0 \lesssim \Gamma(2\bar{n} + 1)$ , the lines with different  $n_0$  overlap. In this case quantum mechanics does not allow

one to identify individual Fock states from the spectrum. As explained in Appendix E, the amplitudes of the transitions with different  $n_0$  are coupled. The overall qubit spectrum shrinks with a decreasing  $\hbar\gamma_{\text{qbt}}/M\omega_0\Gamma$ . When this parameter is small the contribution of the dispersive coupling to the half-width of the qubit spectrum is  $(\hbar\gamma_{\text{qbt}}/M\omega_0\Gamma)^2\Gamma\bar{n}(\bar{n} + 1)/2$  (Krivoglaz, 1965). For systems in thermal equilibrium, the spectrum for an arbitrary  $\hbar\gamma_{\text{qbt}}/M\omega_0\Gamma$  was described by

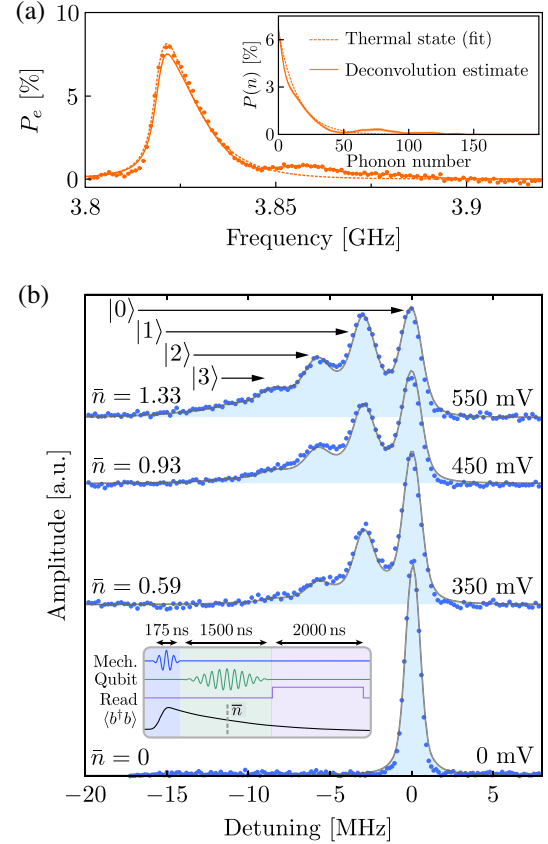


FIG. 13. (a) Spectroscopy of the qubit coupled to the micro-mechanical oscillator (at thermal equilibrium) in a dilution fridge. The qubit excited state probability is measured as a function of frequency of a weak microwave drive. The asymmetry of the peak indicates an oscillator occupation number that is low but significantly larger than 1. The oscillator vibrates at 25 MHz, whereas the qubit frequency is 3.82 GHz. The coupling parameter  $\gamma_{\text{qbt}}$  is positive. Inset: phonon populations extracted from the spectrum with a fit assuming a thermal distribution (dashed line) or with a Bayesian-based deconvolution algorithm (full line). Adapted from Viennot, Ma, and Lehnert, 2018. (b) Pump-probe measurement consisting of a short phonon excitation pulse followed by a longer qubit spectroscopy pulse. The detuning on the horizontal axis is relative to the qubit frequency  $\omega_{\text{qbt}} = 2.317$  GHz in the absence of a phonon excitation pulse; the mechanical oscillator vibrates at 2.405 GHz. The coupling parameter  $\gamma_{\text{qbt}}$  is negative. The initial phonon populations are prepared by the pulse decay over the course of the measurement but are nevertheless visible as individual peaks separated by  $\hbar\gamma_{\text{qbt}}/M\omega_0$ . The blue points are data and the solid lines are a fit using numerical master-equation simulations. Adapted from Arrangoiz-Arriola *et al.*, 2019.

Dykman and Krivoglaz (1987). Using a qubit to study the vibration-number statistics in the case of a driven mode was considered by Clerk and Utami (2007).

In Fig. 13 we present the results of the measurements of the spectrum of Josephson junction qubits coupled to a membrane resonator (Viennot, Ma, and Lehnert, 2018) and to a high-frequency phononic crystal defect (Arrangoiz-Arriola *et al.*, 2019). In the first system the regime was studied where a large number of vibrational states was occupied, whereas in the second system it was possible to reach small occupation numbers and resolve the fine structure of the spectrum.

Note that the experiments by Arrangoiz-Arriola *et al.* (2019) and some of the experiments by Viennot, Ma, and Lehnert (2018) were performed when the vibrational system was away from thermal equilibrium. A full analysis of the spectrum in this case requires one to take into account the coupling of the complex amplitudes of transitions between the states of the mode in the transient regime (Dykman, 1975; Zhang and Dykman, 2017).

### 3. Broadening of the power spectrum due to nonlinear friction

Like conservative nonlinearity, nonlinear friction also leads to a broadening and a change of the shape of the oscillator power spectrum (Dykman and Krivoglaz, 1975). The effect depends on temperature even when the nonlinear friction coefficient  $\Gamma^{(nl)}$  defined by Eq. (53) is temperature independent. In the classical limit, this is already clear from Eq. (55). Indeed, the nonlinear friction force increases with an increasing vibration amplitude. Therefore, as the mean-square amplitude increases with an increasing temperature, so does the nonlinear friction force.

Equation (55) shows that, since in thermal equilibrium  $\langle |u|^2 \rangle = k_B T / 2M\omega_0^2$ , the characteristic parameter of nonlinear friction in the classical theory is  $2\Gamma^{(nl)}k_B T / \hbar\omega_0$ . The evolution of the spectrum with the varying ratio  $\gamma^{(nl)} \equiv 2\Gamma^{(nl)}k_B T / \hbar\omega_0\Gamma$  is shown in Fig. 36. If the vibration frequency does not depend on the amplitude, the spectrum remains symmetric, but it becomes profoundly non-Lorentzian. Its width increases with increasing nonlinear friction, and thus with increasing temperature.

Generally, both nonlinear friction and conservative nonlinearity are present in NEMS and MEMS. Their interplay leads to characteristic features in the spectrum that should allow one to identify the presence of both mechanisms (Dykman and Krivoglaz, 1975). An important indicator of the effect of the conservative nonlinearity that has been seen in experiments is an asymmetry of the spectrum. We are not aware of experiments where a change of the spectrum due to nonlinear friction would have been established. Contrast this with the observation of nonlinear friction in strongly driven systems described in Sec. VI.B.

## VII. NONLINEAR RESONANT PHENOMENA: A LABORATORY FOR STUDYING PHYSICS FAR FROM THERMAL EQUILIBRIUM

Nonlinear resonant response of vibrational modes to an external drive leads to several groups of phenomena, which are of interest in nanomechanics but also make

nanomechanics a testing ground for such diverse areas as statistical physics far from thermal equilibrium, nonlinear dynamics, and quantum cavity or circuit electrodynamics. This is because, for the characteristic small damping, the response already becomes nonlinear for comparatively weak resonant driving. This allows one to study nonlinear effects in a well-controlled fashion over a broad parameter range.

### A. Bistability of resonantly excited vibrations

One of the simplest yet richest nonlinear effects studied in nanomechanics is hysteresis of the vibrations excited by applying a close to resonant driving force. The hysteresis emerges when the frequency  $\omega_F$  or the amplitude  $F$  of a moderately strong drive is swept across a certain range. The onset of hysteresis is a consequence of coexistence of two stable vibrational states of the nonlinear mode, i.e., of the mode bistability (Landau and Lifshitz, 2004). This hysteresis was observed in nanomechanical systems early on (Husain *et al.*, 2003). In most cases it is already well described using the simplest model of vibration nonlinearity, the Duffing model introduced in Sec. VI. In this section we concentrate on the nonlinear resonant response described using this model.

A phenomenological equation of motion (2) extended to include the close to resonance driving  $F \cos \omega_F t$  and the Duffing nonlinearity reads

$$M\ddot{q} + 2M\Gamma\dot{q} + M\omega_0^2 q + M\gamma q^3 = F \cos \omega_F t + f_T(t), \quad |\omega_F - \omega_0| \ll \omega_0. \quad (59)$$

Qualitatively, the occurrence of two stable vibrational states in the absence of noise can be inferred in the following way; cf. Fig. 14. Suppose the drive frequency  $\omega_F$  is close to the eigenfrequency  $\omega_0$  but the detuning  $|\omega_F - \omega_0|$  considerably exceeds the decay rate. One may then expect the amplitude of the forced vibrations to be comparatively small. It is given by the value  $A_1$  in Fig. 14. However, the nonlinearity leads to a

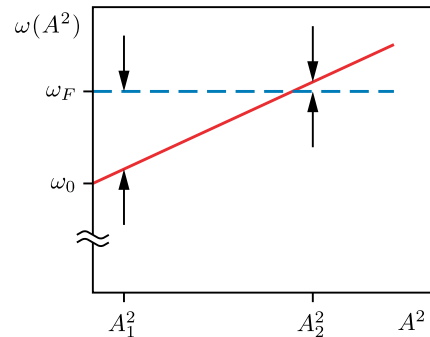


FIG. 14. Dependence of the vibration frequency on the vibration amplitude  $A$  for a comparatively small nonlinearity. Equation (48) indicates that the frequency linearly depends on  $A^2$ , and for the Duffing model  $\omega(A^2) - \omega(0) \approx 3\gamma A^2 / 8\omega(0)$  [note that  $\omega(0) \equiv \omega_0$ ]. When the mode is driven by a field at the frequency  $\omega_F$ , it can have stable vibrational states with comparatively small and comparatively large amplitudes  $A_1$  and  $A_2$ , for which  $\omega(A^2)$  is farther away from or closer to  $\omega_F$ .



change of the mode frequency  $\delta\omega_0$  with the mode amplitude, as described by Eq. (48). If the vibration amplitude is sufficiently large and takes on the value  $A_2$  in Fig. 14, the shifted frequency  $\omega_0 + \delta\omega_0$  can become close to  $\omega_F$  such that there is strong resonance. This resonance will make vibrations with the corresponding large amplitude self-consistent. This leads to two stable states: Forced vibrations can either have large amplitudes and be at good resonance or have small amplitudes and be detuned from the resonance.

Semiquantitatively, the onset of bistability can be understood using the susceptibility of the oscillator  $\chi(\omega)$ . By the definition of the susceptibility, the squared amplitude of the forced vibrations is  $A^2 = |\chi(\omega_F)|^2 F^2$ . If we now use for  $\chi(\omega)$  the familiar expression (5) for the susceptibility of a harmonic oscillator but replace the eigenfrequency  $\omega_0 \rightarrow \omega_0 + \delta\omega_0$  with  $\delta\omega_0$  given by Eq. (48), the resulting equation for the squared amplitude reads

$$A^2 = \frac{F^2}{(2M\omega_0)^2} \left[ \Gamma^2 + \left( \omega_F - \omega_0 - \frac{3\gamma A^2}{8\omega_0} \right)^2 \right]^{-1}. \quad (60)$$

Equation (60) describes the previous qualitative arguments of “tuning” the mode in and out of good resonance, i.e., varying the detuning  $\omega_F - \omega_0 - 3\gamma A^2/8\omega_0$  by changing  $A$ . Formally, Eq. (60) is a cubic equation for  $A^2$ , and it can have three solutions. The solutions with the smallest and the largest  $A^2$  can be shown to be stable (Landau and Lifshitz, 2004). The characteristic dependence of the amplitude  $A$  on the drive frequency detuning  $\omega_F - \omega_0$  for a nanowire measured by Kozinsky *et al.* (2007) is shown in Fig. 15(a).

The dynamics of a resonantly driven mode is conventionally described in terms of the in-phase and quadrature components  $Q$  and  $P$ , respectively. They correspond to the coordinate and momentum of the mode in the rotating frame,

$$\begin{aligned} q(t) &= Q \cos \omega_F t + P \sin \omega_F t, \\ p(t) &= M\omega_F (-Q \sin \omega_F t + P \cos \omega_F t). \end{aligned} \quad (61)$$

The dynamical variables  $Q$  and  $P$  are advantageous from the point of view of the experiment, as they can be directly measured with a lock-in amplifier by setting its frequency to  $\omega_F$ . We note that  $(Q - iP)/2$  has the same form as the complex amplitude  $u(t)$  introduced in Eq. (20) except that the frequency  $\omega_0$  in Eq. (20) is replaced by  $\omega_F$ . In terms of  $Q$  and  $P$ , the vibration amplitude is  $(Q^2 + P^2)^{1/2}$  and the phase is  $-\arctan(P/Q)$ . In a quantum description,  $Q$  and  $P$  are operators, with  $[Q, P] = i\hbar/M\omega_F$ .

The transient dynamics of the mode can be pictured in terms of the motion on the  $(Q, P)$  plane, which is the phase plane in the rotating frame; see Appendix D.1. The time evolution of  $Q$  and  $P$  is slow compared to the fast oscillations at frequency  $\omega_F$ . The stationary values of  $Q$  and  $P$  describe the stationary states of vibrations at frequency  $\omega_F$  in the laboratory frame, as seen in Eq. (61). These values correspond to points on the  $(Q, P)$  plane. If the mode has one stable vibrational state, there is one such point. In the range of bistability, there are three stationary states on the  $(Q, P)$  plane. Two of them correspond to the stable vibrational states with different amplitudes and phases, and the third one corresponds

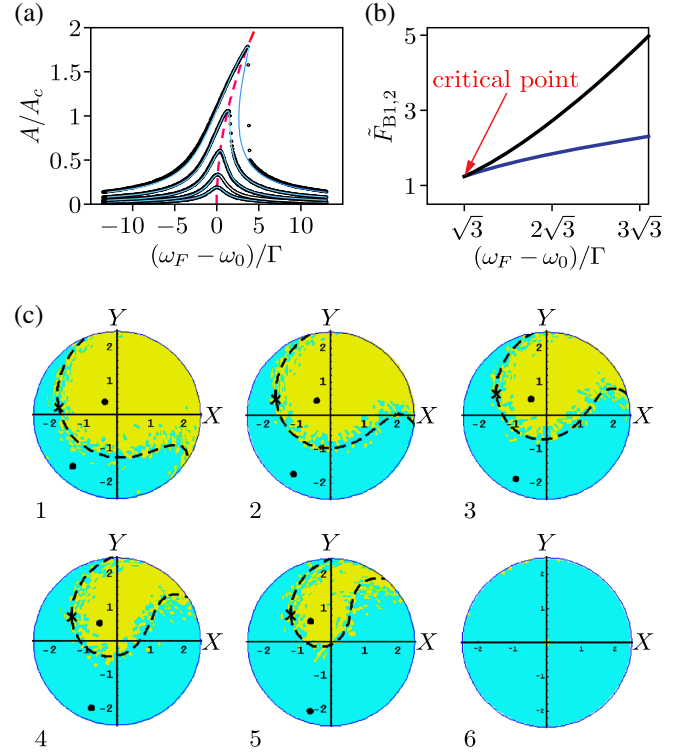


FIG. 15. (a) Vibration amplitude  $A$  of a resonantly driven platinum nanowire vs frequency for various driving powers, showing the onset of bistability. The curves refer to the drive amplitudes  $F/F_c = 0.249, 0.443, 0.788, 1.401, 2.492$ . The amplitudes  $A$  and  $F$  are normalized by their values  $A_c$  and  $F_c$  at the critical point in (b). (b) Bifurcation diagram of a resonantly driven Duffing oscillator; the scaled amplitude of the drive is  $\tilde{F} = (3\gamma/32\omega_F^3\Gamma^3)^{1/2}F$ . The bistability occurs in the interior of the region limited by the bifurcation curves  $\tilde{F}_{B1,2}(\omega_F)$  given by Eq. (D5). At the critical point  $\tilde{F}_{B1} = \tilde{F}_{B2} = \tilde{F}_c$  the three stationary vibrational states (two stable and one unstable) merge [ $\tilde{F}_c = (8/\sqrt{27})^{1/2}$ ]. (c) Basins of attraction of the platinum nanowire resonator at  $(\omega_F - \omega_0)/\Gamma = 4.26$  for increasing drive values:  $F/F_c = (1)1.867, (2)2.049, (3)2.237, (4)2.434, (5)2.640, (6)2.741$ . The variables  $X$  and  $Y$  are the scaled in-phase and quadrature components of the vibrations  $Q$  and  $P$  [Eq. (61)]. Blue and yellow regions indicate the initial states in which the system is prepared by driving it at the frequency  $\omega_F$  with a certain amplitude  $F$ . The amplitude is then switched to a value above  $F/F_c$  and the drive phase is adjusted. After that, the system goes to the final high- or low-amplitude stable state, depending on where it was prepared. The theoretical positions of the stable states and the saddle point and the separatrix curve are indicated by the black points, the black cross, and the dashed black curve, respectively. From Kozinsky *et al.*, 2007.

to an unstable state (a saddle point). The entire  $(Q, P)$  plane is divided into two regions: if prepared initially in one region, the mode evolves toward one stable state, whereas from the other region it evolves to the other stable state.

Kozinsky *et al.* (2007) directly mapped the  $(Q, P)$  plane of a driven nonlinear mode and identified the basins of attraction to different stable states using the vibrations of a doubly clamped platinum nanowire, which were actuated

and detected magnetomotively. The results are shown in Figs. 15(a) and 15(c).

The number of stable vibrational states changes at the bifurcation parameter values, i.e., at the bifurcation points. These points lie on the lines in the space of the parameters of the driving force  $(F, \omega_F)$ , as illustrated in Fig. 15(b). On the upper (black) line the small-amplitude state merges with the unstable state. The experimental results (Kozinsky *et al.*, 2007) in Fig. 15(c) show how, with an increasing driving amplitude, the small-amplitude state (state 1) approaches the unstable state (panels 1–5). Ultimately both of these states disappear (panel 6) and the mode has only one stable vibrational state.

A resonantly driven mode can display bistability if, in addition to conservative nonlinearity, the friction force is also nonlinear. In the presence of nonlinear friction, the decay rate is amplitude dependent. This can be described by replacing  $\Gamma \rightarrow \Gamma + \Gamma^{(\text{nl})}A^2/2q_0^2$  in Eq. (60). The dynamics of the mode in this case was studied by Buks and Yurke (2006).

## B. Parametric excitation

Vibrations of nanomechanical systems can also be resonantly excited using parametric pumping. The corresponding pumping can be described as the modulation of the vibration eigenfrequency  $\omega_0$  at a frequency  $\omega_p$  close to  $2\omega_0$ . If the modulation is weak (it does not excite vibrations), the equilibrium state  $q = p = 0$  is stable. However, a sufficiently strong modulation can make this state unstable. It leads to an onset of two stable vibrational states. In each of these states the system vibrates at the frequency  $\omega_p/2$ . The phases of the vibrations are fixed by the modulation parameters and differ by  $\pi$  in the different states. In optics terms, the system is sometimes called a degenerate parametric oscillator to emphasize that the vibration frequencies are the same in both states. Such parametrically excited vibrations arguably provide the simplest example of the onset of period doubling in a nonlinear system since their period is twice the period of the driving.

The condition for the onset of period-2 vibrations and their amplitude can be obtained using the same naive arguments that led to Eq. (60). Indeed, the simplest phenomenological equation of motion that describes parametric resonance reads

$$M\ddot{q} + 2M\Gamma\dot{q} + M\omega_0^2q + M\gamma q^3 = qF_p \cos \omega_p t + f_T(t), \quad |\omega_p - 2\omega_0| \ll \omega_0. \quad (62)$$

One can again relate the vibration amplitude to the force using the resonant susceptibility  $\chi(\omega_p/2)$ . However, the resonant force now has to be written with account taken of the fact that we are seeking vibrations of the form  $q(t) = A \cos[(\omega_p t/2) + \phi]$ , and therefore the resonant part of the force  $qF_p \cos \omega_p t$  is  $(AF_p/2) \cos[(\omega_p t/2) - \phi]$  (the phase  $\phi$  has to be found separately). Substituting this expression for the force into the equation for the amplitude gives  $A^2 = |\chi(\omega_p/2)|^2 (AF_p/2)^2$ . Using the same expression as in Eq. (60) for the susceptibility, we obtain that either  $A = 0$  (i.e., there are no vibrations) or

$$\frac{F_p^2}{(4M\omega_0)^2} \left[ \Gamma^2 + \left( \delta\omega_p - \frac{3\gamma A^2}{8\omega_0} \right)^2 \right]^{-1} = 1, \quad \delta\omega_p = (\omega_p/2) - \omega_0. \quad (63)$$

Equation (63) shows, in particular, that vibrations at the frequency  $\omega_p/2$  are excited provided that the modulation is sufficiently strong to overcome the dissipation ( $|F_p|/4M\omega_0 > \Gamma$ ). As in the case of the resonant driving discussed in Sec. VII.A, in the presence of nonlinear friction one should replace in Eq. (63)  $\Gamma \rightarrow \Gamma + \Gamma^{(\text{nl})}A^2/2q_0^2$ .

Equation (63) is a quadratic equation for  $A^2$ . It shows that, besides the zero-amplitude state where  $A = 0$ , the modulated mode can have either one or two pairs of period-2 states, depending on whether Eq. (63) has one or two positive roots  $A^2 > 0$ . The stability of these states and the overall dynamics of a parametrically modulated mode can be conveniently described by changing from  $q(t), p(t)$  to the quadratures  $Q(t), P(t)$ . The corresponding transformation is similar to Eq. (61),

$$q + ip/(M\omega_p/2) = (Q + iP) \exp(-i\omega_p t/2).$$

The equations for the quadratures  $Q, P$  are given in Appendix D.2. The stable period-2 states correspond to the symmetrically located fixed points on the phase plane  $(Q, P)$ .

The parameter ranges where a parametrically modulated mode has different numbers of coexisting states are separated by the bifurcation lines shown in Figs. 16(a) and 16(b). An example of the hysteretic behavior of parametrically modulated nanoresonators is shown in Fig. 16(c). The experimental data by Karabalin, Masmanidis, and Roukes (2010) shown in the figure were obtained using doubly clamped piezoelectrically controlled nanobeams. In the simplest case, the occurrence of the hysteresis is a consequence of nonlinear friction. As seen in Fig. 16(b), if one increases the frequency (the parameter  $\mu_p$ ) starting with the negative value, there are excited period-2 vibrations once the solid blue line  $\mu_{B1}$  is crossed. These vibrational states disappear once the higher (green) dashed line is crossed. On the other hand, if one starts from above the green dashed line and decreases the frequency, the zero-amplitude state remains stable until the lower (magenta) dashed line  $\mu_{B2}$  is crossed. It is possible to break the symmetry between the two parametrically driven states that differ by  $\pi$  in the phase by applying a force at  $\omega_p/2$  (Ryvkin and Dykman, 2006), as measured by Mahboob, Froitier, and Yamaguchi (2010) and Leuch *et al.* (2016).

## C. Fluctuations of driven modes

An important aspect of researching resonantly driven or parametrically modulated nanomechanical systems is the possibility to use them for studying fluctuation phenomena far from thermal equilibrium. Because nanomechanical systems are well characterized, they are well suited to such studies. We later discuss several features of fluctuations in driven NVs.

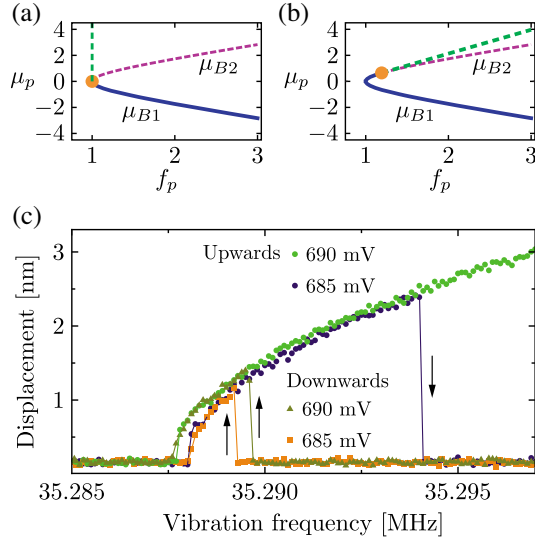


FIG. 16. The bifurcation diagrams of a parametrically modulated mode (a) without and (b) with nonlinear friction. The scaled modulation parameters are  $\mu_p = (\delta\omega_p/\Gamma)\text{sgn}\gamma$  and  $f_p = F_p/2M\Gamma\omega_p$ . (a) With no nonlinear friction, the period-2 states are stable for  $f_p > 1$  and for  $\mu_p > \mu_{B1} = -(f_p^2 - 1)^{1/2}$ . For  $\mu_p > \mu_{B2} = -\mu_{B1}$  the zero-amplitude state also becomes stable, leading to three stable states in the region delimited by the magenta and green dashed lines. (b) In the presence of nonlinear friction the three stable states coexist in the region bound by the line  $\mu_{B2}(f_p)$  and the green (upper) dashed line; cf. Lin, Nakamura, and Dykman (2015). (c) Hysteresis of the response of a modulated nanoresonator for two values of the amplitude of the parametric drive (Karabalin, Masmanidis, and Roukes, 2010). The vibration frequency is  $\omega_p/2$ . “Upwards” and “downwards” refer to the frequency being increased and decreased, respectively, with the resonator initially in the zero-amplitude state. The switching from the upward branch, which refers to the driving amplitude 690 mV, occurs outside of the shown frequency range.

### 1. Fluctuation squeezing

An important generic feature of fluctuations of a periodically driven mode follows from the fact that the driving breaks the continuous time-translation symmetry of the mode dynamics. An immediate consequence of the symmetry breaking is the possibility of fluctuation squeezing. In squeezing, fluctuations of one of the vibrational components (quadratures) are reduced below their level in the absence of driving, whereas fluctuations of the other component are increased. In the absence of driving, the quadratures are the vibration components that oscillate as  $\cos \omega_0 t$  and  $\sin \omega_0 t$ . If the system has a continuous symmetry, the origin of time can be shifted. A shift in time by  $\pi/2\omega_0$  results in an interchange of the quadratures. This shows that the variances of their fluctuations should be equal. A periodically driven system, in contrast, has a discrete time-translation symmetry. It is symmetric only with respect to changing time by the period of the drive. Therefore, the quadratures may no longer be interchanged and their variances are generally different.

Historically, squeezing was first detected in quantum optics (Slusher *et al.*, 1985). It attracted significant attention since it can reduce fluctuations of a quadrature below their level in the

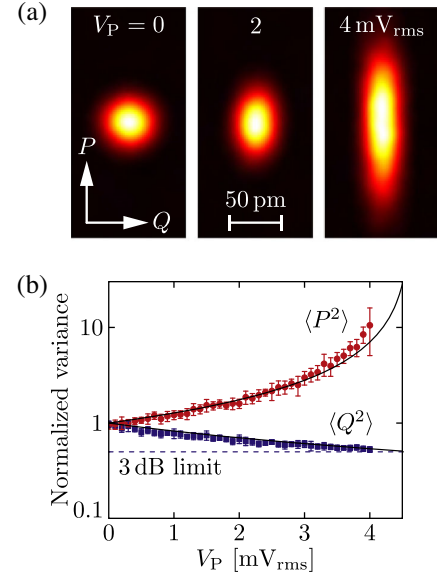


FIG. 17. (a) Thermal vibration noise plotted in the  $(Q, P)$ -phase plane and measured with the pump turned off (thermal equilibrium, pump power  $V_P = 0$  mV) and the pump turned on (non-zero  $V_P$ ). (b) Variance of the  $Q$  and  $P$  quadratures for increasing pump power normalized by the variance at zero pump power. The dashed line indicates the 3 dB limit for parametric squeezing (Poot, Fong, and Tang, 2015).

quantum ground state of the mode and thus enable high-precision measurements (Caves, 1981). The technique has been implemented in laser interferometers for gravitational wave detection (Acernese *et al.*, 2019; Tse *et al.*, 2019). In nanomechanical and micromechanical systems, squeezing in the quantum regime was demonstrated using the techniques of cavity optomechanics (Lecocq *et al.*, 2015; Pirkkalainen, Cho *et al.*, 2015; Wollman *et al.*, 2015).

However, the concept of fluctuation squeezing in vibrational systems equally applies to the classical regime. The squeezing of thermal fluctuations of nanomechanical systems has been achieved in several experiments using parametric pumping (Rugar and Grütter, 1991; Mahboob *et al.*, 2010; Suh *et al.*, 2010). The squeezing is obtained with a comparatively weak pumping below the threshold for exciting period-2 vibrations. For weak noise, it can be described while disregarding the mode nonlinearity; see Appendix D.2.

Figure 17(a) shows the measurements of the thermal vibration noise represented in the  $(Q, P)$ -phase plane (Poot, Fong, and Tang, 2015). The quadratures are measured with a lock-in amplifier by setting its frequency to  $\omega_0$ . Without a pump, the variances of both quadratures are the same, as expected for the continuous time symmetry of the problem. When the resonator is parametrically driven at  $2\omega_0$ , the variances are no longer equal, pointing to time-translation symmetry breaking. The variance of the  $Q$  quadrature is squeezed by the parametric drive. The strongest squeezing corresponds to 3 dB variance suppression, which is reached when the  $P$  quadrature diverges [Fig. 17(b)].

With feedback control (Szorkovszky *et al.*, 2013; Vinante and Falferi, 2013; Poot, Fong, and Tang, 2014; Sonar *et al.*, 2018) it was possible to achieve squeezing by 15.1 dB (Poot,



Fong, and Tang, 2015), well above the conventional 3 dB limit for parametric pumping of a linear mode; cf. Eq. (D14). Classical two-mode squeezing in mechanical resonators by nondegenerate parametric amplification has also been reported (Mahboob, Mounaix *et al.*, 2014; Patil *et al.*, 2015; Pontin *et al.*, 2016), as has the possibility of obtaining squeezing in a two-mode system using postselection (Asano *et al.*, 2019). Classical squeezing was proposed as a way to reduce heating in computers (Klaers, 2019); it also represents an important asset for high-precision sensing (DiFilippo *et al.*, 1992; Natarajan, DiFilippo, and Pritchard, 1995; Mahboob *et al.*, 2010; Szorkovszky *et al.*, 2013), and thus may lead to a new generation of nanomechanical detectors.

Much less attention has been paid to the squeezing of mode fluctuations due to a resonant coordinate-independent force; cf. Eq. (59). The general argument regarding the broken time-translation symmetry applies in this case too. However, for a driven linear mode forced vibrations are simply linearly superimposed on thermal vibrations, and therefore there is no squeezing. The situation changes in the nonlinear regime. Here the fluctuations are affected by the driving and the effect can be resonantly strong.

For weak noise, a resonantly driven mode primarily fluctuates about its state of forced vibrations. These are the fluctuations of the deviations of the quadratures  $\delta Q, \delta P$  from their values in the stable state that become squeezed in the nonlinear regime. The occurrence of the squeezing could be inferred from the strongly asymmetric phase trajectories in the rotating frame in the neglect of dissipation in Fig. 33(b), which were already discussed in an early work on a resonantly driven Duffing oscillator (Dykman and Krivoglaz, 1979; Dmitriev and Dyakonov, 1986); cf. also Siddiqi *et al.* (2004). A theory of squeezing was developed by Buks and Yurke (2006). A strong suppression of a spectral component of a quadrature was observed in a nanomechanical Duffing resonator by Almog *et al.* (2007a) in a narrow parameter range near the critical point in Fig. 15(b) using conventional homodyne detection.

Homodyne measurements are strongly impeded by frequency fluctuations, which play an important role in nanomechanical systems; see Sec. IX. The limitations are particularly pronounced in systems with small damping, where the noise in the in-phase component increases with increasing drive strength (Fong, Pernice, and Tang, 2012); see Fig. 30. However, it appears that for underdamped vibrational modes squeezing can be found by measuring the spectrum of their response to an additional weak probe field (Ochs *et al.*, 2021b) or, for classical fluctuations, by measuring the power spectrum (Huber *et al.*, 2020).

Spectral measurements of squeezing exploit the nature of the dynamics of a driven strongly underdamped mode. When viewed in the rotating frame, this dynamics involves weakly damped oscillations about a stable state of forced vibrations, as described in Appendix D.2.b. The frequency of these oscillations  $\omega_{\text{rot}}$  is much smaller than the strong-drive frequency  $\omega_F$ . When viewed in the laboratory frame, the oscillations at frequency  $\omega_{\text{rot}}$  lead to peaks in the power spectrum at frequencies  $\omega_F \pm \omega_{\text{rot}}$ .

Figure 18 shows the power spectrum of fluctuations of a resonantly driven NVS mode with clearly resolved peaks at

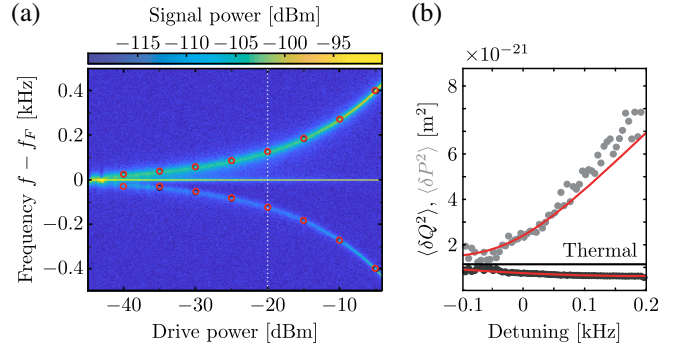


FIG. 18. (a) Power spectrum of a resonantly driven nano-mechanical mode as a function of the frequency  $f$  for  $\omega_F \equiv 2\pi f_F = \omega_0$ . The line at  $f - f_F = 0$  is plotted with reduced brightness to improve the visibility of the satellites, which are due to fluctuations about the stable state of forced vibrations. (b) Variance of the scaled in-phase and quadrature fluctuations  $\langle \delta Q^2 \rangle$  and  $\langle \delta P^2 \rangle$  as a function of the detuning  $(\omega_F - \omega_0)/2\pi$ . The horizontal (black) line indicates thermo-mechanical fluctuations at 293 K in the absence of the drive, and the upper and lower (red) lines indicate the theory for the driven mode. Adapted from Huber *et al.*, 2020.

$\omega_F \pm \omega_{\text{rot}}$  (Huber *et al.*, 2020). The peaks have profoundly different intensities, which is a direct consequence of squeezing.

The peaks at  $\omega_F \pm \omega_{\text{rot}}$  also emerge in the spectrum of the response to an additional weak probe field. The ratio of the areas  $\mathcal{A}^\pm$  of these spectral peaks gives the squeezing parameter  $\phi$  (Dykman, Marthaler, and Peano, 2011; Dykman, 2012; Ochs *et al.*, 2021a),

$$\frac{\langle \delta Q^2 \rangle}{\langle \delta P^2 \rangle} = e^{-4\phi}, \quad \coth^4 \phi = \frac{\mathcal{A}^+}{\mathcal{A}^-}. \quad (64)$$

Equation (64) holds for thermal and quantum fluctuations about the larger-amplitude vibrational state in the range of bistability; cf. Fig. 15(b). For the smaller-amplitude state one should replace  $\coth \phi \rightarrow \tanh \phi$ .

One of the peaks of the response spectrum corresponds to amplification of the probe field by the strong driving field (Dykman and Krivoglaz, 1979; Ochs *et al.*, 2021a). A distinctly double-peak structure of the response spectrum in a suspended nanomembrane was seen by Antoni *et al.* (2012).

#### D. Rare large fluctuations far from thermal equilibrium

Classical and quantum fluctuations in driven nanomechanical systems are not described by the statistical physics of systems in thermal equilibrium, and their probabilities are not determined by the thermodynamic potentials. Revealing general features of such fluctuations is both challenging and important. To a large extent, these features are related to the absence of detailed balance. Detailed balance requires that, in the stationary regime, the probabilities of transitions between the states of a system be balanced pairwise. This means that the probability of a transition  $A \rightarrow B$  between arbitrary states  $A$  and  $B$  is equal to the probability of the transition  $\bar{B} \rightarrow \bar{A}$ . Here the overline indicates that, in the corresponding states, the signs of odd in time variables have been reversed (Lifshitz and Pitaevskii, 1981); we assume that

there is no magnetic field. For a classical vibrational mode, one can associate the mode states with small areas in phase space; for states  $A$  and  $B$  these areas are centered at the points  $q_A, p_A$  and  $q_B, p_B$ , whereas  $\bar{A}$  and  $\bar{B}$  are centered at  $q_A, -p_A$  and  $q_B, -p_B$ , respectively.

Detailed balance is a requisite of thermal equilibrium. It differs from the stationarity condition that the probability to go from  $A$  to  $B, C$ , etc., is equal to the total probability to come to  $A$  from  $B, C$ , etc. Driven nonlinear modes do not have detailed balance as a rule; cf. Roberts, Lingenfelter, and Clerk (2021). They have proved to be invaluable as a means of studying statistical physics with no detailed balance because, on the one hand, they are comparatively simple while, on the other hand, they display a nontrivial behavior.

### 1. Dynamics of nonequilibrium systems in rare large fluctuations

Of special interest in terms of their generic features are nonequilibrium phenomena related to comparatively rare large fluctuations away from a stable state and switching between coexisting stable states. These phenomena encompass chemical and biological reactions as well as switching in lasers, driven nanomagnets, and other systems of current interest. Even though much work has been done on the theory of switching in systems lacking detailed balance, to our knowledge vibrational systems have been the only ones in which the theory could be quantitatively tested in the experiment. Moreover, with these systems the qualitative features of large rare fluctuations, including the involved scaling behavior, have been studied.

For weak on average fluctuations, most of the time the system performs small-amplitude fluctuations about its stable state (or one of its dynamically stable states). Still, occasionally large fluctuations occur in which the system moves far away from this state in phase space. They may result in switching to another stable state.

A key idea behind the understanding of large rare fluctuations was put forward by Onsager and Machlup (1953) and Machlup and Onsager (1953) in the analysis of linear thermal equilibrium systems. They counterintuitively showed that, in a large fluctuation to a given point in phase space, even though the motion is random a system most likely moves along a certain trajectory. Moreover, for an overdamped system this trajectory is the time-reversed trajectory of moving back to the stable state from this point in the absence of fluctuations.

The concept of the corresponding most probable trajectory of a rare fluctuation extends to nonlinear systems and to nonequilibrium systems. However, in systems lacking detailed balance finding such a trajectory is a far from trivial problem, and the topology of such trajectories is also far from trivial (Dykman, Millonas, and Smelyanskiy, 1994). This problem is fundamental in the theory of nonequilibrium systems ranging from physics to biology. It has attracted significant attention over the years (Kamenev, 2011).

A direct experimental observation of the most probable trajectory in a system lacking detailed balance was made with a micromechanical system (Chan, Dykman, and Stambaugh, 2008a, 2008b); see Fig. 19(a). The system was parametrically driven into the range where it had two stable vibrational states  $A_1$  and  $A_2$ ; see Sec. D.2. A comparatively weak noise caused

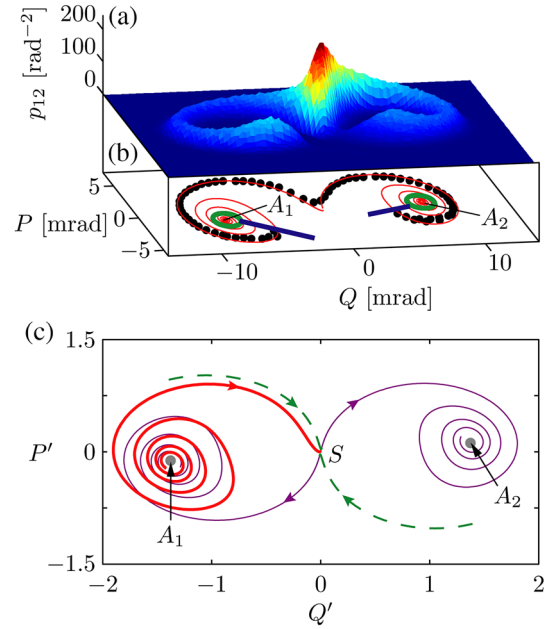


FIG. 19. (a) Probability distribution of the switching paths of a torsional microelectromechanical resonator parametrically driven into bistability. The distribution  $p_{12}(Q, P)$  is measured for switching out of stable state  $A_1$  into state  $A_2$  in the rotating frame;  $Q$  and  $P$  are the quadratures, which are measured in units of the rotation angle of the resonator. (b) Peak locations of the distribution plotted as black circles and the theoretically most probable switching path indicated by a thin red line. All trajectories originate from within the thick green circle in the vicinity of  $A_1$  and later arrive at the thick green circle around  $A_2$ . The radii of the green circles give the typical fluctuation amplitude. The portion of the distribution outside the straight blue lines is omitted. (c) Comparison of the most probable switching path (MPSP) and the noise-free trajectory;  $Q'$  and  $P'$  are the rescaled dimensionless quadratures  $Q$  and  $P$ . The noise-free trajectories from the saddle point  $S$  to the stable states are shown as thin (magenta) solid lines. The thick red line shows the first portion of the MPSP from  $A_1$  to  $S$ , where the system is driven by noise. The MPSP as a whole comprises this trajectory and the noise-free trajectory from  $S$  to  $A_2$ . The green dashed line shows the separatrix. Adapted from Chan, Dykman, and Stambaugh, 2008a, 2008b.

mostly small-amplitude fluctuations about the states but occasionally also led to interstate switching. In the experiment, the system was prepared in the state  $A_1$  and its trajectory was recorded. After it was found in the vicinity of the state  $A_2$ , a portion of the trajectory in the region between the blue lines in Fig. 19(b) was saved and the experiment was repeated. The distribution  $p_{12}$  of the paths followed in switching was obtained by superposing the saved portions of the trajectories.

The sharp peak of the distribution in Fig. 19(a) shows that, indeed, in switching the system is most likely to move along a certain path, the most probable switching path (MPSP). Except for the vicinity of the saddle point  $Q = P = 0$ , the distribution of the trajectories about the MPSP was Gaussian and was in full agreement with the theory, which extended the previously developed approach (Dykman *et al.*, 1992; Luchinsky and McClintock, 1997) to the problem of switching. For switching from the zero-amplitude state of a

parametrically excited microcantilever, an observation of switching paths was reported by Michael and Turner (2007).

Figure 19(c) compares the uphill portion of the MPSP (red line) with the noise-free trajectory (magenta line) along which the system would move from the saddle point to state  $A_1$ . It shows that these trajectories do not have time-reversal symmetry, which would be the symmetry  $(Q, P) \rightarrow (Q, -P)$ . This is an unambiguous indication of the lack of detailed balance.

The form of the MPSP depends not only on the dynamics of the system in the absence of fluctuations but also on the source of the fluctuations, that is, on the properties of the noise, including its spectrum and statistics. The results in Fig. 19 refer to the case where the noise is thermal [cf. Eq. (62)], and therefore is Gaussian and white in slow time; see Sec. IV.

## 2. Scaling behavior of the rates of switching between stable vibrational states

Generally, for a Gaussian and not necessarily white noise the rate of switching between coexisting stable states scales with the noise intensity  $D$  as (Dykman, 1990)

$$W_{\text{sw}} = C_{\text{sw}} \exp(-R/D). \quad (65)$$

Equation (65) is similar to the expression given by Kramers (1940) for the escape rate of a Brownian particle from a potential well. For the Brownian particle the noise intensity is  $k_B T$  and  $R = \Delta U$ , where  $\Delta U$  is the height of the potential barrier to be overcome in escape. In analogy with the Arrhenius law,  $R$  is often called the effective activation energy. To our knowledge, a vibrational mode resonantly driven into bistability was the first physical system with no detailed balance where  $R$  was calculated (Dykman and Krivoglaz, 1979). Both  $R$  and the prefactor  $C_{\text{sw}}$  in Eq. (65) are independent of the noise intensity.

The activation dependence of the switching rate on the noise intensity was demonstrated for a parametrically excited vibrational mode of a single electron in a Penning trap (Lapidus, Enzer, and Gabrielse, 1999). It has been observed in various types of nanomechanical and micromechanical resonators driven into bistability by either a resonant driving force or parametric driving close to twice the mode eigenfrequency; see Aldridge and Cleland (2005), Stambaugh and Chan (2006a), Chan and Stambaugh (2007), Venstra, Westra, and van der Zant (2013), Defoort *et al.* (2015), and Dolleman *et al.* (2019), and references therein. An example is shown in Fig. 20(a).

Another feature of switching in nonequilibrium systems is the scaling behavior of the switching rates, where the activation energy  $R \propto |\ln W_{\text{sw}}|$  scales as a power law of the parameters. For equilibrium systems, where  $R$  corresponds to the barrier height  $\Delta U$ , this scaling was predicted for Josephson junctions (Kurkijärvi, 1972) for the regime in which a junction is not driven by an ac field and is in a quasiequilibrium state. This scaling has been broadly used to determine the junction parameters (Fulton and Dunkelberger, 1974).

Generally, the scaling emerges close to bifurcation points where the stable state from which the system is switching disappears (Dykman and Krivoglaz, 1979, 1980; Knobloch and Wiesenfeld, 1983; Graham and Tél, 1987; Dykman *et al.*,

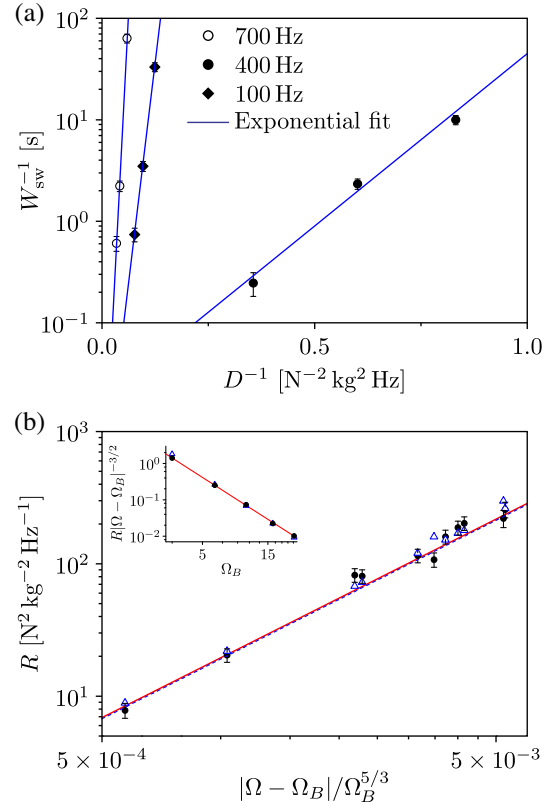


FIG. 20. (a) Activation dependence of the switching rate of a resonantly driven nanomechanical mode  $W_{\text{sw}}$  on the noise intensity  $D$  for different detunings of the drive frequency from its bifurcational value. (b) Effective activation energy  $R$  of the switching rate as a function of the distance from the bifurcational value of the drive frequency;  $\Omega = |\omega_F - \omega_0|/\Gamma$ , and  $\Omega_B$  is the value of  $\Omega$  at the bifurcation point. The filled circles indicate the experimental points, the empty (blue) triangles give the prediction of the full numerical simulation, the (red) solid lines provide the linear fit to the data, and the dashed (blue) lines give the prediction of the asymptotic theory (Dykman and Krivoglaz, 1980). Inset: scaling with the parameter  $\Omega_B$ . Adapted from Defoort *et al.*, 2015.

1998). For resonantly and parametrically driven nonlinear modes, these bifurcation points lie on the lines shown in Figs. 15(b), 16(a), and 16(b). The scaling of  $W_{\text{sw}}$  near bifurcation points was seen in a number of experiments, including those with resonantly driven (Stambaugh and Chan, 2006a; Defoort *et al.*, 2015; Dolleman *et al.*, 2019) and parametrically modulated (Chan and Stambaugh, 2007) micromechanical and nanomechanical modes, parametrically modulated atomic vibrations in a magneto-optical trap (Kim *et al.*, 2005), and resonantly driven vibrations of Josephson junctions (Siddiqi *et al.*, 2006; Vijay, Devoret, and Siddiqi, 2009). The scaling exponents differ in the cases of resonant and parametric driving. Remarkably, not only does the effective activation energy  $R$  scale as the power law of the distance to the bifurcation point (see Appendix D.1.a), but so does the prefactor  $C_{\text{sw}}$  in Eq. (65), with a different exponent (Dykman and Krivoglaz, 1980).

The high degree of control of nanomechanical systems has enabled the scaling exponents not only of  $R$  but also of  $C_{\text{sw}}$  to



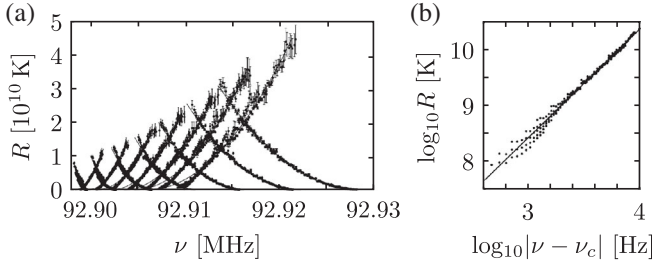


FIG. 21. Measured activation energies of switching between the coexisting large- and small-amplitude states of a resonantly driven nanoresonator. The switching is induced by an externally applied noise that mimics thermal noise. (a) Activation energies as functions of the drive frequency  $\nu = \omega_F/2\pi$  for different values of the resonant force amplitude  $F$ . The activation energy for switching from the large-amplitude state monotonically decreases with an increasing drive frequency, whereas that from the small-amplitude state monotonically increases. (b) Log-log plot showing  $R$  as a function of the difference between  $\nu$  and its critical value  $\nu_c$ . The amplitude of the force  $F$  is close to the critical amplitude and is adjusted to keep the rates of switching between the stable states equal. Adapted from Aldridge and Cleland, 2005.

be measured. Figure 20(b) shows the scaling behavior of  $R$  for a resonantly driven nanomechanical system (Defoort *et al.*, 2015). The data were obtained for different points on the bifurcation line  $F_{B1}$  in Fig. 15(b). It was demonstrated that

$$R \propto |\omega_F - (\omega_F)_B|^{3/2}, \quad C_{sw} \propto |\omega_F - (\omega_F)_B|^{1/2},$$

where  $(\omega_F)_B$  is the bifurcational value of the drive frequency  $\omega_F$ . In agreement with the numerical analysis (Kogan, 2008; Defoort *et al.*, 2015), the scaling holds in an unexpectedly broad range.

The overall change of the effective activation energies of interstate switching with the varying frequency and amplitude of the driving resonant force for a nonlinear nanomechanical beam is shown in Fig. 21(a). Besides the previously discussed bifurcation points, the switching rates display a universal dependence on the parameters near the critical point  $F_c$  in Fig. 15(b) where the two stable vibrational states merge. One can tune the drive amplitude and the frequency in such a way that the rates of switching between the states are equal; see Appendix D.1.a. In this case the activation energy  $R$  is expected to depend on the distance to the critical frequency as  $|\omega_F - (\omega_F)_c|^2$  (Dykman and Krivoglaz, 1979, 1980). This scaling behavior of  $\log W_{sw}$  was demonstrated in the experiment, with  $R$  varying over more than two decades; see Fig. 21(b).

### 3. A kinetic phase transition

Bistable vibrational systems allow one to study another fairly general group of nonequilibrium phenomena. They occur in the parameter range where the rates  $W_{12}$  and  $W_{21}$  of switching between the stable states  $1 \rightarrow 2$  and  $2 \rightarrow 1$  are close to each other. For concreteness, we use 1 and 2 to label the states of a resonantly driven mode with larger and smaller vibration amplitudes, respectively. For weak noise, this

happens where the effective activation energies  $R_1$  and  $R_2$  for switching  $1 \rightarrow 2$  and  $2 \rightarrow 1$  are equal or almost equal [we use that  $W_{ij} \propto \exp(-R_i/D)$ ]. In this range the stationary populations  $w_{1,2}$  of the states are also close to each other, as seen in the balance equation  $w_1/w_2 = W_{21}/W_{12}$ . As the system parameters move away from this range,  $R_1$  and  $R_2$  differ, and the populations quickly become exponentially different. This range was studied by Aldridge and Cleland (2005) close to the critical point.

The range where  $R_1 \approx R_2$  is similar to a smeared first-order phase transition in an equilibrium system. Indeed, in such a phase transition the free energies of the phases are equal, according to the Ehrenfest classification, and the phases (such as liquid and vapor) have comparable volumes (populations). One can conditionally associate the large- and small-amplitude vibrational states with different phases of matter. In this context, the analogs of pressure and temperature in the liquid-vapor transition, i.e., the control parameters, are the amplitude  $F$  and frequency  $\omega_F$  of the driving field. For a certain relation between  $F$  and  $\omega_F$  we have  $R_1 = R_2$ , which can be called a kinetic phase transition. The data in Fig. 21(b) are obtained by moving along the corresponding line on the  $(F, \omega_F)$  plane. The critical point  $[F_c, (\omega_F)_c]$  (see Figs. 15 and 21) is a counterpart of the critical point on the phase transition line.

The kinetic phase transition in a driven mode is accompanied by the onset of extremely narrow peaks in the power spectrum and the spectrum of the response to a probe field (Dykman and Krivoglaz, 1979; Dykman *et al.*, 1994). The peaks are located at the driving frequency. They result from the change of the state populations  $w_1$  and  $w_2$  induced by fluctuations or by the probe field. Such a change leads to the change of the vibration amplitude and phase between their values in the large- and small-amplitude states. The rates at which the populations change, and thus the widths of the peaks, are  $\sim W_{12} \approx W_{21}$ . They are exponentially smaller than the mode decay rate. Therefore, the spectra are extremely sensitive to the parameters of the system, which is similar to the parameter sensitivity at the phase transition in an extended system.

A number of effects related to the kinetic phase transition, including the extremely narrow spectral peaks, have been observed in different types of resonantly driven micromechanical and nanomechanical systems (Chan and Stambaugh, 2006; Stambaugh and Chan, 2006b; Almog *et al.*, 2007b; Venstra, Westra, and van der Zant, 2013; Chowdhury *et al.*, 2017; Dolleman *et al.*, 2019; Huber *et al.*, 2020). Early on it was shown (Cleland, 2005) that these effects enable a 100-fold improvement in frequency resolution compared to a conventional resonant-response-based measurement.

We now discuss the fluctuation-induced response to the probe field and its relation to stochastic resonance. If the probe-field frequency  $\omega_{pr}$  is close to the strong-drive frequency  $\omega_F$ , the probe field can be thought of as a modulation of the strong field amplitude, and hence of the activation energies  $R_{1,2}$ , at frequency  $|\omega_{pr} - \omega_F|$ . As seen in Eq. (65), modulation of  $R_i$  results in an exponentially enhanced modulation of  $W_{ij}$  for weak noise. However, if it is too fast, the populations of the states  $w_{1,2}$  cannot “adjust” to the probe field. Therefore, if the noise intensity  $D$  is small, such that

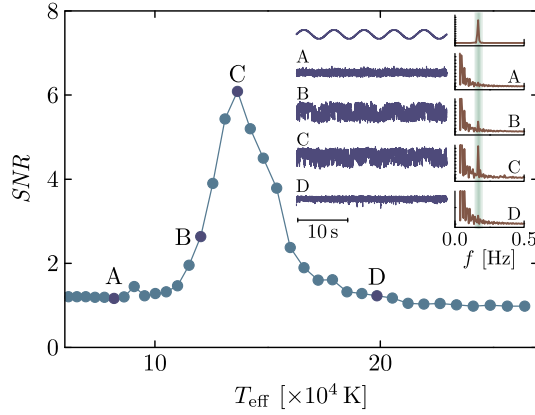


FIG. 22. Noise-enhanced measurement with a nanomechanical cantilever. The cantilever with geometric and inertial nonlinearity is driven into bistability of forced vibrations by a comparatively strong resonant drive. In addition, a broadband noise that emulates thermal noise is applied. The drive is tuned to the kinetic phase transition. The amplitude of the drive is then slowly modulated, mimicking a signal at frequencies equal to the sum and difference of the modulation and drive frequencies. Main panel: signal-to-noise ratio (SNR) as a function of the effective noise temperature. Inset: top row shows the excitation signal in the time (left) and frequency (right) domains. Adapted from Venstra, Westra, and van der Zant, 2013.

$W_{ij} \ll |\omega_{pr} - \omega_F|$ , the response is weak. It exponentially strongly increases with an increasing  $D$  as the rates  $W_{ij}$  approach  $\sim |\omega_{pr} - \omega_F|$ . For large  $D$ , on the other hand, the sensitivity to the modulation of  $R_{1,2}$  falls off. Thus, the response displays a peak as a function of  $D$ . This is reminiscent of stochastic resonance in systems fluctuating in a static double-well potential. This high-frequency stochastic resonance was observed in micromechanical and nanomechanical systems, as Fig. 22 illustrates, and several applications of this effect for sensing were discussed by Chan and Stambaugh (2006), Almog *et al.* (2007b), Venstra, Westra, and van der Zant (2013), and Chowdhury *et al.* (2017).

In the case of resonant parametric excitation at a frequency  $\omega_p \approx 2\omega_0$ , a mode is “automatically tuned” into the kinetic phase transition. Indeed, the period-2 vibrational states have the same amplitude and differ only by phase. Noise-induced interstate transitions are phase-flip transitions, and the stationary populations of the states are equal by symmetry. However, an additional resonant additive drive at a frequency  $\omega_p/2$  lifts this symmetry. As a result, the stationary populations become different. They depend on the phase of the extra drive with respect to the phase of the strong parametric modulation (Ryvkin and Dykman, 2006). This already happens with a weak extra drive, where both states are stable. Such symmetry lifting was observed by Mahboob, Froitier, and Yamaguchi (2010) in a GaAs/AlGaAs-based micromechanical resonator. The corresponding symmetry-breaking detector can resolve frequency shifts  $\delta\omega_0/\omega_0 \sim 10^{-7}$  in a single-shot measurement.

Fluctuation-mediated symmetry lifting has important consequences for coupled parametrically modulated modes. If a

mode vibrates at a frequency  $\omega_p/2$  and is in a state with a given phase, it exerts a symmetry-lifting force on the mode (or modes) that it is coupled to. As a result, depending on the coupling this second mode is biased toward the state with the same or the opposite phase as the primary mode. The modes are on equal footing: they affect each other so as to have the same or opposite phases, and the effect comes through the fluctuations.

The effect of phase ordering in coupled parametrically excited modes was demonstrated by Karabalin *et al.* (2011). In the experiment two almost identical gated nanobeams were driven across the parametric instability. Depending on the sign of the coupling, the mode that experienced the instability later predominantly had the same or the opposite phase as the one that went through the instability first. The coupling could be controlled by the gate voltage, which provided a highly sensitive way of detecting this voltage.

The phase correlations between coupled parametric oscillators mediated by noise were used by Mahboob, Okamoto, and Yamaguchi (2016) to mimic the Ising dynamics of coupled spins with two modes. The two different phases of a parametrically pumped micromechanical mode were associated with two spin projections. Implementations of quantum computation (Goto, 2016, 2019) and Boltzmann sampling (Goto, Lin, and Nakamura, 2018) with coupled nonlinear parametrically excited modes have also been discussed. Of significant importance in this respect is that switching between the period-2 states of a parametrically excited mode can be induced by not only classical but also quantum fluctuations, even for  $T = 0$  (Marthaler and Dykman, 2006). For modulated coupled nanomechanical modes this opens a way of studying quantum phase transitions far from thermal equilibrium, in particular, a transition to a Floquet time-crystalline state (Dykman *et al.*, 2018) in a well-characterized environment.

## VIII. RESONANT MODE COUPLING

A mechanical resonator has a large number of mechanical eigenmodes. These eigenmodes can couple with each other. This leads to a rich variety of different phenomena. We discussed in Sec. VI some of these phenomena, particularly those related to dispersive coupling. Such coupling is important where the modes are far from resonance, but the frequency of a mode depends on the vibration amplitudes of other modes. Here we discuss phenomena originating from resonant linear and nonlinear coupling as well as some resonant multimode effects of an external drive.

### A. Linear resonant coupling

A hallmark of nanoscale mechanical resonators is the wide tunability of their resonance frequencies by electrostatic means. This allows one to bring nanomechanical vibrational modes in and out of linear resonance. Strictly speaking, eigenmodes are defined by diagonalizing the part of the system Hamiltonian that is quadratic in the displacements and momenta. When the resonator modes have significantly different eigenfrequencies, one can speak of approximate modes and disregard the bilinear in the displacements part

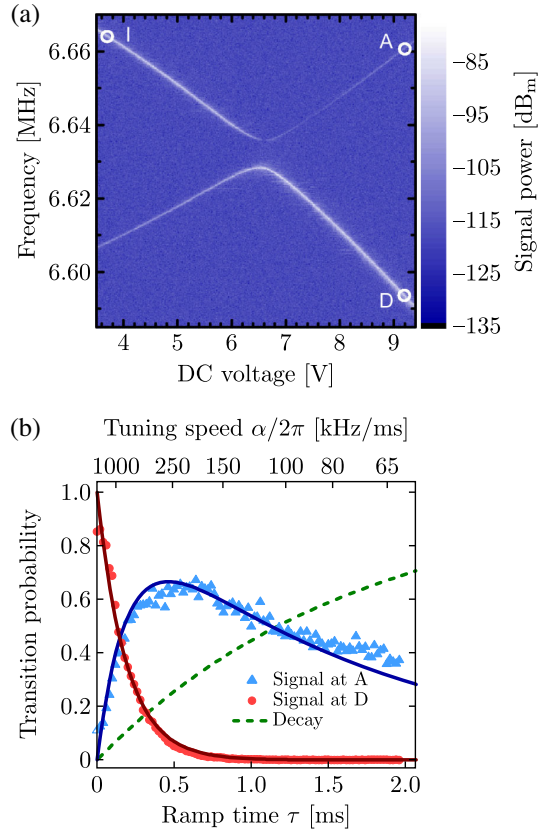


FIG. 23. Resonant mode coupling. (a) Resonant frequencies of two nanomechanical modes as functions of the gate voltage. The two modes hybridize at the anticrossing. (b) Classical analog of the Landau-Zener transition. The high-frequency mode is initially excited [point I in (a)], and the modes are then swept through resonance over time  $\tau$ , which leads to an energy exchange. The data (triangles and dots) show the signal power at points A and D in (a), respectively, as a function of  $\tau$ . The dashed line represents the decay probability of the total energy. From Faust, Rieger *et al.*, 2012.

of the potential energy that couples them. However, when the eigenfrequencies are tuned close to resonance, this part becomes substantial.

In the harmonic approximation, the potential energy of two modes can then be written as

$$U_{12}(q_1, q_2) = \frac{1}{2}M_1\omega_1^2(t)q_1^2 + \frac{1}{2}M_2\omega_2^2(t)q_2^2 + M\Delta_{12}q_1q_2, \quad (66)$$

where  $q_i$  is the displacement of the mode  $i$  ( $i = 1, 2$ ),  $M_i$  is its effective mass,  $\omega_i$  is its eigenfrequency, and  $M\Delta_{12}$  characterizes the coupling strength. If the mode frequencies  $\omega_i(t)$  vary in time in such a way that they go through resonance, the anticrossing shown in Fig. 23(a) occurs. It can be observed while measuring the resonant frequencies of the resonator as functions of the gate voltage that tunes the frequencies (Faust, Rieger *et al.*, 2012; Deng *et al.*, 2016). This anticrossing is similar to the anticrossing of energy levels of a quantum system driven through resonance, even though the considered system is purely classical.

Faust, Rieger *et al.* (2012) also reported observations of a classical analog of the Landau-Zener transition [Fig. 23(b)].

The two-mode system is first prepared by detuning the mode eigenfrequencies by a large amount compared to the coupling. Energy is injected in mode 1, point I in Fig. 23(a). The system is then swept with the gate voltage to the final state where the modes are again practically independent of each other (points A and D). As the modes go through resonance, the energy initially injected in mode 1 gets distributed between the two modes. The distribution depends on the ramp time of the gate voltage [Fig. 23(b)].

An important problem in the Landau-Zener tunneling is the effect of dissipation and noise on the transition; cf. Ao and Rammer (1989), Quintana *et al.* (2013), and Malla, Mishchenko, and Raikh (2017), and references therein. The results by Faust, Rieger *et al.* (2012) suggest that nanomechanical modes can be used to study these effects in a well-controlled experimental setting.

The response of coupled modes to pulses of resonant drive was studied in other experiments with nanomechanical modes (Faust *et al.*, 2013; Okamoto *et al.*, 2013; Zhang *et al.*, 2020). The results allowed Rabi oscillations to be emulated in a classical system.

The reason for the similarity of the classical dynamics of nanomechanical modes and the quantum dynamics of a two-level system is that the interference of linear modes has much in common with the interference of wave functions. We emphasize, however, that nanoresonators and quantum two-state systems such as qubits are entirely different by nature, as seen in the dimensions of their Hilbert spaces, in particular. Coupled classical linear modes may not be used as qubits, since it is the strong nonlinearity of qubits that underlies their application in quantum computing.

Nanomechanical resonators with a symmetric cross section, like cylindrical wires, have degenerate flexural eigenmodes, which are orthogonal. Such modes are highly sensitive to perturbations that cause symmetry lifting. Consider a resonator with degenerate modes polarized in the perpendicular directions  $\hat{\mathbf{r}}_1$  and  $\hat{\mathbf{r}}_2$ . We now place the resonator in an inhomogeneous force field with components  $F_i$  ( $i = 1, 2$ ). The partial derivatives of the force components  $\partial F_i/\partial r_i$  shift the resonance frequencies of the eigenmodes. In contrast, the cross-derivatives  $\partial F_i/\partial r_j$ , with  $i \neq j$ , couple the eigenmodes. As a result, the new eigenmodes have different frequencies and are polarized in different directions. This eigenmode rotation has been directly measured (Gloppe *et al.*, 2014; de Lépinay *et al.*, 2017; Rossi *et al.*, 2017).

The force that drives a nanowire can be nonpotential in nature ( $\partial F_1/\partial r_2 \neq \partial F_2/\partial r_1$ ). Such a force can come if a laser-driven nanowire is placed away from the waist of a focused laser beam. The eigenmodes are then no longer pointing in orthogonal directions. It has been experimentally shown that the angle between them can be reduced to zero (de Lépinay *et al.*, 2018). The power spectra of the modes were found to deviate from the conventional Lorentzian form.

Examples of other effects of resonant coupling of a few NVS modes include the generation of circularly polarized mechanical oscillations using modes polarized in perpendicular directions (Conley *et al.*, 2008; Perisanu *et al.*, 2010) and resonant coupling of an optomechanical resonator and a single bacterium (Gil-Santos *et al.*, 2020). A significant



group of resonant-coupling effects concerns one- and two-dimensional arrays of resonators; in such arrays many modes are brought into resonance. Arrays of NVs can display various types of topological effects (Peano *et al.*, 2015; Cha, Kim, and Daraio, 2018; Ren *et al.*, 2020; Lin *et al.*, 2021; Yamaguchi and Houri, 2021), as well as dynamical phase transitions and symmetry-breaking effects (Dykman *et al.*, 2018; Heugel *et al.*, 2019; Matheny *et al.*, 2019), and can be used as tunable phononic waveguides (Hatanaka, Bachtold, and Yamaguchi, 2019; Kirchhof *et al.*, 2021; Zhang *et al.*, 2021).

## B. Nonlinear resonant coupling

The study of nonlinear resonance has been attracting significant attention and has a long history in quantum and classical mechanics, which goes back at least to Laplace and Poincaré on the classical side and to the Fermi resonance on the quantum side (Fermi, 1931; Arnold, 1989). For two modes, nonlinear resonant mode coupling occurs where the ratio of their eigenfrequencies  $\omega_2/\omega_1$  is close to a rational number  $n/m$ . In nonlinear resonance, modes can exchange energy with each other in a manner similar to linear resonance. The coupling that leads to this exchange comes from the modes nonlinearity and therefore is unavoidable. Generally, it falls off with the increasing order of the resonance, i.e., for two modes, with the increasing  $n$  and  $m$  in the ratio  $n/m$ . Classically, multiple nonlinear resonances pave the road to chaos in conservative systems, a profound understanding that emerged in the 20th century.

A system of coupled nanomechanical modes provides a playground for studying nonlinear resonant effects. One can study them in a well-controlled setting in the regimes of strong to weak dissipation and explore a broad range of phenomena, from the aforementioned resonant energy exchange to various types of dynamical bifurcations, different scenarios for the onset of dynamical chaos, resonant nonlinear friction, etc.

For a two-mode system with the resonant condition  $n\omega_1 \approx m\omega_2$ , the simplest term in the potential energy that directly accounts for the resonant energy exchange in nonlinear resonance has the form

$$U_{\text{nl}}^{\text{res}} = M\Delta_{12}^{(nm)}q_1^nq_2^m, \quad (67)$$

where  $\Delta_{12}^{(nm)}$  is the coupling parameter. The importance of the coupling  $U_{\text{nl}}^{\text{res}}$  is clear from the following argument. If  $q_1$  and  $q_2$  oscillate at frequencies  $\omega_1$  and  $\omega_2$ , respectively,  $U_{\text{nl}}^{\text{res}}$  contains a nonoscillating part. This is the “normal form” term (Guckenheimer and Holmes, 1997): it is of the lowest order in nonlinearity that has a nonoscillating part, drawing the similarity with the harmonic part of the Hamiltonian, which is independent of time.

The effect of the coupling (67) on the energy exchange between the modes is easy to understand in quantum terms. We write the displacement operator of an  $i$ th mode ( $i = 1, 2$ ) in Eq. (67) as  $q_i = (\hbar/2M\omega_i)^{1/2}(a_i + a_i^\dagger)$ , where  $a_i^\dagger$  and  $a_i$  are the raising and lowering operators. Therefore,  $U_{\text{nl}}^{\text{res}}$  contains terms  $(a_1^\dagger)^na_2^m + (a_2^\dagger)^ma_1^n$ . They describe processes in which mode 1 goes up by  $n$  energy levels while mode 2 goes

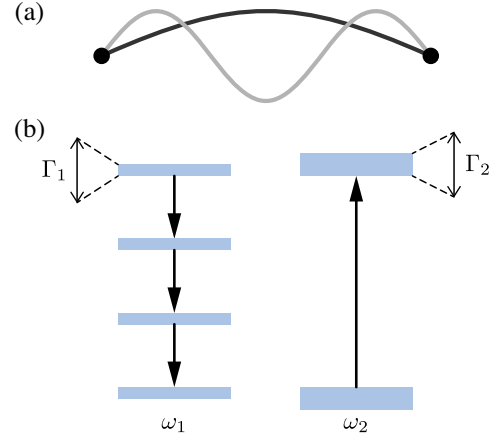


FIG. 24. Nonlinear resonant coupling. (a) Spatial profile of two eigenmodes with resonance frequencies  $\omega_{1,2}$ . (b) Energy diagram showing an energy-exchange process between two harmonic oscillators with  $\omega_2/\omega_1 \simeq 3$ . The process simultaneously annihilates  $n = 3$  quanta in mode 1 and creates  $m = 1$  quantum in mode 2.

down by  $m$  levels, or vice versa, mode 1 goes down by  $n$  energy levels while mode 2 goes up by  $m$  levels. For exact nonlinear resonance, in such processes the modes exchange energy  $\hbar n\omega_1 = \hbar m\omega_2$ , but the total energy of the modes is not changed. This is illustrated in Fig. 24 for  $n = 3$  and  $m = 1$ . If one of the modes is excited, the energy exchange happens periodically in time, as in the case of linear resonance. The energy-exchange frequency is  $\propto |\Delta_{12}^{(nm)}|$  and depends on the mode amplitudes [in fact, one has to take into account that, because of the mode nonlinearity, the frequencies  $\omega_i$  depend on the mode amplitudes  $A_i$ , and a more accurate form of the resonance condition is  $n\omega_1(A_1) = m\omega_2(A_2)$ ]. In quantum terms, the resonating energy levels are split, with the splitting  $\hbar\delta\omega_{\text{nl}}$  that depends on the level numbers.

The onset of resonant nonlinear effects does not require an exact resonance. It suffices for the frequency detuning  $|n\omega_1 - m\omega_2|$  to be smaller or on the order of the sum of the decay rates of the modes or the properly scaled maximal energy-exchange frequency. We also note that the symmetry of the modes may impose restrictions on the coupling: for example, in a uniform straight nanobeam the fundamental flexural mode is not coupled to odd powers of the first excited flexural mode. Selection rules also apply to other types of modes, and therefore in a number of cases special design was implemented to observe particular types of nonlinear resonance (Asadi, Yeom, and Cho, 2021).

An important asset for studying various aspects of nonlinear resonant effects with the NVs is their tunability. The modes can be tuned in and out of resonance by sweeping their eigenfrequencies with the voltage applied to the gate electrode (Eichler *et al.*, 2012) or by dynamically shifting the frequency of one of the modes by driving it into the nonlinear Duffing regime, where the vibration frequency depends on the vibration amplitude [cf. Eq. (48)]; see Antonio, Zanette, and Lopez (2012), Samanta, Yasasvi Gangavarapu, and Naik (2015), Mangussi and Zanette (2016), Chen *et al.* (2017), Hajjaj, Alfossail, and Younis (2018), Asadi, Yu, and Cho (2018),

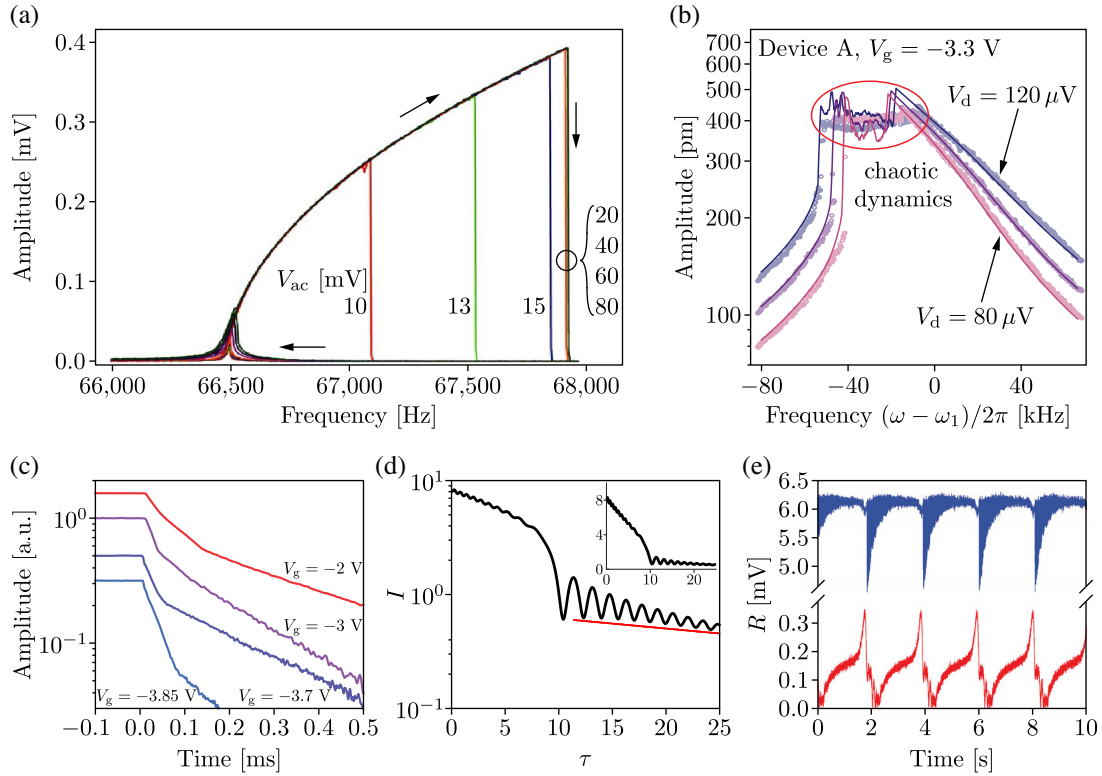


FIG. 25. Experiments and theoretical predictions showing the effects of nonlinear resonant coupling for 1:3 resonance. (a) Nonlinear response of a resonantly driven lower-frequency micromechanical mode as a function of the drive frequency. The mode switches from the large- to the small-amplitude branch at the frequencies that depend on the value of the drive amplitude indicated next to the vertical lines. Adapted from [Antonio, Zanette, and Lopez, 2012](#). (b) Nonlinear response of a multilayer graphene nanoresonator where the nonlinear resonance with a higher-frequency mode results in a plateau. Adapted from [Güttinger \*et al.\*, 2017](#). (c) Nonexponential energy decay in the same system as in (b) and in a similar system, device B. The drive is switched off at  $t = 0$ . The resonators were measured at different gate voltages  $V_g$  to tune the resonance frequencies of the modes. The two upper traces refer to device B, whereas the two lower traces refer to device A. (d) Decay of the scaled squared amplitude of the lower-frequency mode. Calculations show that as the mode goes through the nonlinear resonance the decay is accompanied by oscillations for the coupling larger than the decay rates. Inset: data on a linear scale;  $\tau$  is the scaled time. Adapted from [Shoshani, Shaw, and Dykman, 2017](#). (e) Temporal amplitude of the lower-frequency (blue upper trace) and higher-frequency (red lower trace) responses of the micromechanical resonator showing the bursting behavior as the system is driven close to the saddle-node bifurcation on the invariant cycle. Adapted from [Czaplewski \*et al.\*, 2018](#).

[Houri \*et al.\* \(2019\)](#), [Asadi, Yeom, and Cho \(2021\)](#), [Luo, Gao, and Liu \(2021\)](#), [Shoshani and Shaw \(2021\)](#), and [Arora and Naik \(2022\)](#), and references therein. The latter dependence also leads to the possibility of going through resonance during decay of the mode amplitude after the mode was initially excited.

In nanomechanical systems the nonlinear mode coupling is comparatively weak. It becomes stronger with an increasing mode amplitude, as seen in Eq. (67). Therefore, almost all observations in the classical domain refer to the case where one of the resonating vibrational modes is sufficiently strongly driven or is allowed to decay after being sufficiently strongly excited.

The amplitude dependence of both the mode frequencies and the effective coupling strength makes the nonlinear resonance dynamics much richer than in the case of linear resonance. Several types of ensuing behaviors have been seen in micromechanical and nanomechanical systems. Most observations refer to the cases where a low-frequency mode was driven close to resonance with a high-frequency mode with the frequency ratio 2:1 or 3:1.

For a micromechanical system that displays a 3:1 resonance, it was found ([Antonio, Zanette, and Lopez, 2012](#)) that for the low-frequency mode the Duffing response curve shown in Fig. 15(a) changes due to the nonlinear resonance. As seen in Fig. 25(a), starting with a sufficiently strong driving amplitude, the frequency at which the mode switches from the large- to the small-amplitude branch becomes independent of the drive amplitude. This frequency is determined by the coupling to a mode with a 3 times higher frequency. This coupling opens a new channel of energy relaxation, thereby limiting the increase in the amplitude. On a similar device it was found ([Czaplewski \*et al.\*, 2018](#)) that in the comparatively strong-drive regime the system may display slow and strongly nonsinusoidal vibrations, thus producing a frequency comb with the spectral line spacing smaller than the mode eigenfrequency by a factor approaching  $10^5$  and spanning a bandwidth larger than the mode decay rate by a factor  $\sim 10^2$ ; see Fig. 25(e). This effect was related to a special type of saddle-node bifurcation (cf. Appendix D.1.a), which in this case occurs on an invariant circle ([Shoshani and Shaw, 2021](#)). When the system

is near such a bifurcation point, its trajectory in the rotating frame is of the burst type.

In a nanomechanical resonator studied by Güttinger *et al.* (2017), it was possible to tune the modes into a 3:1 resonance not only by varying the parameters of the drive but also by changing the eigenfrequencies using a gate voltage. It was observed that, when the low-frequency mode was driven sufficiently strongly, the dependence of its amplitude on the drive frequency displayed a plateaulike region; see Fig. 25(b). Numerical simulations suggest that in this region the dynamics in the rotating frame becomes chaotic. The simulations took into account the nonlinear resonant coupling of the form of Eq. (67) and successfully described switching between different vibrational branches of the coupled driven nonlinear modes. Limit cycles and period doubling for 3:1 resonance in a MEMS resonator were observed by Hourì *et al.* (2019).

The results (Chen *et al.*, 2017; Güttinger *et al.*, 2017) also revealed a strongly nonexponential decay of the resonating modes after the low-frequency mode was excited to a large amplitude and the driving was switched off. This can be understood since, during decay, the modes exchange energy with not only the thermal reservoir but also each other. Such an exchange is efficient while the modes are in resonance and the effective coupling strength is larger than the decay rates. This leads to a peculiar form of the time dependence of the amplitude shown in Fig. 25(c), which is in good agreement with the simulations (Güttinger *et al.*, 2017).

Analytically, the time dependence of the mode amplitude has been described in two limiting cases. In the first case, the high-frequency mode has a large decay rate compared to the decay rate of the low-frequency mode and the appropriately scaled coupling, whereas in the second case the decay rates of both modes are small on the coupling scale (Shoshani, Shaw, and Dykman, 2017). In the first case, the high-frequency mode serves as a thermal reservoir that is switched on and off as the amplitude of the low-frequency mode changes, a direct analog of the nonlinear friction discussed in Sec. VI.B; cf. Fig. 11. In the second case, on the other hand, the mode decay is accompanied by strong amplitude oscillations. These oscillations are followed by a steep drop when the system goes through a saddle point of the conservative motion and comes out of resonance, as seen in Fig. 25(d). In both limiting cases, for small amplitudes, where the modes are away from the resonance, the decay becomes exponential.

Besides nonlinear resonance of two modes, nanomechanical and micromechanical systems allow one to study multiple-mode resonance (Mahboob *et al.*, 2013; Luo, Gao, and Liu, 2021). Mahboob *et al.* (2013) observed in a nanomechanical system a resonance of three modes in which  $\omega_1 + \omega_2 \approx \omega_3$  and  $\omega_1 \ll \omega_{2,3}$ . The relevant resonant nonlinear coupling in this case has the form  $U_{nl}^{res} = M\Delta_{123}q_1q_2q_3$ . The resonance was achieved by tuning mode 1 with a piezoelectric transducer. It was shown that resonant driving of the high-frequency mode leads to excitation of coherent self-sustained vibrations of modes 1 and 2, the effect called phonon lasing. A multiple-mode resonance was also studied in a cascade of beams with the frequencies of the successive beams decreasing by a factor of 2 (Qalandar *et al.*, 2014). In this system the energy transfer to a mode with frequency

smaller by a factor of 4 than the excitation frequency was demonstrated.

### C. Parametrically induced resonant coupling

A noteworthy feature of mechanical resonators is that it is possible to resonantly couple two vibrational modes using a parametric drive without any restriction on the ratio of their resonance frequencies  $\omega_2/\omega_1$ . A simple way to achieve such coupling is based on driving a resonator at a frequency  $\omega_p$  equal to either the sum or the difference of the mode eigenfrequencies ( $\omega_1 + \omega_2$  or  $|\omega_1 - \omega_2|$ ) such that the drive resonantly modulates the coupling strength  $\Delta_{12}^{pump}(t)$  in the potential energy

$$U_{12}^{pump} = M\Delta_{12}^{pump}(t)q_1q_2. \quad (68)$$

The parametric drive is often implemented by modulating the stress in the resonator using an electrostatic or piezoelectric force. The coupling (68) may also result from driving one of the modes at the combination frequency  $|\omega_1 \pm \omega_2|$  in the presence of nonlinear mode-mode coupling (Dykman, 1978; Sun *et al.*, 2016). The effect of the coupling (68) is similar to what happens in optomechanical systems (Aspelmeyer, Kippenberg, and Marquardt, 2014b), where the parametric coupling is used to cool and heat mechanical vibrations, realize optomechanically induced transparency in photon cavities, and hybridize mechanical vibrations with the optical field.

If the drive frequency is  $\omega_p = |\omega_1 - \omega_2|$ , the driving leads to an energy exchange between the modes. A simple way to understand this is suggested by Fig. 26(a) if one thinks of the driving as an electromagnetic field. In these terms, the interaction (68) describes a process in which a photon with energy  $\hbar\omega_p$  and a quantum of the lower-frequency mode [mode 1 in Fig. 26(a)] are annihilated and a quantum of the higher-frequency mode is created or, vice versa, a quantum of a higher-frequency mode decays into a photon and a quantum of the lower-frequency mode. For  $\omega_1 < \omega_2$  the energy conservation condition is  $\hbar\omega_p + \hbar\omega_1 = \hbar\omega_2$ .

In other words, if one notices that the mode coordinates  $q_1$  and  $q_2$  oscillate at frequencies  $\omega_1$  and  $\omega_2$ , respectively, whereas  $\Delta_{12}^{pump}(t)$  oscillates at the frequency  $\omega_p = |\omega_1 - \omega_2|$ , in  $U_{12}^{pump}$  there is a term that is independent of time. In the rotating wave approximation it has the same form as the static linear resonant mode-mode coupling discussed in Sec. VIII.A. In terms of the modes' ladder operators, the coupling energy is  $\propto a_1^\dagger a_2 + a_2^\dagger a_1$ . Therefore, the energy exchange is similar to what was considered in Sec. VIII.A.

An important feature of the drive at  $|\omega_1 - \omega_2|$  is that it makes it possible to cool down the low-frequency mode [mode 1 in Fig. 26(a)], given that its relaxation rate is smaller than the relaxation rate of the high-frequency mode (Dykman, 1978). The driving “extracts” the energy from the low-frequency mode and “dumps” it into the high-frequency mode, which then quickly further dumps it into the thermal reservoir coupled to this mode. Thus, the high-frequency mode in this case serves as an effective thermal reservoir for the low-frequency mode.



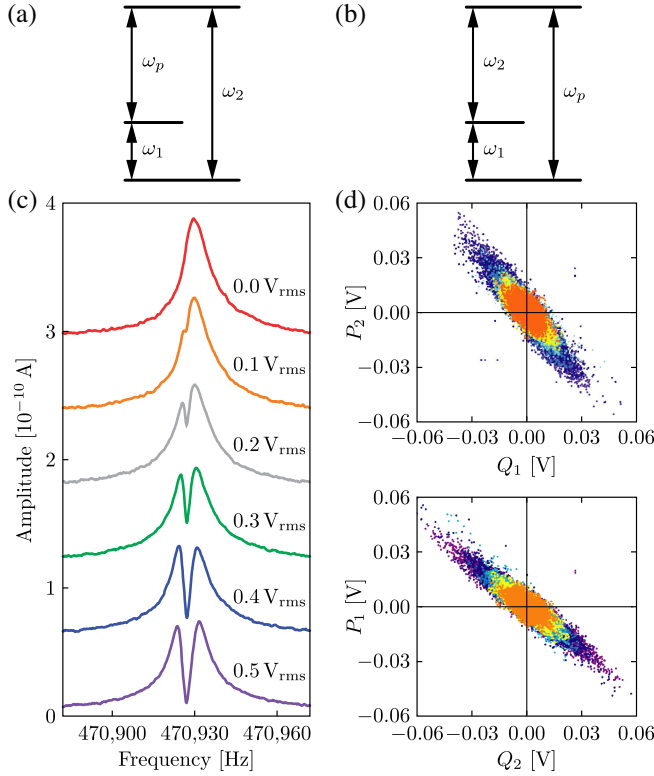


FIG. 26. Resonant mode coupling using a parametric drive. (a),(b) Energy levels when the parametric drive frequency  $\omega_p$  is set at  $\omega_2 - \omega_1$  in (a) and  $\omega_1 + \omega_2$  in (b). (c) Driven response of the displacement of mode 2 to a weak probe field for different parametric drive powers with  $\omega_p = \omega_2 - \omega_1$ . The splitting of the peak at high parametric drive power indicates that modes 1 and 2 are significantly hybridized. (d) Correlations between modes 1 and 2 in the  $(Q_1, P_2)$  and  $(Q_2, P_1)$  phase spaces for  $\omega_p = \omega_2 + \omega_1$  for several parametric drive amplitudes. (c), (d) Adapted from Mahboob *et al.*, 2012, and Mahboob, Okamoto *et al.*, 2014.

If the relaxation rate of the low-frequency mode is dominated by the energy exchange with the high-frequency mode, in the stationary state the populations of the excited states of the modes should be equal. The occupation of the first excited energy level of the high-frequency mode (mode 2) is  $\propto \exp(-\hbar\omega_2/k_B T)$ . The previous argument suggests that the occupation of the first excited state of the low-frequency mode (mode 1) should be  $\propto \exp(-\hbar\omega_1/k_B T_{\text{eff}})$ , with  $T_{\text{eff}} = T\omega_1/\omega_2$ . This means that the effective temperature of mode 1 is significantly lower than  $T$ . Surprisingly, the entire distribution over the excited states of mode 1 is of the Boltzmann form with temperature  $T_{\text{eff}}$  in the absence of nonlinear friction (Dykman, 1978). In the opposite case where the relaxation rate of mode 1 is much higher than that of mode 2, the effective temperature of mode 2 becomes  $T\omega_2/\omega_1$  (i.e., mode heating occurs); see Appendix C.

Mode cooling in coupled mechanical modes was experimentally demonstrated by Mahboob *et al.* (2012) and De Alba *et al.* (2016). The cooling is modest compared to what is achieved with optomechanical devices (Chan *et al.*, 2011; Teufel *et al.*, 2011; Verhagen *et al.*, 2012), where the ratio of the mode frequencies can be much larger.

A profound effect of the driving-induced resonant coupling is seen in the response to a weak probe drive. This response displays Fano resonance. For a not too strong driving-induced coupling and for the driving frequency  $\omega_p \approx |\omega_2 - \omega_1|$ , the amplitude of the response of a faster-decaying mode [mode 2 in Fig. 26(c)] to a probe field displays a narrow dip at a frequency  $\approx \omega_p + \omega_1$ . The dip results from the interference of the direct resonant response of mode 2 and of the response of mode 1 “uplifted” by the drive (68) to the frequency  $\omega_p + \omega_1 \approx \omega_2$ . This is an analog of the optomechanically induced transparency in photon cavities (Weis *et al.*, 2010; Safavi-Naeini *et al.*, 2011; Qu and Agarwal, 2013).

For a stronger driving  $\Delta_{12}^{\text{pump}}(t)$  [Eq. (68)], where the rate of the driving-induced energy exchange between the modes becomes larger than their relaxation rates, the behavior of the modes is reminiscent of that at the mode anticrossing discussed in Sec. VIII.A. The resonance now is between  $\omega_2$  and  $\omega_1 + \omega_p$ . As previously mentioned, the coupling Hamiltonians have the same form in the rotating wave approximation. The modes are strongly hybridized in this regime.

Experimentally, the Fano resonance and the mode hybridization in micromechanics and nanomechanics were first demonstrated in GaAs-based semiconductor resonators (Mahboob *et al.*, 2012; Okamoto *et al.*, 2013). In the response of the mode to a weak probe field shown in Fig. 26(c), the dip associated with the Fano resonance becomes more prominent with the increasing drive  $\Delta_{12}^{\text{pump}}(t)$ . The response for the largest drive is nearly split into two peaks, the analog of anticrossing in Fig. 23(a), indicating a significant mode hybridization. It is comparatively simpler to reach this hybridization regime (also called the strong coupling regime) in resonators based on nanoscale materials, such as graphene and nanotubes, because the stress can be modulated by a larger amount (Liu, Kim, and Lauhon, 2015; De Alba *et al.*, 2016; Mathew *et al.*, 2016; Zhu *et al.*, 2017; Luo *et al.*, 2018; Prasad, Arora, and Naik, 2019).

Parametric drive at the frequency  $\omega_p \approx \omega_1 + \omega_2$  leads to the heating of the Brownian motion of both modes 1 and 2. In the rotating wave approximation, in terms of the modes’ ladder operators the coupling energy is  $\propto a_1^\dagger a_2^\dagger + a_1 a_2$ . The effect of the parametric drive can be thought of as a decay of a drive photon with creation of a quantum of mode 1 and a quantum of mode 2; cf. Fig. 26(b). This excitation corresponds to “negative damping” and is associated with a decrease of the dissipation rates of the modes. If in the absence of the driving one mode is decaying much faster than the other, the effect is described as the decrease of the linear friction coefficient and the increase of the effective temperature of the slower-decaying mode. When the dissipation rate is positive, this mode (mode 1, for concreteness) can amplify an externally applied weak drive at the frequency  $\omega_p - \omega_1$ . When its dissipation rate goes through zero, the mode switches to the regime of self-sustained vibrations (Dykman, 1978).

Amplification of a weak radiation by a nanomechanical mode coupled to an optical cavity mode was observed by Massel *et al.* (2011). For coupled micromechanical modes, both the resonant parametric heating and the onset of oscillations were observed by Mahboob, Okamoto *et al.*

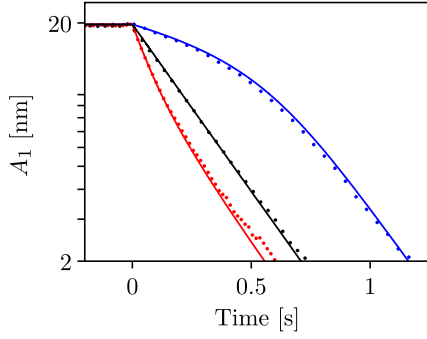


FIG. 27. Tailoring nonlinear friction with parametrically modulated mode coupling. The vibration amplitude of mode 1 is shown as a function of time in a ringdown measurement. The middle (black) curve corresponds to linear friction. The lowest (red) and highest (blue) curves correspond to positive and negative nonlinear friction when the device is pumped at  $\omega_2 \mp 2\omega_1$ , respectively. Adapted from Dong, Dykman, and Chan, 2018.

(2014). In the parametric heating regime, a correlation in the displacement noise of the two modes was measured and two-mode squeezing was found; see Fig. 26(d).

An interesting regime arises when both modes are pumped into the regime of self-sustained vibrations (Sun *et al.*, 2016). The measurements show that the phase fluctuations of the two modes feature near-perfect anticorrelation, so the sum of the phases  $\phi_1(t) + \phi_2(t)$  remains nearly constant. Such anticorrelation is a consequence of the discrete time-translation symmetry imposed by the periodic drive. This regime has not been accessed with the optomechanical systems fabricated thus far, since the dissipation rate of the optical cavity could not be driven to zero.

Parametric drive of the mode coupling can also be used to generate nonlinear friction in a controlled way. Pumping at  $\omega_2 - 2\omega_1$  leads to positive nonlinear friction in mode 1 if the damping rate of mode 2 is large enough that any additional energy arriving from mode 1 is rapidly transferred to the environment. This results in a relaxation process where two quanta of mode 1 are simultaneously extracted and transferred to mode 2 along with a drive photon, in contrast to the previously discussed linear friction that involves a transfer of one quantum of mode 1. Energy decay measurements of this nonlinear friction show that the vibrational amplitude decreases the fastest at high amplitude (red data in Fig. 27) (Dong, Dykman, and Chan, 2018). Pumping at  $\omega_2 + 2\omega_1$  generates negative nonlinear friction, where the measured decay is the slowest at high amplitude (blue data in Fig. 27). Ultimately, such negative nonlinear friction leads to the possibility of self-sustained vibrations in the system of coupled modes.

## IX. FREQUENCY FLUCTUATIONS

Frequency fluctuations are one of the least understood chapters of the dynamics of nanomechanical systems. In a way, even the word “frequency” has been used somewhat ambivalently. Strictly speaking, the angular frequency is equal to  $2\pi$  divided by the vibration period. It is thus associated with a discrete time interval. However, in classical vibrational

systems there is also considered an “instantaneous” frequency that continuously depends on time and is given by the derivative of the vibration phase  $\varphi(t)$  over time. For perfect sinusoidal vibrations the two definitions of the frequency coincide, but in the presence of fluctuations they generally differ. Frequency fluctuations in NVs have attracted significant attention, as they often impose a limit on mass sensitivity (Cleland, 2005; Ekinci and Roukes, 2005; Yang, Callegari *et al.*, 2006; Naik *et al.*, 2009; Chaste *et al.*, 2012) and other applications in sensing, like force and force gradient measurements (Weber *et al.*, 2016; Braakman and Poggio, 2019); they are also a major limiting factor in the application of micromechanical systems such as clocks, gyroscopes, and other devices (Ng *et al.*, 2013; Zaliasl *et al.*, 2015; Miller *et al.*, 2018).

For an isolated linear mode, the displacement can be written as

$$q(t) = A \cos \varphi(t), \quad \varphi(t) = \omega_0 t + \phi.$$

Here  $\omega_0$  is the mode eigenfrequency, i.e., a parameter of the system, whereas  $\phi$  and the amplitude  $A$  are determined by the initial conditions. Coupling of the mode to the environment causes fluctuations of both  $\phi$  and  $\omega_0$ , as well as amplitude fluctuations, making all these parameters time dependent. The fluctuations of  $\phi$  and  $\omega_0$ , which are of primary interest in this section, come from physically different sources and are called, respectively, phase and eigenfrequency fluctuations. Both of them contribute to fluctuations in the full vibrational phase, which can be now written as

$$\varphi(t) = \int_0^t \omega_0(t') dt' + \phi(t). \quad (69)$$

The time-dependent phase  $\phi(t)$  is also often called the phase in the rotating frame. In high- $Q$  systems, of relevance are fluctuations of  $\phi$  and  $\omega_0$  that are slow on the timescale  $\omega_0^{-1}$ .

Fluctuations of  $\phi(t)$  have been studied broadly, initially in various systems of self-sustained vibrations. These studies can be traced back to the 1930s–1950s (Berstein, 1938; Rytov, 1956a, 1956b). They were later carried out for lasers [see Lax (1967), and Lax and Yuen (1968), and references therein] and for time metrology (Allan, 1966; Allan *et al.*, 1988). A major feature of self-sustained vibrations is that the phase  $\phi$  is arbitrary unless the vibrations are synchronized using an external source. Therefore, phase fluctuations can accumulate in time. Generally, this leads to phase diffusion on a long timescale that is independent of the nature of the vibrational system.

In micromechanical and nanomechanical systems, an unavoidable source of phase fluctuations is the thermal (thermomechanical) noise. It comes along with friction from the coupling to a thermal reservoir and is described by the force  $f_T(t)$  in Eq. (2) (Cleland and Roukes, 2002; Schmid, Villanueva, and Roukes, 2016). It sets the so-called noise floor and thus imposes a fundamental limit on the precision with which the full phase  $\varphi(t)$ , and thus the frequency  $\dot{\varphi}(t)$ , can be determined; cf. Fig. 28.

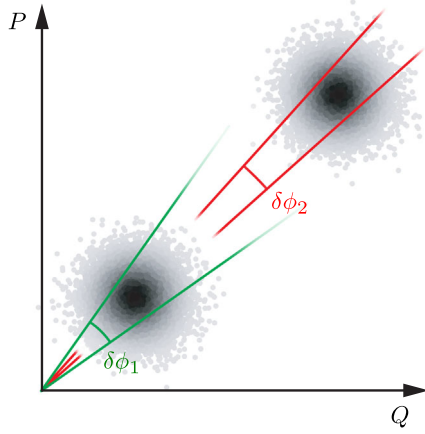


FIG. 28. Effect of thermal phase noise. The noise is sketched as a smearing of the values of the quadratures  $Q$  and  $P$  of the mode. The uncertainty in the phase  $\delta\varphi$  depends on the vibration amplitude. For a small amplitude its value  $\delta\varphi_1$  is larger than the value  $\delta\varphi_2$  for a larger amplitude.

Fluctuations of the vibration eigenfrequency are a different source of fluctuations of the overall phase  $\varphi(t)$ . A simple mechanism of such fluctuations is random attachment and detachment of molecules and the associated change of the mass, and thus the eigenfrequency of a nanoresonator (Yong and Vig, 1989; Cleland and Roukes, 2002; Ekinci, Yang, and Roukes, 2004; Dykman *et al.*, 2010; Yang *et al.*, 2011).

Understanding frequency fluctuations requires one to separate the fluctuations of the eigenfrequency and of the slow part  $\phi$  of the phase and to characterize both the spectra and the statistics of these fluctuations. In turn, this characterization provides a means of identifying the fluctuation sources. We concentrate here primarily on “open-loop” measurements done to this end. These measurements are performed with no feedback loop. They are therefore free from the effect of the noise that comes from the feedback. In studying nanomechanical and micromechanical systems, feedback-based methods are also often employed, including those utilizing self-sustained vibrations (Feng *et al.*, 2008) as well as the phase-locked loop method (Albrecht *et al.*, 1991; Naik *et al.*, 2009; Hanay *et al.*, 2012; Olcum *et al.*, 2015); see Schmid, Villanueva, and Roukes (2016), and Demir (2021), and references therein.

We note that in quantum terms frequency fluctuations are usually associated with decoherence. A familiar source of decoherence in quantum systems is fluctuations of the level spacing, i.e., of the transition frequencies. The thermomechanical noise described by Eq. (2) does not lead to fluctuations of the level spacing of a quantum oscillator in the absence of nonlinearity. In that sense, there is a significant difference between the quantum and classical pictures of frequency fluctuations. The pictures can be reconciled, though, by realizing that, because of dissipation, for a nonzero temperature a quantum oscillator makes transitions between its energy levels. The transitions happen at random, and this is a quantum analog of the effect of thermal noise. The power spectra of quantum and classical linear oscillators have the same shape; see Sec. IV.C.

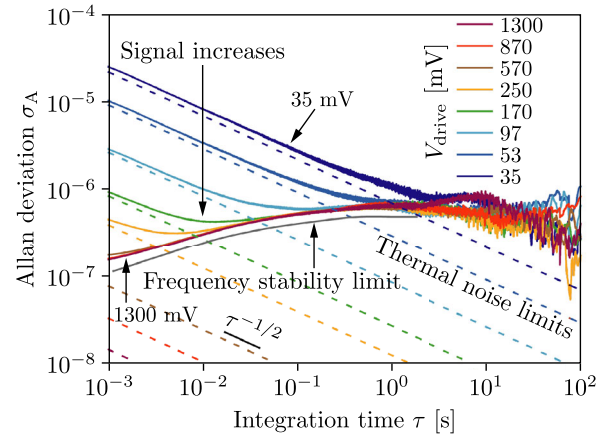


FIG. 29. Allan deviation as a function of integration time, from 1 ms to 100 s, for different amplitudes of the resonant drive  $V_{\text{drive}}$ . The curves are numbered from top to bottom in order of decreasing  $V_{\text{drive}}$ . Dashed lines indicate the expected stability from the output signal at each drive voltage and the total additive noise in the system, including thermal and measurement-related noises. The lowest solid line is a visual guide highlighting the experimentally measured lower bound for frequency stability. Adapted from Sansa *et al.*, 2016.

#### A. Allan variance

The most broadly used method of characterizing frequency fluctuations is based on measuring the Allan variance. To find it, following the original approach (Allan, 1966) one has to measure the average frequency  $\bar{f}(\tau)$  over time  $\tau$  and compare the values of this frequency obtained as the system evolves. Specifically, an  $m$ th value of the average frequency  $\bar{f}_m \equiv \bar{f}_m(\tau)$  is determined by the increment of the overall vibration phase  $\varphi$  over the time from  $t_m$  to  $t_m + \tau$ , and then  $\bar{f}_m = [\varphi(t_m + \tau) - \varphi(t_m)]/2\pi\tau$ . If  $f_0 = \omega_0/2\pi$  is the mean value of  $\bar{f}_m$ , the Allan variance found from  $N$  measurements is defined as

$$\sigma_A^2(\tau) = \frac{1}{2(N-1)f_0^2} \sum_{m=1}^{N-1} (\bar{f}_{m+1} - \bar{f}_m)^2. \quad (70)$$

The Allan variance can be expressed in terms of the power spectrum of the full phase  $\varphi$ . This gives  $\sigma_A^2(\tau)$  in a simple explicit form for several types of noise and for a different relation between  $\tau$  and the mode relaxation time  $\Gamma^{-1}$ , in the closed-loop and open-loop measurements; see Appendix H. The Allan variance as defined by Eq. (70) does not distinguish between fluctuations of the eigenfrequency and the rotating-frame phase  $\phi$ . It also does not provide information about the statistics of the fluctuations.

Figure 29 shows the measurements of the Allan deviation  $\sigma_A$  in a single-crystal Si nanoresonator based on the described approach (Sansa *et al.*, 2016). The studied nanoresonators had  $Q$  in the range  $(5-7) \times 10^3$  and the experiments were done at room temperature. It is seen that the experimentally observed noise can be several orders of magnitude higher than the one expected from thermal fluctuations of the phase  $\phi$  and described by



$$\sigma_A^2(\tau) = (2\Gamma k_B T / \omega_0^4 A^2) \tau^{-1}, \quad (71)$$

cf. Eq. (H3). A significantly larger Allan deviation than what would be expected from thermal noise has been reported for essentially all nanomechanical systems studied thus far. These observations suggest that a major contribution to  $\sigma_A$  comes from other noise sources. Fluctuations of the mode eigenfrequency are of particular importance in this respect.

### B. Eigenfrequency fluctuations

Several mechanisms of eigenfrequency fluctuations of nanoresonators have been discussed in the literature. Besides the fluctuations due to the mode nonlinearity and nonlinear mode coupling discussed in Sec. VI.C.1, they include the aforementioned noise due to the random attachment and detachment of molecules, molecule diffusion along the resonator (Atalaya, Isacsson, and Dykman, 2011b; Yang *et al.*, 2011; Schwender *et al.*, 2018), tension fluctuations due to temperature fluctuations, defect motion, transitions between the states of two-level systems within a material or on the surface (Fong, Pernice, and Tang, 2012; Hamoumi *et al.*, 2018; MacCabe *et al.*, 2020), and local charge fluctuations (Yazdani *et al.*, 2009; Siria *et al.*, 2012; Miao *et al.*, 2014; Dash *et al.*, 2021).

Different fluctuation mechanisms lead to eigenfrequency fluctuations with different timescales, i.e., with different correlation times  $t_c$ . The fluctuation statistics is also different. Often several fluctuation mechanisms with different  $t_c$  and different statistics jointly affect the mode dynamics.

The presence of eigenfrequency fluctuations can be revealed by comparing the power spectrum of a mode or the spectrum of its response to a resonant drive with the results of a ringdown measurement where the decay of initially excited vibrations is studied. In the absence of nonlinear friction the decay is exponential in time, with the decrement given by the friction coefficient  $\Gamma$ , as seen in Eq. (21). If there are no eigenfrequency fluctuations,  $\Gamma$  is also the half-width of the power spectrum  $S(\omega)$ ; cf. Eq. (5). However, the shape of the spectrum often deviates from the Lorentzian and the half-width  $\Delta\omega$  exceeds  $\Gamma$  even when the vibrations are linear (Schneider *et al.*, 2014; Güttinger *et al.*, 2017; MacCabe *et al.*, 2020). This is a consequence of eigenfrequency fluctuations.

An advantageous approach to separating and characterizing eigenfrequency fluctuations is based on studying the mode dynamics in the presence of a close to resonance drive (Maizelis, Roukes, and Dykman, 2011; Fong, Pernice, and Tang, 2012; Gavartin, Verlot, and Kippenberg, 2013; Zhang *et al.*, 2014; Sun *et al.*, 2015; Zhang and Dykman, 2015; Kalaei *et al.*, 2019). The drive breaks the time-translation symmetry of the system; cf. Sec. VII.C. As a result, fluctuations of the in-phase and quadrature vibration components become different, which leads to several observable consequences.

One of these consequences is pronounced in the correlators  $\langle u(t_1) \dots u(t_n) \rangle$  of the complex amplitude of the driven mode

$$u(t) = (2M\omega_F)^{-1} [M\omega_F q(t) - ip(t)] \exp(-i\omega_F t),$$

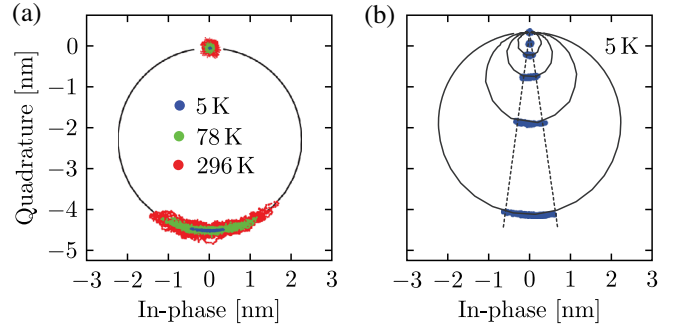


FIG. 30. Fluctuations of the in-phase and quadrature components of a resonantly driven SiN nanoresonator. The black circles show the driven response when the driving frequency  $\omega_F$  is swept across the resonance. (a) Increase of the fluctuations with increasing temperature. (b) Dependence on the driving amplitude. With no driving the mode fluctuates about zero (the data points at the top). Adapted from Fong, Pernice, and Tang, 2012.

where  $\omega_F$  is the drive frequency; cf. Eq. (H4). These correlators are nonzero only because of the broken time-translation symmetry, and it follows from the time-symmetry arguments that for a linear mode they do not depend on thermal noise and the corresponding phase fluctuations. However, they explicitly depend on fluctuations  $\delta\omega_0(t)$  of the eigenfrequency. Studying these correlators provides a direct way to characterize the spectrum and statistics of the eigenfrequency fluctuations and enables one to measure the correlators  $\langle \delta\omega_0(t_1) \dots \delta\omega_0(t_n) \rangle$  (Maizelis, Roukes, and Dykman, 2011). The ratio  $\langle u^2 \rangle / \langle u \rangle^2$  was used by Gavartin, Verlot, and Kippenberg (2013) to characterize eigenfrequency fluctuations in a nanomechanical beam; they also showed that the fluctuations can be suppressed with a feedback using a second mechanical mode as a frequency noise detector. The experiment on a micromechanical resonator in which the eigenfrequency was modulated by telegraph noise (Sun *et al.*, 2015) demonstrated the possibility of revealing the noise statistics by measuring the moments  $\langle u^n \rangle$ .

The role of eigenfrequency fluctuations is seen in Fig. 30, which shows fluctuations of the quadrature and in-phase components of a driven high- $Q$  nanomechanical resonator (Fong, Pernice, and Tang, 2012). Whereas the fluctuational spread of the quadrature component is essentially independent of the amplitude of forced vibrations  $A$ , the spread of the in-phase component increases with an increasing amplitude. The observed spread of the vibration phase counted off from  $\omega_F t$  ( $\omega_F$  is the drive frequency),  $\phi(t) - \omega_F t$ , is practically independent of  $A$  at low temperatures. For the thermomechanical noise, on the other hand, it would fall off with an increasing  $A$ ,  $\sigma_A^2 \propto A^{-2}$ ; cf. Eq. (71) and Appendix H. The observed phase spread is a direct consequence of the fluctuations of  $\omega_0$ , with the phase deviation

$$\delta\phi(t) \approx \int_{-\infty}^t dt' \exp[-\Gamma(t-t')] \delta\omega_0(t')$$

for a weak eigenfrequency noise. The data allowed Fong, Pernice, and Tang (2012) to study the low-frequency part of the spectrum of the fluctuations  $\delta\omega_0(t)$ . It was found to be of

the  $1/f$  type and was related to reorienting two-state elastic dipoles.

The power spectrum of the eigenfrequency fluctuations in a broad frequency range can be extracted directly from the power spectrum of a driven mode  $S(\omega)$  (Zhang *et al.*, 2014; Zhang and Dykman, 2015). For a linear mode this can be qualitatively explained as follows. With no noise, a resonant force  $F \cos \omega_F t$  leads to the mode displacement (cf. Sec. VII.A)

$$q(t) = \frac{F}{2M\omega_F} \text{Re} \frac{i \exp(-i\omega_F t)}{\Gamma - i(\omega_F - \omega_0)}. \quad (72)$$

If in Eq. (72)  $\omega_0$  is fluctuating [that is, if  $\omega_0$  is formally replaced by  $\omega_0 + \delta\omega_0(t)$ ], the displacement  $q(t)$  is also fluctuating. This should lead to an extra peak in the power spectrum of the mode. The form of this peak strongly depends on the interrelation between the correlation time  $t_c$  of the fluctuations  $\delta\omega_0(t)$  and the relaxation time of the mode  $\Gamma^{-1}$ . Since the power spectrum is quadratic in  $q(t)$ , it is clear from Eq. (72) that the peak is proportional to  $F^2$ , which allows one to identify it and separate it from other spectral features.

The replacement of  $\omega_0$  with  $\omega_0 + \delta\omega_0(t)$  in Eq. (72) is applicable if the correlation time of the eigenfrequency fluctuations  $t_c$  is large compared to the mode relaxation time  $\Gamma^{-1}$ , so the mode adiabatically follows these fluctuations. The fluctuation-induced slow time variation of the amplitude and phase of the forced vibrations at frequency  $\omega_F$  lead to a narrow spectral peak that is centered at  $\omega_F$ . The width of this peak is  $\sim t_c^{-1}$ . For small  $|\delta\omega_0(t)|$  the peak is proportional to the power spectral density  $S_{\delta\omega_0}(\omega - \omega_F)$  of  $\delta\omega_0(t)$ . Therefore, the shape of the peak allows one to directly read off this spectral density. In an experiment on a carbon nanotube resonator (Zhang *et al.*, 2014) carried out at  $T = 1.2$  K, the spectral density of the eigenfrequency fluctuations was found to be  $S_{\delta\omega_0}(\omega) \propto \omega^{-\alpha}$  for small  $\omega$ , with  $\alpha \approx 0.5$ . A similar measurement was done for a silicon nanobeam, where such  $1/f$ -type scaling was also observed, with the exponent  $\alpha \approx 0.7$  (Sun *et al.*, 2016).

Slow eigenfrequency fluctuations determine the long-term stability of devices based on nanoresonators and microresonators, including clocks. However, they do not lead to a broadening of the spectral response in the absence of the drive if the response is measured over a short time compared to  $t_c$ . The position of the spectral peak shifts from measurement to measurement in this case. If the duration of a measurement is  $\gtrsim t_c$  and  $\langle \delta\omega_0^2 \rangle \gtrsim \Gamma^2$ , the spectrum is broadened. This is an analog of the inhomogeneous spectral broadening. The effect was observed for a nanotube resonator (Moser *et al.*, 2014) and for a breathing mode in a phononic crystal (MacCabe *et al.*, 2020).

The opposite limit of comparatively fast eigenfrequency fluctuations ( $t_c \ll \Gamma^{-1}$ ) is not directly described by Eq. (72). A qualitative picture is somewhat more involved (Zhang *et al.*, 2014), but, roughly, one can consider the major spectral effect of the drive in this case as coming from the effective heating of the mode, with  $\delta T \propto F^2$ .

Fast fluctuations  $\delta\omega_0(t)$  lead to a broadening of the power spectrum of a mode  $S(\omega)$  in the absence of driving. The power spectrum and the mode susceptibility have a Lorentzian shape

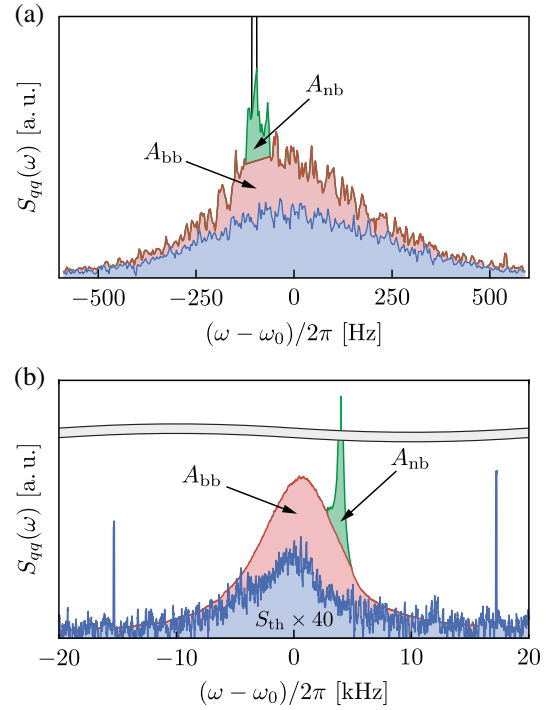


FIG. 31. Power spectra of driven modes with fluctuating eigenfrequencies. (a) Flexural mode of a carbon nanotube with the eigenfrequency  $\omega_0/2\pi = 6.3$  MHz (Zhang *et al.*, 2014). (b) Breathing mode of a nanobeam phononic crystal with the eigenfrequency  $\omega_0/2\pi \approx 425$  MHz (Kalaee *et al.*, 2019). The lowest (blue) curves show the thermal power spectra without drive [multiplied by 40 in (b)]. The regions marked as  $A_{bb}$  and  $A_{nb}$  indicate the driving-induced parts of the power spectrum, which are due to the fast (broadband) and slow (narrowband) eigenfrequency fluctuations. The narrow peaks are centered at the drive frequencies.

with a half-width  $\Delta\omega$ , which is the sum of  $\Gamma$  and the characteristic intensity of the eigenfrequency fluctuations. This feature holds regardless of the statistics of the fluctuations provided that  $\Delta\omega \ll \omega_0$ . It has often been used to describe experiments; cf. Eq. (10).

Studying the spectrum in the presence of driving allows one to separate the contribution of fast frequency fluctuations. The corresponding driving-induced part of the spectrum  $S_F(\omega)$  can be written as

$$S_F(\omega) \approx C_F F^2 \frac{(\Delta\omega - \Gamma)/\Gamma}{\Delta\omega^2 + (\omega_F - \omega_0)^2} \frac{S(\omega)}{k_B T}. \quad (73)$$

Here, strictly speaking,  $\omega_0$  is also renormalized by the frequency fluctuations if they are non-Gaussian; the explicit form of  $C_F$  depends on the statistics of the fluctuations  $\delta\omega_0(t)$  (Zhang *et al.*, 2014). The spectrum  $S_F(\omega)$  has the same shape  $S(\omega)$  as in the absence of driving but is proportional to the squared driving amplitude. It is also proportional to the difference between the fluctuation- and decay-induced broadening  $\Delta\omega - \Gamma$ .

In Fig. 31 we show the results of two experiments (Zhang *et al.*, 2014; Kalaee *et al.*, 2019) that demonstrate how the interplay of the driving and the eigenfrequency fluctuations

affects the power spectrum. Even though the studied systems were significantly different, the observations show the occurrence of a narrow peak centered at the drive frequency and a broad spectrum with a shape similar to that in the absence of driving. Comparing the areas of the peaks with and without driving allowed the contribution of the fast eigenfrequency fluctuations to the observed spectral broadening  $\Delta\omega$  to be estimated. In both experiments this contribution was  $\gtrsim 50\%$ .

## X. OUTLOOK AND CHALLENGES

The goal of this review is to demonstrate the nontrivial physics of nanomechanical systems and the possibility of using them as a platform for studying a broad range of nonlinear and nonequilibrium phenomena in a controlled setting, and also to indicate their numerous applications. These intertwined aspects of nanomechanics make it a fairly unique interdisciplinary area of research and underlie the growing interest in NVs. The interest is further stimulated by the rapid progress in nanotechnology, which allows existing types of NVs to be improved and qualitatively new NVs to be made. In closing the review, we present some of the nascent directions for research in the field. Unavoidably, such a list will be incomplete, particularly given the high rate at which new results are obtained.

An important aspect of the mesoscopic dynamics of NVs are coherent effects. Among them, of significant current interest are the effects of coupling nanomechanical modes to qubits (Lee *et al.*, 2017; Arrangoiz-Arriola *et al.*, 2019) (see also Sec. VI.C.2), as well as the use of qubits to entangle different mesoscopic modes (Wollack *et al.*, 2022). Related is a significant effort to develop nanomechanical resonators with high- $Q$  modes with microwave frequencies (MacCabe *et al.*, 2020; Wollack *et al.*, 2022). These modes can be brought to the ground quantum state for temperatures  $\lesssim 0.1$  K without sideband or active feedback cooling (that reduces the  $Q$  factor) and can be in resonance with superconducting qubits (Mirhosseini *et al.*, 2020). Vibrations localized around engineered defects in phononic crystals with frequencies in the gap of the spectrum of propagating modes are an important type of these modes.

A promising direction in the context of quantum information and coherent effects in nanomechanics is developing qubits based on the NVs. This requires vibration nonlinearity that remains large compared to the decay rate down to the quantum regime. Resonant driving at the frequency of the transition from the ground to the first excited vibrational state does not lead to transitions to higher-energy states, similar to the case of superconducting qubits. The corresponding nonlinearity can be achieved by coupling mechanical vibrations to the charge states of a double-quantum dot. For a qubit based on a carbon nanotube resonator, the coherence time is predicted to be particularly long (Pistolesi, Cleland, and Bachtold, 2021). A strong nonlinearity can also be achieved near a bifurcation point where a nanotube or a nanomembrane is close to collapse due to the strong gate voltage and can tunnel into the collapsed state (Sillanpää *et al.*, 2011).

Topological effects form another group of coherent phenomena that attract current attention. The possibility of observing such effects in phononic crystals in an

optomechanical setting was indicated by Peano *et al.* (2015), and thermal phonons traveling along a topological edge channel with weak backscattering have been observed in an array of over 800 submicron silicon membranes, the largest optomechanical array thus far (Ren *et al.*, 2020). A two-dimensional metamaterial made out of submicron SiN membranes, which has time-reversal symmetry, has been demonstrated to have pseudospin-type edge states, which are robust to waveguide distortion (Cha, Kim, and Daraio, 2018). The possibility to control the phononic band structure electrostatically makes nanoresonator-based metamaterials interesting even where they are topologically trivial. Such control can be used for dynamical tuning of acoustic transparency and waveform engineering in phononic waveguides (Cha and Daraio, 2018; Kurosu *et al.*, 2018; Hatanaka, Bachtold, and Yamaguchi, 2019).

Yet another group of coherent effects is related to the dynamics of NVs in a driving field with frequency  $\omega_F$  close to an overtone of the mode eigenfrequency  $\omega_F \approx n\omega_0$ . This drive can resonantly excite vibrational states at a frequency  $\omega_F/n$ , with  $n > 1$ . The case of  $n = 2$  corresponds to the parametric excitation discussed for a single mode in Sec. VII.B. For coupled NVs, the interaction between driven modes may lead to formation of time crystals where the discrete time-translation symmetry imposed by the periodic drive is broken; i.e., phase-matched vibrations occur at a frequency  $\omega_F/n \approx \omega_0$  (Dykman *et al.*, 2018). The properties of such dissipation-free Floquet time crystals are strongly affected by the nontrivial geometric phase (Lörch *et al.*, 2019) that emerges for  $n \geq 3$  (Guo, Marthaler, and Schön, 2013; Zhang *et al.*, 2017). The resonant-driving-induced time crystals are expected to take an exponentially long time until they are heated up and ultimately melted by the drive.

The “incoherent” side of the dynamics of coupled NVs, i.e., the dynamics in the presence of relaxation and thermal fluctuations, is closely connected to the “coherent” side. Arrays of dissipative resonantly driven NVs can display time-crystalline behavior (Dykman *et al.*, 2018; Heugel *et al.*, 2019), which in this case can have features related to the breaking of the detailed balance. These arrays should enable, in particular, study of the effects of disorder in the eigenfrequencies and the coupling on the quantum and classical time-symmetry-breaking transitions. Coupled NVs can also display topological solitons (Lin *et al.*, 2021; Yamaguchi and Houri, 2021). Topologically nontrivial dissipative networks with interesting dynamics can also be created by driving coupled resonators with radiation modulated at the difference of their frequencies (del Pino, Slim, and Verhagen, 2021). Challenging observations of broken-symmetry states with complex dynamics have been reported for networks of NVs that display self-sustained vibrations (Matheny *et al.*, 2019). Overall, the dynamics of coupled NVs, which has been attracting attention for a long time (Buks and Roukes, 2002; Lifshitz and Cross, 2003, 2008; Cross and Greenside, 2009; Karabalin, Cross, and Roukes, 2009), is significantly enriched by the topological and Floquet aspects.

NVs are playing an increasingly important role in studying condensed-matter systems. One of the pursued directions is to establish microscopic mechanisms of energy relaxation in vibrational modes. A significant effort has recently been put



into identifying Landau-Rumer and Akhiezer relaxation, with experiments covering a range from ultralow temperatures to room temperature (Rodriguez *et al.*, 2019; MacCabe *et al.*, 2020; Tepsic *et al.*, 2021). Understanding nonlinear damping and its dependence on the material, geometry, and temperature is on the horizon (Atalaya *et al.*, 2016; Steeneken *et al.*, 2021), as is the origin of the low quality factor of graphene, carbon nanotubes, and MoS<sub>2</sub> resonators at room temperature (Sazonova *et al.*, 2004; Bunch *et al.*, 2007; Castellanos-Gomez *et al.*, 2013). Another direction involves thermal effects in nanostructures. Heat transfer has been measured in graphene and MoSe<sub>2</sub> monolayers down to cryogenic temperatures, and slow equilibration between different vibrational branches of graphene has been established using photothermal response (Morell *et al.*, 2019; Dolleman *et al.*, 2020); see also Sullivan *et al.* (2017). The mechanical detection and control of magnetic states and magnetic phase transitions in two-dimensional layered antiferromagnetic CrI<sub>3</sub> and FePS<sub>3</sub> materials have been demonstrated down to two layers (Jiang *et al.*, 2020; Šiškins *et al.*, 2020). The charge density wave transition has also been measured in 2H-TaS<sub>2</sub> and 2H-TaSe<sub>2</sub> layered materials (Lee *et al.*, 2021). Regarding electron-vibrational coupling, it has been shown using carbon nanotubes that where the coupling is sufficiently strong it results in controlled vibration cooling or excitation of self-sustained vibrations in response to source-drain voltage (Urgell *et al.*, 2020; Wen *et al.*, 2020).

Substantial work is being done to characterize two-level fluctuators with NVs. A promising direction is opened by passively cooling NVs down to low temperatures (MacCabe *et al.*, 2020; Maillet *et al.*, 2020; Gisler *et al.*, 2021; Kampainen, Mäkinen, and Eltsov, 2022), including submillikelvin temperatures, where even megahertz-range modes are close to the quantum ground state (Cattiaux *et al.*, 2021). The characteristic temperature dependencies of the decay rate and the frequency shift of the NV modes found using the ringdown measurements and the measurements of the response and fluctuation spectra provide an insight into the relaxation mechanisms of two-level systems in nanostructures.

NVs have demonstrated superior sensitivity and spatial resolution in the study of superfluid <sup>3</sup>He and <sup>4</sup>He. They have been used to detect Cooper pair breaking in <sup>3</sup>He (Defoort *et al.*, 2016), as well as to measure helium viscosity, detect modulated “phonon wind” (Guénault *et al.*, 2019, 2020), trap a single vortex (Guthrie *et al.*, 2021), and study new effects of quantum turbulence at ultralow temperatures (Barquist *et al.*, 2020, 2021) in <sup>4</sup>He. A series of first-order layering transitions of liquid helium on a carbon nanotube observed by Noury *et al.* (2019) suggested the possibility of new types of phase transitions on smooth defect-free cylindrical surfaces.

Nanomechanics has essentially opened up the field of experimental studies of nonlinear dynamics of fluctuating vibrational systems. The field is vibrant. Fluctuations can now be measured in real time. For a carbon nanotube, such measurements have revealed a weakly chaotic regime in which, at room temperature, the energy concentrates in low-frequency modes, disperses into higher-frequency modes, and then returns (Barnard *et al.*, 2019), reminiscent of the Fermi-Pasta-Ulam-Tsingou behavior. The interplay of

fluctuations and nonlinearity leads to rich dynamics in systems with a few or even one vibrational mode away from thermal equilibrium, which is related to the breaking of the detailed balance (Roberts, Lingenfelter, and Clerk, 2021), see Sec. VII.C. This includes the scaling behavior of fluctuations near various types of bifurcation points (Jessop, Li, and Armour, 2020; Tadokoro, Tanaka, and Dykman, 2020), the onset of chaos in the rotating frame (Güttinger *et al.*, 2017; Hourì, Asano *et al.*, 2020), and new types of fluctuation squeezing in driven systems in the nonlinear regime (Huber *et al.*, 2020; Yang *et al.*, 2021). Noise squeezing in a nonlinear regime may improve measurement sensitivity, particularly for phase-based measurements (see Sec. IX), by reducing the detrimental effect of thermal noise. Reducing measurement noise is also on the agenda, and to this end new detection methods are explored, such as focused electron beams (Pairis *et al.*, 2019).

Among various nonlinear resonant phenomena that can be accessed with NVs, of increasing interest are nanomechanical frequency combs. These combs have been generated in coupled modes that display nonlinear resonance or in a single mode using feedback control (Hourì *et al.*, 2019, 2021; Hourì, Hatanaka *et al.*, 2020; Singh *et al.*, 2020). A large number of spectral lines have been observed in nanomechanical systems with coupled modes displaying a saddle node on an invariant circle bifurcation (Czaplewski *et al.*, 2018) (see Sec. VIII.B), or by parametrically inducing resonant mode coupling (Chiout *et al.*, 2021). However, driven nonlinear NVs are expected to display a multipleline comb even when there is only a single mode involved but the dissipation is nonlinear (Dykman *et al.*, 2019). An observation of such a comb was recently reported by Ochs *et al.* (2022).

The high sensitivity of the NVs provides a means for addressing fundamental physics problems. Some of these problems are related to the Casimir force at small distances and its dependence on the material properties and the geometry, as well as thermal and nonequilibrium effects (Tang *et al.*, 2017; Gong *et al.*, 2021; Liu *et al.*, 2021; Wang *et al.*, 2021). The possibility of studying the interplay of quantum mechanics and gravity (Schmölle *et al.*, 2016; Liu, Mummery, and Sillanpää, 2021) is being explored. The study of non-Newtonian gravity and even physics beyond the standard model, particularly with levitated particles (which can now be cooled down to their ground quantum state), is also being discussed (Gonzalez-Ballesterio *et al.*, 2021; Moore and Geraci, 2021). Slowly decaying vibrations (with a decay rate < 100 μHz) of levitated nanoparticles are being considered in a somewhat exotic context of the wave-function collapse (Pontin *et al.*, 2020).

Various coherent quantum effects in coupled NVs have attracted substantial attention (Ockeloen-Korppi *et al.*, 2018; de Lépinay *et al.*, 2021; Kotler *et al.*, 2021). These and a number of other quantum effects, such as the cooling of vibrations to their ground state by coupling them to an electromagnetic cavity (see Sec. VIII.C), using NVs to convert microwave-frequency excitation of a superconducting qubit into an optical photon (Mirhosseini *et al.*, 2020), or optically reading out a transmon qubit (Delaney *et al.*, 2022), are often studied in the context of optomechanics, a burgeoning area borne out of nanomechanics (Aspelmeyer,

Kippenberg, and Marquardt, 2014b). Recent improvements of nanofabricated NVs (MacCabe *et al.*, 2020; Beccari *et al.*, 2022; Seis *et al.*, 2022) will lead to further advances in optomechanics.

One of the most important applications of NVs is the emerging technology of single-molecule mass spectrometry with potentially high throughput. It will take advantage of NVs-based inertial imaging (Hanay *et al.*, 2015; Sage *et al.*, 2018). Nanowires and nanotubes hold promise as cantilevers for the next-generation scanning probe microscopes. By utilizing the fundamental modes polarized in perpendicular directions, these cantilevers enable direct imaging of the components of the force fields and allow one to establish whether the field is a potential field (de Lépinay *et al.*, 2017; Rossi *et al.*, 2017). Cantilevers functionalized with a magnetic material at their free end (Rossi *et al.*, 2019) hold promise for imaging a large range of physical phenomena, such as skyrmions, superconducting vortices, and current-carrying edge states in two-dimensional systems (Braakman and Poggio, 2019). Magnetic resonance force microscopy with single nuclear spin sensitivity is another direction of great interest (Rose *et al.*, 2018; Grob *et al.*, 2019).

## LIST OF SYMBOLS AND ABBREVIATIONS

$q$	mode coordinate; it is proportional to the displacement at the antinode of the mode
$p$	momentum conjugate to the coordinate $q$
$M$	effective mass of the mode
$u$	complex vibration amplitude
$S(\omega)$	spectral density of fluctuations of $q$ at frequency $\omega$
$\chi(\omega)$	susceptibility of the coordinate at frequency $\omega$
$\omega_0 = 2\pi f_0$	eigenfrequency of the mode
$\gamma$	parameter of the Duffing, or Kerr, nonlinearity
$\Gamma$	linear friction coefficient; decay rate of the vibration amplitude in the linear regime
$Q = \omega_0/2\Gamma$	quality factor from energy decay measurements
$\Delta\omega$	spectral bandwidth of mechanical resonance; half width at half maximum of the resonant peak in $S(\omega)$
$Q_\omega = \omega_0/2\Delta\omega$	quality factor from spectral measurements
$\omega_F$	angular frequency of a resonant driving force

## ACKNOWLEDGMENTS

A. B. acknowledges ERC Advanced Grant No. 692876, AGAUR (Grant No. 2017SGR1664), MICINN Grant

No. RTI2018-097953-B-I00, the Fondo Europeo de Desarrollo, the Spanish Ministry of Economy and Competitiveness through Quantum CCAA and CEX2019-000910-S (MCIN/AEI/10.13039/501100011033), the QuantERA grant (No. PCI2022-132951), MCIN with funding from European Union NextGenerationEU (PRTR-C17.I1), Fundación Cellex, Fundació Mir-Puig, and Generalitat de Catalunya through CERCA. J.M. was supported by the National Natural Science Foundation of China through Grants No. 62150710547 and No. 62074107. M. I. D. was supported in part by the National Science Foundation through Grants No. DMR-1806473 and No. CMMI-1661618, and by the Google Faculty Research Award.

## APPENDIX A: METHOD OF AVERAGING: WEAK NONLINEARITY AND WEAK DAMPING

### 1. Nonlinear vibrations with no damping

The Bogoliubov-Krylov method of averaging used to derive the equation of motion for the complex amplitude of the mode is similar to the rotating wave approximation (RWA) in quantum mechanics. One thinks of the mode dynamics as vibrations at the mode frequency  $\omega_0$  with an amplitude  $A(t)$  and a phase  $\phi(t)$  that slowly vary on the timescale of the vibration period  $2\pi/\omega_0$ ; that is, the mode coordinate is  $q(t) = A(t) \cos[\omega_0 t + \phi(t)]$ . We note that  $\phi(t)$  here is the “reduced” phase: it does not contain the term  $\omega_0 t$ . The complex slow variable  $u(t)$  (the complex amplitude) defined by Eq. (20) is simply related to  $A$  and  $\phi$ ,

$$u(t) = \frac{1}{2} \left( q - i \frac{p}{M\omega_0} \right) e^{-i\omega_0 t} = \frac{1}{2} A(t) \exp[i\phi(t)]. \quad (\text{A1})$$

For a harmonic mode that is not coupled to a bath,  $A$  and  $\phi$  are independent of time and  $u(t) = \text{const}$ . A more general form of the averaging method is discussed in Appendix F.

In this section we show how the dynamics is modified by the weak nonlinearity of the mode. To simplify the reading we repeat some equations from the main text. We illustrate the Bogoliubov-Krylov method by applying it to the Duffing oscillator. The goal is to describe the dynamics on times that largely exceed the vibration period  $2\pi/\omega_0$ . A direct perturbation theory in the nonlinearity does not apply, as it leads to a secular ( $\propto t$ ) correction to the oscillator displacement. Instead, one should use the asymptotic perturbation theory.

The Hamiltonian of a nonlinear mode is

$$H_0 = \frac{1}{2M} p^2 + U(q). \quad (\text{A2})$$

For the Duffing model the potential energy is

$$U(q) = \frac{1}{2} M \omega_0^2 q^2 + \frac{1}{4} M \gamma q^4,$$

cf. Eq. (46).

With account taken of the relation  $p = M\dot{q}$ , we obtain from the definition of  $u(t)$  [Eq. (A1)]  $\dot{u} \exp(i\omega_0 t) + \dot{u}^* \exp(-i\omega_0 t) = 0$ . Therefore,

$$\ddot{q} + \omega_0^2 q = 2i\omega_0 \dot{u} e^{i\omega_0 t} = -2i\omega_0 \dot{u}^* e^{-i\omega_0 t}, \quad (\text{A3})$$

and the Hamiltonian equation of motion for  $u(t)$  reads

$$\dot{u} = i \frac{\gamma}{2\omega_0} (u e^{i\omega_0 t} + u^* e^{-i\omega_0 t})^3 e^{-i\omega_0 t}. \quad (\text{A4})$$

The timescale on which  $u(t)$  varies because of the non-linearity is seen from Eq. (A4) to be  $\sim \omega_0/|\gamma||u|^2 \gg \omega_0^{-1}$ . The right-hand side of Eq. (A4) contains the smooth term  $\propto u|u|^2$ , which is a constant for a time  $\delta t \ll \omega_0/|\gamma||u|^2$  [since practically  $u(t)$  does not change over this time] and the terms that oscillate as  $\exp(\pm 2i\omega_0 t)$  and  $\exp(-4i\omega_0 t)$ . All these terms are of the same order of magnitude. However, if we now integrate them over time  $\delta t \gg \omega_0^{-1}$ , the contribution of the smooth term will be  $\propto \delta t$ , whereas the contribution of the fast-oscillating terms will be  $\propto \omega_0^{-1} \ll \delta t$ . Therefore, to describe the dynamics of the oscillator on times  $\gg \omega_0^{-1}$  the fast-oscillating terms can be disregarded and the equation of motion becomes

$$\dot{u} \approx 3i\gamma u|u|^2/2\omega_0, \quad u(t) \approx u(0)e^{3i\gamma|u|^2 t/2\omega_0}. \quad (\text{A5})$$

In this approximation  $|u(t)|$  does not change in time, i.e., the vibration amplitude  $A \approx (4|u|^2)^{1/2}$  does not change. However, the vibration phase acquires an extra term  $3\gamma|u|^2 t/2\omega_0$ . Comparing Eq. (A5) to the expression  $q(t) = u(t) \exp(i\omega_0 t) + \text{c.c.}$  [cf. Eq. (A1)], one can see that it corresponds to the change of the oscillator frequency (48),

$$\omega_0 \rightarrow \omega_0 + 3\gamma|u|^2/2\omega_0 = \omega_0 + 3\gamma A^2/8\omega_0.$$

## 2. Effect of the coupling to a bath

We now extend the Bogoliubov-Krylov method to describe the dynamics of the mode where it is weakly coupled to a thermal reservoir. There are two parts to this description that are closely intertwined. One part is the evaluation of the average reaction force from the bath in slow time compared to  $\omega_0^{-1}$ . The second part refers to the random part of the force from the bath, the noise in the equations of motion for  $u(t)$ , and its properties in slow time. In the ensuing approximation, the mode dynamics in *slow time* is Markovian.

For the coupling to the bath of the form  $H_i = qh_b$ , the part of the force from the bath that describes the reaction of the bath to the mode (the backaction) is [cf. Eq. (16)]

$$F_b^{(r)}(t) = -\delta h_b(t) \approx -\langle \delta h_b(t) \rangle \approx \int_0^\infty \mathcal{X}_b(t') [u(t-t') e^{i\omega_0(t-t')} + \text{c.c.}]. \quad (\text{A6})$$

Here  $\mathcal{X}_b(t)$  is the time-dependent bath susceptibility. Remember that Eq. (A6) is an approximation, as we have replaced the full reaction force  $\delta h_b(t)$  with its ensemble-averaged value  $\langle \delta h_b(t) \rangle$  and kept in the latter only the lowest-order term, which describes the linear response of the bath to the bath-mode coupling.

We now expand  $u(t-t') = u(t) - t'\dot{u}(t) + \dots$  and keep only the first term in this expansion (Dykman and Krivoglaz, 1971), relying on the smoothness of  $u(t)$  (discussed later). Using the definition of the Fourier transform of the bath susceptibility

$$\chi_b(\omega) = \int_0^\infty dt \exp(i\omega t) \mathcal{X}_b(t) \quad (\text{A7})$$

and taking into account that  $\chi_b(\omega) = \chi_b^*(-\omega)$  (Landau and Lifshitz, 1980), we obtain for the reaction force

$$F_b^{(r)}(t) \approx \chi_b^*(\omega_0) u(t) e^{i\omega_0 t} + \text{c.c.} \quad (\text{A8})$$

This force is determined by the instantaneous value of  $u(t)$  rather than the evolution of  $u(t')$  for  $t' \leq t$ .

Substituting the force (A8) into the full equation of motion for the mode coordinate  $q(t)$  and using Eq. (A3), we obtain the equation of motion (21) for  $u(t)$ , which we reproduce here for completeness,

$$\begin{aligned} \dot{u} &= -(\Gamma - iP)u + \xi(t), & \Gamma &= \text{Im} \chi_b(\omega_0)/2M\omega_0, \\ P &= -\text{Re} \chi_b(\omega_0)/2M\omega_0. \end{aligned} \quad (\text{A9})$$

Here the term  $\xi(t)$  describes the noise; it does not come from  $F_b^{(r)}$  and is discussed later. In Eq. (A9) we assumed that  $\Gamma \ll \omega_0$  and, in the spirit of the averaging method, disregarded the fast-oscillating term  $\propto \Gamma u^* \exp(-2i\omega_0 t)$  compared with  $\Gamma u$ .

In deriving Eqs. (A8) and (A9), we further assumed that the bath susceptibility  $\chi_b(\omega)$  weakly varies with  $\omega$  in a band of width  $\sim \Gamma$ ,  $|P| \ll \omega_0$  centered at  $\omega_0$ . It is this assumption that justifies disregarding the term  $t'\dot{u}(t)$  and higher-order derivatives of  $u(t)$  in the expansion of  $u(t-t')$  in Eq. (A6). In particular, the term  $t'\dot{u}$  gives the correction

$$\sim |(d\chi_b/d\omega)_{\omega=\omega_0} \dot{u}| \sim \Gamma |u(d\chi_b/d\omega)_{\omega=\omega_0}|,$$

which is assumed to be small compared to the term  $\sim |\chi_b(\omega_0)u|$  kept in Eq. (A9). The assumption holds for  $|d \log \chi_b/d\omega| \ll 1$ . The higher derivatives of  $\chi_b$  are assumed to be relatively small near  $\omega_0$  as well. The typical frequency on which  $\chi_b(\omega)$  changes provides the other reciprocal “fast” time of the mode + bath system, in addition to  $\omega_0^{-1}$ . It is sometimes called the correlation time of the thermal reservoir  $t_{\text{corr}}$ ; note, however, that  $\chi_b(\omega)$  characterizes not only the reservoir but also the coupling of the oscillator to the reservoir.

The approximation (A9) is a Markovian approximation in slow time. It holds if the response of the bath to the oscillator remains essentially unchanged where the oscillator frequency is changed not only by  $\Gamma$  but also by the polaronic frequency shift  $P$ . In our analysis of the nonlinear oscillator we further assume that the response of the bath does not change due to the change of the oscillator frequency caused by the dependence of this frequency on the vibration amplitude.

The Bogoliubov-Krylov method of averaging can also be applied to the analysis of the effect of the thermal noise on the slow variables. The noise in Eq. (A9) is



$$\xi(t) = (i/2M\omega_0)h_b^{(0)}(t)\exp(-i\omega_0 t),$$

where  $-h_b^{(0)}(t)$  is the force on the oscillator from the bath calculated by disregarding the reaction of the bath to the oscillator. The noise correlator is simply expressed in terms of the bath power spectrum

$$S_b(\omega) = \int_{-\infty}^{\infty} dt e^{i\omega t} \langle h_b^{(0)}(t) h_b^{(0)}(0) \rangle. \quad (\text{A10})$$

Clearly,  $\langle \xi^*(t) \xi(t') \rangle \propto \int d\omega S_b(\omega) \exp[-i(\omega - \omega_0)(t - t')]$ . We note that  $S_b(\omega)$  also defines the bath susceptibility, and thus the mode decay rate, via the fluctuation-dissipation theorem (cf. Sec. IV),

$$\text{Im} \chi_b(\omega) = S_b(\omega)/2\hbar[\bar{n}(\omega) + 1].$$

If we replace  $S_b(\omega) \rightarrow S_b(\omega_0)$  and use the relation (A9) between  $\Gamma$  and  $\chi_b(\omega_0)$ , we obtain

$$\langle \xi^*(t) \xi(t') \rangle = (\Gamma k_B T / M \omega_0^2) \delta(t - t').$$

As indicated in Sec. IV.B, the  $\delta$  function here is not a true  $\delta$  function but, effectively, a  $\delta$  function on the timescale  $\gg \omega_0^{-1}, t_{\text{corr}}$ . By expanding  $S_b(\omega)$  in a series about  $\omega_0$ , we find that  $\langle \xi^*(t) \xi(t') \rangle$  has a peak at  $t = t'$  with width  $|t - t'| \lesssim |S_b^{-1} d^2 S_b / d\omega^2|^{1/2} = t_{\text{corr}}$ , where the derivative of  $S_b$  is calculated for  $\omega = \omega_0$ ; this expression may be considered a definition of  $t_{\text{corr}}$ . The width  $t_{\text{corr}}$  is much smaller than  $\Gamma^{-1}$  for  $S_b(\omega)$  smooth near  $\omega_0$ . The argument here coincides with the argument used in disregarding delay in Eq. (A8).

The correlator  $\langle \xi^*(t) \xi^*(t') \rangle$  has an extra factor  $\exp[i\omega_0(t + t')]$  compared to the correlator  $\langle \xi^*(t) \xi(t') \rangle$ . This fast-oscillating factor averages out to zero on a timescale that is large compared to  $\omega_0^{-1}$ . Therefore, in an analysis of the evolution of the slow variables  $u(t)$  and  $u^*(t)$ , one can set  $\langle \xi^*(t) \xi^*(t') \rangle = 0$ . The analysis of the higher-order correlators shows that the noise  $\xi(t)$  is approximately Gaussian on a timescale that is large compared to  $\omega_0^{-1}, t_{\text{corr}}$ . For a bath modeled by a set of harmonic oscillators with the coupling  $h_b$  nonlinear in the coordinates of these oscillators, this was shown by Dykman and Krivoglaz (1971, 1973). This analysis applies to both classical and quantum cases. We note that a similar analysis has to be carried out to justify the expression for the reaction force in terms of the linear response of the bath to the mode.

### 3. Ohmic dissipation

Here for completeness we describe the effect of coupling to the bath in a more restrictive but important case where the power spectrum  $S_b(\omega)$  is flat in a broad range from  $\omega \ll \omega_0$  to  $\omega \gg \omega_0$ . The scale of the flatness is now  $\omega_0$ , not  $\Gamma$ ,  $|P|$ . For a flat  $S_b(\omega)$ , in the classical limit we can approximate the correlation function  $s_b(t)$  by a  $\delta$  function,

$$s_b(t) \equiv \langle h_b^{(0)}(t) h_b^{(0)}(0) \rangle = 4M\Gamma k_B T \delta(t). \quad (\text{A11})$$

Equation (A11) is essentially the definition of the parameter  $\Gamma$  in terms of the correlator  $s_b(t)$ , temperature, and the mode mass  $M$  for the case considered in this section.

Taking into account that, for a classical bath,  $\chi_b(t) = -(k_B T)^{-1} ds_b/dt$ , one obtains from Eq. (A6) the reaction force in the form

$$F_b^{(r)}(t) = \frac{s_b(0)}{k_B T} q(t) - \int_0^\infty dt' \frac{s_b(t')}{k_B T} \frac{dq(t - t')}{dt}. \quad (\text{A12})$$

For the  $\delta$ -correlated noise (A11), the last term in Eq. (A12) gives the friction force  $-2M\Gamma \dot{q}$  in the equation of motion (2). Thus, the reaction of the bath leads to viscous friction, with the friction force proportional to the mode velocity. With account taken of Eq. (A11), the overall dynamics of the mode is mapped on Brownian motion.

The first term on the right-hand side of Eq. (A12) renormalizes the mode frequency  $\omega_0^2 \rightarrow \omega_0^2 - s_b(0)/Mk_B T$ . This is a classical polaronic effect. In calculating  $s_b(0)$  one should keep in mind that the power spectrum  $S_b(\omega)$  falls off for high frequencies, which makes  $s_b(0)$  finite.

To our knowledge, for a classical oscillator the frequency shift was first found by Bogolyubov (1945) for a model where the bath is a set of harmonic oscillators and  $h_b$  is linear in the coordinates  $q_k$  of these oscillators. The corresponding Hamiltonian of the bath  $H_b$  reads

$$H_b = \frac{1}{2} \sum_k (p_k^2 + \omega_k^2 q_k^2), \quad (\text{A13})$$

whereas the coupling Hamiltonian is  $qh_b = \sum_k \epsilon_k q q_k$ . The coupling was weak and the dynamics was Markovian only in the rotating frame.

In quantum theory, the constraint on the coupling parameters in the model (A13) that leads to a viscous friction force in the laboratory frame was found by Caldeira and Leggett (1981). The expression for the friction coefficient  $\Gamma$  comes out if one assumes that the density of states of the bath weighted with the interaction has the form

$$\sum_k (\epsilon_k^2 / \omega_k) \delta(\omega - \omega_k) = (4/\pi) M \Gamma \omega.$$

## APPENDIX B: OSCILLATOR DECAY RATE IN THE BORN APPROXIMATION AND THE QUANTUM KINETIC EQUATION

Equation (A9) for the oscillator decay rate  $\Gamma$  can also be easily obtained from a slightly different point of view. We first recall that the coordinate and momentum of the oscillator are expressed in terms of the ladder operators  $a$  and  $a^\dagger$  as  $q = (\hbar/2M\omega_0)^{1/2}(a + a^\dagger)$  and  $p = -i(\hbar M\omega_0/2)^{1/2}(a - a^\dagger)$ . In an analysis of the quantum dynamics it is convenient to use the eigenfunctions  $|k\rangle$  of the occupation number operator  $a^\dagger a$ . The energy of the isolated harmonic oscillator in a state  $|k\rangle$  is  $\hbar\omega_0(k + 1/2)$ .

The coupling  $qh_b$  of the quantum oscillator to a thermal bath leads to transitions between the nearest oscillator energy levels in Fig. 32(a). The matrix elements of the coordinate  $q$

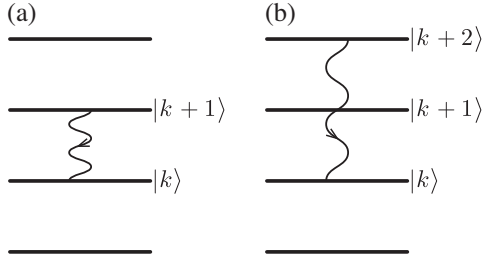


FIG. 32. Transitions between the oscillator energy levels with emission of excitations into a thermal bath. (a) Transitions between nearest levels lead, in the classical description, to a linear friction force proportional to the oscillator velocity. (b) Transitions between next-nearest levels lead, in the classical description, to a nonlinear friction force proportional to the oscillator velocity multiplied by the squared coordinate (in the van der Pol model) or by the squared velocity (in the Rayleigh model).

are  $\langle k|q|k-n\rangle = [\hbar k/2M\omega_0]^{1/2}\delta_{n,1}$  for  $n \geq 0$ . Therefore, to the leading order the linear in  $q$  coupling to the bath leads to transitions only between neighboring levels. From the Fermi golden rule, the rate  $W_{k+1 \rightarrow k}$  of the transition  $|k+1\rangle \rightarrow |k\rangle$  averaged over the states of the thermal bath is

$$W_{k+1 \rightarrow k} = (2\pi/\hbar)[\hbar(k+1)/2M\omega_0] \times \left\langle \sum_{\nu_b} |\langle \nu_b | h_b | \mu_b \rangle|^2 \delta(E_{\mu_b} - E_{\nu_b} + \hbar\omega_0) \right\rangle_{\mu_b}, \quad (\text{B1})$$

where  $\mu_b$  and  $\nu_b$  enumerate the bath states,  $E_{\mu_b}$  and  $E_{\nu_b}$  are the energies of these states, and  $\langle \cdot \rangle_{\mu_b}$  indicates thermal averaging over the states  $\mu_b$ , i.e., a summation with the weight  $\propto \exp(-E_{\mu_b}/k_B T)$ .

We now relate Eq. (B1) to the power spectrum  $S_b(\omega)$  of the operator  $h_b$ , which determines the coupling of the bath to the oscillator,

$$S_b(\omega) = \int_{-\infty}^{\infty} dt e^{i\omega t} \langle h_b(t) h_b(0) \rangle = 2\pi \hbar Z_b^{-1} \times \sum_{\nu_b} |\langle \nu_b | h_b | \mu_b \rangle|^2 \delta(E_{\mu_b} - E_{\nu_b} + \hbar\omega) e^{-E_{\mu_b}/k_B T}, \quad (\text{B2})$$

where  $Z_b$  is the bath partition function. In Eq. (A10) and the main text we used  $h_b^{(0)}$  instead of  $h_b$  in the definition of  $S_b(\omega)$  to emphasize that we are calculating the power spectrum in the absence of coupling to the oscillator.

Combining Eqs. (A9) and (B2), we obtain

$$W_{k+1 \rightarrow k} = 2\Gamma(k+1)(\bar{n}+1), \quad \Gamma = S_b(\omega_0)/4\hbar M\omega_0(\bar{n}+1) \quad (\text{B3})$$

[we recall that  $\bar{n} \equiv \bar{n}(\omega_0)$ ]. Equation (B3) shows that  $\Gamma$  determines the rate of the transitions between the states of a quantum oscillator due to its coupling to a thermal bath. In particular,  $\Gamma = [W_{1 \rightarrow 0}/2]_{\bar{n}=0}$ . The transition rates (B1) linearly increase with the level number.

## 1. Master equation

In slow time compared to  $\omega_0^{-1}$ ,  $t_{\text{corr}}$ , quantum dynamics of the oscillator coupled to a bath can be described using a master equation for the oscillator density matrix in the rotating frame  $\rho = U_0^\dagger(t)\rho_0 U_0(t)$ , where  $\rho_0$  is the density matrix in the laboratory frame and  $U_0(t) = \exp(-ia^\dagger a \omega_0 t)$ . For a linear oscillator with a coupling to the bath of the form of  $H_i = qh_b$ , this equation was derived from the microscopic theory and discussed by Schwinger (1961); see also Senitzky (1961). An extension to weakly nonlinear oscillators was done by Dykman and Krivoglaz (1973). Where the conditions of the Markovian approximation discussed in Sec. A.2 hold, the master equation is Markovian in slow time and can be written in the form of a Lindblad equation,

$$\dot{\rho} = 2\Gamma\{(\bar{n}+1)\mathcal{D}[a]\rho + \bar{n}\mathcal{D}[a^\dagger]\rho\} - iP[a^\dagger a, \rho] - i\hbar^{-1}[H_{\text{nl}}, \rho], \quad (\text{B4})$$

where

$$\mathcal{D}[L]\rho = L\rho L^\dagger - (L^\dagger L\rho + \rho L^\dagger L)/2 \quad (\text{B5})$$

and  $H_{\text{nl}}$  describes nonlinear terms of the oscillator Hamiltonian; for example, for the Duffing nonlinearity of the oscillator potential energy, which in the coordinate representation is described by  $M\gamma q^4/4$  [cf. Eq. (46)], we have

$$H_{\text{nl}} = 3\hbar^2\gamma a^\dagger a(a^\dagger a + 1)/8M\omega_0^2.$$

The term  $\propto P$  describes the polaronic effect of the shift of the oscillator frequency due to the coupling to a thermal bath.

Equation (B4) corresponds to a linear friction force  $-2M\Gamma\dot{q}$  in the phenomenological theory, as discussed in Appendix A, and in the microscopic theory comes from the bath-induced transitions between neighboring energy levels of the oscillator. In contrast, the phenomenological nonlinear friction force

$$f_{\text{vdP}} = -4M\Gamma^{(\text{nl})}(q/q_0)^2\dot{q}, \quad q_0 = (\hbar/2M\omega_0)^{1/2},$$

corresponds, in the microscopic theory, to the bath-induced transitions over two energy levels of the oscillator; see Fig. 32(b). It comes from the interaction with the bath with energy  $q^2 h_b^{(\text{nl})}$  [see Eq. (52)], and specifically from the terms  $a^2$  and  $a^{\dagger 2}$  in  $q^2$ . In the master equation the nonlinear friction is described by the term (Dykman and Krivoglaz, 1975)

$$(\dot{\rho})_{\text{nl}} = 2\Gamma^{(\text{nl})}\{[\bar{n}(2\omega_0) + 1]\mathcal{D}[a^2]\rho + \bar{n}(2\omega_0)\mathcal{D}[a^{\dagger 2}]\rho\}. \quad (\text{B6})$$

The nonlinear friction coefficient  $\Gamma^{(\text{nl})}$  is [cf. Eq. (53)]

$$\Gamma^{(\text{nl})} = \frac{q_0^4}{2\hbar^2[\bar{n}(2\omega_0) + 1]} S_b^{(\text{nl})}(2\omega_0), \quad S_b^{(\text{nl})}(\omega) = \int_{-\infty}^{\infty} dt e^{i\omega t} \langle h_b^{(\text{nl})}(t) h_b^{(\text{nl})}(0) \rangle. \quad (\text{B7})$$

In the classical limit  $k_B T \gg \hbar\omega_0$ , Eq. (B4) goes into the Fokker-Planck equation for the probability distribution of a

nonlinear oscillator, which corresponds to the stochastic classical equation of motion (55). Among other things, Eqs. (B4) and (B6) allow one to calculate the power spectrum of a nonlinear oscillator. The results on the spectra are discussed in the main text and in Appendix E.

The master equation is easily extended to describe resonant and parametric driving. It allows studying the stationary probability distribution of a driven nonlinear oscillator, as well as various transient quantum phenomena.

### APPENDIX C: DRIVING-INDUCED COOLING AND HEATING FOR COUPLED MODES

The possibility to cool a mechanical mode using a driving that resonantly couples it to a high-frequency optical mode in a cavity plays a fundamental role in optomechanics (Aspelmeyer, Kippenberg, and Marquardt, 2014b). However, a mechanical mode can also be cooled down or heated up by coupling it to another mechanical mode or a mode of a different physical nature or simply a thermal reservoir. An interesting and not *a priori* obvious part of the effect is that the stationary distribution of the driven mode is of the Boltzmann form with an effective temperature. This happens if there is no nonlinear friction and the relaxation rate of the considered mode is much smaller than the relaxation rate of the mode it is coupled to (Dykman, 1978).

Formally, we consider two modes with eigenfrequencies  $\omega_1$  and  $\omega_2$  and the pumping (modulation) of the form of Eq. (68), with energy

$$U_{12}^{\text{pump}} = M q_1 q_2 \bar{\Delta}_{12} \cos \omega_p t.$$

This corresponds to setting  $\Delta_{12}^{\text{pump}}(t) = \bar{\Delta}_{12} \cos \omega_p t$  in Eq. (68). For brevity we set the effective masses of the modes to be equal to the same value  $M$ . The modulation frequency  $\omega_p$  is close to either  $|\omega_1 - \omega_2|$  or  $\omega_1 + \omega_2$ . In what follows we assume for concreteness that  $\omega_1 < \omega_2$ . We introduce  $\epsilon_p = \pm 1$  such that  $\omega_p$  is close to  $\omega_2 - \epsilon_p \omega_1$ , i.e., either to  $\omega_2 - \omega_1$  or to  $\omega_2 + \omega_1$ .

In writing the master equation for the modes we assume that each mode is coupled to its thermal reservoir and, in the absence of driving, the mode decay rates are  $\Gamma_1$  and  $\Gamma_2$ . We further assume that the decay rates do not change if the mode eigenfrequencies are slightly changed, for example, if  $\omega_2$  is changed to  $\omega_p + \epsilon_p \omega_1$ ; for the considered resonant pumping  $|\omega_p + \epsilon_p \omega_1 - \omega_2| \ll \omega_{1,2}, t_{\text{corr}}^{-1}$ . We write the master equation using the ladder operators  $a_1, a_1^\dagger$  and  $a_2, a_2^\dagger$  for modes 1 and 2, similar to how it was done in Appendix B for a single mode. We also switch to the rotating frame and use the rotating wave approximation. A unitary transformation to the rotating frame is

$$U(t) = \exp[-i\omega_1 t a_1^\dagger a_1 - i(\omega_p + \epsilon_p \omega_1) t a_2^\dagger a_2].$$

In the rotating wave approximation, the master equation for the density matrix  $\rho$  of the coupled modes reads

$$\begin{aligned} \dot{\rho} &= \sum_j \hat{\Gamma}_j \rho + i\delta\omega_p [a_2^\dagger a_2, \rho] - i[\hat{h}_{12}, \rho], \\ \hat{\Gamma}_j \rho &= 2\Gamma_j [(\bar{n}_j + 1)\mathcal{D}[a_j]\rho + \bar{n}_j \mathcal{D}[a_j^\dagger]\rho], \\ \delta\omega_p &= \omega_p + \epsilon_p \omega_1 - \omega_2, \end{aligned} \quad (\text{C1})$$

where  $\bar{n}_k = \bar{n}(\omega_k)$  ( $k = 1, 2$ ). The Lindblad superoperators  $\mathcal{D}[L]$  are defined in Eq. (B5). Compared to Eq. (B4), in Eq. (C1) we have disregarded the nonlinearity of the modes and their eigenfrequency shifts due to the coupling to the thermal reservoirs.

The operator  $\hat{h}_{12}$  describes the resonantly induced mode coupling,

$$\begin{aligned} \hat{h}_{12} &= \Delta_{12}(a_1^\dagger a_2 + a_2^\dagger a_1), & \omega_p \approx \omega_2 - \omega_1, \\ \hat{h}_{12} &= \Delta_{12}(a_1 a_2 + a_1^\dagger a_2^\dagger), & \omega_p \approx \omega_2 + \omega_1, \end{aligned} \quad (\text{C2})$$

where  $\Delta_{12} = \bar{\Delta}_{12}/4\sqrt{\omega_1 \omega_2}$ . This parameter is of central importance, as it characterizes the coupling strength.

The physical picture of the mode dynamics is simplified in the case where the relaxation rates  $\Gamma_1$  and  $\Gamma_2$  are significantly different. For concreteness, we assume that

$$\Gamma_2 \gg \Gamma_1.$$

In this case mode 2 adiabatically follows mode 1. If the coupling is sufficiently weak ( $|\Delta_{12}| \ll \Gamma_2$ ), one can consider the linear response of mode 2 to the state of mode 1. This response is formed over time  $\sim 1/\Gamma_2$ , whereas the state of mode 1 varies over a significantly longer time.

In the adiabatic approximation the dynamics of mode 1 can be described by tracing out mode 2. We introduce the following density matrix of mode 1:  $\rho_1 = \text{Tr}_2 \rho$ , where  $\text{Tr}_2$  denotes the trace over the states of mode 2. Similarly,  $\langle a_2 \rangle_2 = \text{Tr}_2(a_2 \rho)$  and  $\langle a_2^\dagger \rangle_2 = \text{Tr}_2(a_2^\dagger \rho)$ . We emphasize that these averages over the states of mode 2 are operators with respect to mode 1.

By taking the trace over mode 2 in Eq. (C1), we obtain for  $\epsilon_p = 1$

$$\dot{\rho}_1 = \hat{\Gamma}_1 \rho_1 - i\Delta_{12}([\langle a_1^\dagger, \langle a_2 \rangle_2] + [a_1, \langle a_2^\dagger \rangle_2]). \quad (\text{C3})$$

For  $\epsilon_p = -1$  one should interchange in this equation  $a_1$  and  $a_1^\dagger$ . The equation for  $\langle a_2 \rangle_2$  has the form

$$\begin{aligned} \frac{d}{dt} \langle a_2 \rangle_2 &= \hat{\Gamma}_1 \langle a_2 \rangle_2 - (\Gamma_2 - i\delta\omega_p) \langle a_2 \rangle_2 \\ &\quad - i\text{Tr}_2(a_2 [\hat{h}_{12}, \rho]). \end{aligned} \quad (\text{C4})$$

In the considered regime of the fast relaxation rate  $\Gamma_2$ , we can look for the quasistationary solution of Eq. (C4). Respectively, we disregard  $d\langle a_2 \rangle_2/dt$ . We also disregard the term  $\propto \Gamma_1$  compared to the term  $\propto \Gamma_2$ . To describe the linear response of mode 2 to the coupling, we calculate the last term in Eq. (C4) to the lowest order in the coupling, i.e., we set  $\langle a_2^\dagger a_2 \rangle_2 \approx \bar{n}_2 \rho_1$ , whereas the term  $\langle a_2^2 \rangle_2$  is disregarded. This gives for  $\epsilon_p = 1$

$$\langle a_2 \rangle_2 \approx -i \frac{\Delta_{12}}{\Gamma_2 - i\delta\omega_p} [(\bar{n}_2 + 1)a_1 \rho_1 - \bar{n}_2 \rho_1 a_1].$$



For  $\epsilon_p = -1$  one should replace here  $a_1$  with  $a_1^\dagger$ . Substituting  $\langle a_2 \rangle_2$  and the similar expression for  $\langle a_2^\dagger \rangle_2$  into Eq. (C3), we obtain

$$\begin{aligned} \dot{\rho}_1 = & -\Gamma_{\text{eff}}\{(\bar{n}_{\text{eff}} + 1)\mathcal{D}[a_1]\rho_1 + \bar{n}_{\text{eff}}\mathcal{D}[a_1^\dagger]\rho_1\} \\ & - iP_{\text{eff}}[a_1^\dagger a_1, \rho_1], \end{aligned} \quad (\text{C5})$$

where

$$\begin{aligned} \Gamma_{\text{eff}} = & \Gamma_1 + \epsilon_p \Gamma_2 \frac{\Delta_{12}^2}{\Gamma_2^2 + \delta\omega_p^2}, \\ \bar{n}_{\text{eff}} = & \Gamma_{\text{eff}}^{-1} \left[ \Gamma_1 \bar{n}_1 + \Gamma_2 \frac{\Delta_{12}^2}{\Gamma_2^2 + \delta\omega_p^2} \left( \bar{n}_2 - \frac{\epsilon_p - 1}{2} \right) \right] \end{aligned} \quad (\text{C6})$$

and  $P_{\text{eff}} = \delta\omega_p \Delta_{12}^2 / (\Gamma_2^2 + \delta\omega_p^2)$ .

Remarkably, Eq. (C5) maps the dynamics of the driven slowly decaying mode (mode 1) onto the dynamics of an undriven mode with an effective decay rate  $\Gamma_{\text{eff}}$  and an effective mean occupation number  $\bar{n}_{\text{eff}}$  (Dykman, 1978). As seen from Eq. (C5),  $\Gamma_{\text{eff}}$  exceeds  $\Gamma_1$  for  $\omega_2 \approx \omega_p + \omega_1$  and is smaller than  $\Gamma_1$  for  $\omega_2 + \omega_1 \approx \omega_p$ . At the same time, the effective occupation number  $\bar{n}_{\text{eff}}$  is smaller or larger than  $\bar{n}_1$ . In the stationary regime the effective temperature of the mode  $k_B T_{\text{eff}} = \hbar\omega_1 / \ln[(\bar{n}_{\text{eff}} + 1)/\bar{n}_{\text{eff}}]$  is lower or higher than the temperature of the thermal reservoir. This describes the sideband cooling for  $\omega_2 \approx \omega_p + \omega_1$  by “superposing” onto a low-frequency mode the distribution over the states of a higher-frequency mode. On the other hand, a sufficiently strong drive with  $\omega_p \approx \omega_2 + \omega_1$  leads to  $\Gamma_{\text{eff}}$  becoming equal to zero, which manifests an instability of the system.

## APPENDIX D: FORCED VIBRATIONS

### 1. Resonant driving

A classical Duffing oscillator driven by a resonant force  $F \cos \omega_F t$  experiences the same friction force and the same noise from the thermal bath as in the absence of driving, provided that the detuning of the drive frequency from the eigenfrequency  $|\omega_F - \omega_0|$  is small compared to the reciprocal correlation time of the bath  $\tau_{\text{corr}}^{-1}$ . We assume that the driving is not extremely strong so that the amplitudes of the vibration overtones remain small compared to the amplitude of the main tone. It is then convenient to describe the dynamics by switching to the rotating frame and using the real variables  $Q$  and  $P$ , which are related to the coordinate and momentum of the driven oscillator by the expression

$$Q + iP = [q + i(p/M\omega_F)] \exp(i\omega_F t) \quad (\text{D1})$$

[cf. Eq. (61)]. These variables are similar to (twice) the real and imaginary parts of the complex amplitude in the absence of driving  $u^*(t)$  [Eq. (A1)], except that for a driven oscillator it is more convenient to change to the frame oscillating at frequency  $\omega_F$  rather than  $\omega_0$ .

The equations for  $Q$  and  $P$  are derived similarly to the equation for  $u(t)$ . Disregarding small corrections to  $Q$  and  $P$  that oscillate at frequency  $\omega_F$  and its overtones, we obtain

$$\begin{aligned} \dot{Q} = & \partial_P g_r(Q, P) - \Gamma Q + \xi_Q(t), \\ \dot{P} = & -\partial_Q g_r(Q, P) - \Gamma P + \xi_P(t), \end{aligned} \quad (\text{D2})$$

where

$$\begin{aligned} g_r = & \frac{3\gamma}{32\omega_F} (Q^2 + P^2)^2 - \frac{1}{2} \delta\omega (Q^2 + P^2) - \frac{F}{2M\omega_F} Q, \\ \delta\omega = & \omega_F - \omega_0, \quad |\delta\omega| \ll \omega_F \end{aligned} \quad (\text{D3})$$

(the subscript  $r$  here stands for “resonant”). The major difference from Eq. (A9) is that Eqs. (D2) are written in real variables and include the Duffing nonlinearity  $\propto \gamma$  and the driving force  $\propto F$ ; the bath-induced frequency shift has been incorporated into  $\omega_0$ .

The variables  $Q$  and  $P$  and the time can be rescaled so that the equations of motion contain only two parameters in the absence of noise (Dykman, 2012). The noise components  $\xi_Q(t)$  and  $\xi_P(t)$  are independent  $\delta$ -correlated Gaussian noises with the same intensity as in the absence of the driving,

$$\langle \xi_Q(t) \xi_Q(0) \rangle = \langle \xi_P(t) \xi_P(0) \rangle = (2\Gamma k_B T / M\omega_0^2) \delta(t). \quad (\text{D4})$$

If the decay and the noise are disregarded, Eqs. (D2) become Hamiltonian equations for the coordinate  $Q$  and momentum  $P$  of the oscillator in the rotating frame (the in-phase and quadrature components). The function  $g_r(Q, P)$  is the Floquet Hamiltonian. In the parameter range where the oscillator is bistable in the presence of weak dissipation, it has the form of a tilted Mexican hat; see Fig. 33(a). The cross sections of the surface  $g_r(Q, P)$  in Fig. 33(b) show the oscillator trajectories (D2) in the rotating frame in the limit of zero dissipation. Note the strong asymmetry (a horseshoe-like shape) of the trajectories that go around the minimum of  $g_r(Q, P)$ .

In the absence of noise, Eqs. (D2) have three stationary solutions in the region inside the “curvilinear triangle” on the  $(F, \omega_F)$  plane in Fig. 15(b). The solutions with the largest and smallest values of  $Q^2 + P^2$  are stable, and the solution with the intermediate  $Q^2 + P^2$  is the saddle point. In the limit  $\Gamma \rightarrow 0$  these states correspond, respectively, to the local minimum and maximum of the function  $g_r(Q, P)$  and to its saddle point; see Fig. 33(a). Near the saddle point  $g_r(Q, P)$  has the shape of a hyperboloid. Through this point goes the separatrix that separates the basins of attraction of the stable states for a finite damping. The phase portrait of the system in the range of bistability is shown in Fig. 33(c), which complements Fig. 15(c).

The boundaries of the range of the bistability, i.e., the sides of the curvilinear triangle in Fig. 15(b), are the bifurcation lines. On the line with smaller  $F$  the stable state with the larger amplitude merges with the saddle point, whereas on the line with larger  $F$  it is the smaller-amplitude state that merges with the saddle point. The bifurcational values  $F_{B1,2} \equiv F_{B1,2}(\Omega_r)$  of the drive amplitude as a function of the drive frequency are given by the expression

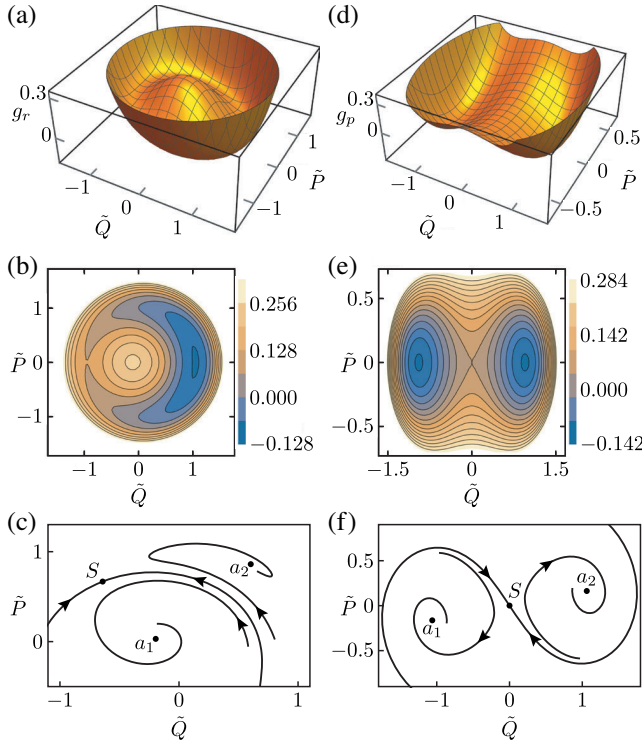


FIG. 33. Left and right columns refer to the resonantly driven and parametrically driven modes in the range of their bistability. The variables  $\tilde{Q}$  and  $\tilde{P}$  for the resonantly driven mode are, respectively, the in-phase and quadrature components  $Q$  and  $P$  multiplied by  $[8\omega_F(\omega_F - \omega_0)/3\gamma]^{1/2}$ . For the parametrically driven mode,  $\tilde{Q}$  and  $\tilde{P}$  are the quadratures  $Q$  and  $P$  scaled by the factor  $|2F_p/3\gamma M|^{1/2}$ . (a),(b) Effective Hamiltonian in the rotating frame for the resonantly driven mode  $g_r$  [Eq. (D3)] and its cross-sections (the phase trajectories in the absence of decay) for the scaled driving field intensity  $\beta = 3\gamma F^2/32M^2\omega_F^3(\delta\omega)^3 = 0.01$ . (c) Phase portrait in the presence of dissipation for  $\beta = 1/27$  and scaled decay rate  $\Gamma/|\delta\omega| = 0.15$ . The phase plane is separated into two parts by the separatrix, which goes through the saddle points  $S$ . The trajectories on the opposite sides of the separatrix approach the stable states  $a_1$  and  $a_2$ . As the decay rate goes to zero, the stable states  $a_2$  and  $a_1$  move toward the minimum and the maximum of  $g_r$ , respectively. (d) Effective Hamiltonian in the rotating frame  $g_p$  [Eq. (D11)] and (e) its cross sections (phase trajectories in the absence of dissipation) for the scaled frequency detuning  $\mu_p = -0.1$  defined in Eq. (D12). (f) Phase portrait in the presence of dissipation for  $\mu_p = 0.2, 2M\omega_p\Gamma/F_p = 0.3$ . As the decay rate goes to zero, the stable states  $a_1$  and  $a_2$  move toward the minima of  $g_p$ .

$$\tilde{F}_{B1,2}^2 = \frac{2}{27} [\Omega_r^3 + 9\Omega_r \mp (\Omega_r^2 - 3)^{3/2}],$$

$$\tilde{F} = (3\gamma/32\omega_F^3\Gamma^3)^{1/2} F, \quad \Omega_r = (\omega_F - \omega_0)/\Gamma. \quad (\text{D5})$$

Equation (D5) is written for the Duffing nonlinearity parameter  $\gamma > 0$ ; for  $\gamma < 0$  one should replace  $\gamma \rightarrow |\gamma|$  in the expression for  $\tilde{F}_{B1,2}$  and  $\delta\omega \equiv \omega_F - \omega_0 \rightarrow -\delta\omega$  in the expression for the scaled frequency detuning  $\Omega_r$ .

### a. Universality of fluctuations near a bifurcation point

The dynamics and fluctuations display universal features near bifurcation points. These features are characteristic, in particular, for merging of a stable state with a saddle point [called the saddle-node bifurcation (Guckenheimer and Holmes, 1997)]. The equations of motion (D2) are simplified where the states are close to each other in phase space. The rates at which the dynamical variables  $Q$  and  $P$  approach their stable values become significantly different. The relaxation rate of the in-phase component  $Q$  is  $\approx 2\Gamma$ , whereas the relaxation rate of the quadrature component  $P$  goes to zero at the bifurcation parameter value; thus  $P$  is a slow variable near the bifurcation point. This variable is an analog of a soft mode in phase transition theory. Its fluctuations can be analyzed in the adiabatic approximation, assuming that the component  $Q(t)$  adiabatically follows  $P(t)$ . As a result, the equation for the time evolution of  $P(t)$  takes the form

$$\dot{P} = -\partial_P U_B(P) + \xi_P(t),$$

$$U_B(P) = -\alpha_{B1}[F - F_B(\Omega_r)](P - P_B) + \alpha_{B2}(P - P_B)^3. \quad (\text{D6})$$

The explicit form of the parameters  $\alpha_{B1,2}$  and the value  $P_B$  of the quadrature at the bifurcation point depend on  $\Omega_r$  (Dykman and Krivoglaz, 1980).

For  $\alpha_{B1}\alpha_{B2}(F - F_B) > 0$  the potential  $U_B$  has a minimum and a maximum, with the minimum corresponding to the stable state of the mode and the maximum corresponding to the saddle point. The relaxation rate near the stable state scales with the distance to the bifurcation point  $F - F_B(\Omega_r)$  as  $\{12\alpha_{B1}\alpha_{B2}[F - F_B(\Omega_r)]\}^{1/2}$ .

The “softening” of the potential  $U_B(P)$  near the bifurcation point leads to an increase in fluctuations. Of particular interest is the effect of the fluctuation-induced switching from the dynamically stable vibrational state to the coexisting state with a strongly different amplitude. Equation (D6) reduces the problem of the switching rate to the problem of escape from a potential well for a static cubic-parabola potential  $U_B(P)$  in a system with no inertia. The rate of escape for this problem is well known (Kramers, 1940),

$$W_{sw} \propto \exp(-M\omega_0^2\Delta U_B/2\Gamma k_B T),$$

where  $\Delta U$  is the height of the potential barrier around the stable state,

$$\Delta U_B = 4|\alpha_{B2}|[\alpha_{B1}(F - F_B)/3\alpha_{B2}]^{3/2}. \quad (\text{D7})$$

This barrier height scales as the distance to the bifurcation point to the power  $3/2$ . Such scaling has been seen in micromechanical and nanomechanical vibrational systems as well as in Josephson junction-based systems (Stambaugh and Chan, 2006a; Siddiqi *et al.*, 2006; Vijay, Devoret, and Siddiqi, 2009; Defoort *et al.*, 2015). We note that, since  $F_B \equiv F_B(\Omega_r)$ , the bifurcation point can be approached by varying the drive amplitude, the drive frequency, or both.

The values of the driving amplitude and frequency where  $F_{B1} = F_{B2}$  give the critical point in Fig. 15. Near this point the

variables  $Q$  and  $P$  also separate into comparatively fast and slow ones, with the equation for the slow variable  $P$  having the form of Eq. (D6), except that the effective potential  $U_B(P)$  has to be replaced by the potential  $U_c(P)$ ,

$$U_c(P) = \alpha_{c1}(P - P_c)^4 - \alpha_{c2}[\omega_F - (\omega_F)_c](P - P_c)^2 + \{\alpha'_{c3}[\omega_F - (\omega_F)_c] + \alpha''_{c3}(F - F_c)\}(P - P_c), \quad (\text{D8})$$

where  $P_c$ ,  $(\omega_F)_c$ , and  $F_c$  are the values of  $P$ ,  $\omega_F$ , and  $F$  at the critical point. These values as well as the parameters  $\alpha_{c1,c2,c3}$  are easy to find using Eqs. (D2) and (D3) (Dykman and Krivoglaz, 1980).

The critical point on the  $(F, \omega_F)$  plane is reminiscent of the critical point on the line of the first-order phase transition. Fluctuations become strong and their correlation time diverges as the oscillator approaches this point. In the range of bistability, as determined by the interrelation between  $F - F_c$  and  $\omega_F - (\omega_F)_c$ , the potential  $U_c(P)$  has two minima. It becomes symmetric on the line on the  $(F, \omega_F)$  plane where the coefficient at the linear in the  $P - P_c$  term is zero. On this line the switching rates between the two minima are equal to each other and the barrier height between the minima is  $\alpha_{c2}^2[\omega_F - (\omega_F)_c]^2/4\alpha_{c1}$ . This barrier height as determined from the switching rate allows the eigenfrequency and the nonlinearity parameter of a nanomechanical mode to be found with extremely high precision (Aldridge and Cleland, 2005).

## 2. Parametrically excited vibrations

Parametric modulation of an oscillator can be described by incorporating the term  $-(F_p q^2/2) \cos \omega_p t$  into its Hamiltonian. The phenomenological equation of motion then takes the form of Eq. (62). For the modulation at frequency  $\omega_p$  close to  $2\omega_0$ , it is convenient to analyze the dynamics by switching to the quadratures  $Q$  and  $P$  that remain almost constant on the timescale  $1/\omega_p$ . The transformation is similar to that for the resonant drive,

$$Q + iP = \left( q + i \frac{p}{M\omega_p/2} \right) \exp(i\omega_p t/2). \quad (\text{D9})$$

As in Eq. (D1),  $Q$  and  $P$  in Eq. (D9) are real. In the rotating wave approximation the equations for  $Q$  and  $P$  have the same form as Eq. (D2), but the function  $g_r$  now has to be replaced with the function  $g_p$ ,

$$\begin{aligned} \dot{Q} &= \partial_P g_p(Q, P) - \Gamma Q + \xi_Q(t), \\ \dot{P} &= -\partial_Q g_p(Q, P) - \Gamma P + \xi_P(t), \end{aligned} \quad (\text{D10})$$

where

$$\begin{aligned} g_p &= \frac{3\gamma}{16\omega_p} (Q^2 + P^2)^2 - \frac{1}{2} \delta\omega_p (Q^2 + P^2), \\ &+ \frac{F_p}{4M\omega_p} (P^2 - Q^2), \quad \delta\omega_p = \frac{\omega_p}{2} - \omega_0. \end{aligned} \quad (\text{D11})$$

Equations (D10) and (D11) apply provided  $|\delta\omega_p| \ll \omega_p$ .

If the decay and the noise are disregarded, Eqs. (D10) become Hamiltonian equations for the coordinate  $Q$  and momentum  $P$  in the rotating frame. The function  $g_p(Q, P)$  is the Hamiltonian; we note that this is not a Floquet Hamiltonian: this is the Hamiltonian in the frame oscillating at frequency  $\omega_p/2$ . In the parameter range where the oscillator has two stable states (in the presence of weak dissipation), it has the form of a symmetric double-well surface; see Fig. 33(d). The cross sections of the surface shown in Fig. 33(e) illustrate the phase trajectories in the rotating frame in the limit of zero dissipation.

The symmetry is a feature of the parametric resonance. Indeed, incrementing the time by the modulation period  $2\pi/\omega_p$  does not change the equation of motion in the laboratory frame [Eq. (62)]. Yet, as seen in Eq. (D9), it leads to the change  $Q \rightarrow -Q, P \rightarrow -P$ .

The phase portrait in the presence of dissipation is shown in Fig. 33(f), which refers to the parameter range where only two vibrational states are stable. As expected from the previous arguments, the phase portrait has inversion symmetry. Similar to the case of a resonantly driven mode, the regions of attraction to the stable states  $a_1$  and  $a_2$  are separated by the separatrix that goes through the saddle point  $S$ .

The variables  $Q$  and  $P$  and the time can be rescaled such that, in the absence of noise, the dynamics is described by two dimensionless parameters  $\mu_p$  and  $f_p$ ,

$$\mu_p = (\delta\omega_p/\Gamma) \text{sgn } \gamma, \quad f_p = F_p/2M\Gamma\omega_p. \quad (\text{D12})$$

Figure 16(a) shows the regions of the  $(f_p, \mu_p)$  plane where there are different numbers of vibrational and steady states in the absence of nonlinear friction. The bifurcation lines  $\mu_{B1,2}$  (the bifurcational values of  $\mu_p$  as functions of  $f_p$ ) are given by

$$\mu_{B1,2} = \mp (f_p^2 - 1)^{1/2}. \quad (\text{D13})$$

For weak modulation or large  $-\mu_p$  the mode is not excited: the vibration amplitude is zero. At  $\mu_p = \mu_{B1}$  the zero-amplitude state becomes unstable, and in the range  $\mu_{B2} > \mu_p > \mu_{B1}$  the system has two stable vibrational states; these are period-2 states with the opposite phases. For  $\mu_p > \mu_{B2}$  and  $f_p > 1$  the zero-amplitude state is also stable; the mode has three stable states and also two unstable period-2 states. On the line  $f_p = 1, \mu_p > 0$  the stable period-2 states merge with the unstable period-2 states and disappear. At the critical point  $\mu_p = 0, f_p = 1$ , all five stationary states merge.

Near the bifurcation lines (D13), the dynamics and fluctuations of the nascent states are controlled by a slow dynamical variable, as in the case of a resonantly driven mode. This variable is a linear combination of  $Q$  and  $P$ . A theory of fluctuations and the scaling of the rates of interstate switching in this parameter range was discussed by Dykman *et al.* (1998) and Lin, Nakamura, and Dykman (2015).

The nonlinear friction significantly modifies the bifurcation diagram, as seen in Fig. 16(b). The line on which the stable and unstable period-2 states merge is tilted, and the critical point shifts. A profound consequence of this change is the hysteresis with the varying modulation frequency, as described in Sec. VII.B.



### a. Fluctuation squeezing in the linear regime

Parametric modulation is often used as a way to squeeze fluctuations of one of the quadratures. The squeezing does not require exciting period-2 vibrations: it occurs already for a weak modulation. This can be seen from Eqs. (D10) and (D11) if one sets  $\gamma = 0$ . In the absence of modulation ( $F_p = 0$ ), one has from these equations  $\langle Q^2 \rangle = \langle P^2 \rangle = k_B T / M \omega_0^2$  in the case where the noise  $\xi_Q(t), \xi_P(t)$  is thermal. The stationary probability distribution  $\rho(Q, P)$  is Gaussian,  $\rho(Q, P) = Z^{-1} \exp[-M \omega_0^2 (Q^2 + P^2) / 2 k_B T]$ ; it is a Boltzmann distribution of a harmonic oscillator,  $Z = M \omega_0^2 / 2 \pi k_B T$ .

In the presence of the modulation but below the excitation threshold ( $f_p^2 < 1 + \mu_p^2$ ), the stationary probability distribution in the rotating frame  $\rho(Q, P)$  is still Gaussian: if one disregards the nonlinearity  $\rho(Q, P) = Z^{-1} \exp(-\sum A_{ij} x_i x_j / 2)$ . Here  $i, j = 1, 2$  and we use  $x_1 \equiv Q, x_2 \equiv P$ ; the normalization factor is  $Z = 2 \pi / (\det \hat{A})^{1/2}$ . The matrix  $\hat{A}$  can easily be found using the Fokker-Planck equation that corresponds to Eq. (D10) [in terms of the theory of stochastic processes, the latter is the Langevin equation for the fluctuating variables  $Q(t)$  and  $P(t)$ ; see Risken (1996)]. We can make a unitary transformation from  $Q, P$  to  $Q', P'$  so as to diagonalize the matrix  $\hat{A}$ . The variances  $\langle Q'^2 \rangle$  and  $\langle P'^2 \rangle$  are given, respectively, by  $A_{\pm}^{-1}$  and  $A_{\mp}^{-1}$ , where  $A_{+}^{-1}$  and  $A_{-}^{-1}$  are the largest and smallest eigenvalues of  $\hat{A}^{-1}$ ,

$$A_{\pm}^{-1} = \frac{k_B T}{M \omega_0^2} \frac{1 + \mu_p^2 \pm |f_p| (1 + \mu_p^2)^{1/2}}{1 + \mu_p^2 - f_p^2}. \quad (\text{D14})$$

One can easily see that  $A_{-}^{-1} < k_B T / M \omega_0^2$  for  $f_p^2 < 1 + \mu_p^2$ , which shows that the variance  $\langle P'^2 \rangle = A_{-}^{-1}$  is smaller than the variance of the quadratures in the absence of driving. This demonstrates squeezing of classical fluctuations. The squeezing becomes more pronounced as the scaled modulation amplitude  $|f_p|$  approaches the critical value  $(1 + \mu_p^2)^{1/2}$  where period-2 vibrations are excited. Close to the critical  $|f_p|$ , the eigenvalue  $A_{-}^{-1}$  is 1/2 of its value in the absence of modulation. This is known as the 3 dB limit of squeezing. While  $A_{-}$  decreases, fluctuations of the other quadrature increase,  $\langle Q'^2 \rangle = A_{+}^{-1} > k_B T / M \omega_0^2$ . The difference between the variances was clearly demonstrated already in the first experiment on squeezing in nanomechanical systems (Rugar and Grütter, 1991).

### b. Squeezing of fluctuations about the state of resonantly or parametrically excited vibrations

Here we expand the discussion in Sec. VII.C to describe what underlies the power spectrum-based detection of fluctuation squeezing in driven underdamped nonlinear modes. The detection exploits the fact that the spectrum of fluctuations about a stable state of forced vibrations of a nonlinear mode is double peaked. The peaks are resolved for sufficiently weak damping. Their occurrence can be understood using the equations of motion for the quadratures of a driven mode (D2) and (D10).

In the limit of zero damping and in the absence of noise, the stationary states of the mode in the rotating frame lie at  $\partial_P g = \partial_Q g = 0$ , where  $g = g_r$  and  $g = g_p$  for the resonant and parametric modulations, respectively. The functions  $g_r$  and  $g_p$  are effective Hamiltonians in the rotating frame, and their extrema play the same role in the dynamics as the minima of the Hamiltonian function  $P^2 / 2M + U(Q)$  of a classical particle with coordinate  $Q$  and momentum  $P$  in a potential  $U(Q)$ , except that  $g_r$  and  $g_p$  do not have the form of a sum of the kinetic and potential energies. An important characteristic of the motion near an extremum of  $g_r$  and  $g_p$  is the frequency

$$\omega_{\text{rot}} = (\partial_P^2 g \partial_Q^2 g)^{1/2}. \quad (\text{D15})$$

For a particle with the Hamiltonian  $P^2 / 2M + U(Q)$ , Eq. (D15) goes into the familiar expression for the vibration frequency near a potential minimum  $(\partial_Q^2 U / M)^{1/2}$ .

In the presence of weak damping and weak noise, after a transient the periodically driven mode approaches one of the stable states, depending on where it was initially prepared (the stable states are slightly shifted from the extrema of  $g_r, g_p$  for weak damping). This is again similar to a particle in a potential well, including the case of a double-well potential. The mode then fluctuates about this state for a long time compared to the relaxation time  $\sim 1/\Gamma$ ; see Sec. VII.D. These fluctuations correspond to random vibrations of  $Q(t)$  and  $P(t)$  at frequency  $\omega_{\text{rot}}$ , as seen when Eqs. (D2) and (D10) are linearized about a stable state. Again, the random vibrations of  $Q(t)$  and  $P(t)$  are similar to thermal vibrations of a particle in a potential well. However, they occur in the rotating frame.

As seen in Eqs. (D1) and (D9), vibrations of  $Q, P$  modulate the forced vibrations of the coordinate and momentum of the driven mode in the laboratory frame  $q(t), p(t)$ . Therefore, the power spectrum of fluctuations of the mode measured in the laboratory frame has peaks at frequencies  $\omega_F \pm \omega_{\text{rot}}$  or  $\omega_p / 2 \pm \omega_{\text{rot}}$  for resonant and parametric modulations, respectively (Drummond and Walls, 1980; Dykman *et al.*, 1994; Dykman, Marthaler, and Peano, 2011). These peaks are “fluctuational analogs” of the peaks in the spectra of the response to an additional weak probe field (Dykman and Krivogla, 1979).

On the experimental side, the double-peak spectrum of fluctuations about a stable vibrational state of a resonantly driven MEMS was observed by Stambaugh and Chan (2006b), but in this experiment the spectral peaks significantly overlapped. In the experiment (Huber *et al.*, 2020) the damping was small and the peaks were well resolved.

As seen in Figs. 33(b) and 33(e), the orbits of motion on the  $(Q, P)$  plane with a given  $g$  are strongly noncircular for both resonant and parametric driving. Therefore, the variances of the quadratures  $Q$  and  $P$  are different, which indicates squeezing. If we disregard dissipation,

$$\begin{aligned} \langle (\delta Q)^2 \rangle &= \frac{k_B T}{2M \omega_0^2} (1 + e^{-4\varphi_*}), & \langle P^2 \rangle &= \frac{k_B T}{2M \omega_0^2} (1 + e^{4\varphi_*}), \\ \exp(2\varphi_*) &= |\partial_Q^2 g|^{1/2} / |\partial_P^2 g|^{1/2}. \end{aligned} \quad (\text{D16})$$

Here  $\delta Q = Q - Q_0$ , where  $Q_0$  is the value of  $Q$  at the considered extremum of  $g$  and the second derivatives of  $g$  are calculated at the extremum, with  $g$  being  $g_r$  or  $g_p$  for the resonant and parametric modulations, respectively.

Along with the squeezing comes the difference in the areas of the spectral peaks at the frequencies  $\omega_F + \omega_{\text{rot}}$  and  $\omega_F - \omega_{\text{rot}}$  for a resonantly driven mode, as well as the peaks at  $(1/2)\omega_p + \omega_{\text{rot}}$  and  $(1/2)\omega_p - \omega_{\text{rot}}$  for a parametrically modulated mode. The difference in the areas is directly related to the squeezing parameter (Dykman, 2012; Huber *et al.*, 2020). The ratio  $\mathfrak{R}_{\text{peak}}$  of the areas of the peaks is

$$\mathfrak{R}_{\text{peaks}} = \tanh^2 \varphi_*.$$

Depending on the parameters and on whether the mode is in the larger- or smaller-amplitude state, for resonant driving, the larger-area peak is on the higher- or lower-frequency side of  $\omega_F$  or  $\omega_p/2$ .

The expression for  $\mathfrak{R}_{\text{peak}}$  also applies to the ratio of the areas of the peaks in the imaginary parts of the susceptibility of a strongly driven, strongly underdamped mode (Ochs *et al.*, 2021b). Such susceptibility describes the response to a weak probe force at frequency  $\omega_{\text{pr}}$  close to resonance. The peaks have opposite signs. The peak that corresponds to resonant amplification of the force always has a smaller area than the one that corresponds to the absorption (Dykman and Krivoglaz, 1979). We note that the expression for the ratio of the areas of the susceptibility peaks also applies in the quantum regime.

#### APPENDIX E: SPECTRA OF NONLINEAR UNDERDAMPED VIBRATIONAL MODES: QUANTUM AND CLASSICAL

The spectra of nonlinear modes (oscillators) are determined by two processes. One is decay of the vibration amplitude. This decay makes the vibrations nonsinusoidal and thus leads to a frequency “uncertainty” and to a spectral broadening. The other is frequency fluctuations. Here we consider the frequency fluctuations that come from the interplay of the dependence of the vibration frequency on the amplitude and the amplitude fluctuations due to thermal noise or a broadband noise from other sources. The two mechanisms of the spectral broadening are not simply superposed but compete, in some sense, because the decay rate of the amplitude  $\Gamma$  is also the reciprocal correlation time of the frequency fluctuations, as explained in Sec. VI.C. Therefore, the shape of the spectrum is determined by the ratio of the fluctuational frequency spread  $\overline{\delta\omega_0}$  to  $\Gamma$ .

The broadening of the spectrum of an oscillator due to the nonlinearity was first discussed for a quantum oscillator (Ivanov, Kvashnina, and Krivoglaz, 1965). The analysis was done for the limiting cases  $\overline{\delta\omega_0} \ll \Gamma$  and  $\Gamma \rightarrow 0$ . A complete solution of the problem that showed the evolution of the spectrum with the varying  $\overline{\delta\omega_0}/\Gamma$  was first obtained in the classical theory (Dykman and Krivoglaz, 1971) and then in the quantum theory (Dykman and Krivoglaz, 1973). It described the interplay of the nonlinearity and decay and offered insight into the paradox of the harmonic oscillator (discussed in Appendix E.1).

In the quantum analysis, it is necessary to take into consideration that the energy levels of a nonlinear oscillator are nonequidistant. In the Duffing model (46), the energy of the  $k$ th level is

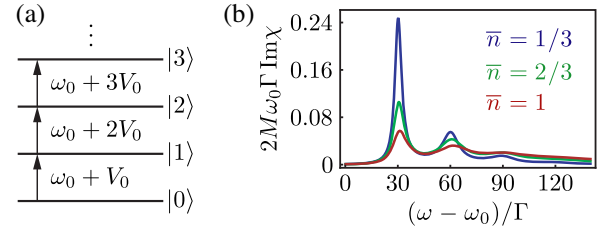


FIG. 34. (a) Transitions between the energy levels of the Duffing oscillator. The difference between the neighboring transition frequencies is  $V_0 = 3\hbar\gamma/4M\omega_0^2$ . (b) Fine structure of the imaginary part of the oscillator susceptibility [the power spectrum is  $S(\omega) \propto (\bar{n} + 1)\text{Im}\chi(\omega)$ ]. The plot refers to the ratio of the nonlinearity parameter  $V_0$  to the decay rate  $V_0/\Gamma = 30$ . The curves from top to bottom at the first maximum ( $\omega - \omega_0 \approx V_0$ ) correspond to  $\bar{n} = 1/3, 2/3$ , and 1. For  $\bar{n} \rightarrow 0$  the spectrum becomes a Lorentzian curve,  $2M\omega_0\text{Im}\chi(\omega) = \Gamma/[\Gamma^2 + (\omega - \omega_0)^2]$ .

$$E_k = \hbar k[\omega_0 + V_0(k+1)/2], \quad V_0 = 3\hbar\gamma/4M\omega_0^2$$

for  $|V_0|k \ll \omega_0$ . The transition frequencies  $(E_k - E_{k-1})/\hbar$  are shown in Fig. 34. They depend on the level number  $k$ , that is, on the energy  $E_k$ . This is the quantum analog of the energy dependence of the oscillator vibration frequency in the classical limit. The parameter  $V_0$  is proportional to the Duffing nonlinearity parameter  $\gamma$ . It is the discreteness of the transition frequencies that determines the quantum effects of the nonlinearity on the susceptibility and the power spectrum.

Thus far in nanomechanical systems studied in the quantum regime (O’Connell *et al.*, 2010; Chu *et al.*, 2018; Satzinger *et al.*, 2018; Arrangoiz-Arriola *et al.*, 2019; Wang *et al.*, 2019; MacCabe *et al.*, 2020; Cattiaux *et al.*, 2021), including the systems studied in quantum optomechanics (Aspelmeyer, Kippenberg, and Marquardt, 2014a, 2014b; de Lépinay *et al.*, 2021; Kotler *et al.*, 2021), the Duffing nonlinearity  $|V_0|$  was small compared to the decay rate  $\Gamma$ . This impeded an observation of quantum effects of the nonlinearity in the spectra. However, quantum effects can be pronounced for electromagnetic modes in nonlinear microwave cavities and for Josephson junction-based systems; cf. Schuster *et al.* (2007) and Bertet *et al.* (2012). They underlie the operation of the transmon qubit (Koch *et al.*, 2007), which is the basic element of the current superconducting quantum computers.

A quantum picture of the nonlinearity-induced spectral change is in some sense more intuitive than the classical, and the classical results follow from the quantum results as a limiting case. Therefore, we present this picture first.

#### 1. “Paradox” of the quantum harmonic oscillator

The oscillator susceptibility  $\chi(\omega)$  near resonance ( $\omega \approx \omega_0$ ) is formed by the transitions between neighboring levels. A naive way to describe this is to think of the oscillator as a set of two-level systems formed by the pairs of neighboring states  $|k-1\rangle, |k\rangle$  with  $k = 1, 2, \dots$ . Each such system makes a partial contribution to the resonant susceptibility, which is described by a function  $\phi(k, \omega)$ . The overall susceptibility of

the oscillator can then be sought in the form of a sum of such partial susceptibilities,

$$\chi(\omega) = (2M\omega_0)^{-1} \sum_{k=1} \phi(k, \omega). \quad (\text{E1})$$

One might further assume that a partial susceptibility  $\phi(k, \omega)$  is given by the familiar expression for the susceptibility of a two-level system (Weisskopf and Wigner, 1930a)

$$\begin{aligned} \phi_W(k, \omega) &= \frac{k}{\bar{n} + 1} \frac{\rho_{k-1}}{\Gamma_W(k) - i(\omega - \omega_0 - V_0 k)}, \\ \Gamma_W(k) &= \Gamma[2k(2\bar{n} + 1) - 1]. \end{aligned} \quad (\text{E2})$$

Here  $\omega_0 + V_0 k$  is the transition frequency of the  $|k-1\rangle \rightarrow |k\rangle$  transition, as seen in Fig. 34(a). The parameter  $\Gamma_W(k)$  is given by the half sum of the reciprocal lifetimes of the states  $|k-1\rangle$  and  $|k\rangle$ . In calculating it we took the reciprocal lifetime of a state  $|k\rangle$  to be  $W_{k \rightarrow k+1} + W_{k \rightarrow k-1}$ , where the transition rates  $W_{k \rightarrow k \pm 1}$  are given by Eq. (B1), and we also took into account that  $W_{k \rightarrow k+1}/W_{k+1 \rightarrow k} = \bar{n}/(\bar{n} + 1)$  [the Einstein relation (Landau and Lifshitz, 1980)], with  $\bar{n} = [\exp(\hbar\omega_0/k_B T) - 1]^{-1}$ . Further along the lines of the Weisskopf-Wigner theory, in Eq. (E2) the coefficient  $\rho_{k-1}$  is the population of the state  $k-1$  from which the system makes a transition,  $\rho_k = \exp(-\hbar k\omega_0/k_B T)/(\bar{n} + 1)$ . The function  $\text{Im } \phi_W(k, \omega)$  has the familiar form of a Lorentzian centered at the transition frequency  $\omega_0 + V_0 k$  and having the half-width  $\Gamma_W(k)$ .

An obvious flaw of this picture, already noticed by Weisskopf and Wigner (1930b), is that it does not describe the susceptibility of a harmonic oscillator in the limit  $V_0 = 0$ . In this limit the functions  $\text{Im } \phi_W(k, \omega)$  are Lorentzians centered at the same frequency, but their half-widths  $\Gamma_W(k)$  are different, so the entire spectrum is not Lorentzian. This has become known as the paradox of the harmonic oscillator (Belavin *et al.*, 1969; Zeldovich, Perelomov, and Popov, 1969). Weisskopf and Wigner (1930b) studied the effect for a three-state system with equal transition frequencies and showed that, indeed, such a system is not described by a set of two independent two-level systems.

The breakdown of the approximation (E2) with decreasing  $|V_0|/\Gamma$  is a characteristic quantum effect. The transition frequencies  $\omega_0 + V_0 k$  with different  $k$  are close to each other, and to distinguish the partial spectra  $\phi_W(k, \omega)$  one has to wait for a time  $t \gg |V_0|^{-1}$ . However, because of the coupling to a thermal bath, the oscillator stays in a state  $k$  for a time  $\sim \Gamma_W^{-1}(k)$ . If this time is less than  $|V_0|^{-1}$ , the partial spectra may not be distinguished.

The time  $\Gamma_W^{-1}(k)$  can be thought of as the time it takes to “switch” from one two-level system to another. The switching couples the partial spectra with different  $k$  to each other. This coupling is described by a system of linear equations (Dykman and Krivoglaz, 1984) that can be obtained from the quantum master equation for the oscillator density matrix  $\rho$  [Eq. (B4)].

Following the standard Kubo formula, we relate the susceptibility of the oscillator to the Fourier transform of the correlator  $\langle a(t)a^\dagger(0) \rangle = \text{Tr}[a \exp(-iHt) a^\dagger \rho_{\text{full}} \exp(iHt)]$ , where  $\rho_{\text{full}}$  is the density matrix of the system and the bath.

Tracing out the bath and switching to the rotating frame, we reduce the trace to that over the states of the oscillator, with the density matrix satisfying Eq. (B4) with the initial condition

$$\rho(0) = a^\dagger \exp(-\hbar\omega_0 a^\dagger a/k_B T)/(\bar{n} + 1).$$

The Fourier transform of the latter trace, i.e., of the trace over the oscillator states  $|k\rangle$ , is a sum over  $k$  of the Fourier transforms of the corresponding matrix elements

$$\phi(k, \omega) = \int_0^\infty dt \exp[i(\omega - \omega_0)t] k^{1/2} \langle k | \rho(t) | k-1 \rangle.$$

From Eq. (B4) we obtain a system of equations for  $\phi(k, \omega)$ . It reads

$$\begin{aligned} &[\Gamma_W(k) - i(\omega - \omega_0 - V_0 k)]\phi(k, \omega) - 2\Gamma k[\bar{n}\phi(k-1, \omega) \\ &+ (\bar{n} + 1)\phi(k+1, \omega)] \\ &= k\rho_{k-1}/(\bar{n} + 1). \end{aligned} \quad (\text{E3})$$

Equation (E3) shows that, for  $|V_0| \gg \Gamma_W(k)$ , the partial spectra  $\phi(k, \omega)$  near their maxima are indeed given by Eq. (E2). However, one can easily verify that, for a harmonic oscillator,  $V_0 = 0$ , the solution is

$$\phi(k, \omega) = \frac{k}{\bar{n} + 1} \frac{\rho_{k-1}}{\Gamma - i(\omega - \omega_0)} \quad (V_0 = 0).$$

In other words, all partial spectra have the same spectral shape, a profound quantum effect. With the account taken of Eq. (E1), this expression gives the familiar expression (5) for the susceptibility of a harmonic oscillator.

## 2. The susceptibility in the explicit form

Equation (E3) can be solved and the expression for the susceptibility  $\chi(\omega)$  can be obtained in the form of an integral of an elementary function (Dykman and Krivoglaz, 1973),

$$\begin{aligned} \chi(\omega) &= \int_0^\infty dt e^{i\omega t} \mathcal{X}(t), \quad \mathcal{X}(t) = \frac{i}{2M\omega_0} e^{-i\omega_0 t} e^{\Gamma t} \psi_{00}^{-2}(t), \\ \psi_{00}(t) &= \cosh(\mathfrak{N}_0 \Gamma t) + \Lambda_0 \sinh(\mathfrak{N}_0 \Gamma t), \\ \mathfrak{N}_0 &= \left[ 1 + i \frac{V_0}{\Gamma} (2\bar{n} + 1) - \frac{V_0^2}{4\Gamma^2} \right]^{1/2} \quad (\text{Re } \mathfrak{N}_0 > 0), \\ \Lambda_0 &= \mathfrak{N}_0^{-1} \left[ 1 + i \frac{V_0}{2\Gamma} (2\bar{n} + 1) \right]. \end{aligned} \quad (\text{E4})$$

The explicit expression (E4) shows that the susceptibility of a quantum Duffing oscillator is determined by two dimensionless parameters: the ratio  $V_0/\Gamma$  of the difference of the transition frequencies [cf. Fig. 34(a)] to the decay rate and the oscillator thermal occupation number  $\bar{n}$ . The power spectrum  $S(\omega) \propto \text{Im } \chi(\omega)$  has a peak near  $\omega = \omega_0$  that not only is non-Lorentzian but is actually asymmetric, in contrast to the case of a harmonic oscillator. For  $|V_0| \gg \Gamma(2\bar{n} + 1)$  the power spectrum can have a fine structure, with the spectral peaks centered at frequencies  $\approx \omega_0 + kV_0$ ; cf. Eq. (E2). This fine structure is illustrated in Fig. 34(b). It exists in a



temperature range limited from above and below. On the one hand, the temperature should be sufficiently high that the excited states of the oscillator are populated. On the other hand, the fine structure smears out with the increasing temperature, as the linewidths  $2\Gamma_W(k)$  increase and the condition  $|V_0| \gg \Gamma_W(k)$  ceases to hold for smaller and smaller  $k$ .

### 3. Dispersively coupled vibrational modes

A similar effect on the susceptibility of the considered mode  $n = 0$  comes from its dispersive coupling to other modes. The energy of the dispersive coupling is

$$U_{\text{disp}} = \frac{3}{4} M \sum_{n_1 \neq n_2} \gamma_{n_1 n_1 n_2 n_2} q_{n_1}^2 q_{n_2}^2,$$

where the subscripts  $n_{1,2}$  enumerate the modes. This is part of the total energy of the nonlinear mode coupling described by Eq. (50).

Because of the dispersive coupling, the frequency  $\omega_0$  of the mode  $n = 0$  becomes dependent on the states  $|k_n\rangle$  of other modes,

$$\begin{aligned} \omega_0 &\rightarrow \omega_0\{k_n\} = \omega_0 + \sum_{n>0} V_n[k_n + (1/2)], \\ V_n &= \frac{3\hbar}{2M_n} \frac{\gamma_{00nn}}{\omega_0 \omega_n}. \end{aligned} \quad (\text{E5})$$

In Eq. (E5) we assume that the coupling parameters  $\gamma_{n_1 n_1 n_2 n_2}$  have been renormalized to allow for the cubic in the mode coordinate terms in the potential energy of the modes [cf. Eq. (50)];  $M_n$  is the effective mass of mode  $n > 0$  ( $M_0 \equiv M$ ). Equation (E5) is the quantum analog of Eq. (51) for the frequency shift in terms of the mode amplitudes.

The frequencies  $\omega_0\{k_n\}$  form a ladder for each  $n$  in a manner similar to the frequency ladder in Fig. 34. As in the case of the internal mode nonlinearity, the susceptibility of the mode  $n = 0$  is affected by the coupling of the transition amplitudes for different  $k_n$ . The overall expression for the susceptibility of the mode  $n = 0$  can be written in the same form as Eq. (E4) provided that one replaces (Dykman and Krivoglaz, 1973)

$$\begin{aligned} e^{\Gamma t} \psi_{00}^{-2}(t) &\rightarrow \psi_{00}^{-1}(t) \prod_n e^{\Gamma_n t} \psi_{0n}^{-1}(t), \\ \psi_{0n}(t) &= \cosh(\mathfrak{S}_n \Gamma_n t) + \Lambda_n \sinh(\mathfrak{S}_n \Gamma_n t). \end{aligned} \quad (\text{E6})$$

Here the parameters  $\mathfrak{S}_n$  and  $\Lambda_n$  are again given by Eq. (E4) with the replacement

$$V_0 \rightarrow V_n, \quad \Gamma \rightarrow \Gamma_n, \quad \bar{n} \rightarrow \bar{n}_n = [\exp(\hbar\omega_n/k_B T) - 1]^{-1}. \quad (\text{E7})$$

In Eqs. (E6) and (E7)  $\Gamma_n$  is the decay rate of mode  $n$  and  $\bar{n}_n$  is its thermal occupation number. We also use  $\Gamma_0 \equiv \Gamma$  and  $\bar{n}_0 \equiv \bar{n}$ .

Where the difference in the frequencies of transitions with different  $k_n$  is large compared to the decay rates of the

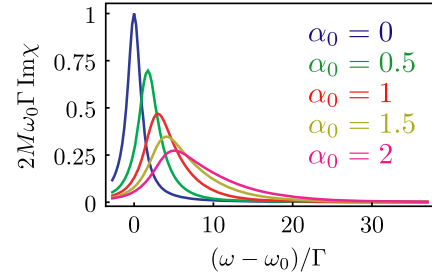


FIG. 35. Imaginary part of the susceptibility of the classical Duffing oscillator  $\text{Im}\chi(\omega) \propto S(\omega)$ . The shape of the spectrum is determined by the single parameter  $\alpha_0$  [Eq. (E8)]. The curves from top to bottom at the maximum refer to  $\alpha_0 = 0$  (a Lorentzian spectrum with half-width  $\Gamma$ ),  $\alpha_0 = 0.5, 1, 1.5, 2$ .

involved modes [ $|V_n| \gg \Gamma_n(2\bar{n}_n + 1)$ ], the susceptibility given by Eqs. (E4)–(E7) becomes a sum of partial susceptibilities for the transitions where modes  $n$  are in different Fock states  $|k_n\rangle$ , as in Eq. (E2). On the other hand, the modes with  $|V_n|(2\bar{n}_n + 1) \ll \Gamma_n$ , i.e., the modes that are weakly dispersively coupled to the considered mode  $n = 0$  compared to their decay rates, only slightly perturb  $\chi(\omega)$ .

### 4. Classical limit

The expressions for the susceptibility simplify in the classical limit. In this limit, the thermal occupation numbers of the modes are  $\bar{n}_n \approx k_B T / \hbar\omega_n$ . Since the nonlinearity parameters  $V_n$ , which are explicitly related to the discreteness of the modes energy spectra, are  $\propto \hbar$ , they can enter only in combination with  $\bar{n}_n$ . Respectively, in the classical limit we have in Eqs. (E4)–(E7)

$$\begin{aligned} \mathfrak{S}_n &\rightarrow (1 + 4i\alpha_n)^{1/2}, \quad \Lambda_n \rightarrow \mathfrak{S}_n^{-1}(1 + 2i\alpha_n), \\ \alpha_n &= 3\gamma_{00nn}k_B T(2 - \delta_{n,0})/8M_n\omega_0\omega_n^2\Gamma_n. \end{aligned} \quad (\text{E8})$$

In the classical limit, the susceptibility does not have a fine structure. However, it is significantly different from the simple Lorentzian limit (10). The power spectrum  $S(\omega) \propto \text{Im}\chi(\omega)$  becomes asymmetric with an increasing  $|\alpha_n|$ , because of both the internal nonlinearity and the dispersive coupling to fluctuating modes (Dykman and Krivoglaz, 1971).

The evolution of the spectrum of a single mode  $n = 0$  with the varying single parameter of the internal nonlinearity  $\alpha_0$  is shown in Fig. 35. The width of the spectrum increases with an increasing  $\alpha_0$ . We note that  $\alpha_0 \propto T$  if the decay rate is independent of temperature. For  $\alpha_0 = 0$  the spectrum is Lorentzian, whereas for  $|\alpha_0| \gg 1$  the spectrum near the maximum has the form  $S(\omega) \propto |\omega - \omega_0| \exp[-(\omega - \omega_0)/2\alpha_0\Gamma]$  for  $\alpha_0(\omega - \omega_0) > 0$ . The expression for the power spectrum of a classical oscillator that coincides with the presented result was given by Renz (1985).

For comparison, we show in Fig. 36 the effect of nonlinear friction on the susceptibility spectrum in the absence of conservative nonlinearity. The spectrum remains symmetric in this case but is strongly non-Lorentzian. The deviation from the Lorentzian form is a signature of the vibration nonlinearity,

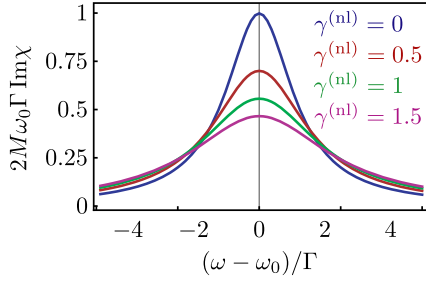


FIG. 36. Imaginary part of the susceptibility of an oscillator with nonlinear friction in the absence of the dependence of the vibration frequency on the amplitude. The dynamics is described by Eqs. (B4)–(B7) in the classical limit [cf. Eq. (55)] with the Duffing nonlinearity parameter  $\gamma = 0$ . The spectra from top to bottom at the maximum correspond to the scaled nonlinear friction coefficient  $\gamma^{(nl)} \equiv 2\Gamma^{(nl)}k_B T/\hbar\omega_0\Gamma = 0, 0.5, 1$ , and  $1.5$ . The nonlinear friction parameter  $\Gamma^{(nl)}$  is defined in Eq. (B7).

while the symmetry of the spectrum enables the effects of conservative and dissipative nonlinearity to be distinguished.

An interesting behavior occurs when the number of the modes  $N$  dispersively coupled to the considered mode is large even while the coupling to each mode is small. One would expect some version of the central limit theorem to apply in this case, leading to a Gaussian power spectrum  $S(\omega)$  (Barnard *et al.*, 2012). This is indeed the case (Zhang and Dykman, 2015). A Gaussian spectrum emerges if  $|\alpha_n| \ll 1$  for all  $n$ , but  $\sum_n \alpha_n^2 \gg 1$  and  $\sum_n \alpha_n^2 \Gamma_n^2 \gg \Gamma_m^2$  ( $\forall m$ ). In this case  $S(\omega) \propto \exp[-(\omega - \tilde{\omega}_0)^2/2\sigma^2]$ , with  $\tilde{\omega}_0 = \omega_0 + 2\sum_n \alpha_n \Gamma_n$  and  $\sigma^2 = 4\sum_n \alpha_n^2 \Gamma_n^2$ .

To conclude this section, we note that the coupling of interstate transitions and the related distortion of the spectral lines is a generic property of systems with close transition frequencies. Such coupling occurs in different types of systems. Besides various vibrational systems, like Josephson-junction-based systems, microwave cavities, and NVSSs, examples range from the cyclotron resonance in semiconductors to electron spin resonance in strong magnetic fields in systems with  $S > 1/2$ . The coupling of transitions is also important for classical vibrational systems with fluctuating frequency. An example is provided by nanomechanical and micromechanical resonators with a fluctuating number and/or positions of attached molecules (Vig and Kim, 1999; Yang *et al.*, 2011). The spectra of such systems can also be asymmetric and can display a fine structure (Dykman *et al.*, 2010). On the formal side, for different physical mechanisms the full spectra can often be described by linear equations for coupled partial spectra. These equations are convenient for a numerical analysis.

## APPENDIX F: THE ACTION-ANGLE VARIABLES

The Duffing model has been successful in describing many observations of nanomechanical systems, and in the majority of cases the analysis was based on the Bogoliubov-Krylov method of averaging outlined in Appendix A.1. As previously indicated, this method is similar to the RWA and is used throughout this review. However, we note that it may become inapplicable even when the nonlinearity is still comparatively weak, that is, the nonparabolic in  $q$  terms in the potential

energy of a vibrational mode  $U(q)$  are still small compared to  $M\omega_0^2 q^2/2$ . A simple example is provided by a mode with a broken inversion symmetry. In this case, in the nonlinear part of the potential one has to keep the cubic in  $q$  term [cf. Eq. (50)],

$$U(q) = \frac{1}{2}M\omega_0^2 q^2 + \frac{1}{3}M\beta q^3 + \frac{1}{4}M\gamma q^4.$$

Such modes have been extensively studied in the literature; see Kozinsky *et al.* (2006), Chan, Dykman, and Stambaugh (2008a), Eichler, Moser *et al.* (2011), Meerwaldt *et al.* (2012), Eichler *et al.* (2013), Huang *et al.* (2019), and Ochs *et al.* (2021a). In fact, the lack of inversion symmetry is fairly generic for flexural nanomechanical modes, as it comes, for example, whenever a gate voltage is applied and a nanoresonator is bent or simply from the capacitive part of the potential energy  $\propto (\partial^3 C_g/\partial q^3)(V_g^{\text{dc}})^2$ ; cf. Eq. (9).

Cubic nonlinearity leads to several effects, including vibrations at the second overtone of the eigenfrequency, i.e., at the frequency  $\approx 2\omega_0$ , and the change of the dependence of the vibration frequency on the amplitude. In the RWA, the latter is described by the renormalization of the Duffing parameter (Landau and Lifshitz, 2004),

$$\gamma \rightarrow \gamma_{\text{eff}} = \gamma - \frac{10\beta^2}{9\omega_0^2} \quad (\text{F1})$$

[see Eichler *et al.* (2013) and Huang *et al.* (2019) for some other effects].

It is immediately seen in Eq. (F1) that the term  $\propto \beta^2$  can significantly change the character of the amplitude dependence of the mode frequency (48). Indeed, if  $\gamma > 0$  but  $\gamma_{\text{eff}} < 0$ , even the sign of the slope  $d\omega/dA^2$  of the frequency dependence on the amplitude changes. However, it is clear that for large amplitudes the term  $\propto q^4$  in  $U(q)$  becomes more important than the term  $\propto q^3$ . Simple dimensional arguments show that for the amplitudes  $A^2 \gtrsim \omega_0^2 \gamma_{\text{eff}}/\gamma^2$  the conventional RWA approximation (F1) becomes inapplicable. For small  $\gamma_{\text{eff}}/\gamma$  this happens when the nonlinear part of the energy  $\sim M\gamma A^4$  is still small compared to the harmonic part  $\sim M\omega_0^2 A^2$ . Therefore, it is necessary to find an alternative approach that would not rely on the conventional RWA.

An appropriate analysis of the mode dynamics is simplified in the case of weak damping, where the decay rate  $\Gamma \ll \omega_0$ . Here it is convenient to use the method of averaging in the form developed in the dynamics of Hamiltonian systems (Arnold, 1989). In this method one changes from the coordinate and momentum of the mode to its action-angle variables. This is a canonical transformation of variables. The coordinate and momentum are functions of the action  $I$  and the phase (angle)  $\varphi$  and are periodic in  $\varphi$ ,

$$q(I, \varphi + 2\pi) = q(I, \varphi), \quad p(I, \varphi + 2\pi) = p(I, \varphi).$$

The action and phase variables of the Hamiltonian system are defined as (Landau and Lifshitz, 2004)

$$I = (2\pi)^{-1} \oint p dq, \quad \varphi = \frac{\partial}{\partial I} \int p dq.$$

The vibration frequency of the mode is a function of  $I$  or, equivalently, of the mode energy  $E$ ,

$$\omega(I) = (\partial I / \partial E)^{-1}$$

and  $\omega(I)\partial_\varphi q = p/M$ , whereas  $\omega(I)\partial_\varphi p = -\partial_q U(q)$ .

To describe the mode dynamics in the presence of a friction force  $-2\Gamma p$  and a driving force  $F \cos \omega_F t$ , one can change the variables from  $(q, p)$  to  $(I, \varphi)$ . The resulting equations for  $I$  and  $\varphi$  read

$$\begin{aligned} \dot{I} &= R\partial_\varphi q, & \dot{\varphi} &= \omega(I) - R\partial_I q, \\ R &= -2\Gamma p + F \cos \omega_F t. \end{aligned} \quad (\text{F2})$$

The key observation that underlies the averaging principle is that the action varies in time only because of the friction and the driving, which are assumed to be small. In contrast, the phase accumulates at frequency  $\omega(I)$ , which is assumed to be large. Therefore, the time evolution of  $q$  and  $p$  is fast oscillations with a slowly varying in time action  $I$ . The contribution of fast oscillations to  $\dot{I}$  does not accumulate in time. Therefore, on a timescale that is large compared to  $\omega_F^{-1}, \omega^{-1}(I)$ , the motion can be described by averaging over the fast oscillations for a given action.

The effect of the driving is most pronounced (see Appendix D.1) when the driving is resonant. This means that the vibrations occur at frequencies  $\omega(I)$  close to  $\omega_F$ , that is,  $|\omega(I) - \omega_F| \ll \omega_F$  (the analysis of parametric driving can be done similarly). We can then write

$$\varphi = \omega_F t + \varphi_0(t), \quad \dot{\varphi}_0 = \omega(I) - \omega_F - R\partial_I q. \quad (\text{F3})$$

The phase  $\varphi_0$  is also a slow variable. For a given  $\varphi_0$  the functions  $q(I, \varphi), p(I, \varphi)$  are periodic in  $\omega_F t$ .

It follows from the previous arguments that the equations for  $I, \varphi_0$  can be obtained by averaging the full equations (F2) over fast oscillations,

$$\dot{I} = \overline{R\partial_\varphi q}, \quad \dot{\varphi}_0 = \omega(I) - \omega_F - \overline{R\partial_I q}. \quad (\text{F4})$$

In Eqs. (F4)

$$\overline{L(I, \varphi)} = (2\pi)^{-1} \int_0^{2\pi} d\theta L(I, \theta + \varphi_0),$$

where  $L$  is an arbitrary function of  $I, \varphi$  that is periodic in  $\varphi$  (in  $R$  we replace  $F \cos \omega_F t$  with  $F \cos \theta$ ; in fact, the averaging is done over the period  $2\pi/\omega_F$  for fixed  $I, \varphi_0$ ).

Stationary states of forced vibrations are given by Eq. (F4), in which one sets  $\dot{I} = \dot{\varphi}_0 = 0$ . One can see that, to the leading order in the Duffing nonlinearity, one obtains the same result for the vibration amplitude and phase as Eqs. (D2) and (D3) or, equivalently, Eq. (60) by assuming  $I$  to be small and keeping a linear in  $I$  term in the expansion of  $\omega(I)$ .

One can go beyond the conventional analysis of the resonant nonlinear response described in Appendix D while still staying in the region of comparatively weak nonlinearity. This is particularly important for small  $\gamma_{\text{eff}}/\gamma$  or for  $\gamma_{\text{eff}} < 0$  and  $\gamma > 0$ , in which case one may have to keep a quadratic in  $I$  term in the expansion of  $\omega(I)$ ; i.e., one can write (Ochs *et al.*, 2022)

$$\omega(I) = \omega_0 + \alpha_1 I + \alpha_2 I^2.$$

Here  $\alpha_1 \propto \gamma_{\text{eff}}$ . The parameters  $\alpha_{1,2}$  include all relevant renormalizations and the terms in the mode potential up to the sixth order in the coordinate  $q$ . The parameters  $\alpha_{1,2}$  are essentially the only parameters accessible to the experiment on resonant weakly damped dynamics. They can describe a nonmonotonic backbone curve. Moreover, in an analysis of the mode dynamics one can approximate  $q \approx (2I/M\omega_0)^{1/2} \cos \phi$  in Eq. (F4), which significantly simplifies the analysis.

However, the action-angle formulation allows one to go beyond the weak-nonlinearity range (Dykman *et al.*, 1990; Soskin, Mannella, and McClintock, 2003; Shoshani, Shaw, and Dykman, 2017; Huang *et al.*, 2019; Miller, Shaw, and Dykman, 2021; Ochs *et al.*, 2021a). We note that if the involved characteristic frequencies  $\omega(I)$  become significantly different from  $\omega_0$ , the approximation of the frequency-independent coefficients of linear and nonlinear friction may become inapplicable. A more general approach to describing dissipation may be necessary in this case.

## APPENDIX G: THERMOELASTIC AND AKHIEZER RELAXATION

In this section we consider the mechanisms of Akhiezer and thermoelastic relaxation of NVS modes. These mechanisms have a common origin and can be described within the same general framework, as indicated in Sec. IV. In both mechanisms, relaxation comes from inelastic scattering of thermal phonons off the low-frequency NVS mode. The process is sketched in Fig. 37. The mechanisms are particularly important if the mode eigenfrequency  $\omega_0$  is small compared to the temperature in frequency units,  $\hbar\omega_0 \ll k_B T$ . To find the mode decay rate  $\Gamma$  in this case it is usually necessary to take into consideration the fact that thermal phonons are scattered off each other, and their scattering rate can be comparable to  $\omega_0$ .

The coupling Hamiltonian that describes the scattering of thermal phonons off the low-frequency NVS mode has the form

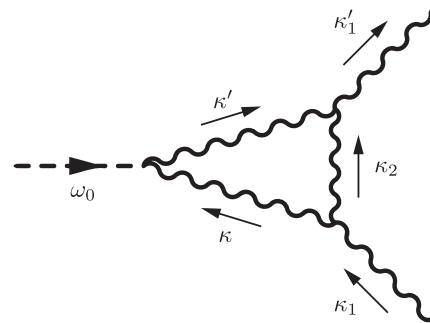


FIG. 37. Feynman diagram showing the scattering of phonon  $\kappa$  off the NVS mode into phonon  $\kappa'$ . The phonons  $\kappa$  and  $\kappa'$  themselves are scattered off other phonons, and the diagram provides an example of such scattering. The resulting lifetime of the involved phonons can be smaller than the reciprocal eigenfrequency  $\omega_0^{-1}$  of the NVS mode.



$$H_i = qh_b^{\text{scatt}}, \quad h_b^{\text{scatt}} = \sum_{\kappa, \kappa'} V_{\kappa\kappa'} b_{\kappa}^{\dagger} b_{\kappa'}, \quad (\text{G1})$$

where  $b_{\kappa}$  and  $b_{\kappa}^{\dagger}$  are annihilation and creation operators of the vibrational modes coupled to the NVS, cf. Eq. (34). These modes provide a thermal reservoir. We call them phonons and assume that their frequencies  $\omega_{\kappa}$  have a quasicontinuous spectrum.

It follows from the results of Sec. IV, see also Eqs. (A9) and (A10), that, to the leading order in  $H_i$ , the decay rate of the considered low-frequency mode can be expressed in terms of the power spectrum of the operator  $h_b^{\text{scatt}}$ . It is convenient to write this expression as

$$\Gamma = -\frac{\hbar}{2Mk_B T} \text{Im} \sum_{\kappa, \kappa'} V_{\kappa\kappa'}^* \int_0^{\infty} dt e^{i\omega_0 t - \varepsilon t} \phi_{\kappa\kappa'}(t), \quad (\text{G2})$$

$$\phi_{\kappa\kappa'}(t) = \frac{-i}{\hbar} \sum_{\kappa_0, \kappa'_0} V_{\kappa_0 \kappa'_0} \langle b_{\kappa}^{\dagger}(t) b_{\kappa'}(t) b_{\kappa'_0}^{\dagger}(0) b_{\kappa_0}(0) \rangle,$$

where  $\varepsilon \rightarrow +0$ . The function  $\phi_{\kappa\kappa'}(t)$  is a two-phonon correlation function.

Equation (G2) immediately gives the Landau-Rumer-Krivoglaz-type result (35) if one disregards the interaction between the high-frequency phonons, in which case  $\phi_{\kappa\kappa'}(t) = (-i/\hbar) V_{\kappa\kappa'} \bar{n}(\omega_{\kappa}) [\bar{n}(\omega_{\kappa'}) + 1] \exp[i(\omega_{\kappa} - \omega_{\kappa'})t]$ .

The interaction between the phonons can be taken into account by deriving a quantum kinetic equation for  $\phi_{\kappa\kappa'}$ . The modes  $\kappa$  can be well defined and the calculation can be done in a fairly general case where the resonator is spatially nonuniform, but the nonuniformity is smooth on the wavelength of thermal phonons  $\lambda_T$  (Atalaya *et al.*, 2016). This means, for example, that the size of the ripples on a nanomembrane or the scale of nanotube bending or twisting largely exceed  $\lambda_T$ .

Here we outline an analysis of the phonon-phonon scattering for a simple case where the resonator is spatially uniform. In a uniform system, thermal phonons are characterized by their wave vector  $\mathbf{k}$  and the branch  $\alpha$ , i.e., the phonon label  $\kappa$  is  $\kappa \equiv (\mathbf{k}, \alpha)$ . For thin resonators,  $\alpha$  includes the number of the quantized state of motion in the direction of the confinement. The strain of the considered low-frequency mode varies on the length  $L$  that largely exceeds the thermal wavelength of phonons  $\lambda_T$ ; for a flexural mode,  $L$  is the length of the resonator. Therefore, the modes  $\kappa$  and  $\kappa'$  coupled to it have close wave vectors,  $|\mathbf{k} - \mathbf{k}'| \ll |\mathbf{k}| \sim 1/\lambda_T$ . For thermal modes to resonantly scatter off the low-frequency mode, their frequencies should also be close,  $|\omega_{\kappa} - \omega_{\kappa'}| \sim \tau_{\kappa}^{-1}$ ,  $\omega_0 \ll \omega_{\kappa}$ , where  $\tau_{\kappa}$  is the relaxation time of mode  $\kappa$ . The conditions on the wave vectors and the mode frequencies are usually met in a sufficiently broad range of  $\mathbf{k}$  if the modes  $\kappa, \kappa'$  belong to the same branch  $\alpha$  [the situation may be more complicated in anisotropic systems (Herring, 1954)]. Here we consider coupling to modes of the same branch.

Given the difference in the spatial scales  $L$  and  $\lambda_T$ , it is convenient to switch from  $\phi_{\kappa\kappa'}$  to its Wigner transform. For a spatially uniform system [ $\kappa \equiv (\mathbf{k}, \alpha), \kappa' \equiv (\mathbf{k}', \alpha)$ ] it has the form

$$\Phi_{\alpha}(\mathbf{r}, \mathbf{k}, t) = \frac{\mathbb{V}}{(2\pi)^d} \int d\mathbf{k}_1 d\mathbf{k}'_1 e^{i(\mathbf{k}'_1 - \mathbf{k}_1) \cdot \mathbf{r}} \phi_{\mathbf{k}_1 \alpha \mathbf{k}'_1 \alpha}(t) \times \delta\left(\frac{\mathbf{k}_1 + \mathbf{k}'_1}{2} - \mathbf{k}\right), \quad (\text{G3})$$

where  $d$  is the dimensionality of thermal phonons and  $\mathbb{V}$  is the volume, area, or length of the resonator, depending on the dimensionality. The function  $\Phi_{\alpha}(\mathbf{r}, \mathbf{k}, t)$  is the two-phonon correlation function for the branch  $\alpha$ .

One can also introduce the coefficient  $V_{\alpha}(\mathbf{r}, \mathbf{k})$ , which is given by the same expression as  $\Phi_{\alpha}$ , except that  $\phi_{\mathbf{k}_1 \alpha \mathbf{k}'_1 \alpha}(t)$  is replaced by  $V_{\mathbf{k}'_1 \alpha \mathbf{k}_1 \alpha}$ . The decay rate (G2) can then be written as

$$\Gamma = -\frac{\hbar}{2Mk_B T} \text{Im} \int \frac{d\mathbf{r} d\mathbf{k}}{(2\pi)^d} \sum_{\alpha} V_{\alpha}^*(\mathbf{r}, \mathbf{k}) \times \int_0^{\infty} dt \Phi_{\alpha}(\mathbf{r}, \mathbf{k}, t) \exp(i\omega_0 t - \varepsilon t). \quad (\text{G4})$$

Equation (G4) presents the decay rate as an integral of the local (for a given  $\mathbf{r}$ ) decay rate “density.”

The parameters  $V_{\alpha}(\mathbf{r}, \mathbf{k})$  take a simple form for the deformation potential coupling of the considered mode to phonons (Gurevich, 1988). The deformation potential model assumes that the phonon wavelengths are much smaller than the length over which the mode-induced displacement field  $q\boldsymbol{\varphi}(\mathbf{r})$  varies. In the model the change of the phonon frequency  $\delta\omega_{\kappa}$  is proportional to the divergence of the displacement field, cf. Eq. (39),

$$\delta\omega_{\kappa} = -\omega_{\kappa} \gamma_{\kappa}^{(\text{G})} q \nabla \boldsymbol{\varphi}(\mathbf{r}). \quad (\text{G5})$$

From Eq. (G5) and from Eq. (G3) written for  $V_{\alpha}(\mathbf{r}, \mathbf{k})$  we can directly express the coupling parameters in terms of the Grüneisen parameters  $\gamma_{\mathbf{k}\alpha}^{(\text{G})}$ ,

$$V_{\alpha}(\mathbf{r}, \mathbf{k}) = -\hbar \omega_{\mathbf{k}\alpha} \gamma_{\mathbf{k}\alpha}^{(\text{G})} \nabla \boldsymbol{\varphi}(\mathbf{r}). \quad (\text{G6})$$

Equations (G4) and (G6) reduce the problem of finding the decay rate of a low-frequency mode to calculating the correlation function  $\Phi_{\alpha}$  of thermal phonons in the Wigner representation. We note that it is not assumed that the mode is described by a plane wave, as in the Akhiezer theory of ultrasound absorption (Akhiezer, 1938). The following analysis does not use the model (G5).

## 1. Kinetic equation

Time evolution of the function  $\Phi_{\alpha}(\mathbf{r}, \mathbf{k}, t)$  is determined by phonon-phonon scattering. If the phonon-phonon coupling and the disorder are weak, one can sum the perturbation series for the functions  $\phi_{\kappa\kappa'}$  (Atalaya *et al.*, 2016) and obtain a Markov kinetic equation for  $\Phi_{\alpha}$  (strictly speaking, with a renormalized phonon spectrum),

$$\partial_t \Phi_{\alpha} + \mathbf{v}_{\mathbf{k}\alpha} \partial_{\mathbf{r}} \Phi_{\alpha} = \text{St}[\Phi_{\alpha}], \quad \Phi_{\alpha} \equiv \Phi_{\alpha}(\mathbf{r}, \mathbf{k}, t). \quad (\text{G7})$$

Here  $\mathbf{v}_{\mathbf{k}\alpha}$  is the group velocity of the phonon of the branch  $\alpha$  with the wave vector  $\mathbf{k}$  and  $\text{St}$  is the collision integral. The initial condition follows from Eq. (G2),

$$\Phi_\alpha(\mathbf{r}, \mathbf{k}, 0) = -i\hbar^{-1}V_\alpha(\mathbf{r}, \mathbf{k})\bar{n}_{\mathbf{k}\alpha}(\bar{n}_{\mathbf{k}\alpha} + 1), \quad (\text{G8})$$

where  $\bar{n}_{\mathbf{k}\alpha} \equiv \bar{n}(\omega_{\mathbf{k}\alpha})$  is the phonon thermal occupation number.

The typical momentum exchange in a phonon-phonon collision or a collision with a short-range scatterer is  $\sim \hbar/\lambda_T$ . Therefore, the collision rate is independent of  $\mathbf{r}$  and the collision integral is local,

$$\text{St}[\Phi_\alpha(\mathbf{r}, \mathbf{k}, t)] = \frac{\mathbb{V}}{(2\pi)^d} \sum_{\alpha_0} \int d\mathbf{k}_0 L_{\mathbf{k}\alpha}^{\mathbf{k}_0\alpha_0} \Phi_{\alpha_0}(\mathbf{r}, \mathbf{k}_0, t). \quad (\text{G9})$$

For phonon-phonon scattering, the coefficients  $L_{\mathbf{k}\alpha}^{\mathbf{k}_0\alpha_0}$  are quadratic in the parameters of the cubic anharmonicity  $V_{\kappa_1\kappa_2\kappa_3}$  introduced in Eq. (36); they are real and are given by the expression for  $\tilde{\Lambda}_{\mathbf{k}\alpha}^{\mathbf{k}_0\alpha_0}$  by *Atalaya et al.* (2016). The locality of the collision integral also holds in the presence of a smooth disorder, where thermal phonons are no longer plane waves.

An analysis of the dynamics of thermal phonons and ultimately of the decay of the low-frequency mode can be done in terms of the right and left eigenmodes of the collision integral  $\psi_\nu(\mathbf{k}, \alpha)$  and  $\Psi_\nu(\mathbf{k}, \alpha)$ ,

$$\begin{aligned} \text{St}[\psi_\nu(\mathbf{k}, \alpha)] &= -\varepsilon_\nu \psi_\nu(\mathbf{k}, \alpha), \\ [\mathbb{V}/(2\pi)^d] \sum_\alpha \int d\mathbf{k} \Psi_\nu(\mathbf{k}, \alpha) \psi_\nu(\mathbf{k}, \alpha) &= \delta_{\nu,\nu'}. \end{aligned} \quad (\text{G10})$$

Since the coefficients  $L_{\mathbf{k}\alpha}^{\mathbf{k}_0\alpha_0}$  are real, the functions  $\psi_\nu$  and  $\Psi_\nu$  and the eigenvalues  $\varepsilon_\nu$  are real or form complex-conjugate pairs, with  $\text{Re } \varepsilon_\nu \geq 0$ . The real parts of the eigenvalues determine the decay rates of the two-phonon correlation functions. The zeroth eigenvalue,  $\nu = 0$ , is  $\varepsilon_0 = 0$ . It corresponds to the stationary value of the two-phonon correlator,

$$\psi_0(\mathbf{k}, \alpha) = \hbar\omega_{\mathbf{k}\alpha}\bar{n}_{\mathbf{k}\alpha}(\bar{n}_{\mathbf{k}\alpha} + 1), \quad \Psi_0(\mathbf{k}, \alpha) = \frac{\hbar\omega_{\mathbf{k}\alpha}}{k_B T^2 C \rho \mathbb{V}}$$

(we recall that  $C$  is the specific heat per unit mass). The eigenfunctions and eigenvalues with  $\nu > 0$  can be found using the explicit form of the collision operator.

Except for special fine-tuned cases, the eigenfunctions  $\psi_\nu$  form a complete set. One can then seek the solution of the kinetic equation in the form

$$\Phi_\alpha(\mathbf{r}, \mathbf{k}, t) = \sum_\nu T_\nu(\mathbf{r}, t) \psi_\nu(\mathbf{k}, \alpha). \quad (\text{G11})$$

The functions  $T_\nu$  describe the spatial structure of the correlator  $\Phi_\alpha(\mathbf{r}, \mathbf{k}, t)$ . The equation for these functions reads

$$\begin{aligned} \partial_t T_\nu(\mathbf{r}, t) + \sum_{\nu'} \mathbf{v}_{\nu\nu'} \partial_{\mathbf{r}} T_{\nu'}(\mathbf{r}, t) &= -\varepsilon_\nu T_\nu(\mathbf{r}, t), \\ \mathbf{v}_{\nu\nu'} &= \frac{\mathbb{V}}{(2\pi)^d} \sum_\alpha \int d\mathbf{k} \Psi_\nu(\mathbf{k}, \alpha) \mathbf{v}_{\mathbf{k}\alpha} \psi_{\nu'}(\mathbf{k}, \alpha). \end{aligned} \quad (\text{G12})$$

We now outline the solution of this equation in the limiting cases of the thermoelastic and Akhiezer relaxation.

### a. Thermoelastic relaxation

The decay rate  $\Gamma$  of the low-frequency mode is determined by the evolution of  $\Phi_\alpha(\mathbf{r}, \mathbf{k}, t)$  on the timescale  $\lesssim \omega_0^{-1}$ , as seen from Eq. (G4). We start with the case where  $\omega_0^{-1}$  is large compared to the relaxation time of thermal phonons  $\tau_{\text{ph}} = \max[\text{Re } \varepsilon_{\nu>0}^{-1}]$ . As seen from Eq. (G12),  $\tau_{\text{ph}}$  determines the long-time decay of the functions  $T_{\nu>0}$ . The decay of  $T_0$  can be slower, and this is the case that we now consider.

The slow evolution of  $T_0(\mathbf{r}, t)$  can be described in the adiabatic approximation in which the functions  $T_{\nu>0}$  adiabatically follow  $T_0$ . We then have  $T_\nu(\mathbf{r}, t) \approx -\varepsilon_\nu^{-1} \mathbf{v}_{\nu 0} \partial_{\mathbf{r}} T_0(\mathbf{r}, t)$  for  $\nu > 0$  and  $t \gg \tau_{\text{ph}}$ . Equation (G12) for  $T_0$  then takes the form

$$\begin{aligned} \partial_t T_0(\mathbf{r}, t) &= \sum_{ij} D_{ij} \partial_{r_i} \partial_{r_j} T_0(\mathbf{r}, t), \\ D_{ij} &= \sum_{\nu>0} (\mathbf{v}_{0\nu})_i (\mathbf{v}_{\nu 0})_j / \varepsilon_\nu. \end{aligned} \quad (\text{G13})$$

Using the explicit form of  $\Phi_\alpha(\mathbf{r}, \mathbf{k}, t)$  and  $\psi_0(\mathbf{k}, \alpha)$ , one can show that  $iT_0(\mathbf{r}, t)$  can be interpreted as the scaled coordinate-dependent increment of the temperature of high-frequency phonons compared to the ambient temperature. Respectively, Eq. (G13) has the form of the standard equation of thermal diffusion. Using the completeness of the set of the eigenfunctions  $\psi_\nu$ , one can further show that the expression for  $D_{ij}$  coincides with the standard expression (Lifshitz and Pitaevskii, 1981) for thermal diffusivity. In an isotropic medium  $D_{ij} = D\delta_{ij}$ . In terms of the thermal conductivity and the specific heat,  $D = \kappa_T / C\rho$ .

The boundary conditions for the function  $T_0(\mathbf{r}, t)$  follow from its proportionality to the temperature increment. At a free side of a nanoresonator there is no heat flux in the direction  $\hat{\mathbf{n}}$  normal to the side, and then  $\hat{\mathbf{n}} \partial_{\mathbf{r}} T_0 = 0$ . This boundary condition on the temperature increment was used in the analysis of thermoelastic relaxation by Lifshitz and Roukes (2000). On the other hand, at the surfaces where the resonator is clamped the temperature may be equal to the ambient temperature, and then  $T_0 = 0$  (but the clamping area can also have a thermal contact resistance).

A convenient strategy is to find the eigenvalues  $\mu_n$  and eigenfunctions  $T_{0n}(\mathbf{r})$  of the diffusion equation (G13), express  $T_0(\mathbf{r}, t)$  as a sum of  $T_{0n} \exp(-\mu_n t)$ , and then find the decay rate of the low-frequency mode from Eqs. (G4) and (G11), in which we keep only the term with  $\nu = 0$  (Atalaya et al., 2016). We illustrate this strategy for an important type of NVS (Zener, 1938; Landau and Lifshitz, 1986; Lifshitz and Roukes, 2000), a long and thin rectangular nanobeam. We assume that the beam is clamped at  $x = 0$  and  $x = L$ , has width  $W$  in the  $y$  direction and thickness  $l_\perp$  in the  $z$  direction, with the length  $L \gg W, l_\perp$  and with  $W, l_\perp \gg l_T$  ( $l_T$  is the phonon mean free path). The beam bends in the  $z$  direction. Therefore, the temperature is nonuniform in the  $z$  direction, but it can be uniform in the  $y$  direction. Since  $l_\perp \ll L$ , the low-lying eigenvalues of the diffusion equation (G13) correspond to the eigenmode  $\propto \sin(\pi z / l_\perp)$ . If we choose  $T_0 = 0$  at  $x = 0$  and  $x = L$ , the eigenmodes of Eq. (G13) are  $T_{0n}(\mathbf{r}) = (2/\sqrt{V}) \sin(\pi z / l_\perp) \sin(n\pi x / L)$ , and the corresponding

eigenvalues are  $\mu_n = \pi^2 D(l_\perp^{-2} + n^2 L^{-2})$ . For small  $n$ , where the term  $\propto L^{-2}$  in  $\mu_n$  can be disregarded,  $\mu_n \approx \tau_Z^{-1} = D(\pi/l_\perp)^2$ . This expression coincides with the Zener relaxation rate  $\tau_Z^{-1}$  used in the equation for the thermoelastic decay rate (38).

The phenomenological analysis of the thermoelastic relaxation corresponds to the assumption that the Grüneisen parameter is the same for all phonons:  $\gamma_{\mathbf{k}\alpha}^{(G)} \equiv \gamma^{(G)} = E\alpha_T / C\rho(1 - 2\nu_P)$ , where  $\alpha_T$  is the linear thermal expansion coefficient and  $\nu_P$  is the Poisson ratio. From Eqs. (G6), (G8), and (G11), with the account taken of the explicit form of  $\psi_0(\mathbf{k}, \alpha)$ , we have

$$T_0(\mathbf{r}, 0) = i\hbar^{-1}\gamma^{(G)}\nabla\varphi.$$

To find  $T_0(\mathbf{r}, t)$  one should expand  $T_0(\mathbf{r}, 0)$  in the eigenmodes  $T_{0n}(\mathbf{r})$ . Integration over time in Eq. (G4) then gives the decay rate  $\Gamma$  of the NVS mode in the form

$$\Gamma = \frac{E^2\alpha_T^2 T}{2MC\rho(1 - 2\nu_P)^2} \sum_n \frac{\mu_n^{-1}}{1 + (\omega_0/\mu_n)^2} \left| \int d\mathbf{r} \nabla\varphi T_{0n}(\mathbf{r}) \right|^2. \quad (\text{G14})$$

The eigenfunctions of the thermal diffusion equation were also used by Zener (1938) in the analysis of the  $Q$  factor of the beam vibrations based on the coupled equations of motion of a slow mode and temperature. These equations were derived from thermodynamic arguments and only diffusion transverse to the beam was considered.

For a flexural mode we have

$$\nabla\varphi = -(1 - 2\nu_P)L^{1/2}z\partial_x^2\zeta \left( \int \zeta^2 dx \right)^{-1/2},$$

where  $\zeta(x)$  is the displacement of the central plane in the  $z$  direction (Landau and Lifshitz, 1986). Using the explicit form of  $\zeta(x)$  for the lowest flexural mode and the expression for the mode eigenfrequency  $\omega_0 \approx 6.5(l_\perp/L^2)(E/\rho)^{1/2}$ , and setting  $\mu_n \approx \mu_0$ , from Eq. (G14) we obtain

$$\Gamma = \Gamma^{\text{TER}} \approx 0.98 \frac{E\alpha_T^2 T \omega_0}{2C\rho} \frac{\omega_0 \tau_Z}{1 + (\omega_0 \tau_Z)^2}, \quad (\text{G15})$$

which essentially coincides with Eq. (38).

We note that it is necessary to keep several terms in the sum over the eigenmodes  $T_{0n}$  in Eq. (G14) [Eq. (G15) includes the entire sum]. If the aspect ratio  $L/l_\perp$  is not large, one should take the dependence of the relaxation times of the thermal modes  $\mu_n^{-1}$  on the mode number into account. The described method applies to any geometry. It also allows one to take the difference between the values of the Grüneisen parameter for different phonons into account and, moreover, to go beyond the deformation potential approximation (G5) altogether.

## B. Akhiezer relaxation

When the mode eigenfrequency significantly exceeds the rate of thermal diffusion,  $\omega_0 \gg \tau_Z^{-1}$ , one should take into account a finite time it takes for the phonons to locally equilibrate. The corresponding mechanism is the extension to

a resonator mode of the Akhiezer mechanism of decay of ultrasound (Akhiezer, 1938).

In terms of the formalism described here, the Akhiezer damping is determined by the evolution of the function  $T_\nu(\mathbf{r}, t)$  over the phonon relaxation time  $\tau_{\text{ph}} \ll \tau_Z$ . On this timescale one can disregard the drift term in Eq. (G12). Indeed, this term comes from the spatial nonuniformity of the phonon distribution. The characteristic scale of the nonuniformity is the size of the system, which largely exceeds the phonon mean free path  $\sim v_{\text{ph}}\tau_{\text{ph}}$  ( $v_{\text{ph}}$  is the characteristic phonon velocity), so that  $|v_{\text{ph}}\partial_{\mathbf{r}}T_\nu| \ll |T_\nu|/\tau_{\text{ph}}$ . The functions  $T_\nu(\mathbf{r}, t)$  then exponentially decay in time as  $\exp(-\varepsilon_\nu t)$  for  $\nu > 0$ .

From Eqs. (G4) and (G11), the Akhiezer decay rate of the considered low-frequency mode  $\Gamma \equiv \Gamma^{\text{Akh}}$  is

$$\Gamma^{\text{Akh}} = \frac{1}{2Mk_B T} \frac{\mathbb{V}}{(2\pi)^{2d}} \text{Re} \sum_{\alpha, \alpha'} \int d\mathbf{r} d\mathbf{k} d\mathbf{k}' V_\alpha^*(\mathbf{r}, \mathbf{k}) \times \sum_{\nu > 0} \frac{\psi_\nu(\mathbf{k}, \alpha) \Psi_\nu(\mathbf{k}', \alpha')}{\varepsilon_\nu - i\omega_0} V_{\alpha'}(\mathbf{r}, \mathbf{k}') \bar{n}_{\mathbf{k}'\alpha'} (\bar{n}_{\mathbf{k}'\alpha'} + 1). \quad (\text{G16})$$

The term  $\nu = 0$ , which describes thermal diffusion, does not contribute to the Akhiezer relaxation.

In deriving Eq. (G16) no assumptions have been made about the structure of the considered low-frequency mode and the symmetry of the medium. It is important, though, that if we describe the coupling to phonons by the deformation potential (G6) and assume that the coupling parameters  $\gamma_{\mathbf{k}\alpha}^{(G)}$  are the same for all phonons, it follows from Eq. (G10) that  $\Gamma^{\text{Akh}} = 0$ . This means that to describe the Akhiezer relaxation it is necessary to allow for the dependence of  $\gamma_{\mathbf{k}\alpha}^{(G)}$  on the phonon quantum numbers  $\mathbf{k}$  and  $\alpha$ .

In the analysis of the Akhiezer relaxation the phonon decay rates  $\text{Re} \varepsilon_\nu$  are often replaced by a characteristic parameter  $\tau_{\text{ph}}^{-1}$ ; see Maris (1968), Iyer and Candler (2016), and references therein. In this approximation we can simplify Eq. (G16) using the completeness of the eigenfunctions  $\psi_\nu$ ,  $\sum_{\nu > 0} \psi_\nu(\mathbf{k}, \alpha) \Psi_\nu(\mathbf{k}', \alpha') = [(2\pi)^d / \mathbb{V}] \delta(\mathbf{k} - \mathbf{k}') \delta_{\alpha\alpha'} - \psi_0(\mathbf{k}, \alpha) \times \Psi_0(\mathbf{k}', \alpha')$ . If we denote the averaging over phonons by an overline,

$$\overline{B_\alpha(\mathbf{r}, \mathbf{k})} = \frac{\hbar^2}{(2\pi)^d C\rho k_B T^2} \sum_\alpha \int d\mathbf{k} B_\alpha(\mathbf{r}, \mathbf{k}) \omega_{\mathbf{k}\alpha}^2 \bar{n}_{\mathbf{k}\alpha} (\bar{n}_{\mathbf{k}\alpha} + 1) \quad (\text{G17})$$

[here  $B_\alpha(\mathbf{r}, \mathbf{k})$  is an arbitrary function of  $\mathbf{r}$ ,  $\mathbf{k}$ , and  $\alpha$ ], we can rewrite Eq. (G16) as

$$\Gamma^{\text{Akh}} = \frac{q_0^2}{\hbar} C\rho T \frac{\omega_0 \tau_{\text{ph}}}{1 + \omega_0^2 \tau_{\text{ph}}^2} \times \int d\mathbf{r} [|\overline{v_\alpha(\mathbf{r}, \mathbf{k})}|^2 - |\overline{v_\alpha(\mathbf{r}, \mathbf{k})}|^2], \quad (\text{G18})$$

where  $v_\alpha(\mathbf{r}, \mathbf{k}) = V_\alpha(\mathbf{r}, \mathbf{k})/\hbar\omega_{\mathbf{k}\alpha}$  and  $q_0 = (\hbar/2M\omega_0)^{1/2}$ . Equation (G18) explicitly shows that, to describe the Akhiezer relaxation, one has to take into account the



dependence of the parameters  $\gamma_{\mathbf{k}\alpha}^{(G)}$  on  $\mathbf{k}$ ,  $\alpha$ . From this point of view, it may be more appropriate to interpret the parameter  $(\gamma^{(G)})^2$  in Eq. (40) as the variance rather than the squared mean value of  $\gamma_{\mathbf{k}\alpha}^{(G)}$ .

An advantageous feature of the presented technique is that it allows one to consider an intermediate parameter range between the limits of the thermoelastic and Akhiezer relaxation. It immediately applies to microresonators and nanoresonators of an arbitrary geometry and various boundary conditions.

## APPENDIX H: ALLAN VARIANCE IN THE LIMITING CASES

As indicated in Sec. IX, the most common way to characterize frequency fluctuations is based on the Allan variance  $\sigma_A^2(\tau)$ . It is defined in terms of the frequencies  $\bar{f}_m$  measured from the increments of the full vibrational phase  $\varphi$  over the time intervals  $(t_m, t_m + \tau)$  as

$$\sigma_A^2(\tau) = \frac{1}{2(N-1)\bar{f}_0^2} \sum_{m=1}^{N-1} (\bar{f}_{m+1} - \bar{f}_m)^2, \quad (\text{H1})$$

where  $\bar{f}_0$  is the mean value of  $\bar{f}_m$ ; cf. Eq. (70). We recall that  $\varphi(t)$  determines the displacement in the laboratory frame, which is  $\propto \cos[\varphi(t)]$ ; it should not be confused with the phase  $\phi(t)$  in the rotating frame, which is counted off from  $2\pi f_0 t$ .

If the dead time between the successive measurements is zero,  $t_{m+1} - t_m = \tau$ , the Allan variance can be simply expressed in terms of the power spectrum  $S_\varphi(\omega)$  of the fluctuations of the full vibrational phase,

$$\sigma_A^2(\tau) = \frac{8}{\pi \omega_0^2 \tau^2} \int_0^\infty d\omega \sin^4(\omega\tau/2) S_\varphi(\omega). \quad (\text{H2})$$

Allan variance is used particularly broadly to characterize noise of self-sustained vibrations in systems with feedback. In such systems the vibration amplitude  $A$  is kept almost constant by the feedback loop, but the phase is not fixed (unless the vibrations are synchronized by an external source). Noise causes phase fluctuations, which accumulate in time. If the noise is thermal (thermomechanical), as in the equation of Brownian motion (2) or in Eq. (A9), the phase is diffusing (Berstein, 1938). Then, from the previous equations and Eq. (H2),  $\sigma_A^2(\tau)$  displays a characteristic dependence on  $\tau$  and  $A$ ,

$$\sigma_A^2(\tau) = (2\Gamma k_B T / M \omega_0^4 A^2) \tau^{-1}. \quad (\text{H3})$$

In the range where  $\tau$  is small compared to the decay time of the oscillator  $\Gamma^{-1}$ , Eq. (H3) also applies to a mode driven by a sufficiently strong resonant force  $F \cos \omega_F t$  with no feedback loop. For a strong drive the amplitude of forced vibrations largely exceeds the thermal displacement  $(k_B T / M \omega_0^2)^{1/2}$ , and thus amplitude fluctuations are relatively small. Fluctuations in this case can be analyzed using the equation of motion for the complex amplitude  $u(t)$  of a driven linear mode

$$\begin{aligned} \dot{u} &= -[\Gamma + i(\omega_F - \omega_0)]u(t) - i \frac{F}{4M\omega_F} + \xi(t), \\ u(t) &= \frac{1}{2M\omega_F} [M\omega_F q(t) - ip(t)] \exp(-i\omega_F t), \end{aligned} \quad (\text{H4})$$

where  $\xi(t)$  is thermal noise with the correlator (24); cf. Sec. D.1.

In the absence of noise and in the stationary regime, the vibration amplitude is  $A_{\text{st}} \approx 2|u_{\text{st}}| = (F/2M\omega_F)[(\omega_F - \omega_0)^2 + \Gamma^2]^{-1/2}$ . The vibration phase  $\phi_{\text{st}}$  as counted off from the drive phase is

$$\phi_{\text{st}} = -\frac{1}{2} \pi - \arctan[(\omega_F - \omega_0)/\Gamma]. \quad (\text{H5})$$

For weak thermal noise the vibration phase  $\phi(t) = \varphi(t) - \omega_F t$  fluctuates about  $\phi_{\text{st}}$ . This behavior is significantly different from the phase diffusion for self-sustained vibrations. Interestingly, it follows from Eq. (H4) that the dependence  $\sigma_A^2 \propto \tau^{-1}$  has the same form in both cases provided  $\Gamma\tau \ll 1$ . It is this characteristic dependence that gives the so-called noise floor for thermal-noise-dominated fluctuations in nanomechanical systems; cf. Cleland and Roukes (2002), Ekinci, Yang, and Roukes (2004), Sansa *et al.* (2016), Sadeghi *et al.* (2020), and references therein.

For a resonantly driven mode subject to thermal noise and in the absence of a feedback loop, Eq. (H4) allows one also to find a simple expression for the Allan variance in the opposite limit of a long time  $\tau$ , where  $\Gamma\tau \gg 1$ ,

$$\sigma_A^2(\tau) = (3k_B T / M \omega_0^4 A^2) \tau^{-2}. \quad (\text{H6})$$

Of significant importance is a different regime where the Allan variance is dominated not by thermal fluctuations of the slow part of the phase but rather by eigenfrequency fluctuations. These fluctuations often have a  $1/f$ -type component (the flicker noise). In this case it follows from Eq. (69) that  $S_\varphi(\nu) \propto \nu^{-3}$  for small  $\nu$ . Then from Eq. (H2) we have  $\sigma_A^2 \propto \tau^{-4}$ . As mentioned in Sec. IX, the Allan variance does not distinguish between the eigenfrequency fluctuations and the fluctuations of the rotating-frame phase  $\phi$ .

A convenient approach to an open-loop measurement of the Allan variance is based on measuring the ratio of the quadrature and in-phase components of the vibrations of a driven mode. This ratio gives  $\tan \phi(t)$ . In the measurement, the drive frequency  $\omega_F$  is often chosen to be maximally close to the mean measured mode eigenfrequency  $\omega_0^{\text{meas}}$ . The relation between the phase fluctuation  $\Delta\phi(t)$  and the fluctuation  $\Delta\omega_0^{\text{meas}}$  in this case can be obtained using Eq. (H5). To do this one should replace  $\omega_0$  in this equation with  $\omega_0^{\text{meas}}$  and the stationary phase  $\phi_{\text{st}}$  with the time-dependent phase  $\phi$ . One then finds  $\Delta\omega_0^{\text{meas}} \approx \Gamma \Delta\phi$ . The relation applies in the adiabatic limit, where the change  $\Delta\phi(t)$  is slow compared to the oscillator relaxation time  $\Gamma^{-1}$  and is small.

## REFERENCES

Abrikosov, A. A., L. P. Gorkov, and I. E. Dzyaloshinski, 1975, *Methods of Quantum Field Theory in Statistical Physics* (Dover, New York).

- Acernese, F., *et al.*, 2019, “Increasing the Astrophysical Reach of the Advanced Virgo Detector via the Application of Squeezed Vacuum States of Light,” *Phys. Rev. Lett.* **123**, 231108.
- Akhiezer, A. I., 1938, “On the sound absorption in solids,” *Zh. Eksp. Teor. Fiz.* **8**, 1318.
- Albrecht, T. R., P. Grütter, D. Horne, and D. Rugar, 1991, “Frequency modulation detection using high- $Q$  cantilevers for enhanced force microscope sensitivity,” *J. Appl. Phys.* **69**, 668–673.
- Alda, I., J. Berthelot, R. A. Rica, and R. Quidant, 2016, “Trapping and manipulation of individual nanoparticles in a planar Paul trap,” *Appl. Phys. Lett.* **109**, 163105.
- Aldridge, J. S., and A. N. Cleland, 2005, “Noise-Enabled Precision Measurements of a Duffing Nanomechanical Resonator,” *Phys. Rev. Lett.* **94**, 156403.
- Allan, D., H. Hellwig, P. Kartaschoff, J. Vanier, J. Vig, G. M. R. Winkler, and N. F. Yannoni, 1988, “Standard terminology for fundamental frequency and time metrology,” in *Proceedings of the 42nd Annual Frequency Control Symposium, Baltimore, 1988* (IEEE, New York), pp. 419–425, [10.1109/FREQ.1988.27634](#).
- Allan, D. W., 1966, “Statistics of atomic frequency standards,” *Proc. IEEE* **54**, 221–230.
- Almog, R., S. Zaitsev, O. Shtempluck, and E. Buks, 2007a, “Noise Squeezing in a Nanomechanical Duffing Resonator,” *Phys. Rev. Lett.* **98**, 078103.
- Almog, R., S. Zaitsev, O. Shtempluck, and E. Buks, 2007b, “Signal amplification in a nanomechanical Duffing resonator via stochastic resonance,” *Appl. Phys. Lett.* **90**, 013508.
- Amarouchene, Yacine, Matthieu Mangeat, Benjamin Vidal Montes, Lukas Ondic, Thomas Guérin, David S. Dean, and Yann Louyer, 2019, “Nonequilibrium Dynamics Induced by Scattering Forces for Optically Trapped Nanoparticles in Strongly Inertial Regimes,” *Phys. Rev. Lett.* **122**, 183901.
- Anderson, P. W., 1954, “Mathematical model for the narrowing of spectral lines by exchange or motion,” *J. Phys. Soc. Jpn.* **9**, 316–339.
- Anderson, P. W., B. I. Halperin, and C. M. Varma, 1972, “Anomalous low-temperature thermal properties of glasses and spin glasses,” *Philos. Mag.* **25**, 1–9.
- Anetsberger, G., R. Rivière, A. Schliesser, O. Arcizet, and T. J. Kippenberg, 2008, “Ultralow-dissipation optomechanical resonators on a chip,” *Nat. Photonics* **2**, 627.
- Angelescu, D. E., M. C. Cross, and M. L. Roukes, 1998, “Heat transport in mesoscopic systems,” *Superlattices Microstruct.* **23**, 673.
- Antoni, Thomas, Kevin Makles, Rémy Braive, Tristan Briant, Pierre-François Cohadon, Isabelle Sagnes, Isabelle Robert-Philip, and Antoine Heidmann, 2012, “Nonlinear mechanics with suspended nanomembranes,” *Europhys. Lett.* **100**, 68005.
- Antonio, D., D. H. Zquette, and D. Lopez, 2012, “Frequency stabilization in nonlinear micromechanical oscillators,” *Nat. Commun.* **3**, 806.
- Ao, Ping, and J. Rammer, 1989, “Influence of Dissipation on the Landau-Zener Transition,” *Phys. Rev. Lett.* **62**, 3004–3007.
- Ares, N., T. Pei, A. Mavalankar, M. Mergenthaler, J. H. Warner, G. A. D. Briggs, and E. A. Laird, 2016, “Resonant Optomechanics with a Vibrating Carbon Nanotube and a Radio-Frequency Cavity,” *Phys. Rev. Lett.* **117**, 170801.
- Ari, Atakan B., M. Çağatay Karakan, Cenk Yanık, İsmet İ. Kaya, and M. Selim Hanay, 2018, “Intermodal Coupling as a Probe for Detecting Nanomechanical Modes,” *Phys. Rev. Appl.* **9**, 034024.
- Armour, A. D., M. P. Blencowe, and Y. Zhang, 2004, “Classical dynamics of a nanomechanical resonator coupled to a single-electron transistor,” *Phys. Rev. B* **69**, 125313.
- Arnold, V. I., 1989, *Mathematical Methods of Classical Mechanics* (Springer, New York).
- Arora, Nishta, and A. K. Naik, 2022, “Qualitative effect of internal resonance on the dynamics of two-dimensional resonator,” *J. Phys. D* **55**, 265301.
- Arrangoiz-Arriola, P., E. A. Wollack, Zhaoyou Wang, M. Pechal, Wentao Jiang, T. P. McKenna, J. D. Witmer, R. Van Laer, and A. H. Safavi-Naeini, 2019, “Resolving the energy levels of a nanomechanical oscillator,” *Nature (London)* **571**, 537.
- Asadi, Keivan, Junghoon Yeom, and Hanna Cho, 2021, “Strong internal resonance in a nonlinear, asymmetric microbeam resonator,” *Microsyst. Nanoeng.* **7**, 9.
- Asadi, Keivan, Jun Yu, and Hanna Cho, 2018, “Nonlinear couplings and energy transfers in micro- and nano-mechanical resonators: Intermodal coupling, internal resonance and synchronization,” *Phil. Trans. R. Soc. A* **376**, 20170141.
- Asano, Motoki, Ryuichi Ohta, Takuma Aihara, Tai Tsuchizawa, Hajime Okamoto, and Hiroshi Yamaguchi, 2019, “Optically probing Schwinger angular momenta in a micromechanical resonator,” *Phys. Rev. A* **100**, 053801.
- Aspelmeyer, M., T. Kippenberg, and F. Marquardt, 2014a, Eds., *Cavity Optomechanics: Nano- and Micromechanical Resonators Interacting with Light* (Springer, Berlin).
- Aspelmeyer, M., T. J. Kippenberg, and F. Marquardt, 2014b, “Cavity optomechanics,” *Rev. Mod. Phys.* **86**, 1391.
- Atalaya, J., A. Isacsson, and M. I. Dykman, 2011a, “Diffusion-Induced Bistability of Driven Nanomechanical Resonators,” *Phys. Rev. Lett.* **106**, 227202.
- Atalaya, J., A. Isacsson, and M. I. Dykman, 2011b, “Diffusion-induced dephasing in nanomechanical resonators,” *Phys. Rev. B* **83**, 045419.
- Atalaya, Juan, Thomas W. Kenny, M. L. Roukes, and M. I. Dykman, 2016, “Nonlinear damping and dephasing in nanomechanical systems,” *Phys. Rev. B* **94**, 195440.
- Bahr, B., R. Marathe, and D. Weinstein, 2014, “Phononic Crystals for acoustic confinement in CMOS-MEMS resonators,” in *Proceedings of the 2014 IEEE Frequency Control Symposium, Taipei, 2014* (IEEE, New York), pp. 1–4, [10.1109/FCS.2014.6859980](#).
- Barker, A. S., and A. J. Sievers, 1975, “Optical studies of vibrational properties of disordered solids,” *Rev. Mod. Phys.* **47**, S1–S179.
- Barnard, Arthur W., Vera Sazonova, Arend M. van der Zande, and Paul L. McEuen, 2012, “Fluctuation broadening in carbon nanotube resonators,” *Proc. Natl. Acad. Sci. U.S.A.* **109**, 19093.
- Barnard, Arthur W., Mian Zhang, Gustavo S. Wiederhecker, Michal Lipson, and Paul L. McEuen, 2019, “Real-time vibrations of a carbon nanotube,” *Nature (London)* **566**, 89.
- Barquist, C. S., W. G. Jiang, K. Gunther, N. Eng, Y. Lee, and H. B. Chan, 2020, “Damping of a micro-electromechanical oscillator in turbulent superfluid  $^4\text{He}$ : A novel probe of quantized vorticity in the ultra-low temperature regime,” *Phys. Rev. B* **101**, 174513.
- Barquist, C. S., W. G. Jiang, K. Gunther, and Y. Lee, 2021, “Determining the source of phase noise: Response of a driven Duffing oscillator to low-frequency damping and resonance frequency fluctuations,” *Physica (Amsterdam)* **427D**, 132999.
- Barton, Robert A., *et al.*, 2012, “Photothermal self-oscillation and laser cooling of graphene optomechanical systems,” *Nano Lett.* **12**, 4681–4686.
- Beccari, Alberto, Diego A. Visani, Sergey A. Fedorov, Mohammad J. Bereyhi, Victor Boureau, Nils J. Engelsen, and Tobias J. Kippenberg, 2022, “Strained crystalline nanomechanical resonators with ultralow dissipation,” *Nat. Phys.* **18**, 436–441.

- Behunin, R. O., F. Intravaia, and P. T. Rakich, 2016, “Dimensional transformation of defect-induced noise, dissipation, and nonlinearity,” *Phys. Rev. B* **93**, 224110.
- Belavin, A. A., B. Y. Zeldovich, A. M. Perelomov, and V. S. Popov, 1969, “Relaxation of quantum systems with equidistant spectra,” *J. Exp. Theor. Phys.* **29**, 145, [http://jetp.ras.ru/cgi-bin/dn/e\\_029\\_01\\_0145.pdf](http://jetp.ras.ru/cgi-bin/dn/e_029_01_0145.pdf).
- Bennett, S. D., and A. A. Clerk, 2006, “Laser-like instabilities in quantum nano-electromechanical systems,” *Phys. Rev. B* **74**, 201301.
- Bennett, S. D., L. Cockins, Y. Miyahara, P. Grutter, and A. A. Clerk, 2010, “Strong Electromechanical Coupling of an Atomic Force Microscope Cantilever to a Quantum Dot,” *Phys. Rev. Lett.* **104**, 017203.
- Benyamini, A., A. Hamo, S. Viola Kusminskiy, F. von Oppen, and S. Ilani, 2014, “Real-space tailoring of the electron-phonon coupling in ultraclean nanotube mechanical resonators,” *Nat. Phys.* **10**, 151.
- Bereyhi, Mohammad J., Amirali Arabmoheghi, Sergey A. Fedorov, Alberto Beccari, Guanhao Huang, Tobias J. Kippenberg, and Nils J. Engelsen, 2022, “Perimeter modes of nanomechanical resonators exhibit quality factors exceeding  $10^9$  at room temperature,” *Phys. Rev. X* **12**, 021036.
- Berstein, I. L., 1938, “On fluctuations in the neighborhood of periodic motion of an auto-oscillating system,” *C.R. (Dokl.) Acad. Sci. URSS* **20**, 11.
- Bertet, P., F. R. Ong, M. Boissonneault, A. Bolduc, F. Mallet, A. C. Doherty, A. Blais, D. Vion, and D. Esteve, 2012, “Circuit quantum electrodynamics with a nonlinear resonator,” in *Fluctuating Nonlinear Oscillators: From Nanomechanics to Quantum Superconducting Circuits*, edited by M. I. Dykman (Oxford University Press, Oxford), pp. 1–31.
- Bienfait, A., *et al.*, 2019, “Phonon-mediated quantum state transfer and remote qubit entanglement,” *Science* **364**, 368–371.
- Bindel, David S., and Sanjay Govindjee, 2005, “Elastic PMLs for resonator anchor loss simulation,” *Int. J. Numer. Methods Eng.* **64**, 789–818.
- Blaikie, Andrew, David Miller, and Benjamin J. Aleman, 2019, “A fast and sensitive room-temperature graphene nanomechanical bolometer,” *Nat. Commun.* **10**, 4726.
- Blencowe, M. P., J. Imbers, and A. D. Armour, 2005, “Dynamics of a nanomechanical resonator coupled to a superconducting single-electron transistor,” *New J. Phys.* **7**, 236.
- Bleszynski-Jayich, A. C., W. E. Shanks, B. Peaudecerf, E. Ginossar, F. von Oppen, L. Glazman, and J. G. E. Harris, 2009, “Persistent currents in normal metal rings,” *Science* **326**, 272–275.
- Blien, Stefan, Patrick Steger, Niklas Hüttner, Richard Graaf, and Andreas K. Hüttel, 2020, “Quantum capacitance mediated carbon nanotube optomechanics,” *Nat. Commun.* **11**, 1636.
- Bogoliubov, N. N., and Y. A. Mitropolsky, 1961, *Asymptotic Methods in the Theory of Non-Linear Oscillations* (Gordon and Breach, New York).
- Bogolyubov, N. N., 1945, *On Some Statistical Methods in Mathematical Physics* (National Academy of Sciences of Ukraine, Kiev).
- Bothner, D., S. Yanai, A. Iniguez-Rabago, M. Yuan, Ya. M. Blanter, and G. A. Steele, 2020, “Cavity electromechanics with parametric mechanical driving,” *Nat. Commun.* **11**, 1589.
- Braakman, F. R., and M. Poggio, 2019, “Force sensing with nanowire cantilevers,” *Nanotechnology* **30**, 332001.
- Brout, R., and W. Visscher, 1962, “Suggested Experiment on Approximate Localized Modes in Crystals,” *Phys. Rev. Lett.* **9**, 54–55.
- Buks, E., and M. L. Roukes, 2001, “Stiction, adhesion energy, and the Casimir effect in micromechanical systems,” *Phys. Rev. B* **63**, 033402.
- Buks, E., and M. L. Roukes, 2002, “Electrically tunable collective response in a coupled micromechanical array,” *J. Microelectromech. Syst.* **11**, 802–807.
- Buks, E., and B. Yurke, 2006, “Mass detection with a nonlinear nanomechanical resonator,” *Phys. Rev. E* **74**, 046619.
- Bunch, J. Scott, Arend M. van der Zande, Scott S. Verbridge, Ian W. Frank, David M. Tanenbaum, Jeevak M. Parpia, Harold G. Craighead, and Paul L. McEuen, 2007, “Electromechanical resonators from graphene sheets,” *Science* **315**, 490–493.
- Burg, Thomas P., Michel Godin, Scott M. Knudsen, Wenjiang Shen, Greg Carlson, John S. Foster, Ken Babcock, and Scott R. Manalis, 2007, “Weighing of biomolecules, single cells and single nanoparticles in fluid,” *Nature (London)* **446**, 1066–1069.
- Caldeira, A. O., and A. J. Leggett, 1981, “Influence of Dissipation on Quantum Tunneling in Macroscopic Systems,” *Phys. Rev. Lett.* **46**, 211–214.
- Carr, D. W., and H. G. Craighead, 1997, “Fabrication of nanoelectromechanical systems in single crystal silicon using silicon on insulator substrates and electron beam lithography,” *J. Vac. Sci. Technol. B* **15**, 2760–2763.
- Castellanos-Gomez, Andres, Ronald van Leeuwen, Michele Buscema, Herre S. J. van der Zant, Gary A. Steele, and Warner J. Venstra, 2013, “Single-layer  $\text{MoS}_2$  mechanical resonators,” *Adv. Mater.* **25**, 6719–6723.
- Castellanos-Gomez, Andres, Harold B. Meerwaldt, Warner J. Venstra, Herre S. J. van der Zant, and Gary A. Steele, 2012, “Strong and tunable mode coupling in carbon nanotube resonators,” *Phys. Rev. B* **86**, 041402.
- Catalini, Letizia, Massimiliano Rossi, Eric C. Langman, and Albert Schliesser, 2021, “Modeling and Observation of Nonlinear Damping in Dissipation-Diluted Nanomechanical Resonators,” *Phys. Rev. Lett.* **126**, 174101.
- Cattiaux, D., *et al.*, 2021, “A macroscopic object passively cooled into its quantum ground state of motion beyond single-mode cooling,” *Nat. Commun.* **12**, 6182.
- Caves, Carlton M., 1981, “Quantum-mechanical noise in an interferometer,” *Phys. Rev. D* **23**, 1693–1708.
- Cha, Jinwoong, and Chiara Daraio, 2018, “Electrical tuning of elastic wave propagation in nanomechanical lattices at MHz frequencies,” *Nat. Nanotechnol.* **13**, 1016–1020.
- Cha, Jinwoong, Kun Woo Kim, and Chiara Daraio, 2018, “Experimental realization of on-chip topological nanoelectromechanical metamaterials,” *Nature (London)* **564**, 229–233.
- Chakram, S., Y. S. Patil, L. Chang, and M. Vengalattore, 2014, “Dissipation in Ultrahigh Quality Factor SiN Membrane Resonators,” *Phys. Rev. Lett.* **112**, 127201.
- Chan, H. B., V. A. Aksyuk, R. N. Kleiman, D. J. Bishop, and F. Capasso, 2001, “Quantum mechanical actuation of microelectromechanical systems by the Casimir force,” *Science* **291**, 1941–1944.
- Chan, H. B., Y. Bao, J. Zou, R. A. Cirelli, F. Klemens, W. M. Mansfield, and C. S. Pai, 2008, “Measurement of the Casimir Force between a Gold Sphere and a Silicon Surface with Nanoscale Trench Arrays,” *Phys. Rev. Lett.* **101**, 030401.
- Chan, H. B., M. I. Dykman, and C. Stambaugh, 2008a, “Paths of Fluctuation Induced Switching,” *Phys. Rev. Lett.* **100**, 130602.
- Chan, H. B., M. I. Dykman, and C. Stambaugh, 2008b, “Switching-path distribution in multidimensional systems,” *Phys. Rev. E* **78**, 051109.
- Chan, H. B., and C. Stambaugh, 2006, “Fluctuation-enhanced frequency mixing in a nonlinear micromechanical oscillator,” *Phys. Rev. B* **73**, 224301.



- Chan, H. B., and C. Stambaugh, 2007, "Activation Barrier Scaling and Crossover for Noise-Induced Switching in Micromechanical Parametric Oscillators," *Phys. Rev. Lett.* **99**, 060601.
- Chan, Jasper, T. P. Mayer Alegre, Amir H. Safavi-Naeini, Jeff T. Hill, Alex Krause, Simon Groblacher, Markus Aspelmeyer, and Oskar Painter, 2011, "Laser cooling of a nanomechanical oscillator into its quantum ground state," *Nature (London)* **478**, 89–92.
- Chandorkar, S. A., M. Agarwal, R. Melamud, R. N. Candler, K. E. Goodson, and T. W. Kenny, 2008, "Limits of quality factor in bulk-mode micromechanical resonators," in *Proceedings of the 21st IEEE International Conference on Micro Electro Mechanical Systems, Tucson, 2008* (IEEE, New York), pp. 74–77, [10.1109/MEMSYS.2008.4443596](#).
- Chandorkar, Saurabh A., Robert N. Candler, Amy Duwel, Renata Melamud, Manu Agarwal, Kenneth E. Goodson, and Thomas W. Kenny, 2009, "Multimode thermoelastic dissipation," *J. Appl. Phys.* **105**, 043505.
- Chaste, J., A. Eichler, J. Moser, G. Ceballos, R. Rurali, and A. Bachtold, 2012, "A nanomechanical mass sensor with yoctogram resolution," *Nat. Nanotechnol.* **7**, 301–304.
- Chaste, J., M. Sledzinska, M. Zdrojek, J. Moser, and A. Bachtold, 2011, "High-frequency nanotube mechanical resonators," *Appl. Phys. Lett.* **99**, 213502.
- Chen, C., D. H. Zanette, D. A. Czaplewski, S. Shaw, and D. López, 2017, "Direct observation of coherent energy transfer in nonlinear micromechanical oscillators," *Nat. Commun.* **8**, 15523.
- Chen, Changyao, Vikram V. Deshpande, Mikito Koshino, Sunwoo Lee, Alexander Gondarenko, Allan H. MacDonald, Philip Kim, and James Hone, 2016, "Modulation of mechanical resonance by chemical potential oscillation in graphene," *Nat. Phys.* **12**, 240–244.
- Chen, Changyao, Sami Rosenblatt, Kirill I. Bolotin, William Kalb, Philip Kim, Ioannis Kyriassis, Horst L. Stormer, Tony F. Heinz, and James Hone, 2009, "Performance of monolayer graphene nanomechanical resonators with electrical readout," *Nat. Nanotechnol.* **4**, 861.
- Chen, Changyao, Damián H. Zanette, Jeffrey R. Guest, David A. Czaplewski, and Daniel López, 2016, "Self-Sustained Micromechanical Oscillator with Linear Feedback," *Phys. Rev. Lett.* **117**, 017203.
- Chien, Miao-Hsuan, Mario Bramehuber, Benedikt K. Rossboth, Gerhard J. Schütz, and Silvan Schmid, 2018, "Single-molecule optical absorption imaging by nanomechanical photothermal sensing," *Proc. Natl. Acad. Sci. U.S.A.* **115**, 11150–11155.
- Chiout, Anis, Franck Correia, Meng-Qiang Zhao, A. T. Charlie Johnson, Debora Pierucci, Fabrice Oehler, Abdelkarim Ouerghi, and Julien Chaste, 2021, "Multi-order phononic frequency comb generation within a MoS<sub>2</sub> electromechanical resonator," *Appl. Phys. Lett.* **119**, 173102.
- Chiu, H.-Y., P. Hung, H. W. Ch. Postma, and M. Bockrath, 2008, "Atomic-scale mass sensing using carbon nanotube resonators," *Nano Lett.* **8**, 4342–4346.
- Chowdhury, Avishek, Sylvain Barbay, Marcel G. Clerc, Isabelle Robert-Philip, and Rémy Braive, 2017, "Phase Stochastic Resonance in a Forced Nanoelectromechanical Membrane," *Phys. Rev. Lett.* **119**, 234101.
- Chu, Yiwen, Prashanta Kharel, William H. Renninger, Luke D. Burkhardt, Luigi Frunzio, Peter T. Rakich, and Robert J. Schoelkopf, 2017, "Quantum acoustics with superconducting qubits," *Science* **358**, 199.
- Chu, Yiwen, Prashanta Kharel, Taekwan Yoon, L. Frunzio, P. T. Rakich, and R. J. Schoelkopf, 2018, "Creation and control of multi-phonon Fock states in a bulk acoustic-wave resonator," *Nature (London)* **563**, 666.
- Clark, Jeremy B., Florent Lecocq, Raymond W. Simmonds, Jose Aumentado, and John D. Teufel, 2017, "Sideband cooling beyond the quantum backaction limit with squeezed light," *Nature (London)* **541**, 191.
- Cleland, A. N., 2003, *Foundations of Nanomechanics: From Solid-State Theory to Device Applications* (Springer, Berlin).
- Cleland, A. N., 2005, "Thermomechanical noise limits on parametric sensing with nanomechanical resonators," *New J. Phys.* **7**, 235.
- Cleland, A. N., and M. L. Roukes, 1996, "Fabrication of high frequency nanometer scale mechanical resonators from bulk Si crystals," *Appl. Phys. Lett.* **69**, 2653–2655.
- Cleland, A. N., and M. L. Roukes, 1998, "A nanometre-scale mechanical electrometer," *Nature (London)* **392**, 160.
- Cleland, A. N., and M. L. Roukes, 2002, "Noise processes in nanomechanical resonators," *J. Appl. Phys.* **92**, 2758–2769.
- Clerk, A. A., and S. Bennett, 2005, "Quantum nanoelectromechanics with electrons, quasi-particles and Cooper pairs: Effective bath descriptions and strong feedback effects," *New J. Phys.* **7**, 238.
- Clerk, A. A., M. H. Devoret, S. M. Girvin, Florian Marquardt, and R. J. Schoelkopf, 2010, "Introduction to quantum noise, measurement, and amplification," *Rev. Mod. Phys.* **82**, 1155–1208.
- Clerk, A. A., and D. W. Utami, 2007, "Using a qubit to measure photon-number statistics of a driven thermal oscillator," *Phys. Rev. A* **75**, 042302.
- Cole, Garrett D., Ignacio Wilson-Rae, Katharina Werbach, Michael R. Vanner, and Markus Aspelmeyer, 2011, "Phonon-tunnelling dissipation in mechanical resonators," *Nat. Commun.* **2**, 231.
- Cole, Robin M., George A. Brawley, Vivekananda P. Adiga, Roberto De Alba, Jeevak M. Parpia, Bojan Ilic, Harold G. Craighead, and Warwick P. Bowen, 2015, "Evanescent-Field Optical Readout of Graphene Mechanical Motion at Room Temperature," *Phys. Rev. Appl.* **3**, 024004.
- Collins, K. C., A. A. Maznev, Zh. Tian, K. Esfarjani, K. A. Nelson, and G. Chen, 2013, "Non-diffusive relaxation of a transient thermal grating analyzed with the Boltzmann transport equation," *J. Appl. Phys.* **114**, 104302.
- Conangla, Gerard P., Andreas W. Schell, Raúl A. Rica, and Romain Quidant, 2018, "Motion control and optical interrogation of a levitating single nitrogen vacancy in vacuum," *Nano Lett.* **18**, 3956–3961.
- Conley, William G., Arvind Raman, Charles M. Krougrill, and Saeed Mohammadi, 2008, "Nonlinear and nonplanar dynamics of suspended nanotube and nanowire resonators," *Nano Lett.* **8**, 1590–1595.
- Cross, M., and H. Greenside, 2009, *Pattern Formation and Dynamics in Nonequilibrium Systems* (Cambridge University Press, Cambridge, England).
- Cross, M. C., and Ron Lifshitz, 2001, "Elastic wave transmission at an abrupt junction in a thin plate with application to heat transport and vibrations in mesoscopic systems," *Phys. Rev. B* **64**, 085324.
- Croy, Alexander, Daniel Midtvedt, Andreas Isacsson, and Jari M. Kinaret, 2012, "Nonlinear damping in graphene resonators," *Phys. Rev. B* **86**, 235435.
- Czaplewski, David A., Changyao Chen, Daniel Lopez, Oriel Shoshani, Axel M. Eriksson, Scott Strachan, and Steven W. Shaw, 2018, "Bifurcation Generated Mechanical Frequency Comb," *Phys. Rev. Lett.* **121**, 244302.
- Dash, Aneesh, Swapnil K. More, Nishta Arora, and A. K. Naik, 2021, "Ultra-sensitive charge detection and latch memory using MoS<sub>2</sub>-nanoresonator-based bifurcation amplifiers," *Appl. Phys. Lett.* **118**, 053105.

- Davidovikj, D., F. Alijani, S. J. Cartamil-Bueno, H. S. J. van der Zant, M. Amabili, and P. G. Steeneken, 2017, “Nonlinear dynamic characterization of two-dimensional materials,” *Nat. Commun.* **8**, 1253.
- De, S., K. Kunal, and N. R. Aluru, 2016, “Mixed role of surface on intrinsic losses in silicon nanostructures,” *J. Appl. Phys.* **119**, 114304.
- De Alba, R., F. Massel, I. R. Storch, T. S. Abhilash, A. Hui, P. L. McEuen, H. G. Craighead, and J. M. Parpia, 2016, “Tunable phonon-cavity coupling in graphene membranes,” *Nat. Nanotechnol.* **11**, 741–746.
- de Bonis, S. L., C. Urgell, W. Yang, C. Samanta, A. Noury, J. Vergara-Cruz, Q. Dong, Y. Jin, and A. Bachtold, 2018, “Ultrasensitive displacement noise measurement of carbon nanotube mechanical resonators,” *Nano Lett.* **18**, 5324–5328.
- Debye, P., 1929, *Polar Molecules* (Dover, New York).
- Defoort, M., V. Puller, O. Bourgeois, F. Pistolesi, and E. Collin, 2015, “Scaling laws for the bifurcation escape rate in a nanomechanical resonator,” *Phys. Rev. E* **92**, 050903.
- Defoort, M., *et al.*, 2016, “Probing Bogoliubov quasiparticles in superfluid  $^3\text{He}$  with a ‘vibrating-wire like’ MEMS device,” *J. Low Temp. Phys.* **183**, 284.
- Degen, C. L., M. Poggio, H. J. Mamin, C. T. Rettner, and D. Rugar, 2009, “Nanoscale magnetic resonance imaging,” *Proc. Natl. Acad. Sci. U.S.A.* **106**, 1313.
- Delaney, R. D., M. D. Urmei, S. Mittal, B. M. Brubaker, J. M. Kindem, P. S. Burns, C. A. Regal, and K. W. Lehnert, 2022, “Superconducting-qubit readout via low-backaction electro-optic transduction,” *Nature (London)* **606**, 489–493.
- de Lépinay, Laure Mercier, Caspar F. Ockeloen-Korppi, Matthew J. Woolley, and Mika A. Sillanpää, 2021, “Quantum mechanics–free subsystem with mechanical oscillators,” *Science* **372**, 625–629.
- de Lépinay, Laure Mercier, Benjamin Pigeau, Benjamin Besga, and Olivier Arcizet, 2018, “Eigenmode orthogonality breaking and anomalous dynamics in multimode nano-optomechanical systems under non-reciprocal coupling,” *Nat. Commun.* **9**, 1401.
- de Lépinay, Laure Mercier, Benjamin Pigeau, Benjamin Besga, Pascal Vincent, Philippe Poncharal, and Olivier Arcizet, 2017, “A universal and ultrasensitive vectorial nanomechanical sensor for imaging 2D force fields,” *Nat. Nanotechnol.* **12**, 156.
- Delić, Uroš, Manuel Reisenbauer, Kahan Dare, David Grass, Vladan Vuletić, Nikolai Kiesel, and Markus Aspelmeyer, 2020, “Cooling of a levitated nanoparticle to the motional quantum ground state,” *Science* **367**, 892.
- Delord, T., P. Huillery, L. Nicolas, and G. Hétet, 2020, “Spin-cooling of the motion of a trapped diamond,” *Nature (London)* **580**, 56–59.
- del Pino, Javier, Jesse J. Slim, and Ewold Verhagen, 2021, “Non-Hermitian chiral phononics through optomechanically-induced squeezing,” *arXiv:2110.14710*.
- De Martino, Alessandro, Reinhold Egger, and Alexander O. Gogolin, 2009, “Phonon-phonon interactions and phonon damping in carbon nanotubes,” *Phys. Rev. B* **79**, 205408.
- Demir, Alper, 2021, “Understanding fundamental trade-offs in nanomechanical resonant sensors,” *J. Appl. Phys.* **129**, 044503.
- Deng, Guang-Wei, *et al.*, 2016, “Strongly coupled nanotube electro-mechanical resonators,” *Nano Lett.* **16**, 5456–5462.
- DiFilippo, Frank, Vasant Natarajan, Kevin R. Boyce, and David E. Pritchard, 1992, “Classical Amplitude Squeezing for Precision Measurements,” *Phys. Rev. Lett.* **68**, 2859–2862.
- Dmitriev, A. P., and M. I. Dyakonov, 1986, “Activated and tunneling transitions between the two forced-oscillation regimes of an anharmonic oscillator,” *Zh. Eksp. Teor. Fiz.* **90**, 1430–1439, [http://www.jetp.ras.ru/cgi-bin/dn/e\\_063\\_04\\_0838.pdf](http://www.jetp.ras.ru/cgi-bin/dn/e_063_04_0838.pdf).
- Dolleman, R. J., P. Belardinelli, S. Hour, H. S. J. van der Zant, F. Alijani, and P. G. Steeneken, 2019, “High-frequency stochastic switching of graphene resonators near room temperature,” *Nano Lett.* **19**, 1282–1288.
- Dolleman, Robin J., Samer Hour, Abhilash Chandrashekar, Farbod Alijani, Herre S. J. van der Zant, and Peter G. Steeneken, 2018, “Opto-thermally excited multimode parametric resonance in graphene membranes,” *Sci. Rep.* **8**, 9366.
- Dolleman, Robin J., Gerard J. Verbiest, Yaroslav M. Blanter, Herre S. J. van der Zant, and Peter G. Steeneken, 2020, “Nonequilibrium thermodynamics of acoustic phonons in suspended graphene,” *Phys. Rev. Res.* **2**, 012058.
- Dominguez-Medina, Sergio, *et al.*, 2018, “Neutral mass spectrometry of virus capsids above 100 megadaltons with nanomechanical resonators,” *Science* **362**, 918–922.
- Dong, X., M. I. Dykman, and H. B. Chan, 2018, “Strong negative nonlinear friction from induced two-phonon processes in vibrational systems,” *Nat. Commun.* **9**, 3241.
- Drummond, P. D., and D. F. Walls, 1980, “Quantum-theory of optical bistability. I. Non-linear polarizability model,” *J. Phys. A* **13**, 725–741.
- Dykman, M. I., 1975, “Theory of nonlinear nonequilibrium oscillators interacting with a medium,” *Zh. Eksp. Teor. Fiz.* **68**, 2082–2094, [http://www.jetp.ras.ru/cgi-bin/dn/e\\_041\\_06\\_1042.pdf](http://www.jetp.ras.ru/cgi-bin/dn/e_041_06_1042.pdf).
- Dykman, M. I., 1978, “Heating and cooling of local and quasilocal vibrations by nonresonance field,” *Sov. Phys. Solid State* **20**, 1306–1311, [http://web.pa.msu.edu/people/dykman/pub06/Sov.Phys.Sol.St\\_78.pdf](http://web.pa.msu.edu/people/dykman/pub06/Sov.Phys.Sol.St_78.pdf).
- Dykman, M. I., 1990, “Large fluctuations and fluctuational transitions in systems driven by colored Gaussian noise: A high-frequency noise,” *Phys. Rev. A* **42**, 2020–2029.
- Dykman, M. I., 2012, “Periodically modulated quantum nonlinear oscillators,” in *Fluctuating Nonlinear Oscillators: From Nanomechanics to Quantum Superconducting Circuits*, edited by M. I. Dykman (Oxford University Press, Oxford), pp. 165–197.
- Dykman, M. I., Christoph Bruder, Niels Lörch, and Yaxing Zhang, 2018, “Interaction-induced time-symmetry breaking in driven quantum oscillators,” *Phys. Rev. B* **98**, 195444.
- Dykman, M. I., M. Khasin, J. Portman, and S. W. Shaw, 2010, “Spectrum of an Oscillator with Jumping Frequency and the Interference of Partial Susceptibilities,” *Phys. Rev. Lett.* **105**, 230601.
- Dykman, M. I., and M. A. Krivogla, 1971, “Classical theory of nonlinear oscillators interacting with a medium,” *Phys. Status Solidi B* **48**, 497–512.
- Dykman, M. I., and M. A. Krivogla, 1973, “Quantum theory of nonlinear oscillators interacting with the medium,” *Sov. Phys. JETP* **37**, 506–511, [http://jetp.ras.ru/cgi-bin/dn/e\\_037\\_03\\_0506.pdf](http://jetp.ras.ru/cgi-bin/dn/e_037_03_0506.pdf).
- Dykman, M. I., and M. A. Krivogla, 1975, “Spectral distribution of nonlinear oscillators with nonlinear friction due to a medium,” *Phys. Status Solidi B* **68**, 111–123.
- Dykman, M. I., and M. A. Krivogla, 1979, “Theory of fluctuational transitions between the stable states of a nonlinear oscillator,” *Sov. Phys. JETP* **77**, 30–37, [http://www.jetp.ras.ru/cgi-bin/dn/e\\_050\\_01\\_0030.pdf](http://www.jetp.ras.ru/cgi-bin/dn/e_050_01_0030.pdf).
- Dykman, M. I., and M. A. Krivogla, 1980, “Fluctuations in nonlinear systems near bifurcations corresponding to the appearance of new stable states,” *Physica (Amsterdam)* **104A**, 480–494.
- Dykman, M. I., and M. A. Krivogla, 1984, “Theory of nonlinear oscillators interacting with a medium,” in *Soviet Physics Reviews*, Vol. 5, edited by I. M. Khalatnikov (Harwood Academic,

- New York), pp. 265–441, <http://web.pa.msu.edu/people/dykman/pub06/DKreview84.pdf>.
- Dykman, M. I., and M. A. Krivoglaz, 1987, “Profiles of no-phonon lines of impurity centers interacting with local or quasilocal vibrations,” *Sov. Phys. Solid State* **29**, 210–214, <https://www.mathnet.ru/links/5bf9632913d5dd245c2f85f7c3c0a240/ft900.pdf>.
- Dykman, M. I., D. G. Luchinsky, R. Mannella, P. V. E. McClintock, N. D. Stein, and N. G. Stocks, 1994, “Supernarrow spectral peaks and high-frequency stochastic resonance in systems with coexisting periodic attractors,” *Phys. Rev. E* **49**, 1198–1215.
- Dykman, M. I., C. M. Maloney, V. N. Smelyanskiy, and M. Silverstein, 1998, “Fluctuational phase-flip transitions in parametrically driven oscillators,” *Phys. Rev. E* **57**, 5202–5212.
- Dykman, M. I., R. Mannella, P. V. E. McClintock, S. M. Soskin, and N. G. Stocks, 1990, “Noise-induced narrowing of peaks in the power spectra of underdamped nonlinear oscillators,” *Phys. Rev. A* **42**, 7041–7049.
- Dykman, M. I., M. Marthaler, and V. Peano, 2011, “Quantum heating of a parametrically modulated oscillator: Spectral signatures,” *Phys. Rev. A* **83**, 052115.
- Dykman, M. I., P. V. E. McClintock, V. N. Smelyanskiy, N. D. Stein, and N. G. Stocks, 1992, “Optimal Paths and the Prehistory Problem for Large Fluctuations in Noise-Driven Systems,” *Phys. Rev. Lett.* **68**, 2718–2721.
- Dykman, M. I., M. M. Millonas, and V. N. Smelyanskiy, 1994, “Observable and hidden singular features of large fluctuations in nonequilibrium systems,” *Phys. Lett. A* **195**, 53–58.
- Dykman, M. I., Gianluca Rastelli, M. L. Roukes, and Eva M. Weig, 2019, “Resonantly Induced Friction and Frequency Combs in Driven Nanomechanical Systems,” *Phys. Rev. Lett.* **122**, 254301.
- Eichenfield, M., J. Chan, R. M. Camacho, K. J. Vahala, and O. Painter, 2009, “Optomechanical crystals,” *Nature (London)* **462**, 78–82.
- Eichler, A., J. Chaste, J. Moser, and A. Bachtold, 2011, “Parametric amplification and self-oscillation in a nanotube mechanical resonator,” *Nano Lett.* **11**, 2699.
- Eichler, A., M. del Álamo Ruiz, J. A. Plaza, and A. Bachtold, 2012, “Strong Coupling between Mechanical Modes in a Nanotube Resonator,” *Phys. Rev. Lett.* **109**, 025503.
- Eichler, A., J. Moser, J. Chaste, M. Zdrojek, I. Wilson-Rae, and A. Bachtold, 2011, “Nonlinear damping in mechanical resonators made from carbon nanotubes and graphene,” *Nat. Nanotechnol.* **6**, 339–342.
- Eichler, A., J. Moser, M. I. Dykman, and A. Bachtold, 2013, “Symmetry breaking in a mechanical resonator made from a carbon nanotube,” *Nat. Commun.* **4**, 2843.
- Einstein, A., and L. Hopf, 1910, “Statistical investigation of a resonator’s motion in a radiation field,” *Ann. Phys. (Berlin)* **338**, 1105–1115.
- Ekinci, K. L., and M. L. Roukes, 2005, “Nanoelectromechanical systems,” *Rev. Sci. Instrum.* **76**, 061101.
- Ekinci, K. L., Y. T. Yang, and M. L. Roukes, 2004, “Ultimate limits to inertial mass sensing based upon nanoelectromechanical systems,” *J. Appl. Phys.* **95**, 2682–2689.
- Enss, C., and S. Hunklinger, 2005, *Low-Temperature Physics* (Springer-Verlag, Berlin).
- Erbe, A., C. Weiss, W. Zwerger, and R. H. Blick, 2001, “Nanomechanical Resonator Shuttling Single Electrons at Radio Frequencies,” *Phys. Rev. Lett.* **87**, 096106.
- Fainstein, A., N. D. Lanzillotti-Kimura, B. Jusserand, and B. Perrin, 2013, “Strong Optical-Mechanical Coupling in a Vertical GaAs/AlAs Microcavity for Subterahertz Phonons and Near-Infrared Light,” *Phys. Rev. Lett.* **110**, 037403.
- Faust, T., P. Krenn, S. Manus, J. P. Kotthaus, and E. M. Weig, 2012, “Microwave cavity-enhanced transduction for plug and play nanomechanics at room temperature,” *Nat. Commun.* **3**, 728.
- Faust, T., J. Rieger, M. J. Seitner, J. P. Kotthaus, and E. M. Weig, 2013, “Coherent control of a classical nanomechanical two-level system,” *Nat. Phys.* **9**, 485–488.
- Faust, T., J. Rieger, M. J. Seitner, P. Krenn, J. P. Kotthaus, and E. M. Weig, 2012, “Nonadiabatic Dynamics of Two Strongly Coupled Nanomechanical Resonator Modes,” *Phys. Rev. Lett.* **109**, 037205.
- Faust, Thomas, Johannes Rieger, Maximilian J. Seitner, Jörg P. Kotthaus, and Eva M. Weig, 2014, “Signatures of two-level defects in the temperature-dependent damping of nanomechanical silicon nitride resonators,” *Phys. Rev. B* **89**, 100102.
- Fedorets, D., L. Y. Gorelik, R. I. Shekhter, and M. Jonson, 2004, “Quantum Shuttle Phenomena in a Nanoelectromechanical Single-Electron Transistor,” *Phys. Rev. Lett.* **92**, 166801.
- Feng, Tianli, Bo Qiu, and Xiulin Ruan, 2015, “Coupling between phonon-phonon and phonon-impurity scattering: A critical revisit of the spectral Matthiessen’s rule,” *Phys. Rev. B* **92**, 235206.
- Feng, X. L., Rongrui He, Peidong Yang, and M. L. Roukes, 2007, “Very high frequency silicon nanowire electromechanical resonators,” *Nano Lett.* **7**, 1953–1959.
- Feng, X. L., C. J. White, A. Hajimiri, and M. L. Roukes, 2008, “A self-sustaining ultrahigh-frequency nanoelectromechanical oscillator,” *Nat. Nanotechnol.* **3**, 342–346.
- Fermi, E., 1931, “The Raman effect of carbon dioxide,” *Z. Phys.* **71**, 250–259.
- Feynman, R. P., and F. L. Vernon, Jr., 1963, “The theory of a general quantum system interacting with a linear dissipative system,” *Ann. Phys. (Amsterdam)* **24**, 118.
- Fogliano, Francesco, Benjamin Besga, Antoine Reigie, Laure Mercier de Lépinay, Philip Heringlake, Clement Gouriou, Eric Eyraud, Wolfgang Wernsdorfer, Benjamin Pigeau, and Olivier Arcizet, 2021, “Ultrasensitive nano-optomechanical force sensor operated at dilution temperatures,” *Nat. Commun.* **12**, 4124.
- Fong, King Y., Wolfram H. P. Pernice, and Hong X. Tang, 2012, “Frequency and phase noise of ultrahigh  $Q$  silicon nitride nanomechanical resonators,” *Phys. Rev. B* **85**, 161410(R).
- Ford, G. W., M. Kac, and P. Mazur, 1965, “Statistical mechanics of assemblies of coupled oscillators,” *J. Math. Phys. (N.Y.)* **6**, 504.
- Ford, G. W., J. T. Lewis, and R. F. O’Connell, 1988, “Quantum Langevin equation,” *Phys. Rev. A* **37**, 4419–4428.
- Forstner, S., S. Prams, J. Knittel, E. D. van Ooijen, J. D. Swaim, G. I. Harris, A. Szorkovszky, W. P. Bowen, and H. Rubinsztein-Dunlop, 2012, “Cavity Optomechanical Magnetometer,” *Phys. Rev. Lett.* **108**, 120801.
- Fulton, T. A., and L. N. Dunkelberger, 1974, “Lifetime of the zero-voltage state in Josephson tunnel junctions,” *Phys. Rev. B* **9**, 4760–4768.
- Ganzhorn, Marc, and Wolfgang Wernsdorfer, 2012, “Dynamics and Dissipation Induced by Single-Electron Tunneling in Carbon Nanotube Nanoelectromechanical Systems,” *Phys. Rev. Lett.* **108**, 175502.
- Gao, J., J. Zmuidzinas, B. A. Mazin, H. G. LeDuc, and P. K. Day, 2007, “Noise properties of superconducting coplanar waveguide microwave resonators,” *Appl. Phys. Lett.* **90**, 102507.
- Garanin, D. A., and V. S. Lutovinov, 1992, “Absorption of sound and kinetic coefficients of elastic bodies,” *Ann. Phys. (N.Y.)* **218**, 293–324.



- Garcia-Sanchez, D., A. S. Paulo, M. J. Esplandiu, F. Perez-Murano, L. Forro, A. Aguasca, and A. Bachtold, 2007, “Mechanical Detection of Carbon Nanotube Resonator Vibrations,” *Phys. Rev. Lett.* **99**, 085501.
- Gavartin, E., P. Verlot, and T. J. Kippenberg, 2013, “Stabilization of a linear nanomechanical oscillator to its thermodynamic limit,” *Nat. Commun.* **4**, 2860.
- Ghadimi, A. H., S. A. Fedorov, N. J. Engelsen, M. J. Bereyhi, R. Schilling, D. J. Wilson, and T. J. Kippenberg, 2018, “Elastic strain engineering for ultra-low mechanical dissipation,” *Science* **360**, 764.
- Ghaffari, S., S. A. Chandorkar, S. S. Wang, E. J. Ng, C. H. Ahn, V. Hong, Y. S. Yang, and T. W. Kenny, 2013, “Quantum limit of quality factor in silicon micro and nano mechanical resonators,” *Sci. Rep.* **3**, 3244.
- Ghaffari, S., and T. W. Kenny, 2015, “Damping in resonant MEMS,” in *Resonant MEMS: Fundamentals, Implementation, and Application*, edited by O. Brand, I. Dufour, S. Heinrich, and F. Josse (Wiley, New York), p. 55.
- Gieseler, J., A. Kabcenell, E. Rosenfeld, J. D. Schaefer, A. Safira, M. J. A. Schuetz, C. Gonzalez-Ballester, C. C. Rusconi, O. Romero-Isart, and M. D. Lukin, 2020, “Single-Spin Magnetomechanics with Levitated Micromagnets,” *Phys. Rev. Lett.* **124**, 163604.
- Gieseler, J., L. Novotny, and R. Quidant, 2013, “Thermal nonlinearities in a nanomechanical oscillator,” *Nat. Phys.* **9**, 806.
- Gieseler, Jan, Bradley Deutsch, Romain Quidant, and Lukas Novotny, 2012, “Subkelvin Parametric Feedback Cooling of a Laser-Trapped Nanoparticle,” *Phys. Rev. Lett.* **109**, 103603.
- Gil-Santos, E., C. Baker, D. T. Nguyen, W. Hease, C. Gomez, A. Lemaître, S. Ducci, G. Leo, and I. Favero, 2015, “High-frequency nano-optomechanical disk resonators in liquids,” *Nat. Nanotechnol.* **10**, 810–816.
- Gil-Santos, Eduardo, Daniel Ramos, Javier Martínez, Marta Fernández-Regúlez, Ricardo García, Álvaro San Paulo, Montserrat Calleja, and Javier Tamayo, 2010, “Nanomechanical mass sensing and stiffness spectrometry based on two-dimensional vibrations of resonant nanowires,” *Nat. Nanotechnol.* **5**, 641–645.
- Gil-Santos, Eduardo, Jose J. Ruz, Oscar Malvar, Ivan Favero, Aristide Lemaître, Priscila M. Kosaka, Sergio García-López, Montserrat Calleja, and Javier Tamayo, 2020, “Optomechanical detection of vibration modes of a single bacterium,” *Nat. Nanotechnol.* **15**, 469–474.
- Gisler, Thomas, Mohamed Helal, Deividas Sabonis, Urs Grob, Martin Héritier, Christian L. Degen, Amir H. Ghadimi, and Alexander Eichler, 2021, “Soft-clamped silicon nitride string resonators at millikelvin temperatures,” [arXiv:2112.03730](https://arxiv.org/abs/2112.03730).
- Gloppe, A., P. Verlot, E. Dupont-Ferrier, A. Siria, P. Poncharal, G. Bachelier, P. Vincent, and O. Arcizet, 2014, “Bidimensional nano-optomechanics and topological backaction in a non-conservative radiation force field,” *Nat. Nanotechnol.* **9**, 920–926.
- Gokhale, V. J., and J. J. Gorman, 2017, “Approaching the intrinsic quality factor limit for micromechanical bulk acoustic resonators using phononic crystal tethers,” *Appl. Phys. Lett.* **111**, 013501.
- Golding, Brage, J. E. Graebner, B. I. Halperin, and R. J. Schutz, 1973, “Nonlinear Phonon Propagation in Fused Silica below 1 K,” *Phys. Rev. Lett.* **30**, 223–226.
- Gong, Tao, Matthew R. Corrado, Ahmed R. Mahbub, Calum Shelden, and Jeremy N. Munday, 2021, “Recent progress in engineering the Casimir effect—Applications to nanophotonics, nanomechanics, and chemistry,” *Nanophotonics* **10**, 523–536.
- González, Gabriela I., and Peter R. Saulson, 1994, “Brownian motion of a mass suspended by an anelastic wire,” *J. Acoust. Soc. Am.* **96**, 207–212.
- Gonzalez-Ballester, C., M. Aspelmeyer, L. Novotny, R. Quidant, and O. Romero-Isart, 2021, “Levitodynamics: Levitation and control of microscopic objects in vacuum,” *Science* **374**, eabg3027.
- Gorelik, L. Y., A. Isacsson, M. V. Voinova, B. Kasemo, R. I. Shekhter, and M. Jonson, 1998, “Shuttle Mechanism for Charge Transfer in Coulomb Blockade Nanostructures,” *Phys. Rev. Lett.* **80**, 4526–4529.
- Goto, H., Z. Lin, and Y. Nakamura, 2018, “Boltzmann sampling from the Ising model using quantum heating of coupled nonlinear oscillators,” *Sci. Rep.* **8**, 7154.
- Goto, Hayato, 2016, “Universal quantum computation with a nonlinear oscillator network,” *Phys. Rev. A* **93**, 050301.
- Goto, Hayato, 2019, “Quantum computation based on quantum adiabatic bifurcations of Kerr-nonlinear parametric oscillators,” *J. Phys. Soc. Jpn.* **88**, 061015.
- Götz, K. J., D. R. Schmid, F. J. Schupp, P. L. Stiller, Ch. Strunk, and A. K. Hüttel, 2018, “Nanomechanical Characterization of the Kondo Charge Dynamics in a Carbon Nanotube,” *Phys. Rev. Lett.* **120**, 246802.
- Gouttenoire, V., T. Barois, S. Perisanu, J. L. Leclercq, S. T. Purcell, P. Vincent, and A. Ayari, 2010, “Digital and FM demodulation of a doubly clamped single-walled carbon-nanotube oscillator: Towards a nanotube cell phone,” *Small* **6**, 1060–1065.
- Grabert, H., P. Schramm, and G.-L. Ingold, 1988, “Quantum Brownian motion: The functional integral approach,” *Phys. Rep.* **168**, 115–207.
- Graham, R., and T. Tél, 1987, “Nonequilibrium potentials for local codimension-2 bifurcations of dissipative flows,” *Phys. Rev. A* **35**, 1328–1349.
- Greywall, D. S., B. Yurke, P. A. Busch, A. N. Pargellis, and R. L. Willett, 1994, “Evading Amplifier Noise in Nonlinear Oscillators,” *Phys. Rev. Lett.* **72**, 2992–2995.
- Grob, U., M. D. Krass, M. Héritier, R. Pachlatko, J. Rhensius, J. Košata, B. A. Moores, H. Takahashi, A. Eichler, and C. L. Degen, 2019, “Magnetic resonance force microscopy with a one-dimensional resolution of 0.9 nanometers,” *Nano Lett.* **19**, 7935–7940.
- Gruber, G., C. Urgell, A. Tavemarakis, A. Stavrinadis, S. Tepsic, C. Magén, S. Sangiao, J. M. de Teresa, P. Verlot, and A. Bachtold, 2019, “Mass sensing for the advanced fabrication of nanomechanical resonators,” *Nano Lett.* **19**, 6987–6992.
- Guckenheimer, J., and P. Holmes, 1997, *Nonlinear Oscillators, Dynamical Systems and Bifurcations of Vector Fields* (Springer-Verlag, New York).
- Guénault, A. M., *et al.*, 2019, “Probing superfluid  $^4\text{He}$  with high-frequency nanomechanical resonators down to millikelvin temperatures,” *Phys. Rev. B* **100**, 020506.
- Guénault, A. M., *et al.*, 2020, “Detecting a phonon flux in superfluid  $^4\text{He}$  by a nanomechanical resonator,” *Phys. Rev. B* **101**, 060503.
- Guo, Lingzhen, M. Marthaler, and G. Schön, 2013, “Phase Space Crystals: A New Way to Create a Quasienergy Band Structure,” *Phys. Rev. Lett.* **111**, 205303.
- Gurevich, L. E., and B. I. Shklovskii, 1968, “Absorption of ultrasound in dielectric crystals with high impurity concentrations,” *Sov. Phys. JETP* **26**, 989, [http://www.jetp.ras.ru/cgi-bin/dn/e\\_026\\_05\\_0989.pdf](http://www.jetp.ras.ru/cgi-bin/dn/e_026_05_0989.pdf).
- Gurevich, V. L., 1988, *Transport in Phonon Systems* (Elsevier Science, Amsterdam).
- Gustafsson, Martin V., Thomas Aref, Anton Frisk Kockum, Maria K. Ekström, Göran Johansson, and Per Delsing, 2014, “Propagating phonons coupled to an artificial atom,” *Science* **346**, 207–211.

- Guthrie, A., S. Kafanov, M. T. Noble, Yu. A. Pashkin, G. R. Pickett, V. Tsepelin, A. A. Dorofeev, V. A. Krupenin, and D. E. Presnov, 2021, “Nanoscale real-time detection of quantum vortices at millikelvin temperatures,” *Nat. Commun.* **12**, 2645.
- Güttinger, J., A. Noury, P. Weber, A. M. Eriksson, C. Lagoon, J. Moser, C. Eichler, A. Wallraff, A. Isacsson, and A. Bachtold, 2017, “Energy-dependent path of dissipation in nanomechanical resonators,” *Nat. Nanotechnol.* **12**, 631.
- Hajjaj, A. Z., F. K. Alfossail, and M. I. Younis, 2018, “Two-to-one internal resonance of MEMS arch resonators,” *Int. J. Non-Linear Mech.* **107**, 64–72.
- Hamoumi, M., P. E. Allain, W. Hease, L. Morgenroth, B. Gérard, A. Lemaître, G. Leo, and I. Favero, 2018, “Microscopic Nanomechanical Dissipation in Gallium Arsenide Resonators,” *Phys. Rev. Lett.* **120**, 223601.
- Hanay, M. S., S. Kelber, A. K. Naik, D. Chi, S. Hentz, E. C. Bullard, E. Colinet, L. Duraffourg, and M. L. Roukes, 2012, “Single-protein nanomechanical mass spectrometry in real time,” *Nat. Nanotechnol.* **7**, 602–608.
- Hanay, M. Selim, Scott I. Kelber, Cathal D. O’Connell, Paul Mulvaney, John E. Sader, and Michael L. Roukes, 2015, “Inertial imaging with nanomechanical systems,” *Nat. Nanotechnol.* **10**, 339–344.
- Hann, Connor T., Chang-Ling Zou, Yaxing Zhang, Yiwen Chu, Robert J. Schoelkopf, S. M. Girvin, and Liang Jiang, 2019, “Hardware-Efficient Quantum Random Access Memory with Hybrid Quantum Acoustic Systems,” *Phys. Rev. Lett.* **123**, 250501.
- Hatanaka, D., A. Bachtold, and H. Yamaguchi, 2019, “Electrostatically Induced Phononic Crystal,” *Phys. Rev. Appl.* **11**, 024024.
- Hauer, B. D., C. Doolin, K. S. D. Beach, and J. P. Davis, 2013, “A general procedure for thermomechanical calibration of nano/micro-mechanical resonators,” *Ann. Phys. (N.Y.)* **339**, 181–207.
- Hauer, B. D., P. H. Kim, C. Doolin, F. Souris, and J. Davis, 2018, “Two-level system damping in a single-crystal silicon optomechanical resonator,” *Phys. Rev. B* **98**, 214303.
- He, Rongrui, X. L. Feng, M. L. Roukes, and Peidong Yang, 2008, “Self-transducing silicon nanowire electromechanical systems at room temperature,” *Nano Lett.* **8**, 1756–1761.
- Heisenberg, W., 1927, “Über den anschaulichen inhalt der quantentheoretischen kinematik und mechanik,” *Z. Phys.* **43**, 172–198.
- Henry, Tania, Kyungkun Kim, Zaiyuan Ren, Christopher Yerino, Jung Han, and Hong X. Tang, 2007, “Directed growth of horizontally aligned gallium nitride nanowires for nanoelectromechanical resonator arrays,” *Nano Lett.* **7**, 3315–3319.
- Heritier, M., A. Eichler, Y. Pan, U. Grob, I. Shorubalko, M. D. Krass, Y. Tao, and C. L. Degen, 2018, “Nanoladder cantilevers made from diamond and silicon,” *Nano Lett.* **18**, 1814–1818.
- Herring, Conyers, 1954, “Role of low-energy phonons in thermal conduction,” *Phys. Rev.* **95**, 954–965.
- Heugel, Toni L., Matthias Oscity, Alexander Eichler, Oded Zilberberg, and R. Chitra, 2019, “Classical Many-Body Time Crystals,” *Phys. Rev. Lett.* **123**, 124301.
- Hoehne, F., Y. A. Pashkin, O. Astafiev, L. Faoro, L. B. Ioffe, Y. Nakamura, and J. S. Tsai, 2010, “Damping in high-frequency metallic nanomechanical resonators,” *Phys. Rev. B* **81**, 184112.
- Houri, S., D. Hatanaka, M. Asano, R. Ohta, and H. Yamaguchi, 2019, “Limit cycles and bifurcations in a nonlinear MEMS resonator with a 1:3 internal resonance,” *Appl. Phys. Lett.* **114**, 103103.
- Houri, S., D. Hatanaka, M. Asano, and H. Yamaguchi, 2020, “Demonstration of Multiple Internal Resonances in a Microelectromechanical Self-Sustained Oscillator,” *Phys. Rev. Appl.* **13**, 014049.
- Houri, Samer, Motoki Asano, Hajime Okamoto, and Hiroshi Yamaguchi, 2021, “Self-Sustained Libration Regime in Nonlinear Microelectromechanical Devices,” *Phys. Rev. Appl.* **16**, 064015.
- Houri, Samer, Motoki Asano, Hiroshi Yamaguchi, Natsue Yoshimura, Yasuharu Koike, and Ludovico Minati, 2020, “Generic Rotating-Frame-Based Approach to Chaos Generation in Nonlinear Micro- and Nanoelectromechanical System Resonators,” *Phys. Rev. Lett.* **125**, 174301.
- Hsu, Jen-Feng, Peng Ji, Charles W. Lewandowski, and Brian D’Urso, 2016, “Cooling the motion of diamond nanocrystals in a magneto-gravitational trap in high vacuum,” *Sci. Rep.* **6**, 30125.
- Huang, L., S. M. Soskin, I. A. Khovanov, R. Mannella, K. Ninios, and H. B. Chan, 2019, “Frequency stabilization and noise-induced spectral narrowing in resonators with zero dispersion,” *Nat. Commun.* **10**, 3930.
- Huang, X. M. H., C. A. Zorman, M. Mehregany, and M. L. Roukes, 2003, “Nanoelectromechanical systems: Nanodevice motion at microwave frequencies,” *Nature (London)* **421**, 496–496.
- Huber, J. S., G. Rastelli, M. J. Seitner, J. Kölbl, W. Belzig, M. I. Dykman, and E. M. Weig, 2020, “Spectral Evidence of Squeezing of a Weakly Damped Driven Nanomechanical Mode,” *Phys. Rev. X* **10**, 021066.
- Husain, A., J. Hone, H. W. C. Postma, X. M. H. Huang, T. Drake, M. Barbic, A. Scherer, and M. L. Roukes, 2003, “Nanowire-based very-high-frequency electromechanical resonator,” *Appl. Phys. Lett.* **83**, 1240–1242.
- Hüttel, A. K., G. A. Steele, B. Witkamp, M. Poot, L. P. Kouwenhoven, and H. S. J. van der Zant, 2009, “Carbon nanotubes as ultrahigh quality factor mechanical resonators,” *Nano Lett.* **9**, 2547–2552.
- Imboden, Matthias, and Pritiraj Mohanty, 2014, “Dissipation in nanoelectromechanical systems,” *Phys. Rep.* **534**, 89–146.
- Islam, Arnob, Anno van den Akker, and Philip X.-L. Feng, 2018, “Anisotropic thermal conductivity of suspended black phosphorus probed by opto-thermomechanical resonance spectromicroscopy,” *Nano Lett.* **18**, 7683–7691.
- Ivanov, M. A., M. A. Krivoglaz, D. N. Mirlin, and I. I. Reshina, 1966, “Widening of infrared absorption lines by local high-frequency oscillations,” *Sov. Phys. Solid State* **8**, 150.
- Ivanov, M. A., L. B. Kvashnina, and M. A. Krivoglaz, 1965, “Spectral distribution of localized vibrations,” *Sov. Phys. Solid State* **7**, 1652.
- Iyer, Srikanth S., and Robert N. Candler, 2016, “Mode- and Direction-Dependent Mechanical Energy Dissipation in Single-Crystal Resonators due to Anharmonic Phonon-Phonon Scattering,” *Phys. Rev. Appl.* **5**, 034002.
- Jessop, Matthew R., Weibin Li, and Andrew D. Armour, 2020, “Phase synchronization in coupled bistable oscillators,” *Phys. Rev. Res.* **2**, 013233.
- Jiang, Shengwei, Hongchao Xie, Jie Shan, and Kin Fai Mak, 2020, “Exchange magnetostriction in two-dimensional antiferromagnets,” *Nat. Mater.* **19**, 1295–1299.
- Judge, John A., Douglas M. Photiadis, Joseph F. Vignola, Brian H. Houston, and Jacek Jarzynski, 2007, “Attachment loss of micro-mechanical and nanomechanical resonators in the limits of thick and thin support structures,” *J. Appl. Phys.* **101**, 013521.
- Jung, Minkyung, Peter Rickhaus, Simon Zihlmann, Alexander Eichler, Peter Makk, and Christian Schönenberger, 2019, “GHz nanomechanical resonator in an ultraclean suspended graphene *p-n* junction,” *Nanoscale* **11**, 4355–4361.
- Kacem, N., and S. Hentz, 2009, “Bifurcation topology tuning of a mixed behavior in nonlinear micromechanical resonators,” *Appl. Phys. Lett.* **95**, 183104.

- Kagan, Yu., and Ya. A. Ioselevskii, 1962, “The Mössbauer effect for an impurity nucleus in a crystal. I,” *Sov. Phys. JETP* **15**, 182, [http://jetp.ras.ru/cgi-bin/dn/e\\_015\\_01\\_0182.pdf](http://jetp.ras.ru/cgi-bin/dn/e_015_01_0182.pdf).
- Kalaei, M., M. Mirhosseini, P. B. Dieterle, M. Peruzzo, J. M. Fink, and O. Painter, 2019, “Quantum electromechanics of a hypersonic crystal,” *Nat. Nanotechnol.* **14**, 334–339.
- Kamenev, A., 2011, *Field Theory of Non-Equilibrium Systems* (Cambridge University Press, Cambridge, England).
- Kamppinen, T., J. T. Mäkinen, and V. B. Eltsov, 2022, “Dimensional control of tunneling two-level systems in nanoelectromechanical resonators,” *Phys. Rev. B* **105**, 035409.
- Karabalin, R. B., M. C. Cross, and M. L. Roukes, 2009, “Nonlinear dynamics and chaos in two coupled nanomechanical resonators,” *Phys. Rev. B* **79**, 165309.
- Karabalin, R. B., R. Lifshitz, M. C. Cross, M. H. Matheny, S. C. Masmanidis, and M. L. Roukes, 2011, “Signal Amplification by Sensitive Control of Bifurcation Topology,” *Phys. Rev. Lett.* **106**, 094102.
- Karabalin, R. B., S. C. Masmanidis, and M. L. Roukes, 2010, “Efficient parametric amplification in high and very high frequency piezoelectric nanoelectromechanical systems,” *Appl. Phys. Lett.* **97**, 183101.
- Karabalin, R. B., M. H. Matheny, X. L. Feng, E. Defay, G. Le Rhun, C. Marcoux, S. Hentz, P. Andreucci, and M. L. Roukes, 2009, “Piezoelectric nanoelectromechanical resonators based on aluminum nitride thin films,” *Appl. Phys. Lett.* **95**, 103111.
- Kenig, Eyal, M. C. Cross, Jeff Moehlis, and Kurt Wiesenfeld, 2013, “Phase noise of oscillators with unsaturated amplifiers,” *Phys. Rev. E* **88**, 062922.
- Kenig, Eyal, M. C. Cross, L. G. Villanueva, R. B. Karabalin, M. H. Matheny, Ron Lifshitz, and M. L. Roukes, 2012, “Optimal operating points of oscillators using nonlinear resonators,” *Phys. Rev. E* **86**, 056207.
- Keşkekler, Ata, Oriel Shoshani, Herre S. J. van der Zant, Peter G. Steeneken, and Farbod Alijani, 2021, “Tuning nonlinear damping in graphene nanoresonators by parametric-direct internal resonance,” *Nat. Commun.* **12**, 1099.
- Khivrich, Ilya, Aashish A. Clerk, and Shahal Ilani, 2019, “Nanomechanical pump-probe measurements of insulating electronic states in a carbon nanotube,” *Nat. Nanotechnol.* **14**, 161–167.
- Kim, Bongsang, Rob N. Candler, Matthew A. Hopcroft, Manu Agarwal, Woo-Tae Park, and Thomas W. Kenny, 2007, “Frequency stability of wafer-scale film encapsulated silicon based MEMS resonators,” *Sens. Actuators A* **136**, 125–131.
- Kim, K., M. S. Heo, K. H. Lee, H. J. Ha, K. Jang, H. R. Noh, and W. Jhe, 2005, “Noise-induced transition of atoms between dynamic phase-space attractors in a parametrically excited atomic trap,” *Phys. Rev. A* **72**, 053402.
- Kim, Minjin, Jihwan Kim, Yaseen Hou, Dong Yu, Yong-Joo Doh, Bongsoo Kim, Kun Woo Kim, and Junho Suh, 2019, “Nanomechanical characterization of quantum interference in a topological insulator nanowire,” *Nat. Commun.* **10**, 4522.
- Kim, P. H., B. D. Hauer, C. Doolin, F. Souris, and J. P. Davis, 2016, “Approaching the standard quantum limit of mechanical torque sensing,” *Nat. Commun.* **7**, 13165.
- Kim, SunPhil, Jaehyung Yu, and Arend M. van der Zande, 2018, “Nano-electromechanical drumhead resonators from two-dimensional material bimorphs,” *Nano Lett.* **18**, 6686–6695.
- Kippenberg, T. J., and K. J. Vahala, 2008, “Cavity optomechanics: Back-action at the mesoscale,” *Science* **321**, 1172–1176.
- Kirchhof, Jan N., Kristina Weinle, Sebastian Heeg, Victor Deinhardt, Sviatoslav Kovalchuk, Katja Höflich, and Kirill I. Bolotin, 2021, “Tunable graphene phononic crystal,” *Nano Lett.* **21**, 2174–2182.
- Kiselev, A. A., and G. J. Iafrate, 2008, “Phonon dynamics and phonon assisted losses in Euler-Bernoulli nanobeams,” *Phys. Rev. B* **77**, 205436.
- Klaers, Jan, 2019, “Landauer’s Erasure Principle in a Squeezed Thermal Memory,” *Phys. Rev. Lett.* **122**, 040602.
- Kleybolte, L., P. Gewecke, A. Sawadsky, M. Korobko, and R. Schnabel, 2020, “Squeezed-Light Interferometry on a Cryogenically Cooled Micromechanical Membrane,” *Phys. Rev. Lett.* **125**, 213601.
- Klimchitskaya, G. L., U. Mohideen, and V. M. Mostepanenko, 2009, “The Casimir force between real materials: Experiment and theory,” *Rev. Mod. Phys.* **81**, 1827–1885.
- Knobel, Robert G., and Andrew N. Cleland, 2003, “Nanometre-scale displacement sensing using a single electron transistor,” *Nature (London)* **424**, 291.
- Knobloch, E., and K. A. Wiesenfeld, 1983, “Bifurcations in fluctuating systems: The center-manifold approach,” *J. Stat. Phys.* **33**, 611–637.
- Koch, Jens, Terri M. Yu, Jay Gambetta, A. A. Houck, D. I. Schuster, J. Majer, Alexandre Blais, M. H. Devoret, S. M. Girvin, and R. J. Schoelkopf, 2007, “Charge-insensitive qubit design derived from the Cooper pair box,” *Phys. Rev. A* **76**, 042319.
- Koenig, D. R., and E. M. Weig, 2012, “Voltage-sustained self-oscillation of a nano-mechanical electron shuttle,” *Appl. Phys. Lett.* **101**, 213111.
- Kogan, Oleg, 2008, “Scaling crossovers in activated escape of nonequilibrium systems: A resonantly driven oscillator,” *arXiv*: 0805.0972.
- Kotler, Shlomi, *et al.*, 2021, “Direct observation of deterministic macroscopic entanglement,” *Science* **372**, 622–625.
- Kozinsky, I., H. W. Ch. Postma, O. Kogan, A. Husain, and M. L. Roukes, 2007, “Basins of Attraction of a Nonlinear Nanomechanical Resonator,” *Phys. Rev. Lett.* **99**, 207201.
- Kozinsky, I., H. W. Ch. Postma, I. Bargatin, and M. L. Roukes, 2006, “Tuning nonlinearity, dynamic range, and frequency of nanomechanical resonators,” *Appl. Phys. Lett.* **88**, 253101.
- Kramers, H., 1940, “Brownian motion in a field of force and the diffusion model of chemical reactions,” *Physica (Utrecht)* **7**, 284–304.
- Krivoglaz, M. A., 1961, “Theory of inelastic scattering of neutrons by imperfect crystals,” *Sov. Phys. JETP* **13**, 397–409, [http://jetp.ras.ru/cgi-bin/dn/e\\_013\\_02\\_0397.pdf](http://jetp.ras.ru/cgi-bin/dn/e_013_02_0397.pdf).
- Krivoglaz, M. A., 1964, “Effect of anharmonicity on the intensity of the Mössbauer line,” *Sov. Phys. JETP* **19**, 432, [http://jetp.ras.ru/cgi-bin/dn/e\\_019\\_02\\_0432.pdf](http://jetp.ras.ru/cgi-bin/dn/e_019_02_0432.pdf).
- Krivoglaz, M. A., 1965, “Theory of broadening of spectral lines and nonradiative transitions in systems with weak coupling,” *Sov. Phys. JETP* **21**, 204, [http://jetp.ras.ru/cgi-bin/dn/e\\_021\\_01\\_0204.pdf](http://jetp.ras.ru/cgi-bin/dn/e_021_01_0204.pdf).
- Kryloff, N., and N. Bogoliubov, 1947, *Introduction to Non-Linear Mechanics* (Princeton University Press, Princeton, NJ).
- Kubo, R., 1954, “Note on the stochastic theory of resonance absorption,” *J. Phys. Soc. Jpn.* **9**, 935–944.
- Kunal, K., and N. R. Aluru, 2014, “Intrinsic dissipation in a nanomechanical resonator,” *J. Appl. Phys.* **116**, 094304.
- Kurkijärvi, J., 1972, “Intrinsic fluctuations in a superconducting ring closed with a Josephson junction,” *Phys. Rev. B* **6**, 832–835.
- Kurosu, M., D. Hatanaka, K. Onomitsu, and H. Yamaguchi, 2018, “On-chip temporal focusing of elastic waves in a phononic crystal waveguide,” *Nat. Commun.* **9**, 1331.
- LaHaye, M. D., O. Buu, B. Camarota, and K. C. Schwab, 2004, “Approaching the quantum limit of a nanomechanical resonator,” *Science* **304**, 74.



- LaHaye, M. D., J. Suh, P. M. Echternach, K. C. Schwab, and M. L. Roukes, 2009, "Nanomechanical measurements of a superconducting qubit," *Nature (London)* **459**, 960–964.
- Laird, Edward A., Fei Pei, Wei Tang, Gary A. Steele, and Leo P. Kouwenhoven, 2012, "A high quality factor carbon nanotube mechanical resonator at 39 GHz," *Nano Lett.* **12**, 193–197.
- Landau, L. D., and I. M. Khalatnikov, 1949a, "Theory of viscosity of helium II. I. Collisions of elementary excitations in helium II," *Zh. Eksp. Teor. Fiz.* **19**, 637, [10.1016/B978-0-08-010586-4.50074-2](#).
- Landau, L. D., and I. M. Khalatnikov, 1949b, "Theory of viscosity of helium II. II. Calculation of the viscosity coefficient," *Zh. Eksp. Teor. Fiz.* **19**, 709, [10.1016/B978-0-08-010586-4.50075-4](#).
- Landau, L. D., and E. M. Lifshitz, 1980, *Statistical Physics: Part 1*, 3rd ed. (Pergamon Press, New York).
- Landau, L. D., and E. M. Lifshitz, 1986, *Theory of Elasticity*, 3rd ed. (Butterworth-Heinemann, Oxford).
- Landau, L. D., and E. M. Lifshitz, 2004, *Mechanics*, 3rd ed. (Elsevier, Amsterdam).
- Landau, L. D., and G. Rumer, 1937, "On the absorption of sound in solids," *Phys. Z. Sowjetunion* **11**, 18, [10.1016/B978-0-08-010586-4.50033-X](#).
- Lapidus, L. J., D. Enzer, and G. Gabrielse, 1999, "Stochastic Phase Switching of a Parametrically Driven Electron in a Penning Trap," *Phys. Rev. Lett.* **83**, 899–902.
- Larsen, Tom, Silvan Schmid, Luis G. Villanueva, and Anja Boisen, 2013, "Photothermal analysis of individual nanoparticulate samples using micromechanical resonators," *ACS Nano* **7**, 6188–6193.
- Lassagne, B., Y. Tarakanov, J. Kinaret, D. Garcia-Sanchez, and A. Bachtold, 2009, "Coupling mechanics to charge transport in carbon nanotube mechanical resonators," *Science* **325**, 1107–1110.
- Lax, M., 1967, "Classical noise. V. Noise in self-sustained oscillators," *Phys. Rev.* **160**, 290.
- Lax, M., and H. Yuen, 1968, "Quantum noise. XIII. Six-classical-variable description of quantum laser fluctuations," *Phys. Rev.* **172**, 362.
- Lecocq, F., J. B. Clark, R. W. Simmonds, J. Aumentado, and J. D. Teufel, 2015, "Quantum Nondemolition Measurement of a Nonclassical State of a Massive Object," *Phys. Rev. X* **5**, 041037.
- Lee, Donghun, Kenneth W. Lee, Jeffrey V. Cady, Preeti Ovarthaiyapong, and Ania C. Bleszynski Jayich, 2017, "Topical review: Spins and mechanics in diamond," *J. Opt.* **19**, 033001.
- Lee, Jaesung, Zenghui Wang, Keliang He, Jie Shan, and Philip X.-L. Feng, 2013, "High frequency MoS<sub>2</sub> nanomechanical resonators," *ACS Nano* **7**, 6086–6091.
- Lee, Martin, Makars Šiškins, Samuel Mañas-Valero, Eugenio Coronado, Peter G. Steeneken, and Herre S.J. van der Zant, 2021, "Study of charge density waves in suspended 2H-TaS<sub>2</sub> and 2H-TaSe<sub>2</sub> by nanomechanical resonance," *Appl. Phys. Lett.* **118**, 193105.
- Lee, Shih-Wei, Stuart Truax, Liu Yu, Cosmin Roman, and Christoffer Hierold, 2013, "Carbon nanotube resonators with capacitive and piezoresistive current modulation readout," *Appl. Phys. Lett.* **103**, 033117.
- Leghtas, Z., *et al.*, 2015, "Confining the state of light to a quantum manifold by engineered two-photon loss," *Science* **347**, 853–857.
- Lescanne, Raphaël, Marius Villiers, Théau Peronnin, Alain Sarlette, Matthieu Delbecq, Benjamin Huard, Takis Kontos, Mazhar Mirrahimi, and Zaki Leghtas, 2020, "Exponential suppression of bit-flips in a qubit encoded in an oscillator," *Nat. Phys.* **16**, 509–513.
- Leuch, A., L. Papariello, O. Zilberberg, C. L. Degen, R. Chitra, and A. Eichler, 2016, "Parametric Symmetry Breaking in a Nonlinear Resonator," *Phys. Rev. Lett.* **117**, 214101.
- Li, M., H. X. Tang, and M. L. Roukes, 2007, "Ultra-sensitive NEMS-based cantilevers for sensing, scanned probe and very high-frequency applications," *Nat. Nanotechnol.* **2**, 114–120.
- Li, Mo, E. B. Myers, H. X. Tang, S. J. Aldridge, H. C. McCaig, J. J. Whiting, R. J. Simonson, N. S. Lewis, and M. L. Roukes, 2010, "Nanoelectromechanical resonator arrays for ultrafast, gas-phase chromatographic chemical analysis," *Nano Lett.* **10**, 3899–3903.
- Li, T. C., S. Kheifets, and M. G. Raizen, 2011, "Millikelvin cooling of an optically trapped microsphere in vacuum," *Nat. Phys.* **7**, 527–530.
- Lifshitz, E. M., and L. P. Pitaevskii, 1981, *Physical Kinetics* (Butterworth-Heinemann, Oxford).
- Lifshitz, I. M., 1942a, "2. Absorption due to the presence of isotopes," *J. Exp. Theor. Phys.* **12**, 137.
- Lifshitz, I. M., 1942b, "3. Crystals containing impurities and low-concentration mixed crystals," *J. Exp. Theor. Phys.* **12**, 156.
- Lifshitz, I. M., 1942c, "Optical behavior of nonideal crystal lattices in the infrared. 1. General theory," *J. Exp. Theor. Phys.* **12**, 117.
- Lifshitz, R., and M. C. Cross, 2003, "Response of parametrically driven nonlinear coupled oscillators with application to micro-mechanical and nanomechanical resonator arrays," *Phys. Rev. B* **67**, 134302.
- Lifshitz, R., and M. C. Cross, 2008, "Nonlinear dynamics of nanomechanical and micromechanical resonators," in *Reviews of Nonlinear Dynamics and Complexity*, edited by H. G. Schuster (Wiley, Weinheim), pp. 1–52.
- Lifshitz, Ron, and M. L. Roukes, 2000, "Thermoelastic damping in micro- and nanomechanical systems," *Phys. Rev. B* **61**, 5600–5609.
- Lin, Shaochun, Liang Zhang, Tian Tian, Chang-Kui Duan, and Jiangfeng Du, 2021, "Dynamic observation of topological soliton states in a programmable nanomechanical lattice," *Nano Lett.* **21**, 1025–1031.
- Lin, Z. R., Y. Nakamura, and M. I. Dykman, 2015, "Critical fluctuations and the rates of interstate switching near the excitation threshold of a quantum parametric oscillator," *Phys. Rev. E* **92**, 022105.
- Lindenfeld, Ze'ev, and Ron Lifshitz, 2013, "Damping of mechanical vibrations by free electrons in metallic nanoresonators," *Phys. Rev. B* **87**, 085448.
- Liu, Chang-Hua, In Soo Kim, and Lincoln J. Lauhon, 2015, "Optical control of mechanical mode-coupling within a MoS<sub>2</sub> resonator in the strong-coupling regime," *Nano Lett.* **15**, 6727–6731.
- Liu, M., Y. Zhang, G. L. Klimchitskaya, V. M. Mostepanenko, and U. Mohideen, 2021, "Demonstration of an Unusual Thermal Effect in the Casimir Force from Graphene," *Phys. Rev. Lett.* **126**, 206802.
- Liu, Yulong, Jay Mummery, and Mika A. Sillanpää, 2021, "Gravitational forces between nonclassical mechanical oscillators," *Phys. Rev. Appl.* **15**, 034004.
- Londoño, J. M., S. A. Neild, and J. E. Cooper, 2015, "Identification of backbone curves of nonlinear systems from resonance decay responses," *J. Sound Vib.* **348**, 224–238.
- Lörch, Niels, Yaxing Zhang, Christoph Bruder, and M. I. Dykman, 2019, "Quantum state preparation for coupled period tripling oscillators," *Phys. Rev. Res.* **1**, 023023.
- Losby, J. E., *et al.*, 2015, "Torque-mixing magnetic resonance spectroscopy," *Science* **350**, 798.
- Louisell, W. H., 1990, *Quantum Statistical Properties of Radiation* (Wiley-VCH, Berlin).
- Luchinsky, D. G., and P. V. E. McClintock, 1997, "Irreversibility of classical fluctuations studied in analogue electrical circuits," *Nature (London)* **389**, 463–466.

- Lulla, K. J., M. Defoort, C. Blanc, O. Bourgeois, and E. Collin, 2013, "Evidence for the Role of Normal-State Electrons in Nanoelectromechanical Damping Mechanisms at Very Low Temperatures," *Phys. Rev. Lett.* **110**, 177206.
- Luo, Gang, Zhuo-Zhi Zhang, Guang-Wei Deng, Hai-Ou Li, Gang Cao, Ming Xiao, Guang-Can Guo, Lin Tian, and Guo-Ping Guo, 2018, "Strong indirect coupling between graphene-based mechanical resonators via a phonon cavity," *Nat. Commun.* **9**, 383.
- Luo, Wenyao, Naikun Gao, and Duo Liu, 2021, "Multimode non-linear coupling induced by internal resonance in a microcantilever resonator," *Nano Lett.* **21**, 1062–1067.
- MacCabe, Gregory S., Hengjiang Ren, Jie Luo, Justin D. Cohen, Hengyun Zhou, Alp Sipahigil, Mohammad Mirhosseini, and Oskar Painter, 2020, "Nano-acoustic resonator with ultralong phonon lifetime," *Science* **370**, 840–843.
- Machlup, S., and L. Onsager, 1953, "Fluctuations and irreversible process. II. Systems with kinetic energy," *Phys. Rev.* **91**, 1512–1515.
- Magrini, Lorenzo, Philipp Rosenzweig, Constanze Bach, Andreas Deutschmann-Olek, Sebastian G. Hofer, Sungkun Hong, Nikolai Kiesel, Andreas Kugi, and Markus Aspelmeyer, 2021, "Real-time optimal quantum control of mechanical motion at room temperature," *Nature (London)* **595**, 373–377.
- Mahboob, I., R. Dupuy, K. Nishiguchi, A. Fujiwara, and H. Yamaguchi, 2016, "Hopf and period-doubling bifurcations in an electromechanical resonator," *Appl. Phys. Lett.* **109**, 073101.
- Mahboob, I., E. Flurin, K. Nishiguchi, A. Fujiwara, and H. Yamaguchi, 2010, "Enhanced force sensitivity and noise squeezing in an electromechanical resonator coupled to a nanotransistor," *Appl. Phys. Lett.* **97**, 253105.
- Mahboob, I., C. Froitier, and H. Yamaguchi, 2010, "A symmetry-breaking electromechanical detector," *Appl. Phys. Lett.* **96**, 213103.
- Mahboob, I., M. Mounaix, K. Nishiguchi, A. Fujiwara, and H. Yamaguchi, 2014, "A multimode electromechanical parametric resonator array," *Sci. Rep.* **4**, 4448.
- Mahboob, I., K. Nishiguchi, A. Fujiwara, and H. Yamaguchi, 2013, "Phonon Lasing in an Electromechanical Resonator," *Phys. Rev. Lett.* **110**, 127202.
- Mahboob, I., K. Nishiguchi, H. Okamoto, and H. Yamaguchi, 2012, "Phonon-cavity electromechanics," *Nat. Phys.* **8**, 387–392.
- Mahboob, I., H. Okamoto, K. Onomitsu, and H. Yamaguchi, 2014, "Two-Mode Thermal-Noise Squeezing in an Electromechanical Resonator," *Phys. Rev. Lett.* **113**, 167203.
- Mahboob, I., H. Okamoto, and H. Yamaguchi, 2016, "An electromechanical Ising Hamiltonian," *Sci. Adv.* **2**, e1600236.
- Mahboob, I., N. Perrissin, K. Nishiguchi, D. Hatanaka, Y. Okazaki, A. Fujiwara, and H. Yamaguchi, 2015, "Dispersive and dissipative coupling in a micromechanical resonator embedded with a nanomechanical resonator," *Nano Lett.* **15**, 2312–2317.
- Mahboob, I., and H. Yamaguchi, 2008a, "Bit storage and bit flip operations in an electromechanical oscillator," *Nat. Nanotechnol.* **3**, 275–279.
- Mahboob, I., and H. Yamaguchi, 2008b, "Piezoelectrically pumped parametric amplification and  $Q$  enhancement in an electromechanical oscillator," *Appl. Phys. Lett.* **92**, 173109.
- Maillet, O., X. Zhou, R. Gazizulin, A. Maldonado Cid, M. Defoort, A. D. Fefferman, O. Bourgeois, and E. Collin, 2017, "Non-linear frequency transduction of nano-mechanical Brownian motion," *Phys. Rev. B* **96**, 165434.
- Maillet, Olivier, Dylan Cattiaux, Xin Zhou, Rasul R. Gazizulin, Olivier Bourgeois, Andrew D. Fefferman, and Eddy Collin, 2020, "Nanomechanical damping via electron-assisted relaxation of two-level systems," [arXiv:2009.03804](https://arxiv.org/abs/2009.03804).
- Maizelis, Z. A., M. L. Roukes, and M. I. Dykman, 2011, "Detecting and characterizing frequency fluctuations of vibrational modes," *Phys. Rev. B* **84**, 144301.
- Malla, Rajesh K., E. G. Mishchenko, and M. E. Raikh, 2017, "Suppression of the Landau-Zener transition probability by weak classical noise," *Phys. Rev. B* **96**, 075419.
- Malvar, O., J. J. Ruz, P. M. Kosaka, C. M. Domínguez, E. Gil-Santos, M. Calleja, and J. Tamayo, 2016, "Mass and stiffness spectrometry of nanoparticles and whole intact bacteria by multimode nanomechanical resonators," *Nat. Commun.* **7**, 13452.
- Mangussi, F., and D. H. Zanette, 2016, "Internal resonance in a vibrating beam: A zoo of nonlinear resonance peaks," *PLoS One* **11**, e0162365.
- Maris, H. J., 1966, "The vibrational spectrum of an isotopically disordered crystal," *Philos. Mag.* **13**, 465–476.
- Maris, H. J., 1968, "Ultrasonic attenuation in dirty dielectric crystals," *Phys. Rev.* **175**, 1077–1081.
- Marthaler, M., and M. I. Dykman, 2006, "Switching via quantum activation: A parametrically modulated oscillator," *Phys. Rev. A* **73**, 042108.
- Masmanidis, Sotiris C., Rasul B. Karabalin, Iwijn De Vlaminck, Gustaaf Borghs, Mark R. Freeman, and Michael L. Roukes, 2007, "Multifunctional nanomechanical systems via tunably coupled piezoelectric actuation," *Science* **317**, 780–783.
- Massel, F., T. T. Heikkilä, J.-M. Pirkkalainen, S. U. Cho, H. Saloniemi, P. J. Hakonen, and M. A. Sillanpää, 2011, "Microwave amplification with nanomechanical resonators," *Nature (London)* **480**, 351.
- Matheny, M. H., L. G. Villanueva, R. B. Karabalin, J. E. Sader, and M. L. Roukes, 2013, "Nonlinear mode-coupling in nanomechanical systems," *Nano Lett.* **13**, 1622–1626.
- Matheny, Matthew H., *et al.*, 2019, "Exotic states in a simple network of nanoelectromechanical oscillators," *Science* **363**, eaav7932.
- Mathew, J. P., R. N. Patel, A. Borah, R. Vijay, and M. M. Deshmukh, 2016, "Dynamical strong coupling and parametric amplification of mechanical modes of graphene drums," *Nat. Nanotechnol.* **11**, 747–751.
- Mathew, John P., Raj Patel, Abhinandan Borah, Carina B. Maliakkal, T. S. Abhilash, and Mandar M. Deshmukh, 2015, "Nanoscale electromechanics to measure thermal conductivity, expansion, and interfacial losses," *Nano Lett.* **15**, 7621–7626.
- Meenehan, S. M., J. D. Cohen, S. Groeblacher, J. T. Hill, A. H. Safavi-Naeini, M. Aspelmeyer, and O. Painter, 2014, "Silicon optomechanical crystal resonator at millikelvin temperatures," *Phys. Rev. A* **90**, 011803.
- Meerwaldt, H. B., G. Labadze, B. H. Schneider, A. Taspinar, Ya. M. Blanter, H. S. J. van der Zant, and G. A. Steele, 2012, "Probing the charge of a quantum dot with a nanomechanical resonator," *Phys. Rev. B* **86**, 115454.
- Meerwaldt, H. B., Gary A. Steele, and Herre S. J. van der Zant, 2012, "Carbon nanotubes: Nonlinear high- $Q$  resonators with strong coupling to single-electron tunneling," in *Fluctuating Nonlinear Oscillators*, edited by M. I. Dykman (Oxford University Press, Oxford), pp. 312–340.
- Miao, T. F., S. Yeom, P. Wang, B. Standley, and M. Bockrath, 2014, "Graphene nanoelectromechanical systems as stochastic-frequency oscillators," *Nano Lett.* **14**, 2982–2987.
- Micchi, G., R. Avriker, and F. Pistolesi, 2015, "Mechanical Signatures of the Current Blockade Instability in Suspended Carbon Nanotubes," *Phys. Rev. Lett.* **115**, 206802.

- Michael, V. Requa, and Kimberly L. Turner, 2007, “Precise frequency estimation in a microelectromechanical parametric resonator,” *Appl. Phys. Lett.* **90**, 173508.
- Millen, J., P. Z. G. Fonseca, T. Mavrogordatos, T. S. Monteiro, and P. F. Barker, 2015, “Cavity Cooling a Single Charged Levitated Nanosphere,” *Phys. Rev. Lett.* **114**, 123602.
- Miller, James M. L., Dongsuk D. Shin, Hyun-Keun Kwon, Steven W. Shaw, and Thomas W. Kenny, 2019, “Phase Control of Self-Excited Parametric Resonators,” *Phys. Rev. Appl.* **12**, 044053.
- Miller, James M. Lehto, Azadeh Ansari, David B. Heinz, Yunhan Chen, Ian B. Flader, Dongsuk D. Shin, L. Guillermo Villanueva, and Thomas W. Kenny, 2018, “Effective quality factor tuning mechanisms in micromechanical resonators,” *Appl. Phys. Rev.* **5**, 041307.
- Miller, Nicholas J., Steven W. Shaw, and M. I. Dykman, 2021, “Suppressing Frequency Fluctuations of Self-Sustained Vibrations in Underdamped Nonlinear Resonators,” *Phys. Rev. Appl.* **15**, 014024.
- Mirhosseini, Mohammad, Alp Sipahigil, Mahmoud Kalaei, and Oskar Painter, 2020, “Superconducting qubit to optical photon transduction,” *Nature (London)* **588**, 599–603.
- Mohammadi, S., A. A. Eftekhar, W. D. Hunt, and A. Adibi, 2009, “High- $Q$  micromechanical resonators in a two-dimensional phononic crystal slab,” *Appl. Phys. Lett.* **94**, 051906.
- Möller, Christoffer B., Rodrigo A. Thomas, Georgios Vasilakis, Emil Zeuthen, Yeghishe Tsaturyan, Mikhail Balabas, Kasper Jensen, Albert Schliesser, Klemens Hammerer, and Eugene S. Polzik, 2017, “Quantum back-action-evading measurement of motion in a negative mass reference frame,” *Nature (London)* **547**, 191–195.
- Montinaro, Michele, Gunter Wöst, Mathieu Munsch, Yannik Fontana, Eleonora Russo-Averchi, Martin Heiss, Anna Fontcuberta i Morral, Richard J. Warburton, and Martino Poggio, 2014, “Quantum dot opto-mechanics in a fully self-assembled nanowire,” *Nano Lett.* **14**, 4454–4460.
- Moore, David C., and Andrew A. Geraci, 2021, “Searching for new physics using optically levitated sensors,” *Quantum Sci. Technol.* **6**, 014008.
- Morell, N., A. Reserbat-Plantey, I. Tsioutsios, K. G. Schadler, F. Dubin, F. H. L. Koppens, and A. Bachtold, 2016, “High quality factor mechanical resonators based on  $\text{WSe}_2$  monolayers,” *Nano Lett.* **16**, 5102–5108.
- Morell, Nicolas, Slaven Tepsic, Antoine Reserbat-Plantey, Andrea Cepellotti, Marco Manca, Itai Epstein, Andreas Isacsson, Xavier Marie, Francesco Mauri, and Adrian Bachtold, 2019, “Optomechanical measurement of thermal transport in two-dimensional  $\text{MoSe}_2$  lattices,” *Nano Lett.* **19**, 3143–3150.
- Moser, J., A. Eichler, J. Guetinger, M. I. Dykman, and A. Bachtold, 2014, “Nanotube mechanical resonators with quality factors of up to 5 million,” *Nat. Nanotechnol.* **9**, 1007–1011.
- Moser, J., J. Güttinger, A. Eichler, M. J. Esplandiú, D. E. Liu, M. I. Dykman, and A. Bachtold, 2013, “Ultrasensitive force detection with a nanotube mechanical resonator,” *Nat. Nanotechnol.* **8**, 493.
- Moskovtsev, Kirill, and M. I. Dykman, 2017, “Strong vibration nonlinearity in semiconductor-based nanomechanical systems,” *Phys. Rev. B* **95**, 085426.
- Mozyrsky, D., I. Martin, and M. B. Hastings, 2004, “Quantum-Limited Sensitivity of Single-Electron-Transistor-Based Displacement Detectors,” *Phys. Rev. Lett.* **92**, 018303.
- Nabholz, U., W. Heinzelmann, J. E. Mehner, and P. Degenfeld-Schonburg, 2018, “Amplitude- and gas pressure-dependent nonlinear damping of high- $Q$  oscillatory MEMS micro mirrors,” *J. Microelectromech. Syst.* **27**, 383–391.
- Naik, A., O. Buu, M. D. LaHaye, A. D. Armour, A. A. Clerk, M. P. Blencowe, and K. C. Schwab, 2006, “Cooling a nanomechanical resonator with quantum back-action,” *Nature (London)* **443**, 193–196.
- Naik, A. K., M. S. Hanay, W. K. Hiebert, X. L. Feng, and M. L. Roukes, 2009, “Towards single-molecule nanomechanical mass spectrometry,” *Nat. Nanotechnol.* **4**, 445–450.
- Natarajan, V., F. DiFilippo, and D. E. Pritchard, 1995, “Classical Squeezing of an Oscillator for Subthermal Noise Operation,” *Phys. Rev. Lett.* **74**, 2855–2858.
- Nayfeh, A. H., and D. T. Mook, 2004, *Nonlinear Oscillations* (Wiley-VCH, Weinheim).
- Ng, Eldwin J., Hyung Kyu Lee, Chae Hyuck Ahn, Renata Melamud, and Thomas W. Kenny, 2013, “Stability of silicon microelectromechanical systems resonant thermometers,” *IEEE Sens. J.* **13**, 987–993.
- Nichol, John M., Eric R. Hemesath, Lincoln J. Lauhon, and Raffi Budakian, 2008, “Displacement detection of silicon nanowires by polarization-enhanced fiber-optic interferometry,” *Appl. Phys. Lett.* **93**, 193110.
- Nichol, John M., Tyler R. Naibert, Eric R. Hemesath, Lincoln J. Lauhon, and Raffi Budakian, 2013, “Nanoscale Fourier-Transform Magnetic Resonance Imaging,” *Phys. Rev. X* **3**, 031016.
- Niguès, A., A. Siria, and P. Verlot, 2015, “Dynamical backaction cooling with free electrons,” *Nat. Commun.* **6**, 8104.
- Ning, Z. Y., T. W. Shi, M. Q. Fu, Y. Guo, X. L. Wei, S. Gao, and Q. Chen, 2014, “Transversally and axially tunable carbon nanotube resonators *in situ* fabricated and studied inside a scanning electron microscope,” *Nano Lett.* **14**, 1221–1227.
- Norte, R. A., J. P. Moura, and S. Gröblacher, 2016, “Mechanical Resonators for Quantum Optomechanics Experiments at Room Temperature,” *Phys. Rev. Lett.* **116**, 147202.
- Noury, Adrien, Jorge Vergara-Cruz, Pascal Morfin, Bernard Plaçais, Maria C. Gordillo, Jordi Boronat, Sébastien Balibar, and Adrian Bachtold, 2019, “Layering Transition in Superfluid Helium Adsorbed on a Carbon Nanotube Mechanical Resonator,” *Phys. Rev. Lett.* **122**, 165301.
- Nowick, S., and B. S. Berry, 1972, *Anelastic Relaxation in Crystal-line Solids* (Academic Press, New York).
- O’Brien, M. C., S. Dunn, J. E. Downes, and J. Twamley, 2019, “Magneto-mechanical trapping of micro-diamonds at low pressures,” *Appl. Phys. Lett.* **114**, 053103.
- Ochs, J. S., D. K. J. Boness, G. Rastelli, M. Seitner, W. Belzig, M. I. Dykman, and E. M. Weig, 2022, “Frequency comb from a single driven nonlinear nanomechanical mode,” *arXiv:2207.04030*.
- Ochs, J. S., G. Rastelli, M. Seitner, M. I. Dykman, and E. M. Weig, 2021a, “Resonant nonlinear response of a nanomechanical system with broken symmetry,” *Phys. Rev. B* **104**, 155434.
- Ochs, J. S., M. Seitner, M. I. Dykman, and E. M. Weig, 2021b, “Amplification and spectral evidence of squeezing in the response of a strongly driven nanoresonator to a probe field,” *Phys. Rev. A* **103**, 013506.
- Ockeloen-Korppi, C. F., E. Damskägg, J.-M. Pirkkalainen, M. Asjad, A. A. Clerk, F. Massel, M. J. Woolley, and M. A. Sillanpää, 2018, “Stabilized entanglement of massive mechanical oscillators,” *Nature (London)* **556**, 478–482.
- Ockeloen-Korppi, C. F., E. Damskägg, J.-M. Pirkkalainen, A. A. Clerk, M. J. Woolley, and M. A. Sillanpää, 2016, “Quantum Backaction Evading Measurement of Collective Mechanical Modes,” *Phys. Rev. Lett.* **117**, 140401.
- O’Connell, A. D., *et al.*, 2010, “Quantum ground state and single-phonon control of a mechanical resonator,” *Nature (London)* **464**, 697–703.



- Ofek, Nissim, *et al.*, 2016, “Extending the lifetime of a quantum bit with error correction in superconducting circuits,” *Nature (London)* **536**, 441–445.
- Okamoto, H., T. Kamada, K. Onomitsu, I. Mahboob, and H. Yamaguchi, 2009, “Optical tuning of coupled micromechanical resonators,” *Appl. Phys. Express* **2**, 062202.
- Okamoto, Hajime, Adrien Gourgout, Chia-Yuan Chang, Koji Onomitsu, Imran Mahboob, Edward Yi Chang, and Hiroshi Yamaguchi, 2013, “Coherent phonon manipulation in coupled mechanical resonators,” *Nat. Phys.* **9**, 480–484.
- Okazaki, Yuma, Imran Mahboob, Koji Onomitsu, Satoshi Sasaki, and Hiroshi Yamaguchi, 2016, “Gate-controlled electromechanical backaction induced by a quantum dot,” *Nat. Commun.* **7**, 11132.
- Olcum, Selim, Nathan Cermak, Steven C. Wasserman, and Scott R. Manalis, 2015, “High-speed multiple-mode mass-sensing resolves dynamic nanoscale mass distributions,” *Nat. Commun.* **6**, 7070.
- Onsager, L., and S. Machlup, 1953, “Fluctuations and irreversible processes,” *Phys. Rev.* **91**, 1505–1512.
- Pairis, S., F. Donatini, M. Hocevar, D. Tumanov, N. Vaish, J. Claudon, J.-P. Poizat, and P. Verlot, 2019, “Shot-Noise-Limited Nanomechanical Detection and Radiation Pressure Backaction from an Electron Beam,” *Phys. Rev. Lett.* **122**, 083603.
- Pandey, M., R. B. Reichenbach, A. T. Zehnder, A. Lal, and H. G. Craighead, 2009, “Reducing anchor loss in MEMS resonators using mesa isolation,” *J. Microelectromech. Syst.* **18**, 836–844.
- Park, Y.-H., and K. C. Park, 2004, “High-fidelity modeling of MEMS resonators. Part I. Anchor loss mechanisms through substrate,” *J. Microelectromech. Syst.* **13**, 238–247.
- Patil, Y. S., S. Chakram, L. Chang, and M. Vengalattore, 2015, “Thermomechanical Two-Mode Squeezing in an Ultrahigh- $Q$  Membrane Resonator,” *Phys. Rev. Lett.* **115**, 017202.
- Peano, V., C. Brendel, M. Schmidt, and F. Marquardt, 2015, “Topological Phases of Sound and Light,” *Phys. Rev. X* **5**, 031011.
- Perisanu, S., T. Barois, A. Ayari, P. Poncharal, M. Choueib, S. T. Purcell, and P. Vincent, 2010, “Beyond the linear and duffing regimes in nanomechanics: Circularly polarized mechanical resonances of nanocantilevers,” *Phys. Rev. B* **81**, 165440.
- Perisanu, S., P. Vincent, A. Ayari, M. Choueib, S. T. Purcell, M. Bechelany, and D. Cornu, 2007, “High  $Q$  factor for mechanical resonances of batch-fabricated sic nanowires,” *Appl. Phys. Lett.* **90**, 043113.
- Pfeifer, H., T. Paraíso, L. Zang, and Oskar Painter, 2016, “Design of tunable GHz-frequency optomechanical crystal resonators,” *Opt. Express* **24**, 11407–11419.
- Phillips, W. A., 1972, “Tunneling states in amorphous solids,” *J. Low Temp. Phys.* **7**, 351–360.
- Photiadis, Douglas, M., and John A. Judge, 2004, “Attachment losses of high  $Q$  oscillators,” *APL Photonics* **85**, 482–484.
- Pirkkalainen, J.-M., S. U. Cho, F. Massel, J. Tuorila, T. T. Heikkilä, P. J. Hakonen, and M. A. Sillanpää, 2015, “Cavity optomechanics mediated by a quantum two-level system,” *Nat. Commun.* **6**, 6981.
- Pirkkalainen, J.-M., E. Damskagg, M. Brandt, F. Massel, and M. A. Sillanpää, 2015, “Squeezing of Quantum Noise of Motion in a Micromechanical Resonator,” *Phys. Rev. Lett.* **115**, 243601.
- Pistoiesi, F., A. N. Cleland, and A. Bachtold, 2021, “Proposal for a Nanomechanical Qubit,” *Phys. Rev. X* **11**, 031027.
- Pistoiesi, F., and S. Labarthe, 2007, “Current blockade in classical single-electron nanomechanical resonator,” *Phys. Rev. B* **76**, 165317.
- Poggio, M., and C. L. Degen, 2010, “Force-detected nuclear magnetic resonance: Recent advances and future challenges,” *Nanotechnology* **21**, 342001.
- Poggio, M., C. L. Degen, C. T. Rettner, H. J. Mamin, and D. Rugar, 2007, “Nuclear magnetic resonance force microscopy with a microwire rf source,” *Appl. Phys. Lett.* **90**, 263111.
- Poggio, M., M. P. Jura, C. L. Degen, M. A. Topinka, H. J. Mamin, D. Goldhaber-Gordon, and D. Rugar, 2008, “An off-board quantum point contact as a sensitive detector of cantilever motion,” *Nat. Phys.* **4**, 635–638.
- Polunin, P. M., Yu. Yang, M. I. Dykman, T. W. Kenny, and S. W. Shaw, 2016, “Characterization of MEMS resonator nonlinearities using the ringdown response,” *J. Microelectromech. Syst.* **25**, 297.
- Poncharal, Philippe, Z. L. Wang, Daniel Ugarte, and Walt A. de Heer, 1999, “Electrostatic deflections and electromechanical resonances of carbon nanotubes,” *Science* **283**, 1513.
- Pontin, A., M. Bonaldi, A. Borrielli, L. Marconi, F. Marino, G. Pandraud, G. A. Prodi, P. M. Sarro, E. Serra, and F. Marin, 2016, “Dynamical Two-Mode Squeezing of Thermal Fluctuations in a Cavity Optomechanical System,” *Phys. Rev. Lett.* **116**, 103601.
- Pontin, A., N. P. Bullier, M. Toroš, and P. F. Barker, 2020, “Ultrathin linewidth levitated nano-oscillator for testing dissipative wave-function collapse,” *Phys. Rev. Res.* **2**, 023349.
- Poot, M., K. Y. Fong, and H. X. Tang, 2014, “Classical non-Gaussian state preparation through squeezing in an optoelectromechanical resonator,” *Phys. Rev. A* **90**, 063809.
- Poot, M., King Yan Fong, and Hong Tang, 2015, “Deep feedback-stabilized parametric squeezing in an opto-electromechanical system,” *New J. Phys.* **17**, 043056.
- Poot, Menno, and Herre S. J. van der Zant, 2012, “Mechanical systems in the quantum regime,” *Phys. Rep.* **511**, 273–335.
- Prasad, Parmeshwar, Nishta Arora, and A. K. Naik, 2019, “Gate tunable cooperativity between vibrational modes,” *Nano Lett.* **19**, 5862–5867.
- Purcell, S. T., P. Vincent, C. Journet, and Vu Thien Binh, 2002, “Tuning of Nanotube Mechanical Resonances by Electric Field Pulling,” *Phys. Rev. Lett.* **89**, 276103.
- Qalandar, K. R., B. S. Strachan, B. Gibson, M. Sharma, A. Ma, S. W. Shaw, and K. L. Turner, 2014, “Frequency division using a micromechanical resonance cascade,” *Appl. Phys. Lett.* **105**, 244103.
- Qu, Kenan, and G. S. Agarwal, 2013, “Fano resonances and their control in optomechanics,” *Phys. Rev. A* **87**, 063813.
- Quintana, C. M., K. D. Petersson, L. W. McFaul, S. J. Srinivasan, A. A. Houck, and J. R. Petta, 2013, “Cavity-Mediated Entanglement Generation via Landau-Zener Interferometry,” *Phys. Rev. Lett.* **110**, 173603.
- Rayleigh, J. W. S., 1945, *The Theory of Sound*, Vol. 1, 2nd ed. (Dover, New York).
- Rechnitz, S., T. Tabachnik, M. Shlafman, S. Shlafman, and Y. E. Yaish, 2021, “Mode coupling, bi-stability, and spectral broadening in buckled nanotube resonators,” *arXiv:2110.01572*.
- Reed, A. P., *et al.*, 2017, “Faithful conversion of propagating quantum information to mechanical motion,” *Nat. Phys.* **13**, 1163.
- Reinhardt, Christoph, Tina Müller, Alexandre Bourassa, and Jack C. Sankey, 2016, “Ultralow-Noise SiN Trampoline Resonators for Sensing and Optomechanics,” *Phys. Rev. X* **6**, 021001.
- Remus, L. G., M. P. Blencowe, and Y. Tanaka, 2009, “Damping and decoherence of a nanomechanical resonator due to a few two-level systems,” *Phys. Rev. B* **80**, 174103.
- Ren, Hengjiang, Tirth Shah, Hannes Pfeifer, Christian Brendel, Vittorio Peano, Florian Marquardt, and Oskar Painter, 2020, “Topological phonon transport in an optomechanical system,” *arXiv:2009.06174*.

- Renz, W., 1985, "Derivation and solution of a low-friction Fokker-Planck equation for a bound Brownian particle," *Z. Phys. B* **59**, 91–102.
- Reserbat-Plantey, Antoine, Laëticia Marty, Olivier Arcizet, Nedjma Bendiab, and Vincent Bouchiat, 2012, "A local optical probe for measuring motion and stress in a nanoelectromechanical system," *Nat. Nanotechnol.* **7**, 151–155.
- Reulet, B., A. Yu. Kasumov, M. Kociak, R. Deblock, I. I. Khodos, Yu. B. Gorbatov, V. T. Volkov, C. Journet, and H. Bouchiat, 2000, "Acoustoelectric Effects in Carbon Nanotubes," *Phys. Rev. Lett.* **85**, 2829–2832.
- Ricci, F., R. A. Rica, M. Spasenovic, J. Gieseler, L. Rondin, L. Novotny, and R. Quidant, 2017, "Optically levitated nanoparticle as a model system for stochastic bistable dynamics," *Nat. Commun.* **8**, 15141.
- Riedinger, Ralf, Sungkun Hong, Richard A. Norte, Joshua A. Slater, Juying Shang, Alexander G. Krause, Vikas Anant, Markus Aspelmeyer, and Simon Gröblacher, 2016, "Non-classical correlations between single photons and phonons from a mechanical oscillator," *Nature (London)* **530**, 313–316.
- Riedinger, Ralf, Andreas Wallucks, Igor Marinković, Clemens Löschnauer, Markus Aspelmeyer, Sungkun Hong, and Simon Gröblacher, 2018, "Remote quantum entanglement between two micromechanical oscillators," *Nature (London)* **556**, 473–477.
- Rieger, J., A. Isacsson, M. J. Seitner, J. P. Kotthaus, and E. M. Weig, 2014, "Energy losses of nanomechanical resonators induced by atomic force microscopy-controlled mechanical impedance mismatching," *Nat. Commun.* **5**, 3345.
- Risken, H., 1996, *The Fokker-Planck Equation*, 2nd ed. (Springer, Berlin).
- Riviere, R., S. Deleglise, S. Weis, E. Gavartin, O. Arcizet, A. Schliesser, and T. J. Kippenberg, 2011, "Optomechanical sideband cooling of a micromechanical oscillator close to the quantum ground state," *Phys. Rev. A* **83**, 063835.
- Roberts, David, Andrew Lingenfelter, and Aashish Clerk, 2021, "Hidden time-reversal symmetry, quantum detailed balance and exact solutions of driven-dissipative quantum systems," *PRX Quantum* **2**, 020336.
- Robinson, Jeremy T., Maxim Zhalalutdinov, Jeffrey W. Baldwin, Eric S. Snow, Zhongqing Wei, Paul Sheehan, and Brian H. Houston, 2008, "Wafer-scale reduced graphene oxide films for nanomechanical devices," *Nano Lett.* **8**, 3441–3445.
- Rocheleau, T., T. Ndukum, C. Macklin, J. B. Hertzberg, A. A. Clerk, and K. C. Schwab, 2010, "Preparation and detection of a mechanical resonator near the ground state of motion," *Nature (London)* **463**, 72–75.
- Rodriguez, Janna, Saurabh A. Chandorkar, Christopher A. Watson, Grant M. Glaze, C. H. Ahn, Eldwin J. Ng, Yushi Yang, and Thomas W. Kenny, 2019, "Direct detection of Akhiezer damping in a silicon MEMS resonator," *Sci. Rep.* **9**, 1–10.
- Rose, William, Holger Haas, Angela Q. Chen, Nari Jeon, Lincoln J. Lauhon, David G. Cory, and Raffi Budakian, 2018, "High-Resolution Nanoscale Solid-State Nuclear Magnetic Resonance Spectroscopy," *Phys. Rev. X* **8**, 011030.
- Roshan, M. H., *et al.*, 2016, "Dual-MEMS-resonator temperature-to-digital converter with 40  $\mu$ K resolution and FOM of 0.12 pJ/K<sup>2</sup>," in *Proceedings of the 2016 IEEE International Solid-State Circuits Conference (ISSCC), San Francisco, 2016* (IEEE, New York), pp. 200–201.
- Rossi, Massimiliano, David Mason, Junxin Chen, Yeghishe Tsaturyan, and Albert Schliesser, 2018, "Measurement-based quantum control of mechanical motion," *Nature (London)* **563**, 53–58.
- Rossi, N., B. Gross, F. Dirnberger, D. Bougeard, and M. Poggio, 2019, "Magnetic force sensing using a self-assembled nanowire," *Nano Lett.* **19**, 930–936.
- Rossi, Nicola, Floris R. Braakman, Davide Cadeddu, Denis Vasyukov, Gozde Tutuncuoglu, Anna Fontcuberta i Morral, and Martino Poggio, 2017, "Vectorial scanning force microscopy using a nanowire sensor," *Nat. Nanotechnol.* **12**, 150.
- Roszhart, T. V., 1990, "The effect of thermoelastic internal friction on the  $Q$  of micromachined silicon resonators," in *Proceedings of the IEEE 4th Technical Digest on Solid-State Sensor and Actuator Workshop, Hilton Head Island, 1990* (IEEE, New York), pp. 13–16.
- Roy, Swapna K., K. Sauer Vincent T., N. Westwood-Bachman Jocelyn, Venkatasubramanian Anandram, and K. Hiebert Wayne, 2018, "Improving mechanical sensor performance through larger damping," *Science* **360**, eaar5220.
- Rugar, D., and P. Grütter, 1991, "Mechanical Parametric Amplification and Thermomechanical Noise Squeezing," *Phys. Rev. Lett.* **67**, 699–702.
- Rytov, S. M., 1956a, "Fluctuations in oscillating systems of the Thomson type. I," *Sov. Phys. JETP* **2**, 217–224, [http://www.jetp.ras.ru/cgi-bin/dn/e\\_002\\_02\\_0217.pdf](http://www.jetp.ras.ru/cgi-bin/dn/e_002_02_0217.pdf).
- Rytov, S. M., 1956b, "Fluctuations in oscillating systems of the Thomson type. II," *Sov. Phys. JETP* **2**, 225–235, [http://www.jetp.ras.ru/cgi-bin/dn/e\\_002\\_02\\_0225.pdf](http://www.jetp.ras.ru/cgi-bin/dn/e_002_02_0225.pdf).
- Ryvkin, D., and M. I. Dykman, 2006, "Resonant symmetry lifting in a parametrically modulated oscillator," *Phys. Rev. E* **74**, 061118.
- Sachkou, Yauhen P., *et al.*, 2019, "Coherent vortex dynamics in a strongly interacting superfluid on a silicon chip," *Science* **366**, 1480.
- Sadeghi, Pedram, Alper Demir, Luis Guillermo Villanueva, Hendrik Kähler, and Silvan Schmid, 2020, "Frequency fluctuations in nanomechanical silicon nitride string resonators," *Phys. Rev. B* **102**, 214106.
- Safavi-Naeini, A. H., T. P. Mayer Alegre, J. Chan, M. Eichenfield, M. Winger, Q. Lin, J. T. Hill, D. E. Chang, and O. Painter, 2011, "Electromagnetically induced transparency and slow light with optomechanics," *Nature (London)* **472**, 69–73.
- Safavi-Naeini, Amir H., Dries Van Thourhout, Roel Baets, and Raphaël Van Laer, 2019, "Controlling phonons and photons at the wavelength scale: Integrated photonics meets integrated photonics," *Optica* **6**, 213–232.
- Sage, E., *et al.*, 2018, "Single-particle mass spectrometry with arrays of frequency-addressed nanomechanical resonators," *Nat. Commun.* **9**, 3283.
- Sahafi, Pardis, William Rose, Andrew Jordan, Ben Yager, Michèle Piscitelli, and Raffi Budakian, 2020, "Ultralow dissipation patterned silicon nanowire arrays for scanning probe microscopy," *Nano Lett.* **20**, 218–223.
- Sahu, Sudhir Kumar, Supriya Mandal, Sanat Ghosh, Mandar M. Deshmukh, and Vibhor Singh, 2022, "Superconducting vortex-charge measurement using cavity electromechanics," *Nano Lett.* **22**, 1665–1671.
- Samanta, C., P. R. Yasasvi Gangavarapu, and A. K. Naik, 2015, "Nonlinear mode coupling and internal resonances in MoS<sub>2</sub> nanoelectromechanical system," *Appl. Phys. Lett.* **107**, 173110.
- Samanta, Chandan, Nishta Arora, and A. K. Naik, 2018, "Tuning of geometric nonlinearity in ultrathin nanoelectromechanical systems," *Appl. Phys. Lett.* **113**, 113101.
- Sansa, M., *et al.*, 2016, "Frequency fluctuations in silicon nanoresonators," *Nat. Nanotechnol.* **11**, 552.
- Sansa, Marc, Marta Fernandez-Regalez, Alvaro San Paulo, and Francesc Pérez-Murano, 2012, "Electrical transduction in

- nanomechanical resonators based on doubly clamped bottom-up silicon nanowires,” *Appl. Phys. Lett.* **101**, 243115.
- Santamore, D. H., A. C. Doherty, and M. C. Cross, 2004, “Quantum nondemolition measurement of Fock states of mesoscopic mechanical oscillators,” *Phys. Rev. B* **70**, 144301.
- Santamore, D. H., H. S. Goan, G. J. Milburn, and M. L. Roukes, 2004, “Anharmonic effects on a phonon-number measurement of a quantum-mesoscopic-mechanical oscillator,” *Phys. Rev. A* **70**, 052105.
- Satzinger, K. J., *et al.*, 2018, “Quantum control of surface acoustic-wave phonons,” *Nature (London)* **563**, 661.
- Saulson, Peter R., 1990, “Thermal noise in mechanical experiments,” *Phys. Rev. D* **42**, 2437–2445.
- Sazonova, V., Y. Yaish, H. Ustunel, D. Roundy, T. A. Arias, and P. L. McEuen, 2004, “A tunable carbon nanotube electromechanical oscillator,” *Nature (London)* **431**, 284–287.
- Schmid, S., K. D. Jensen, K. H. Nielsen, and A. Boisen, 2011, “Damping mechanisms in high- $Q$  micro and nanomechanical string resonators,” *Phys. Rev. B* **84**, 165307.
- Schmid, S., L. G. Villanueva, and M. L. Roukes, 2016, *Fundamentals of Nanomechanical Resonators* (Springer, Cham, Switzerland).
- Schmölle, Jonas, Mathias Dragosits, Hans Hepach, and Markus Aspelmeyer, 2016, “A micromechanical proof-of-principle experiment for measuring the gravitational force of milligram masses,” *Classical Quantum Gravity* **33**, 125031.
- Schneider, Ben H., Vibhor Singh, Warner J. Venstra, Harold B. Meerwaldt, and Gary A. Steele, 2014, “Observation of decoherence in a carbon nanotube mechanical resonator,” *Nat. Commun.* **5**, 5819.
- Schuster, D. I., *et al.*, 2007, “Resolving photon number states in a superconducting circuit,” *Nature (London)* **445**, 515–518.
- Schwender, J., I. Tsioutsios, A. Tavernarakis, Q. Dong, Y. Jin, U. Staufer, and A. Bachtold, 2018, “Improving the read-out of the resonance frequency of nanotube mechanical resonators,” *Appl. Phys. Lett.* **113**, 063104.
- Schwinger, J., 1961, “Brownian motion of a quantum oscillator,” *J. Math. Phys. (N.Y.)* **2**, 407.
- Seis, Yannick, Thibault Capelle, Eric Langman, Sampo Saarinen, Eric Planz, and Albert Schliesser, 2022, “Ground state cooling of an ultracoherent electromechanical system,” *Nat. Commun.* **13**, 1507.
- Sengupta, Shamashis, Hari S. Solanki, Vibhor Singh, Sajal Dhara, and Mandar M. Deshmukh, 2010, “Electromechanical resonators as probes of the charge density wave transition at the nanoscale in NbSe<sub>2</sub>,” *Phys. Rev. B* **82**, 155432.
- Senitzky, I. R., 1961, “Dissipation in quantum mechanics. The harmonic oscillator. II,” *Phys. Rev.* **124**, 642–648.
- Seoáñez, C., F. Guinea, and A. H. Castro Neto, 2008, “Surface dissipation in nanoelectromechanical systems: Unified description with the standard tunneling model and effects of metallic electrodes,” *Phys. Rev. B* **77**, 125107.
- Shoshani, O., S. W. Shaw, and M. I. Dykman, 2017, “Anomalous decay of nanomechanical modes going through nonlinear resonance,” *Sci. Rep.* **7**, 18091.
- Shoshani, Oriel, and Steven W. Shaw, 2021, “Resonant modal interactions in micro/nano-mechanical structures,” *Nonlinear Dyn.* **104**, 1801.
- Siddiqi, I., R. Vijay, F. Pierre, C. M. Wilson, L. Frunzio, M. Metcalfe, C. Rigetti, and M. H. Devoret, 2006, “The Josephson bifurcation amplifier for quantum measurements,” in *Quantum Computation in Solid State Systems*, edited by B. Ruggiero, P. Delsing, C. Granata, Y. Pashkin, and P. Silvertrini (Springer, New York), pp. 28–37.
- Siddiqi, I., R. Vijay, F. Pierre, C. M. Wilson, M. Metcalfe, C. Rigetti, L. Frunzio, and M. H. Devoret, 2004, “RF-Driven Josephson Bifurcation Amplifier for Quantum Measurement,” *Phys. Rev. Lett.* **93**, 207002.
- Sild, Olev, and Kristjan, Haller, 1988, Eds., *Zero-Phonon Lines and Spectral Hole Burning in Spectroscopy and Photochemistry* (Springer, Berlin).
- Sillanpää, Mika A., Raphaël Khan, Tero T. Heikkilä, and Pertti J. Hakonen, 2011, “Macroscopic quantum tunneling in nanoelectromechanical systems,” *Phys. Rev. B* **84**, 195433.
- Singh, Rajan, A. Faruque Sarkar, Chitres Guria, Ryan J. T. Nicholl, Sagar Chakraborty, Kirill I. Bolotin, and Saikat Ghosh, 2020, “Giant tunable mechanical nonlinearity in graphene-silicon nitride hybrid resonator,” *Nano Lett.* **20**, 4659.
- Singh, V., S. J. Bosman, B. H. Schneider, Y. M. Blanter, A. Castellanos-Gomez, and G. A. Steele, 2014, “Optomechanical coupling between a multilayer graphene mechanical resonator and a superconducting microwave cavity,” *Nat. Nanotechnol.* **9**, 820–824.
- Singh, Vibhor, Bushra Irfan, Ganesh Subramanian, Hari S. Solanki, Shamashis Sengupta, Sudipta Dubey, Anil Kumar, S. Ramakrishnan, and Mandar M. Deshmukh, 2012, “Coupling between quantum Hall state and electromechanics in suspended graphene resonator,” *Appl. Phys. Lett.* **100**, 233103.
- Singh, Vibhor, Shamashis Sengupta, Hari S. Solanki, Rohan Dhall, Adrien Allain, Sajal Dhara, Prita Pant, and Mandar M. Deshmukh, 2010, “Probing thermal expansion of graphene and modal dispersion at low-temperature using graphene nanoelectromechanical systems resonators,” *Nanotechnology* **21**, 165204.
- Singh, Vibhor, Olga Shevchuk, Ya. M. Blanter, and Gary A. Steele, 2016, “Negative nonlinear damping of a multilayer graphene mechanical resonator,” *Phys. Rev. B* **93**, 245407.
- Siria, A., T. Barois, K. Vilella, S. Perisanu, A. Ayari, D. Guillot, S. T. Purcell, and P. Poncharal, 2012, “Electron fluctuation induced resonance broadening in nano electromechanical systems: The origin of shear force in vacuum,” *Nano Lett.* **12**, 3551–3556.
- Šiškins, Makars, Martin Lee, Samuel Mañas-Valero, Eugenio Coronado, Yaroslav M. Blanter, Herre S. J. van der Zant, and Peter G. Steeneken, 2020, “Magnetic and electronic phase transitions probed by nanomechanical resonators,” *Nat. Commun.* **11**, 2698.
- Slusher, R. E., L. W. Hollberg, B. Yurke, J. C. Mertz, and J. F. Valley, 1985, “Observation of Squeezed States Generated by Four-Wave Mixing in an Optical Cavity,” *Phys. Rev. Lett.* **55**, 2409–2412.
- Solanki, Hari S., Shamashis Sengupta, Sajal Dhara, Vibhor Singh, Sunil Patil, Rohan Dhall, Jeevak Parpia, Arnab Bhattacharya, and Mandar M. Deshmukh, 2010, “Tuning mechanical modes and influence of charge screening in nanowire resonators,” *Phys. Rev. B* **81**, 115459.
- Sonar, Sameer, Vitaly Fedoseev, Matthew J. Weaver, Fernando Luna, Elger Vlieg, Harmen van der Meer, Dirk Bouwmeester, and Wolfgang Löffler, 2018, “Strong thermomechanical squeezing in a far-detuned membrane-in-the-middle system,” *Phys. Rev. A* **98**, 013804.
- Song, X., M. Oksanen, J. Li, P. J. Hakonen, and M. A. Sillanpää, 2014, “Graphene Optomechanics Realized at Microwave Frequencies,” *Phys. Rev. Lett.* **113**, 027404.
- Song, Xuefeng, Mika Oksanen, Mika A. Sillanpää, H. G. Craighead, J. M. Parpia, and Pertti J. Hakonen, 2012, “Stamp transferred suspended graphene mechanical resonators for radio frequency electrical readout,” *Nano Lett.* **12**, 198–202.



- Soskin, S. M., R. Mannella, and P. V. E. McClintock, 2003, “Zero-dispersion phenomena in oscillatory systems,” *Phys. Rep.* **373**, 247–408.
- Stambaugh, C., and H. B. Chan, 2006a, “Noise activated switching in a driven, nonlinear micromechanical oscillator,” *Phys. Rev. B* **73**, 172302.
- Stambaugh, C., and H. B. Chan, 2006b, “Supernarrow Spectral Peaks near a Kinetic Phase Transition in a Driven Nonlinear Micromechanical Oscillator,” *Phys. Rev. Lett.* **97**, 110602.
- Stapfner, S., L. Ost, D. Hunger, J. Reichel, I. Favero, and E. M. Weig, 2013, “Cavity-enhanced optical detection of carbon nanotube Brownian motion,” *Appl. Phys. Lett.* **102**, 151910.
- Steele, G. A., A. K. Hüttel, B. Witkamp, M. Poot, H. B. Meerwaldt, L. P. Kouwenhoven, and H. S. J. van der Zant, 2009, “Strong coupling between single-electron tunneling and nanomechanical motion,” *Science* **325**, 1103–1107.
- Steeneken, Peter G., Robin J. Dolleman, Dejan Davidovikj, Farbod Alijani, and Herre S. J. van der Zant, 2021, “Dynamics of 2D material membranes,” *2D Mater.* **8**, 042001.
- Stiller, P. L., S. Kugler, D. R. Schmid, C. Strunk, and A. K. Hüttel, 2013, “Negative frequency tuning of a carbon nanotube nanoelectromechanical resonator under tension,” *Phys. Status Solidi B* **250**, 2518–2532.
- Stomp, Romain, Yoichi Miyahara, Sacha Schaer, Qingfeng Sun, Hong Guo, Peter Grutter, Sergei Studenikin, Philip Poole, and Andy Sachrajda, 2005, “Detection of Single-Electron Charging in an Individual InAs Quantum Dot by Noncontact Atomic-Force Microscopy,” *Phys. Rev. Lett.* **94**, 056802.
- Stoneham, A. M., 2001, *Theory of Defects in Solids* (Oxford University Press, Oxford).
- Stowe, T. D., K. Yasumura, T. W. Kenny, D. Botkin, K. Wago, and D. Rugar, 1997, “Attonewton force detection using ultrathin silicon cantilevers,” *Appl. Phys. Lett.* **71**, 288–290.
- Suh, J., A. J. Weinstein, C. U. Lei, E. E. Wollman, S. K. Steinke, P. Meystre, A. A. Clerk, and K. C. Schwab, 2014, “Mechanically detecting and avoiding the quantum fluctuations of a microwave field,” *Science* **344**, 1262.
- Suh, Junho, Matthew D. LaHaye, Pierre M. Echternach, Keith C. Schwab, and Michael L. Roukes, 2010, “Parametric amplification and back-action noise squeezing by a qubit-coupled nanoresonator,” *Nano Lett.* **10**, 3990–3994.
- Sullivan, Sean, Ajit Vallabhaneni, Iskandar Kholmanov, Xiulin Ruan, Jayathi Murthy, and Li Shi, 2017, “Optical generation and detection of local nonequilibrium phonons in suspended graphene,” *Nano Lett.* **17**, 2049–2056.
- Sun, F., X. Dong, J. Zou, M. I. Dykman, and H. B. Chan, 2016, “Correlated anomalous phase diffusion of coupled phononic modes in a sideband-driven resonator,” *Nat. Commun.* **7**, 12694.
- Sun, F., J. Zou, Z. A. Maizelis, and H. B. Chan, 2015, “Telegraph frequency noise in electromechanical resonators,” *Phys. Rev. B* **91**, 174102.
- Szorkovszky, A., G. A. Brawley, A. C. Doherty, and W. P. Bowen, 2013, “Strong Thermomechanical Squeezing via Weak Measurement,” *Phys. Rev. Lett.* **110**, 184301.
- Tadokoro, Yukihiro, Hiroya Tanaka, and M. I. Dykman, 2020, “Noise-induced switching from a symmetry-protected shallow metastable state,” *Sci. Rep.* **10**, 10413.
- Tang, L., M. Wang, C. Y. Ng, M. Nikolic, C. T. Chan, A. W. Rodriguez, and H. B. Chan, 2017, “Measurement of non-monotonic Casimir forces between silicon nanostructures,” *Nat. Photonics* **11**, 97–101.
- Tao, Y., J. M. Boss, B. A. Moores, and C. L. Degen, 2014, “Single-crystal diamond nanomechanical resonators with quality factors exceeding one million,” *Nat. Commun.* **5**, 3638.
- Tavernarakis, A., J. Chaste, A. Eichler, G. Ceballos, M. C. Gordillo, J. Boronat, and A. Bachtold, 2014, “Atomic Monolayer Deposition on the Surface of Nanotube Mechanical Resonators,” *Phys. Rev. Lett.* **112**, 196103.
- Tavernarakis, A., A. Stavrinadis, A. Nowak, I. Tsioutsios, A. Bachtold, and P. Verlot, 2018, “Optomechanics with a hybrid carbon nanotube resonator,” *Nat. Commun.* **9**, 662.
- Tebbenjohanns, Felix, Martin Frimmer, Vijay Jain, Dominik Windey, and Lukas Novotny, 2020, “Motional Sideband Asymmetry of a Nanoparticle Optically Levitated in Free Space,” *Phys. Rev. Lett.* **124**, 013603.
- Tebbenjohanns, Felix, M. Luisa Mattana, Massimiliano Rossi, Martin Frimmer, and Lukas Novotny, 2021, “Quantum control of a nanoparticle optically levitated in cryogenic free space,” *Nature (London)* **595**, 378–382.
- Tepsic, S., G. Gruber, C. B. Møller, C. Magén, P. Belardinelli, E. R. Hernández, F. Alijani, P. Verlot, and A. Bachtold, 2021, “Interrelation of Elasticity and Thermal Bath in Nanotube Cantilevers,” *Phys. Rev. Lett.* **126**, 175502.
- Teufel, J. D., T. Donner, Dale Li, J. W. Harlow, M. S. Allman, K. Cicak, A. J. Sirois, J. D. Whittaker, K. W. Lehnert, and R. W. Simmonds, 2011, “Sideband cooling of micromechanical motion to the quantum ground state,” *Nature (London)* **475**, 359–363.
- Teufel, J. D., J. W. Harlow, C. A. Regal, and K. W. Lehnert, 2008, “Dynamical Backaction of Microwave Fields on a Nanomechanical Oscillator,” *Phys. Rev. Lett.* **101**, 197203.
- Toda, M. O., 1958, “On the theory of the Brownian motion,” *J. Phys. Soc. Jpn.* **13**, 1266–1280.
- Touzard, S., *et al.*, 2018, “Coherent Oscillations inside a Quantum Manifold Stabilized by Dissipation,” *Phys. Rev. X* **8**, 021005.
- Travis, J., 1994, “Building bridges to the nanoworld,” *Science* **263**, 1702–1703.
- Tsaturyan, Y., A. Barg, E. S. Polzik, and A. Schliesser, 2017, “Ultraslow nanomechanical resonators via soft clamping and dissipation dilution,” *Nat. Nanotechnol.* **12**, 776.
- Tse, M., *et al.*, 2019, “Quantum-Enhanced Advanced LIGO Detectors in the Era of Gravitational-Wave Astronomy,” *Phys. Rev. Lett.* **123**, 231107.
- Tsioutsios, I., A. Tavernarakis, J. Osmond, P. Verlot, and A. Bachtold, 2017, “Real-time measurement of nanotube resonator fluctuations in an electron microscope,” *Nano Lett.* **17**, 1748–1755.
- Turner, K. L., S. A. Miller, P. G. Hartwell, N. C. MacDonald, S. H. Strogatz, and S. G. Adams, 1998, “Five parametric resonances in a microelectromechanical system,” *Nature (London)* **396**, 149–152.
- Ullersma, P., 1966, “An exactly solvable model for Brownian motion. I. Derivation of Langevin equation,” *Physica (Amsterdam)* **32**, 27.
- Unterreithmeier, Q. P., T. Faust, and J. P. Kotthaus, 2010, “Damping of Nanomechanical Resonators,” *Phys. Rev. Lett.* **105**, 027205.
- Unterreithmeier, Q. P., E. M. Weig, and J. P. Kotthaus, 2009, “Universal transduction scheme for nanomechanical systems based on dielectric forces,” *Nature (London)* **458**, 1001–1004.
- Urgell, C., W. Yang, S. L. De Bonis, C. Samanta, M. J. Esplandiú, Q. Dong, Y. Jin, and A. Bachtold, 2020, “Cooling and self-oscillation in a nanotube electromechanical resonator,” *Nat. Phys.* **16**, 32–37.
- Usmani, O., Ya. M. Blanter, and Yu. V. Nazarov, 2007, “Strong feedback and current noise in nanoelectromechanical systems,” *Phys. Rev. B* **75**, 195312.

- van der Pol, B., 1926, "On relaxation-oscillations," *London Edinburgh Dublin Philos. Mag. J. Sci.* **2**, 978–992.
- van der Zande, Arend M., Robert A. Barton, Jonathan S. Alden, Carlos S. Ruiz-Vargas, William S. Whitney, Phi H.Q. Pham, Jiwoong Park, Jeevak M. Parpia, Harold G. Craighead, and Paul L. McEuen, 2010, "Large-scale arrays of single-layer graphene resonators," *Nano Lett.* **10**, 4869–4873.
- van Leeuwen, R., A. Castellanos-Gomez, G. A. Steele, H. S. J. van der Zant, and W. J. Venstra, 2014, "Time-domain response of atomically thin MoS<sub>2</sub> nanomechanical resonators," *Appl. Phys. Lett.* **105**, 041911.
- Venkatasubramanian, Anandram, Vincent T. K. Sauer, Swapan K. Roy, Mike Xia, David S. Wishart, and Wayne K. Hiebert, 2016, "Nano-optomechanical systems for gas chromatography," *Nano Lett.* **16**, 6975–6981.
- Venkatesan, A., K. J. Lulla, M. J. Patton, A. D. Armour, C. J. Mellor, and J. R. Owers-Bradley, 2010, "Dissipation due to tunneling two-level systems in gold nanomechanical resonators," *Phys. Rev. B* **81**, 073410.
- Venstra, W. J., H. J. R. Westra, and H. S. J. van der Zant, 2013, "Stochastic switching of cantilever motion," *Nat. Commun.* **4**, 2624.
- Venstra, Warner J., Ronald van Leeuwen, and Herre S. J. van der Zant, 2012, "Strongly coupled modes in a weakly driven micro-mechanical resonator," *Appl. Phys. Lett.* **101**, 243111.
- Verbridge, Scott S., Jeevak M. Parpia, Robert B. Reichenbach, Leon M. Bellan, and H. G. Craighead, 2006, "High quality factor resonance at room temperature with nanostrings under high tensile stress," *J. Appl. Phys.* **99**, 124304.
- Verhagen, E., S. Deléglise, S. Weis, A. Schliesser, and T. J. Kippenberg, 2012, "Quantum-coherent coupling of a mechanical oscillator to an optical cavity mode," *Nature (London)* **482**, 63–67.
- Viennot, J. J., X. Ma, and K. W. Lehnert, 2018, "Phonon-Number-Sensitive Electromechanics," *Phys. Rev. Lett.* **121**, 183601.
- Vig, J. R., and Y. Kim, 1999, "Noise in microelectromechanical system resonators," *IEEE Trans. Ultrason. Ferroelectr. Freq. Control* **46**, 1558–1565.
- Vigneau, Florian, Juliette Monsel, Jorge Tabanera, Léa Bresque, Federico Fedele, Janet Anders, Juan M. R. Parrondo, Alexia Auffèves, and Natalia Ares, 2021, "Ultrastrong coupling between electron tunneling and mechanical motion," *arXiv:2103.15219*.
- Vijay, R., M. H. Devoret, and I. Siddiqi, 2009, "The Josephson bifurcation amplifier," *Rev. Sci. Instrum.* **80**, 111101.
- Villanueva, L. G., E. Kenig, R. B. Karabalin, M. H. Matheny, Ron Lifshitz, M. C. Cross, and M. L. Roukes, 2013, "Surpassing Fundamental Limits of Oscillators Using Nonlinear Resonators," *Phys. Rev. Lett.* **110**, 177208.
- Villanueva, L. G., and S. Schmid, 2014, "Evidence of Surface Loss as Ubiquitous Limiting Damping Mechanism in SiN Micro- and Nanomechanical Resonators," *Phys. Rev. Lett.* **113**, 227201.
- Vinante, A., 2014, "Thermal frequency noise in micromechanical resonators due to nonlinear mode coupling," *Phys. Rev. B* **90**, 024308.
- Vinante, A., and P. Falferi, 2013, "Feedback-Enhanced Parametric Squeezing of Mechanical Motion," *Phys. Rev. Lett.* **111**, 207203.
- Vinante, A., P. Falferi, G. Gasbarri, A. Setter, C. Timberlake, and H. Ulbricht, 2020, "Ultralow Mechanical Damping with Meissner-Levitated Ferromagnetic Microparticles," *Phys. Rev. Appl.* **13**, 064027.
- Wang, Mingkan, L. Tang, C. Y. Ng, Riccardo Messina, Brahim Guizal, J. A. Crosse, Mauro Antezza, C. T. Chan, and H. B. Chan, 2021, "Strong geometry dependence of the Casimir force between interpenetrated rectangular gratings," *Nat. Commun.* **12**, 600.
- Wang, Zenghui, Jiang Wei, Peter Morse, J. Gregory Dash, Oscar E. Vilches, and David H. Cobden, 2010, "Phase transitions of adsorbed atoms on the surface of a carbon nanotube," *Science* **327**, 552–555.
- Wang, Zhaoyou, Marek Pechal, E. Alex Wollack, Patricio Arrangoiz-Arriola, Maodong Gao, Nathan R. Lee, and Amir H. Safavi-Naeini, 2019, "Quantum Dynamics of a Few-Photon Parametric Oscillator," *Phys. Rev. X* **9**, 021049.
- Weber, P., J. Güttinger, A. Noury, J. Vergara-Cruz, and A. Bachtold, 2016, "Force sensitivity of multilayer graphene optomechanical devices," *Nat. Commun.* **7**, 12496.
- Weber, P., J. Güttinger, I. Tsioutsios, D. E. Chang, and A. Bachtold, 2014, "Coupling graphene mechanical resonators to superconducting microwave cavities," *Nano Lett.* **14**, 2854–2860.
- Weis, Stefan, Rémi Rivière, Samuel Deléglise, Emanuel Gavartin, Olivier Arcizet, Albert Schliesser, and Tobias J. Kippenberg, 2010, "Optomechanically induced transparency," *Science* **330**, 1520–1523.
- Weisskopf, V., and E. Wigner, 1930a, "Calculation of the natural line width based on Dirac's light theory," *Z. Phys.* **63**, 54–73.
- Weisskopf, V., and E. Wigner, 1930b, "On the natural linewidth of radiation of the harmonic oscillator," *Z. Phys.* **65**, 18–29.
- Wen, Yutian, N. Ares, F. J. Schupp, T. Pei, G. A. D. Briggs, and E. A. Laird, 2020, "A coherent nanomechanical oscillator driven by single-electron tunnelling," *Nat. Phys.* **16**, 75–82.
- Westra, H. J. R., M. Poot, H. S. J. van der Zant, and W. J. Venstra, 2010, "Nonlinear Modal Interactions in Clamped-Clamped Mechanical Resonators," *Phys. Rev. Lett.* **105**, 117205.
- Will, M., M. Hamer, M. Müller, A. Noury, P. Weber, A. Bachtold, R. V. Gorbachev, C. Stampfer, and J. Güttinger, 2017, "High quality factor graphene-based two-dimensional heterostructure mechanical resonator," *Nano Lett.* **17**, 5950–5955.
- Willick, Kyle, Xiaowu (Shirley) Tang, and Jonathan Baugh, 2017, "Probing the non-linear transient response of a carbon nanotube mechanical oscillator," *Appl. Phys. Lett.* **111**, 223108.
- Wilson, D. J., V. Sudhir, N. Piro, R. Schilling, A. Ghadimi, and T. J. Kippenberg, 2015, "Measurement-based control of a mechanical oscillator at its thermal decoherence rate," *Nature (London)* **524**, 325–329.
- Wilson-Rae, I., 2008, "Intrinsic dissipation in nanomechanical resonators due to phonon tunneling," *Phys. Rev. B* **77**, 245418.
- Wilson-Rae, I., R. A. Barton, S. S. Verbridge, D. R. Southworth, B. Ilic, H. G. Craighead, and J. M. Parpia, 2011, "High-*Q* Nanomechanics via Destructive Interference of Elastic Waves," *Phys. Rev. Lett.* **106**, 047205.
- Wollack, E. Alex, Agneta Y. Cleland, Rachel G. Gruenke, Zhaoyou Wang, Patricio Arrangoiz-Arriola, and Amir H. Safavi-Naeini, 2022, "Quantum state preparation, tomography, and entanglement of mechanical oscillators," *Nature (London)* **604**, 463.
- Wollman, E. E., C. U. Lei, A. J. Weinstein, J. Suh, A. Kronwald, F. Marquardt, A. A. Clerk, and K. C. Schwab, 2015, "Quantum squeezing of motion in a mechanical resonator," *Science* **349**, 952–955.
- Woodruff, T. O., and H. Ehrenreich, 1961, "Absorption of sound in insulators," *Phys. Rev.* **123**, 1553.
- Woodside, Michael T., and Paul L. McEuen, 2002, "Scanned probe imaging of single-electron charge states in nanotube quantum dots," *Science* **296**, 1098.
- Wu, Chung Chiang, and Zhaohui Zhong, 2011, "Capacitive spring softening in single-walled carbon nanotube nanoelectromechanical resonators," *Nano Lett.* **11**, 1448–1451.

- Yamaguchi, H., 2017, “GaAs-based micro/nanomechanical resonators,” *Semicond. Sci. Technol.* **32**, 103003.
- Yamaguchi, H., and I. Mahboob, 2013, “Parametric mode mixing in asymmetric doubly clamped beam resonators,” *New J. Phys.* **15**, 015023.
- Yamaguchi, Hiroshi, and Samer Houry, 2021, “Generation and Propagation of Topological Solitons in a Chain of Coupled Parametric-Micromechanical-Resonator Arrays,” *Phys. Rev. Appl.* **15**, 034091.
- Yang, A., H. J. Lian, M. L. W. Thewalt, M. Uemura, A. Sagara, K. M. Itoh, E. E. Haller, J. W. Ager, and S. A. Lyon, 2006, “Isotopic mass dependence of the lattice parameter in silicon determined by measurement of strain-induced splitting of impurity bound exciton transitions,” *Physica (Amsterdam)* **376B–377B**, 54–56.
- Yang, Fan, Mengqi Fu, Bojan Bosnjak, Robert H. Blick, Yuxuan Jiang, and Elke Scheer, 2021, “Mechanically Modulated Sideband and Squeezing Effects of Membrane Resonators,” *Phys. Rev. Lett.* **127**, 184301.
- Yang, Fan, Felix Rochau, Jana Huber, Alexandre Briussel, Gianluca Rastelli, Eva M. Weig, and Elke Scheer, 2019, “Spatial modulation of nonlinear flexural vibrations of membrane resonators,” *arXiv:1902.01270*.
- Yang, Y., E. J. Ng, P. M. Polunin, Y. Chen, I. B. Flader, S. W. Shaw, M. I. Dykman, and T. W. Kenny, 2016, “Nonlinearity of degenerately doped bulk-mode silicon MEMS resonators,” *J. Microelectromech. Syst.* **25**, 859.
- Yang, Y. T., C. Callegari, X. L. Feng, K. L. Ekinici, and M. L. Roukes, 2006, “Zeptogram-scale nanomechanical mass sensing,” *Nano Lett.* **6**, 583–586.
- Yang, Y. T., C. Callegari, X. L. Feng, and M. L. Roukes, 2011, “Surface adsorbates fluctuations and noise in nanoelectromechanical systems,” *Nano Lett.* **11**, 1753.
- Yasumura, K. Y., T. D. Stowe, E. M. Chow, T. Pfafman, T. W. Kenny, B. C. Stipe, and D. Rugar, 2000, “Quality factors in micron- and submicron-thick cantilevers,” *J. Microelectromech. Syst.* **9**, 117–125.
- Yazdani, Showkat M., Nikolas Hoepker, Seppe Kuehn, Roger F. Loring, and John A. Marohn, 2009, “Quantifying electric field gradient fluctuations over polymers using ultrasensitive cantilevers,” *Nano Lett.* **9**, 2273–2279.
- Yeo, I., *et al.*, 2014, “Strain-mediated coupling in a quantum dot-mechanical oscillator hybrid system,” *Nat. Nanotechnol.* **9**, 106.
- Yong, Y. K., and J. R. Vig, 1989, “Resonator surface contamination—A cause of frequency fluctuations,” *IEEE Trans. Ultrason. Ferroelectr. Freq. Control* **36**, 452–458.
- Yu, P. L., K. Cicak, N. S. Kampel, Y. Tsaturyan, T. P. Purdy, R. W. Simmonds, and C. A. Regal, 2014, “A phononic bandgap shield for high-*Q* membrane microresonators,” *Appl. Phys. Lett.* **104**, 023510.
- Yu, P.-L., T. P. Purdy, and C. A. Regal, 2012, “Control of Material Damping in High-*Q* Membrane Microresonators,” *Phys. Rev. Lett.* **108**, 083603.
- Yuksel, Mert, Ezgi Orhan, Cenk Yanik, Atakan B. Ari, Alper Demir, and M. Selim Hanay, 2019, “Nonlinear nanomechanical mass spectrometry at the single-nanoparticle level,” *Nano Lett.* **19**, 3583–3589.
- Yurke, B., D. S. Greywall, A. N. Pargellis, and P. A. Busch, 1995, “Theory of amplifier-noise evasion in an oscillator employing a nonlinear resonator,” *Phys. Rev. A* **51**, 4211–4229.
- Zaitsev, Stav, Oleg Shtempluck, Eyal Buks, and Oded Gottlieb, 2012, “Nonlinear damping in a micromechanical oscillator,” *Nonlinear Dyn.* **67**, 859.
- Zalalutdinov, Maxim K., *et al.*, 2021, “Acoustic cavities in 2D heterostructures,” *Nat. Commun.* **12**, 3267.
- Zaliasl, Samira, *et al.*, 2015, “A 3 ppm  $1.5 \times 0.8 \text{ mm}^2$   $1.0 \mu\text{A}$  32.768 kHz MEMS-based oscillator,” *IEEE J. Solid-State Circuits* **50**, 291–302.
- Zeldovich, B. Ya., A. M. Perelomov, and V. S. Popov, 1969, “Relaxation of a quantum oscillator,” *Sov. Phys. JETP* **28**, 308–316, [http://www.jetp.ras.ru/cgi-bin/dn/e\\_028\\_02\\_0308.pdf](http://www.jetp.ras.ru/cgi-bin/dn/e_028_02_0308.pdf).
- Zener, C., 1937, “Internal friction in solids. I. Theory of internal friction in reeds,” *Phys. Rev.* **52**, 230–235.
- Zener, C., 1958, “Anelasticity of metals,” *Nuovo Cimento* **7**, 544–568.
- Zener, C. M., 1948, *Elasticity and Anelasticity of Metals* (University of Chicago Press, Chicago).
- Zener, Clarence, 1938, “Internal friction in solids. II. General theory of thermoelastic internal friction,” *Phys. Rev.* **53**, 90–99.
- Zhang, Qing-Hang, Yue Ying, Zhuo-Zhi Zhang, Zi-Jia Su, He Ma, Guo-Quan Qin, Xiang-Xiang Song, and Guo-Ping Guo, 2021, “Graphene-based nanoelectromechanical periodic array with tunable frequency,” *Nano Lett.* **21**, 8571–8578.
- Zhang, Xin, Kevin Makles, Léo Colombier, Dominik Metten, Hicham Majjad, Pierre Verlot, and Stéphane Berciaud, 2020, “Dynamically-enhanced strain in atomically thin resonators,” *Nat. Commun.* **11**, 5526.
- Zhang, Y., J. Moser, J. Güttinger, A. Bachtold, and M. I. Dykman, 2014, “Interplay of Driving and Frequency Noise in the Spectra of Vibrational Systems,” *Phys. Rev. Lett.* **113**, 255502.
- Zhang, Yaxing, and M. I. Dykman, 2015, “Spectral effects of dispersive mode coupling in driven mesoscopic systems,” *Phys. Rev. B* **92**, 165419.
- Zhang, Yaxing, and M. I. Dykman, 2017, “Preparing quasienergy states on demand: A parametric oscillator,” *Phys. Rev. A* **95**, 053841.
- Zhang, Yaxing, J. Gosner, S. M. Girvin, J. Ankerhold, and M. I. Dykman, 2017, “Time-translation-symmetry breaking in a driven oscillator: From the quantum coherent to the incoherent regime,” *Phys. Rev. A* **96**, 052124.
- Zhang, Zhuo-Zhi, Qitao Hu, Xiang-Xiang Song, Yue Ying, Hai-Ou Li, Zhen Zhang, and Guo-Ping Guo, 2020, “A suspended silicon single-hole transistor as an extremely scaled gigahertz nanoelectromechanical beam resonator,” *Adv. Mater.* **32**, 2005625.
- Zhang, Zhuo-Zhi, *et al.*, 2020, “Coherent phonon dynamics in spatially separated graphene mechanical resonators,” *Proc. Natl. Acad. Sci. U.S.A.* **117**, 5582.
- Zhou, X., D. Cattiaux, R. R. Gazizulin, A. Luck, O. Maillet, T. Crozes, J.-F. Motte, O. Bourgeois, A. Fefferman, and E. Collin, 2019, “On-Chip Thermometry for Microwave Optomechanics Implemented in a Nuclear Demagnetization Cryostat,” *Phys. Rev. Appl.* **12**, 044066.
- Zhou, Xin, Srisaran Venkatachalam, Ronghua Zhou, Hao Xu, Alok Pokharel, Andrew Fefferman, Mohammed Zaknounge, and Eddy Collin, 2021, “High-*Q* silicon nitride drum resonators strongly coupled to gates,” *Nano Lett.* **21**, 5738–5744.
- Zhu, Dong, *et al.*, 2017, “Coherent phonon Rabi oscillations with a high-frequency carbon nanotube phonon cavity,” *Nano Lett.* **17**, 915–921.
- Zhu, J., M. Brink, and P. L. McEuen, 2005, “Frequency shift imaging of quantum dots with single-electron resolution,” *Appl. Phys. Lett.* **87**, 242102.